INVESTIGATING THE ROLE OF MLLT11 IN CORTICAL DEVELOPMENT

by

Danielle Stanton-Turcotte

Submitted in partial fulfillment of the requirements for the degree of Doctor of Philosophy

at

Dalhousie University
Halifax, Nova Scotia
July 2023

DEDICATION

This thesis is dedicated to my beloved family and partner, who have supported and encouraged me in moving across borders to pursue my interests.

And of course, to Dexter.

TABLE OF CONTENTS

LIST OF TABLES

LIST OF FIGURES

ABSTRACT

The formation of connections within the mammalian neocortex is highly regulated by both extracellular guidance mechanisms and intrinsic gene expression programs. Dysregulation of these programs has been shown to cause a variety of neurodevelopmental disorders (NDDs) such as autism spectrum disorder (ASD). The regulation of cortical projection morphologies and how their misregulation contributes to NDDs is not yet fully understood at the molecular level. Here, I report a role for Mllt11 (Myeloid/lymphoid or mixed-lineage leukemia; translocated to chromosome 11/All1 Fused Gene From Chromosome 1q) in the migration and neurite outgrowth of callosal projection neurons during mouse brain formation. I show that *Mllt11* expression is exclusive to developing neurons and is enriched in the developing cortical plate (CP) during the formation of the superficial cortical layers. In cultured primary cortical neurons, Mllt11 is detected in varicosities and growth cones as well as the soma. Using conditional loss-of-function and gain-of-function analysis I show that Mllt11 is required for neuritogenesis and proper migration of upper layer (UL) cortical projection neurons (CPNs). Loss of *Mllt11* in the superficial cortex of male and female neonates leads to a severe reduction in fibres crossing the corpus callosum (CC), a progressive loss in the maintenance of UL CPN gene expression, and reduced complexity of dendritic arborization. Proteomic analysis revealed that Mllt11 associates with stabilized microtubules and motor proteins. Additionally, loss of *Mllt11* resulted in a spectrum of mild behavioral deficits similar to those seen in human cases of ASD as well as mouse models of NDDs, which varied by sex and number of intact copies of the *Mllt11* allele. Taken together, our findings support a role for *Mllt11* in promoting the formation of mature UL CPN morphologies and connectivity in the cerebral cortex.

LIST OF ABBREVIATIONS USED

4-HPR	N-(4-Hydroxyphenyl) Retinamide
A2780	Ovarian Endometrioid Adenocarcinoma
ABP	Actin-Binding Protein
ac-α-tub	Acetylated α-Tubulin
ADHD	Attention-Deficit/Hyperactivity Disorder
Af1q/Mllt11	ALL1 Fused From Chromosome 1q
AKT	A Serine/Threonine Kinase Protein B
ApoER2	Apolipoprotein E Receptor 2
ARP	Actin-Related Protein
ARP2/3	Actin-Related Protein 2/3
ASD	Autism Spectrum Disorder
ATP	Adenosine Triphosphate
BAD	BCL2 Associated Agonist of Cell Death
BCL2	B-Cell Leukemia/Lymphoma 2
BD	Bipolar Disorder
BM	Bone Marrow
BP	Binding Protein
BP/IP	Basal Progenitor/Intermediate Progenitor
C57BL/6	C57 Black 6
CamKII	Ca^{2+}/Calmodulin-Dependent Protein Kinase II
CC	Corpus Callosum
CC3	Cleaved Caspase-3
CD7	T-Cell Antigen Cluster Differentiation 7
CD34	Hematopoietic Progenitor Cell Antigen Cluster Differentiation 34
Cdc42	Cell Division Cycle 42
CDK	Cyclin-Dependent Kinase
cDNA	Copy Deoxyribonucleic Acid
CDP/Cux1	CCAAT-Displacement Protein/Cut-Like Homeobox 1
cKO	Conditional Knockout
CNS	Central Nervous System
Co-IP	Co-Immunoprecipitation
CP	Cortical Plate
CPN	Cortical Projection Neuron
CR	Cajal-Rietzus
Ctip2	Coup-TF-Interacting Protein 2
Ctrl	Control
Ctx	Cortex
Cux2	Cut-Like Homeobox 2

Dab1	Disabled-1
DAPI	2-(4-Amidinophenyl)-1H -Indole-6-Carboxamidine
DCX	Doublecortin
Dem	Food Demonstration
DiI	1,1'-Dioctadecyl-3,3,3'3'-Tetramethylindocarbocyanine Perchlorate
DL	Deep Layer
DMEM	Dulbecco's Modified Eagle Medium
DNA	Deoxyribonucleic Acid
DPP	Days Post-Plating
E#	Embryonic Day #
EC	External Capsule
ECL	Enhanced Chemiluminescence
ECM	Extracellular Matrix
EdU	5-Ethynyl-2′-Deoxyuridine
EFP	Estrogen-Responsive Finger Protein
eGFP	Enhanced Green Fluorescent Protein
ER	Endoplasmic Reticulum
ESC	Embryonic Stem Cell
Ets-1	Erythroblast Transformation Specific 1
FBS	Fetal Bovine Serum
Fezf2	FEZ Family Zinc Finger 2
Flox	Flanked Locus of X-Over P1
Foxp2	Forkhead Box Protein 2
FR	Food Restriction
FVB	Friend Virus B
GFAP	Glial Fibrillary Acidic Protein
GFP	Green Fluorescent Protein
GST	Glutathione Sepharose Transferase
HEK293	Human Embryonic Kidney
HPP	Hours Post-Plating
HRP	Horseradish Peroxidase
IC	Internal Capsule
ICC	Immunocytochemistry
ID	Intellectual Deficiency
IHC	Immunohistochemistry
IN	Inhibitory Interneuron
IP/BP	Intermediate Progenitor/Basal Progenitor
IPTG	Isopropyl β-D-1-Thiogalactopyranoside
IRES	Internal Ribosome Entry Site
ISH	In Situ Hybridization

IZ	Intermediate Zone
JNK	c-Jun N-Terminal Kinase
Ki67	Marker of Proliferation Kiel67
KIF	Kinesin Superfamily Protein
L	Layer
lacZ	β-Galactosidase
LAMP-2A	Lyososomal Associated Membrane Protein 2A
LGE	Lateral Ganglionic Eminence
Lis1	Lissencephaly 1
LoxP	Locus of X-Over P1
MAP	Microtubule-Associated Protein
MAP2	Microtubule-Associated Protein 2
MDA-MB-435-HM	M.D. Anderson Metastatic Breast 435 High Metastatic
MGE	Medial Ganglionic Eminence
Mllt11/Af1q	Myeloid/Lymphoid or Mixed-Lineage Leukemia Translocated to Chromosome 11
MLL	Mixed-Lineage Leukemia
MMP	Matrix Metalloprotease
mRNA	Messenger Ribonucleic Acid
mTOR	Mammalian Target of Rapamycin
Myo5a	Unconventional Myosin Va
Myh9	Non-Muscle Myosin Heavy Chain 9
Myh10	Non-Muscle Myosin Heavy Chain 10
MZ	Marginal Zone
NDD	Neurodevelopmental Disorder
NESC	Neuroepithelial Stem Cell
NeuN	Neuronal Nuclei
NF	Neurofilament
N.S.	Not Significant
NS1	Nonsocial Odor 1
NS2	Nonsocial Odor 2
OCD	Obsessive-Compulsive Disorder
OCT	Optimal Cutting Temperature
OVCAR-3	Ovarian Adenocarcinoma
P#	Postnatal Day #
p53	Tumor Protein 53
p73	Tumor Protein 73
Pax6	Paired Box 6
PCR	Polymerase Chain Reaction
PFA	Paraformaldehyde
PI3K	Phosphatidylinositol-3 Kinase

PBS	Phosphate Buffered Saline
PLAB	Placental Bone Morphogenetic Protein
PSD95	Postsynaptic Density Protein 95
PVDF	Polyvinylidene Fluoride
qPCR	Quantitative Polymerase Chain Reaction
Ras	Rat Sarcoma
REST1	RE1-Silencing Transcription Factor
RFU	Relative Fluorescence Units
RGC	Radial Glial Cell
RGP	Radial Glial Progenitor
RhoC	Ras Homolog Family Member C
RNA	Ribonucleic Acid
RNP	Ribonucleoprotein
RORB	RAR-Related Orphan Receptor Beta
ROS	Reactive Oxygen Species
S1	Social Odor 1 (P30)/Stranger 1 (P37)
S2	Social Odor 2 (P30)/Stranger 2 (P37)
Satb2	Special AT-Rich Sequence-Binding Protein
SDS-PAGE	Sodium Dodecyl-Sulfate Polyacrylamide Gel Electrophoresis
siRNA	Small Interfering Ribonucleic Acid
Sox2	SRY-Box Transcription Factor 2
Sox5	SRY-Box Transcription Factor 5
Spec1	Stronglyocentrotus Purpuratus Ectoderm 1
Str	Striatum
SVZ	Subventricular Zone
Tau	Tubulin-Associated Unit
Tbr1	T-Box Brain Protein 1
Tbr2	T-Box Brain Protein 2
Td	Tandem Dimer
Th	Thalamus
Tom	Tomato
Tuj1/Tubb3	β-Tubulin 3 Class III
UL	Upper Layer
VLDLR	Very Low Density Lipoprotein Receptor
VZ	Ventricular Zone
WCL	Whole Cell Lysate
WM	White Matter
Wnt	Wingless/Integrated

ACKNOWLEDGEMENTS

To my supervisor, Dr. Angelo Iulianella, thank you for your guidance, mentorship, and generous provision of time, resources, and wisdom during my time under your supervision. Thank you for providing me with this once-in-a-lifetime opportunity and giving me a chance to begin a career in science. Your enthusiasm for the pursuit of knowledge is infectious and inspiring.

To the members of my examining committee, Dr. Kazue Semba, Dr. Stefan Krueger, and Dr. James Fawcett, thank you for your invaluable knowledge, feedback, and guidance over the past six years.

To the members of the Iulianella lab, past and present, thank you for sharing this experience with me. To Emily C., thank you for being my first lab mate and showing me the ropes. To Sam, thank you for the wonderful company, endless laughs, and emotional support in the trenches. To Karolynn, thank you for being the most brilliant and capable lab mom; this project would not have been possible without your knowledge and guidance. To Kaitlin, thank you for your company and the atmosphere that your wit and presence brought to the lab. To Mohsen, thank you for being such great company and enriching my days and broadening my horizons with intriguing philosophical discussions. To Marley, thank you for always being a wonderful teammate and companion in the lab, and for sharing in my love and enthusiasm for movies and science. To Dr. Emily Witt, thank you for imparting your knowledge of all things behavior, assisting with my frequent technological difficulties, giving me the opportunity to learn skills in a field outside

of my own, keeping me sane during those *long* days inside of that *tiny* behavior room, and, of course, for your friendship.

To my wonderful partner Erin, who helped and supported me in more ways than I could possibly list here, thank you. None of this would have been possible without your endless love and support.

Finally, thank you to the members of the Department of Medical Neuroscience who came along on this journey with me.

CHAPTER 1. INTRODUCTION

The mammalian neocortex is a complex structure, underlying the capacity for executive function, sensory processing, emotion, motor output, and cognition. It is a laminated structure organized into six molecularly and morphologically distinct layers populated by a heterogeneous collection of excitatory pyramidal cortical projection neurons (CPNs) and inhibitory interneurons (INs). This anatomical organization emerges from the tight regulation of neurogenesis coupled with migration of newborn neurons to their final laminar position, where they acquire distinct molecular identities and morphological traits necessary to form functional circuitry within the brain. A fundamental question concerns how the migration of newborn neurons is controlled in the sequential generation of more superficial cortical layers and their subsequent connectivity patterns. While it is clear that the cytoskeleton plays a key role in neuronal translocation, how it impacts CPN subtype-specific neurite morphogenesis and the maintenance of laminar transcriptional programs is not well understood.

The sorting of differentiating CPN subtypes into discrete, functional layers occurs as cells migrate radially from progenitor domains located along the ventricular zone (VZ) and adjacent subventricular zone (SVZ) along the apicobasal axis to invade the cortical plate (CP). Early in cortical development newly born neurons migrate along radial glial fibres projecting from the basal surface of VZ progenitors to the pia via somal translocation (Miyata et al., 2001).

In both neuronal migration and neurite extension, inherent properties of microtubules dictate the translation of interaction with guidance cues to growth

and steering of nascent projections. Microtubule growth, retraction, and stabilization are controlled by complex signaling events induced by extracellular cues, and the coordination of these events is necessary for appropriate neuronal migration and neurite extension. The ability to couple developmental cues with construction or degradation of microtubule networks underlies the propensity of CPNs to form connections both intracortically and with other brain regions. As such, mutations of tubulin subtypes have been linked to neurodevelopmental disorders (NDDs) that affect cortical formation, stabilization, and projections. Much like tubulin, mutations of microtubule-associated proteins (MAPs), including stabilizing or nucleating proteins, motor proteins, and cargo-specific adapter proteins that govern trafficking of organelles and proteins to specific regions of a neuron, have also been linked with various forms of NDDs (Moffat et al., 2015; Moon & Wynshaw-Boris, 2013).

Although axonal regulatory mechanisms are conserved throughout the cortex, the targeting and wiring of each cortical layer is also dependent upon its unique molecular characteristics. For instance, each cortical layer expresses a unique program of transcription factors that provide the necessary molecular context crucial for synapse formation with the appropriate target regions of the brain (Kumamoto et al., 2013; Toma et al., 2014). This system of transcription factor activation and repression functioning in cross-repressive networks regulates the organized chronological generation of cortical layers and functional diversity of projection neuron subtypes (Toma et al., 2014).

While cortical cell fates are primed by interactions of transcription factors in developing neurons, the expression of these transcriptional programs must be stabilized throughout terminal differentiation. It is known that localization within the cortex can impact acquisition and maintenance of transcriptional programs, but the mechanism remains unclear. Here I report a role for Myeloid/lymphoid or mixed-lineage leukemia; translocated to chromosome 11/All1 Fused Gene From Chromosome 1q (Mllt11/Af1q) in regulating cortical specification and localization within the maturing CP.

Mllt11 was first identified in an infant with acute myelomonocytic leukemia carrying the t(1;11)(q21;q23) translocation that creates a fusion protein consisting of Mllt11 and Mll (Tse et al., 1995b). Mllt11 is a novel vertebrate-specific protein that possesses a nuclear export signal but otherwise has poorly defined functional domains. In addition to an oncogenic function, we previously showed that *Mllt11* is expressed in all post-mitotic neurons during development and is enriched in the developing cortical plate (Yamada et al., 2014). *Mllt11* transcription is down-regulated by RE1 silencing transcription factor (REST), a key factor involved in regulating neural differentiation (Hu et al., 2015), but is up-regulated during neurogenesis (Lin et al., 2004a). However, its role in neural development and differentiation is largely unknown.

Here I report that Mllt11 is a neural-specific tubulin-interacting protein and its conditional inactivation in the superficial layers of the mouse brain results in improper localization and specification of upper layer (UL) neurons, as well as commissural projection defects. Inability to initiate and maintain functional

projections was accompanied by aberrant expression of layer-specific transcriptional programs and localization in the *Mllt11* mutant cortex. Additionally, I show that *Mllt11* loss led to dysplasia of the superficial cortex characterized by a severe abrogation of UL CPN dendritic morphologies resulting from neurite outgrowth defects. Alternatively, *Mllt11* overexpression causes rapid invasion of the cortical plate by differentiating neurons, a process which relies heavily on cytoskeletal architecture of basal processes of radial glial progenitors (RGPs). Mechanistically, I provide evidence that Mllt11 interacts with stabilized microtubules, explaining the phenocopy of *Mllt11* mutants with brain tubulinopathies (Bahi-Buisson et al., 2014). Behaviorally, *Mllt11* mutants exhibit a spectrum of deficits in a sex- and intact copy number-dependent manner, reminiscent of those characteristic of Autism Spectrum Disorder (ASD). Altogether, these findings suggest a role for *Mllt11* in migration of CPNs as well as formation and maintenance of functional connections required for morphological complexity and phenotypic stability of projection neurons.

1.1. The Genetics of Cortical Development: The Cortical De-Repression Circuit

The dorsal telencephalon consists of neuroepithelial stem cells (NESCs) in a pseudostratified layer, which serves as the progenitor pool containing cells fated to multiply mitotically and differentiate into all cell types of the neocortex. These cells express Sox2, a marker of stemness and self-renewal and repressor of differentiation associated genes (Zhang et al., 2020). Beginning at embryonic

day 8-9 (E8-9), the NESCs in this layer, the ventricular zone, undergo mitosis and divide symmetrically to increase the initial pool of precursors before converting to RGPs, which express Pax6 (Götz et al., 1998). Pax6 and Sox2 regulate many common promoters in progenitor cells to coordinately activate proneural genes while repressing other fates in order to restrict the lineage toward neuronal differentiation (Scardigli et al., 2003). Many downstream targets of Pax6 include genetic regulators which further restrict the neuronal lineage, such as Tbr2 (Scardigli et al., 2003) as well as numerous patterning molecules and signaling components (Andrews & Mastick, 2003; Stoykova et al., 1997; Thakurela et al., 2016). As the progenitor pool expands and the neural tube thickens, Pax6+ RGPs divide asymmetrically, giving rise to either an excitatory cortical projection neuron (CPN) or basal or intermediate progenitors (BP/IPs) which populate the subventricular zone (SVZ). These BPs are limited in their potency and ability to divide such that each will produce two neurons through symmetrical division (Gao et al., 2014).

As spatial segregation of apical (VZ) and basal (SVZ) regions of the neural tube increases, different regions become more or less exposed to unique signaling cues as a result of their location. These cells in their varying spatial distribution are made more or less susceptible to environmental cues through expression of such signaling receptors conferred by Pax6 and its downstream targets. As such, RGP morphology, featuring a long, radial process extending to the pial surface, allows for sampling and integration of cues from the full extent of the dorsal telencephalon, including those excreted from the meninges,

developing blood vessels, and those expressed on the surface of or excreted from nascent neurons inhabiting more superficial regions, while more superficial Tbr2+ IPs of the SVZ, are differentially exposed based on their location within the developing pseudostratfication of cells (Taverna et al., 2014; Yuzwa et al., 2016).

Expression of Sox5 at approximately E10 activates expression of *Tbr1*, defining the preplate (Arlotta et al., 2005; Hevner et al., 2001a; Kwan et al., 2008; Lai et al., 2008). This structure consists of a thick layer of cells which will eventually split to give rise to deep layer (DL) 6 and layer (L) 1 (D'Arcangelo et al., 1995a; Ogawa et al., 1995a). This process occurs mechanistically through migration of later born neurons which invade this layer and populate the center, physically splitting the layer in two distinct laminae, guided by the most superficial region of the preplate comprised of Cajal-Rietzus (CR) cells, which secrete guidance molecule Reelin (D'Arcangelo et al., 1995b; Moore & Iulianella, 2021; Ogawa et al., 1995b). As subsequent waves of nascent neurons are born in the VZ and SVZ, they migrate superficially in response to Reelin through differential regulation of Reelin receptors ApoER2 and VLDLR. Through interaction with cytoplasmic adaptor protein Dab1, interaction of Reelin with transmembrane receptors signals downstream effectors to regulate the cytoskeleton, thus activating migration superficially toward the source of Reelin signaling. In the presence of a high concentration of Reelin most superficially in the CP, downregulation of APOER2 results in a braking effect, depositing the newly born neuron just beneath L1 and superficial to Tbr1+ layer, resulting in the splitting of

the preplate into L1 and the subplate, which later becomes DL6 (Figure 1.1., Duit et al., 2010; Hevner et al., 2001b). The earliest born neurons to migrate in this way and facilitate splitting of the preplate are Ctip2+ DL5 CPNs, beginning at approximately E12. Expression of Fezf2 activates Ctip2 in these neurons, in turn repressing the Tbr1+ fate as well as UL fates which have yet to be specified (Figure 1.1., Han et al., 2011; Hirata et al., 2004; McKenna et al., 2011). Expression of Satb2 is initiated in nascent neurons born from the intermediate zone (IZ) fated for L4, which in turn suppresses expression of Ctip2 (Figure 1.1.). Through subsequent coordinate expression of CCAAT-Displacement Protein/Cut-Like Homeobox 1 (CDP/Cux1) and Cux2 along with Satb2, neurons become fated for UL2/3, beginning at E14 and concluding by approximately E18 (Figure 1.1., Alcamo et al., 2008; Franco et al., 2012a; Nieto et al., 2004; Sylvén et al., 1991).

It is known that cortical layer markers exert their effects and carve out diverse subtypes of CPNs through numerous downstream genetic and molecular interactions which act to specify gene transcriptional networks, expression of signaling machinery resulting in ability to respond to environmental cues, regulation of morphology, targeting of projections, and electrical properties through expression of ion channels. As such, expression of each marker correlates to a unique cellular identity, characteristic axonal projection path through which developing neurites contribute to the interconnected networks of white matter (WM) tracts in the central nervous system (CNS), as well as

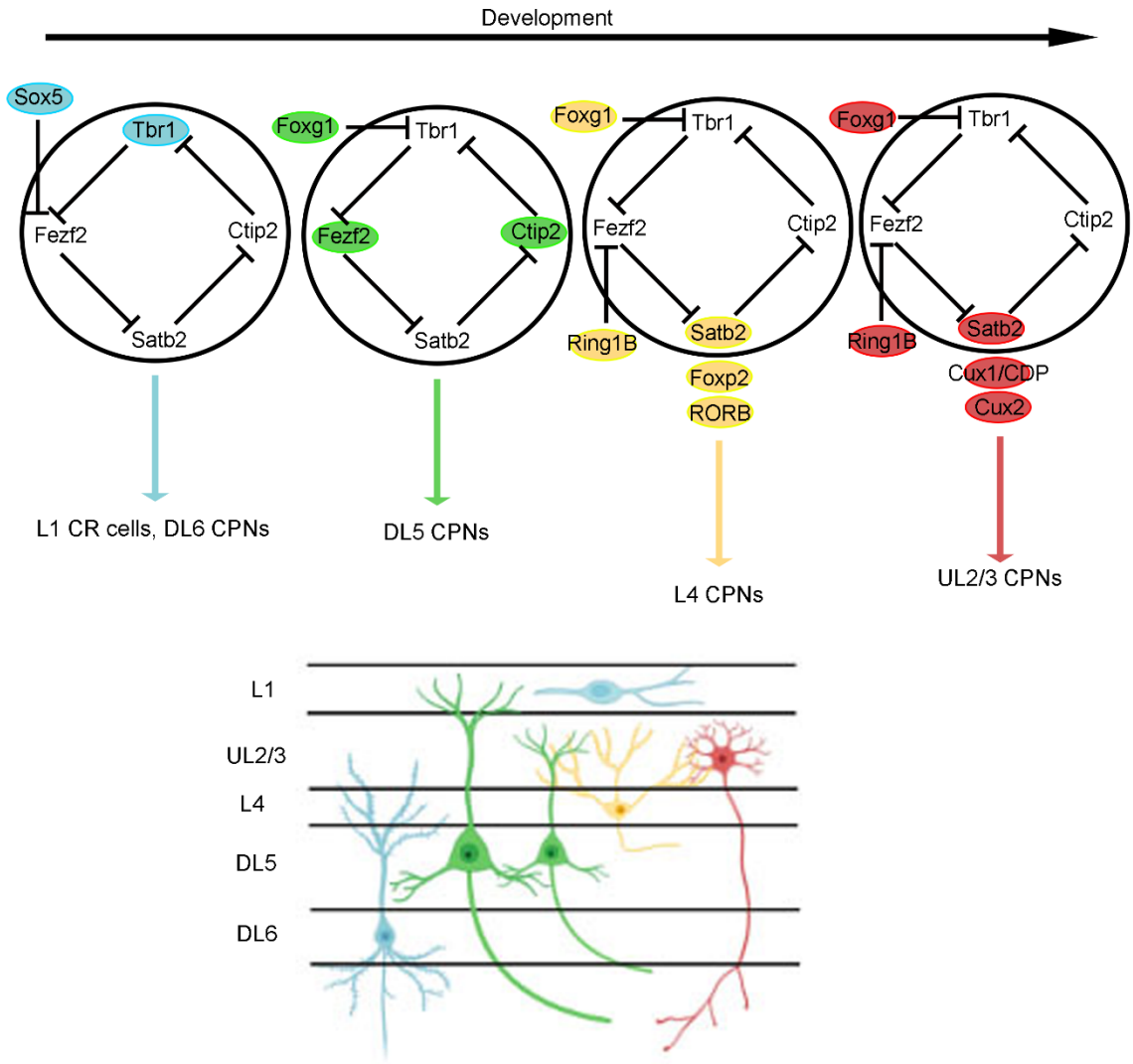

Figure 1.1. Cortical Derepression Loop Specifies CPN Subtypes Destined for Discrete Layers During Cortical Lamination. L, layer; CR, Cajal-Rietzus; DL, deep layer; CPN, cortical projection neuron; UL, upper layer.

stereotypical morphology (Franco et al., 2012b). With the exception of the CR cells of L1, which are born first during corticogenesis and secrete Reelin to guide the radial migration of nascent neurons (Chai et al., 2009; Chai et al., 2016; Frotscher, 1998; Gil-Sanz et al., 2013), this process begins with Tbr1+ neurons which populate DL6 and project to the thalamus (Hevner et al., 2001; Thomson, 2010). Subsequently, the Ctip2+ neurons of DL5 are born, which mostly connect to subcerebral regions (Arlotta et al., 2005). L4 neurons, which receive input from the thalamus, can be identified by their co-expression of Foxp2, RORB, and Satb2 (Figure 1.1., Hisaoka et al., 2010; Leone et al., 2015; Lopez-Bendito and Molnar, 2003, Scala et al., 2019a). The last cortical cell types generated are those of UL2/3 in the superficial cortex, identified by the expression of CDP/Cux1, Cux2 (Figure 1.1., Nieto et al., 2004; Zimmer et al., 2004), and Satb2 (Alcamo et al., 2008; Britanova et al., 2008a; Leone et al., 2015).

Tbr1 initially regulates the identity of CPNs in the preplate, and eventually DL6, via downstream activation by Sox5 (Figure 1.1.). These CPNs typically possess dendrites which receive inputs from UL2/3, and corticofugal axons which primarily project to the thalamus via the corticothalamic tracts of the internal capsule (IC) and external capsule (EC, espo et al., 2022). Loss of *Tbr1* results in improper targeting of projections which become rerouted to the hypothalamus and cerebral peduncles. Additionally, as Tbr1 represses *Ctip2* activation in DL6 neurons, its loss results in an expansion of the Ctip2+ DL5 domain through de-repression of *Ctip2* (Bedogni et al., 2010). Conversely, misexpression of *Tbr1* in cells fated to become UL CPNs results in acquisition of

DL6 fate by UL CPNs, accumulation in deeper cortical layers, and decreased ability to project neurons across the CC and conversely direct their axons subcortically (Crespo et al., 2022).

As *Tbr1* expression becomes repressed by Fezf2, *Ctip2* expression is activated by this de-repression, priming a DL5 CPN fate (Figure 1.1.). Ctip2 acts downstream of Fezf2 to regulate the targeting of subcortical regions such as the hindbrain and spinal cord during axonogenesis, though a small portion of DL5 CPNs also project contralaterally across the midline via the CC (O'Leary & Koester, 1993). These Ctip2+ cells have apical dendrites which extend into L1, though DL5 cells possessing callosal axons have shorter, less arborescent apical dendrites which terminate in UL2/3 (Kasper et al., 1994). Loss of *Ctip2* from the developing cortex results in adoption of UL callosally-projecting neuronal fate, as well as increased expression of Satb2 and expansion of its expression domain into DL5 (Chen et al., 2008a). Much like *Tbr1*, ectopic expression of *Ctip2* or its upstream regulator *Fezf2* in UL CPNs results in subcortical axon targeting reminiscent of DL5 CPNs (Chen et al., 2008b).

Following expression of *Ctip2* and its delineation of DL5 CPNs, Satb2 expression becomes derepressed and in turn represses Ctip2+ DL5 identity in layers 2-4 of the developing cortex (Figure 1.1.). Co-expression of *RORB* with *Satb2* delineates L4, made up of spiny stellate pyramidal cells which possess arborescent, densely spinous dendrites and receive input from the thalamus via the thalamocortical tracts in the IC and EC (Scala et al., 2019a). These cells also possess thin, ramifying axons that mostly project within L4 with some synapsing

on cells in L1 and UL2/3 (Scala et al., 2019b; Weiler et al., 2023a). Co-expression of *CDP/Cux1* and *Cux2* with *Satb2* specifies UL2/3 CPNs (Figure 1.1.). UL2/3 CPNs possess dendrites which receive inputs from L4, and axons which project to UL2/3 and L1 (Cubelos et al., 2010; Y. Liu et al., 2021; Weiler et al., 2023b). Of these cortico-cortical connections, approximately 80% form contralaterally via the CC and 20% occur ipsilaterally to more local regions (Nieto et al., 2004; Zimmer et al., 2004). Loss of *Satb2* from the cerebral cortex results in CC agenesis, as well as upregulation of DL5 marker *Ctip2* and expansion of its expression domain into putative ULs, which project subcerebrally via the corticospinal tract (Britanova et al., 2008b).

Interestingly, ectopic expression of UL markers in DLs following their fate specification does not change the fate of differentiated, postmitotic DL CPNs, suggesting that the cross-repressive regulatory network of genes which sculpt the cortical lamninae becomes fate-restricted in the same inside-out spatiotemporal manner in which they invade the CP, with later born neurons exhibiting more potential to be converted to other cell types than earlier born and specified CPNs. This phenomenon is likely due to increasingly restrictive chromatin landscapes over the course of development (Britanova et al., 2008c; Heavner et al., 2020; Yang et al., 2018).

Forces exerted on the cytoskeleton couple with motor proteins to enable appropriate mechanotransduction to push and pull the nucleus toward the pia until a neuron reaches its terminal location (Bellion et al., 2005; Tsai et al., 2007). This process involves coordination of two distinct events in which the leading

edge of a growing process is guided toward the pia, followed by transport of the microtubules that form the perinuclear cage, a dynamic structure consisting of detyrosinated, nonacetylated tubulin which encases the nucleus, effectively pulling the nucleus in the direction of migration (Umeshima et. al, 2007). As the somas of these cells reach the VZ, previously anchored apical junctional complexes are downregulated, releasing the soma from the VZ, and the trailing apical pole of the cells becomes the nascent axon projecting apically to form WM tracts (Ayala et al., 2007; Marín & Rubenstein, 2003; Nadarajah et al., 2001; Sakakibara et al., 2014). Consequently, the IZ and CP become more densely populated with neurons and projections, and multiple modes of motility must be employed by later-born neurons to overcome the previously deposited neuronal layers. These events also rely on coordinated cytoskeletal reorganization as cells transiently acquire multipolarity to weave through the dense IZ, and then reacquire bipolarity upon invasion of the CP via somal translocation (Sakakibara et al., 2014). The growth of axons during brain formation also involves dynamic cytoskeletal reorganization at the growth cone in response to external guidance cues or cell-cell contacts (Ayala et al., 2007; Hirokawa & Takemura, 2004). The cytoskeletal components involved in axon growth, steering, and development of neuronal morphology will be discussed in the following section.

1.2. The Actin and Microtubule Cytoskeleton and Its Role in Neuronal Development

The cytoskeleton and its interactors play numerous roles in neuronal development as well as functioning and maintenance of mature, differentiated neurons. These functions include structural support, acting as conduits for intracellular trafficking, stabilization of scaffolding complexes required for inter- and intracellular signaling, generation of contractile and motile forces. As such, cytoskeletal dysregulation can manifest in many ways and impact various aspects of cellular morphology and development. The individual components of the cytoskeleton and their role in neural development will be discussed herein.

1.2.1. Actin

There are three isoforms of actin present in human tissue: α, found in muscles, β, found in non-muscle tissue such as neurons, and γ, found in smooth muscle and non-muscle tissues (Dominguez & Holmes, 2011). Actin polymerization occurs spontaneously following hydrolysis of ATP in the presence of monovalent or divalent cations (Kang et al., 2013), however in a cellular context this process is more efficient and exhibits faster dynamics due to the presence of actin-related proteins (ARPs, Muller et al., 2005). Nucleation of actin occurs through two energetically unfavorable steps including dimerization of monomeric globular or free (G-) actin into filamentous (F-) actin and addition of a third subunit to form an unstable and highly dissociative trimer (De La Cruz & Pollard, 1995; Sept & McCammon, 2001). Elongation of the trimer then proceeds from both ends, though the rate of monomer addition to the barbed end is higher

and thus most growth occurs at this end. The opposite pointed ends experience a lower rate of ATP dissociation and therefore undergoes monomer addition at a slower rate, coupled with a higher rate of monomer dissociation, or catastrophe (Fujiwara et al., 2007). The properties of each end of this polarized F-actin structure allow for differential regulation and fine-tuning of dynamics at each end, allowing for a process of coupled growth and catastrophe known as treadmilling, which allows for generation of force when anchored to other cytoskeletal components and motor proteins (Campellone & Welch, 2010; Dominguez & Holmes, 2011; Fujiwara et al., 2007; Lin et al., 1996).

In neurons, a whole host of actin binding proteins interact with actin at each state of nucleation and elongation to increase the efficiency of actin growth. Actin monomer BPs such as Profilin and Formin, bind to barbed ends to enhance growth locally while sterically inhibiting nucleation and elongation from pointed ends (Lu & Pollard, 2001; Mockrin & Korn, 1980). Some actin monomer BPs, such as Thymosin β_4, conversely prevent nucleation and elongation by sequestering actin monomers or competitively binding through motifs shared with actin to prevent polymerization (Pantaloni & Carlier, 1993). Other polymeric actin BPs, such as Gelsolins and Cofilins, aid in actin nucleation and elongation by severing actin polymers to create new nucleation sites, giving rise to multiple actin chains with barbed ends available for nucleation (Ohki et al., 2009; Paredez et al., 2011).

Interaction with actin bps also allows for formation of more complex actin-based structures such as networks and bundles. Branching of growing actin

polymers occurs through binding of the Arp2/3 complex, which allows for nucleation from multiple points along the barbed end (Oma & Harata, 2011). In nervous tissue, Spire and Cordon Bleu bind actin to create a complex which energetically favors branching of actin into short polymers such as dimers or trimers, creating multiple short branches (Campellone & Welch, 2010; Quinlan et al., 2005). Fimbrins, Filamins, and Fascins contain actin binding domains (ABDs) spaced at non-uniform distances to promote actin growth in various directions, giving rise to complex, cross-linked networks. These diverse actin-based structures underlie the intricate cytoskeletal anatomy of the growing tip of the developing axon, responsible for integrating extracellular cues and coordinating strategic motion in response, thus guiding the neurite towards its target, and initiating neuronal migration (Pollard, 2016). This structure is known as the growth cone.

Growth cones consist of several distinct domains, each with unique properties conferred by the presence of particular actin dynamics and structures. The peripheral or P domain is characterized by the presence of protrusions called filopodia, containing thick bundles of filamentous or F-actin. Filopodia extend through concerted cycling of actin and generation of forward motion of these bundles in response to guidance cues (Argiro et al., 1984, 1985; Bray & Chapman, 1985). Microtubules are also interspersed throughout this region, providing points of traction for actin cycling (Yamada et al., 1970, 1971). At these sites, actin, tubulin, and motor protein Myosin II interact to create an actin treadmilling effect, in which coupling of actin polymerization at proximal barbed

ends with propulsion of the growing actin filament along a microtubule by Myosin II, generates force that propels actin bundles forward from pointed ends located at the periphery. Through interaction between these ends and protein complexes in the membrane, forward motion of the filopodia is generated (Diefenbach et al., 2002; Lin et al., 1996; Sayyad et al., 2015).

This cytoskeletal reorganization is coupled with signaling cascades which cause local changes in ion concentrations and mobilization of signaling molecules, making it more or less energetically favorable for this actin cycling to occur, or impeding this process altogether, giving rise to lamellipodia. Lamellipodia are regions between the filopodia, consisting of more diffuse networks of F-actin which cross-link into a complex meshwork, providing a substrate for binding of ABPs which provide structure and stability for filopodia formation and extension (Goldberg & Burmeister, 1986). These regions play a crucial role in steering, as they retract and collapse in response to deterrent chemical signaling, allowing growth to proceed in a more favorable or attractant direction in response to guidance cues such as Wnt signaling, which guides axons across the midline of the dorsal forebrain to form the corpus callosum (Burden, 2000; He et al., 2018; Purro et al., 2008). As intracellular stores of Ca^{2+} are sequestered to one side of the growth cone, activation of CamKII and Calmodulin compete to increase stabilization and polymerization on one side while preferentially reducing growth on the other, resulting in steering toward an attractive cue and/or away from a repulsive cue (Nesler et al., 2016; Xi et al., 2019).

Proximal to the peripheral domain is the transition, or T domain. This region contains F-actin bundles arranged perpendicular to filopodia formation, which serve as anchor points and nucleation sites for filopodia (Dent & Gertler, 2003a). Most proximally is the central, or C-domain, which is characterized by the presence of bundles of stabilized microtubules whose ends diverge from one another as they approach the T-domain, creating a widening at the base of the growth cone. The C domain also contains organelles such as mitochondria which provide ATP to meet local energy needs and aid in actin polymerization, as well as vesicles containing signaling machinery and membrane components, ribonucleoprotein (RNP) granules for local translational control, and cytoskeletal components required for continuous axon growth (Dent & Gertler, 2003b).

1.2.2. Tubulin

Much like actin filaments, microtubules play a crucial role in the structure and function of neurites, both during growth and the maintenance of their stability. Microtubules are tube-like structures consisting of tubulin protofilaments arranged into a tube. These protofilaments consist of various isoforms of α- and β-tubulin, which form heterodimers which make up the building blocks of protofilaments. The human genome contains 9 genes for α- and β-tubulin isoforms, which are differentially expressed across cell and tissue types. This genetically encoded diversity among tubulin subunits confers structural consequence through unique molecular moieties that allow for specific interactions and addition of regulatory post-translational modifications. Structural diversity facilitates fine-tuning of microtubule construction and regulation in cell or

tissue-specific contexts, while more highly conserved domains allow for more generalized, large-scale regulation.

The contexts in which tubulin isotypes and post-translational modifications are structurally necessary reflects the heterogeneous expression profiles of tubulin subunits across and within cell types and cellular compartments. In the growth cone, for instance, tyrosination of tubulin subunits governs the dynamic mode of rapid polymerization and depolymerization responsible for growth and steering (Brown et al., 1993; Marcos et al., 2009). Phosphorylation precludes incorporation of tubulin subunits into microtubules and strengthens their interaction with membranes to form scaffolding complexes within growth cones and nerve terminals (Hargreaves et al., n.d.; Ramkumar et al., 2018). In contrast, polyamination has a stabilizing effect on microtubules by preventing depolymerization (Hargreaves et al., n.d.). Similarly, acetylation of α-tubulin subunits confers stability and structural integrity by protecting against breakage in projections in the longest-lived axons of mature neurons which are subject to mechanical stress (Ahmad et al., 1993; LeDizet & Piperno, 1987; Song et al., 2013). Trafficking of organelles, vesicles containing pre-synaptic machinery, and cytoskeletal components themselves are also crucial for growth, development, and maintenance of projections, and this can only occur through interaction of motor proteins and microtubules composed of subunits with specific modifications making these reactions energetically favorable (Cai et al., 2009; Even et al., 2019; Monroy et al., 2018).

For instance, mutation of α-tubulin isoforms cause lissencephaly and other gyrification defects, as well as reduction in white matter resulting in abnormalities of the CC and IC Bahi-Buisson et al., 2008; Jansen et al., 2011; Keays et al., 2007; Kumar et al., 2010; Poirier et al., 2007; Tian et al., 2010). β-tubulin mutations have been linked with cortical dysplasia, epilepsy, decreased neuronal density, enlarged ventricles, WM thinning, and defects in migration and radial glial fibre extension due to their role in axonal growth, guidance, and cell cycle-dependent proliferation (Breuss et al., 2012; Breuss et al., 2017; Cushion et al., 2014; Ejaz et al., 2017; Hersheson et al., 2013; Jaglin et al., 2009; Jamuar et al., 2014; Ngo et al., 2014; Poirier et al., 2010; Rodan et al., 2017; Tischfield et al., 2010; Whitman et al., 2016). Mutation of γ-tubulin has also been shown to cause a wide range of phenotypes common to other tubulin isoforms due to its role in stabilizing growth and nucleation of microtubules (Brock et al., 2018; Draberova et al., 2017; Ivanova et al., 2019; Poirier et al., 2013; Yuba-Kubo et al., 2005).

Much like tubulin, mutations of microtubule-associated proteins (MAPs) including stabilizing or nucleating proteins, motor proteins, and cargo-specific adapter proteins that govern trafficking of organelles and proteins to specific regions of a neuron, have also been linked with various forms of NDDs (Moffat et al., 2015; Moon and Wynshaw-Boris, 2013). Mutations of these proteins can also affect neuronal development at the level of mitosis, axon guidance, disturbance of fasciculation of axonal tracts, or impaired migration. Doublecortin (DCX), for instance, is a MAP which binds to microtubules to promote polymerization and formation of the perinuclear cage. Mutations to DCX as well as mutations to

Lissencephaly 1 (Lis1), an adaptor which links dynein to microtubules during transport, impair the process of nucleokinesis and somal translocation, affecting the ability of neurons to migrate within the cortex, resulting in lissencephaly, cortical heterotopias, cognitive and language deficits in humans, and abnormal electrical activity in the brain causing seizures (Adam, 2007; Bodakuntla et al., 2019a). Some MAPs possess both microtubule- and actin-binding domains, implicating them in growth cone filopodial interactions as well as dendritic spine development. Microtubule stabilizing proteins Tau and MAP2 are two examples of such proteins, with Tau being specific to axons and MAP2 initially expressed in all developing neurites but later segregated to dendrites (Bodakuntla et al., 2019b). This pre-axonal filtering of compartment-specific MAPs is mediated by another MAP family known as KIFs, which act as cargo adaptor proteins bound to microtubules during axonal and dendritic transport, precluding cargo from entering the incorrect cellular compartment (Gumy et al., 2017a). Mutations to Tau, the MAP family, or KIFs can result in hypo- or hyper-stabilized microtubules, causing reduced or improper trafficking of vesicles and organelles along microtubules of axons and dendrites, altered axonodendritic morphology, neurite function, and overall neurological function in the form of ataxia, tremors, and degenerative diseases (Goedert, 2005; Gumy et al., 2017b; Liu et al., 2015).

Within the context of neuronal development, migration, and neurite extension, motor proteins play a particularly important role in tandem with the cytoskeletal components with which they interact. Dynein, Kinesin, and Myosins are examples of such proteins. The regulation of cargo trafficking along

microtubules by Kinesin and Dynein motor proteins ensure delivery of intracellular cargo to the appropriate target. While Dyneins move in a plus-to-minus direction, generating forces to propel microtubules away from the soma toward the axon terminal, Kinesins traverse microtubules in a minus-to-plus direction, allowing them to utilize microtubules as a highway to carry cargo throughout the extent of the axon (Barlan et al., 2013; Bhabha et al., 2016; Hirokawa et al., 2009; Semenova et al., 2014). Though Myosins are typically thought of as actin-specfic molecular motors, some Myosins also interact with microtubules, such as Myosin Va, which binds both actin and microtubules, allowing it to cross-link and couple microtubules to actin filaments, making it ideal for short-range vesicle transport of cargo delivered from microtubules of the distal axon into the growth cone, (Cao et al., 2004; Langford, 2002; Rogers et al., 1999; Rogers & Gelfand, 1998). Mutation of Myosin Va results in severe seizures and death (Bridgman, 1999). Mutations and aberrant localization of neurofilaments mediated by microtubule-based transport via molecular motors have also been linked with schizophrenia, bipolar disorder (BD), and ASD (Clark et al., 2007; English et al., 2009; Kristiansen et al., 2006; Pennington et al., 2008; Sivagnanasundaram et al., 2007; Yao et al., 2021).

Many of these common cortical morphologies and cytoarchitectural features indicative of dysregulation of cytoskeletal architecture are shared among autistic individuals. The growth of neurites and synapse formation are facilitated by a dynamic network of microtubules, actin, intermediate filaments, and associated proteins that provide support for axonal and dendritic structures. A

common thread between all mutations of tubulin isotypes and associated proteins is their propensity to give rise to phenotypes commonly associated with NDDs through migration, cell fate specification, and axonal regulatory mechanisms required for functional connectivity within the cortex and between the cortex and other regions. Mutations in microtubules and MAPs have been associated with tubulinopathies, a group of related disorders classified as NDDs. Some individuals with tubulinopathies exhibit both physical and behavioral characteristics similar to and overlapping with those seen in NDDs like ASD. ASD will be discussed further in the subsequent section.

1.3. Neurodevelopmental Disorder: Mutations Affecting Morphology, Connectivity, and Function Underlie ASD

The development of the cerebral cortex depends on the synchronization of molecular processes allowing cells segregated to distinct brain regions to create functional connections by projecting to each other in the proper spatiotemporal manner. This is a highly complex process requiring careful coordination of genetic regulation and protein interactions on a subcellular level. These subcellular events change the internal landscape of the cell in such a manner that informs overall cell morphology and therefore the connectivity between cells. Due to the complexity of this process, there are innumerable opportunities for variable outcomes. Some of this variability is mostly benign and can be compensated for or overcome, resulting in little-to-no impact on overall brain function. Other times, mutations can occur which change the structure and

function of a protein to the extent that cognitive, sensory, motor, emotional, and outward behavioral experiences are altered substantially. Events such as these which occur during neural development are categorized as NDDs, one such example being ASD.

ASD is characterized by core behavioral symptoms, including repetitive or restricted behaviors, interests, and social deficits. Often accompanying these core symptoms are language deficits, intellectual disability, higher than average rates of epilepsy, anxiety, obsessive compulsive disorder (OCD), Attention Deficit Hyperactivity Disorder (ADHD), and a reduced threshold for distress or emotional disturbance when faced with environmental changes (Al-Beltagi, 2021; Hodges et al., 2020; Meier et al., 2015). Symptoms typically begin to present early in childhood, though levels of severity vary, and it is not uncommon for some individuals to be diagnosed later in life due to the ability to compensate, or camouflage stereotypical ASD-related behaviors (McQuaid et al., 2022a).

One such factor that plays a role in ease of diagnosis is differences in behavioral manifestations of the disorder across sexes and gender identities (Giarelli et al., 2010). Such variation has been studied in depth, and males have been shown to display external symptoms which are more readily apparent and easily diagnosable, while it is more common for females to present symptoms with more subtlety, which are less outwardly apparent and more internally focused. For instance, autistic males tend to be diagnosed at a much higher rate, and have a higher prevalence of repetitive or restricted behaviors and reduced sociability. Females on the other hand, tend to display communication difficulties

and anxiety, but exhibit reduced instances of outwardly visible social deficits (Begeer et al., 2013; McQuaid et al., 2022b). This begs the question of whether there are differences across sexes in behavioral manifestations strictly due to the impact of the mutations that underlie the disease, whether societal norms and expectations imposed across sexes and gender identities impact the development of such behaviors differentially, or a combination of the two, a topic which is still under active investigation (Baron-Cohen et al., 2011; Begeer et al., 2013; Giarelli et al., 2010; McQuaid et al., 2022b).

Despite such differences in manifestation of symptoms and diagnoses across sexes, there are shared features between the manifestation of the various mutations that give rise to ASD behavioral phenotypes, such as their contribution to abnormal neural connectivity and activity. Therefore, a more holistic approach to understanding the disorder has emerged, which seeks to combine mutation models with synaptic and connectivity deficit models, thus creating a more well-rounded understanding of the underlying mechanisms, as well as precisely how they contribute to the specific cognitive and sensory experiences characteristic of ASD. This approach focuses on the developmental emergence of altered connectivity between brain regions and coupling this with behavioral analyses to gain insight into the specific behavioral impact of various mechanistic components. Such dysfunctions include synaptogenesis, vesicle trafficking, signaling, and neuritogenesis. Each of these factors are highly interconnected and contribute to the functional disconnect seen in ASD (Belmonte et al., 2004; Brock et al., 2002; Geschwind & Levitt, 2007).

As such, one common characteristic of the different mutations that cause ASD-related behaviors is their role in disrupting normal neural connectivity and activity through mutations at the genetic level which impact the morphology and function of these circuits. Numerous genetic determinants and effectors of ASD development have been identified, many of which act concurrently and coordinately with multiple and often overlapping functions in a convoluted way that makes it difficult to parse out the roles of individual causal genes. This is consistent with the diverse range of symptoms of ASD which present across a spectrum of behavioral outcomes, cognitive capabilities, and sensory experiences that all feed into each other through altered cortical networks.

Over 234 individual loci have been flagged as potential contributors to ASD through exome sequencing, and the majority of cases lack any known underlying mutation (Parikshak et al., 2016; Sanders et al., 2011). Consistent trends among known causal mutations have provided some insight into the nature of the disorder. It is known that ASD-associated mutations are often protein-disrupting de novo mutations. Given that behavioral symptoms of ASD typically manifest before age 3, a critical time point for synapse formation, it is unsurprising that many such mutations occur in genes that affect synaptogenesis as well as synaptic transmission (Gilman et al., 2011; Hlushchenko et al., 2018; Li et al., 2014). These implicated genes include *Neurexins*, *Neuroligins*, *Cadherins*, *Contactins*, *Shanks*, *Integrins*, and *Reelin* (Abrahams & Geschwind, 2008; Buxbaum, 2009; Lintas & Persico, 2009; Südhof, 2008; Wang et al., 2009). Other identified mutations also affect developmentally relevant events that

precede synaptogenesis and maturation, such as transcription of signaling components and machinery, posttranslational modification of these signaling receptors which are crucial in guiding neuronal migration and differentiation in response to external cues, as well as ion channels that allow the cell to respond to these cascades (Bassell & Warren, 2008; Benayed et al., 2005; Bucan et al., 2009; Hashimoto et al., 2006; Kelleher & Bear, 2008; Levitt & Campbell, 2009; Nishimura et al., 2007; Sadakata et al., 2007). Further complicating our ability to parse individual causal genes is the fact that genes whose protein products act in cascades upstream of other identified ASD-related loci have also been implicated. One such well-studied example is mTOR, which plays roles in various neurodevelopmental processes including neuronal differentiation, axonogenesis and steering, neuronal migration, large scale patterning of cortical regions, and synaptic protein synthesis, maturation, and pruning, in addition to its broadly-sweeping regulatory roles in metabolism and regulation of the cell cycle (Fingar et al., 2004; Saxton & Sabatini, 2017; Thomas et al., 2023).

From a morphological perspective, these mutations commonly result in alterations at the level of the cortex. Much like every other aspect of this disorder, morphological features also present across a broad spectrum with a high degree of variability, but differences in cortical thickness in various regions have been documented in many studies (Shen et al., 2022; Yang et al., 2016). Alterations in WM thickness, specifically within the CC and subcortical WM tracts, have also been reported, and in some cases were shown to correlate with severity of certain sensory modalities (Hong et al., 2019; Ohta et al., 2020). Additionally, at

the cytoarchitectural level, in some studies utilizing postmortem brains from autistic humans as well as mouse models of common genetic mutations linked to ASD, loss of layer-specific morphology and genetic identity has been reported (Casanova et al., 2013; Stoner et al., 2014; Fujimoto et al., 2021).

Though many events and processes underlying the proper formation of the cortex are well-understood, our understanding of the regulation of these events is lacking. Identification of genes expressed during cortical development as well as those misregulated in disorders where the cortex exhibits altered morphogenesis or genetic regulation have shed light on underlying mechanistic processes crucial to proper development. Additionally, due to the variability in phenotypes seen across ASD mutant models as well as the diverse symptomology with which autistic individuals present, there is a need for genetic models that provide insight into direct mechanisms underlying the spectrum of pathologies and behaviors unique to ASD and to elucidate how each gene contributes individually and within its functional network. One such gene which has been identified as a potential ASD-linked gene is *Mllt11*, an oncogene implicated in neuronal development, which will be discussed in the following section.

1.4. Review of Mllt11

Myeloid/lymphoid or mixed lineage leukemia translocated to chromosome 11 (Mllt11) was first identified through a translocation event implicated in leukemia (Li et al., 2003; So et al., 2000a; Watanabe et al., 2003) and its

presence in immature hematopoietic cells (So et al., 2000b). Expression levels of *Mllt11* in various diseases also implicated its significance in disease progression. Elevated expression of *Mllt11* was identified as an independent adverse prognostic factor in pediatric acute myeloid leukemia, as its expression level increased from 0- to 154-fold compared to normal expression levels in marrow cells and correlated positively with a decreased survival rate and increased severity of the disease progression (Tse et al., 2004). *Mllt11* was also identified as a poor prognostic marker for adult acute myeloid leukemia (Gregory et al., 2009; Strunk et al., 2009a) potentially through a consequently increased incidence of tyrosine kinase 3 internal tandem duplication (Strunk et al., 2009b). Increased levels of *Mllt11* expression were also found in cases of high-risk myelodysplastic syndrome, albeit lower than in leukemia, but were still significantly increased compared to low and intermediate-risk groups (Tse et al., 2005).

As awareness of its role in tumorogenesis increased and it emerged and gained notoriety as an oncogene, elevated expression of *Mllt11* was identified in other diseases. One analysis of transcriptional signatures of thyroid oncocytic tumours revealed overexpression of *Mllt11* in 56% of cases (Jacques et al., 2005). Testicular germ cell tumors also displayed increased expression of *Mllt11* (Skotheim et al., 2006). Additionally, *Mllt11* transcript levels were found to be increased in mammary tissue following exposure of environmental toxin benzo(a)pyrene, a known carcinogen (Keshava et al., 2005).

Investigation of its protein structure by Tse and colleagues revealed a 90 amino acid protein product which shared structural features with cytokines (Tse et al., 1995a). Among these are the presence of RNA-destabilizing consensus sequences at the untranslated 3' end, and the presence of an AT hook in the N-terminal domain, a DNA binding motif characteristic of proteins such as high-mobility group family members which function in DNA-dependent regulatory processes (Reeves & Beckerbauer, 2001; Tse et al., 1995c). This motif is commonly associated with methyltransferase activity specifically. The localization of transcription also resembled cytokine activity closely in that it is mainly restricted in normal tissues but exhibits abnormal expression in tumor cells (Busson-Le Coniat et al., 1999a).

Subsequent exploration of *Mllt11*'s structure and role in the genetic landscape continued to reveal a role in abnormal and cancerous cell development. In leukemia, a translocation event was identified in which *Mll* translocates to chromosome 11 to form a fusion partner with *Mllt11* to promote a tumorogenic fate (Busson-Le Coniat et al., 1999b). Additionally, a hallmark feature of non-hodgkin lymphoma is duplication or alterations to chromosome 1, and more specifically loci in proximity to and including *Mllt11* (Lestou et al., 2003a), implying that its location in the genome may have effects on disease progression distinct from mechanistic roles of its protein product.

Continued exploration of the role of *Mllt11* revealed the nuance of its mechanistic role in cancer progression. Expression of *Mllt11* in HEK293 cells induced expression of Tuj1/Tubb3, a neuronally-restricted β- tubulin isoform, and

formation of neurite-like projections in a small percentage of transfected cells (Lin et al., 2004b). Although the significance of this finding was controversial due to the tendency of HEK293 cells to spontaneously extend projections in this manner, it hinted at a potential mechanism for Mllt11 in projection of processes, a feature shared between tumorogenic and metastatic activity, and neuritogenesis. This was further corroborated by an analysis of the gene expression profile of an isogenic tumor metastasis model, which revealed that *Mllt11* exhibits high levels of endogenous expression in MDA-MB-435-HM breast cancer cells. Stable transfection of *Mllt11* increased the invasive and metastatic potential of this line, which correlated strongly with upregulation of *Ets-1* and *RhoC*. *Ets-1* expression activates promoters of MMP genes and is correlated with tumor progression, and RhoC, a member of the Ras superfamily of small GTPases regulates cell motility and invasivity. Unsurprisingly, subsequently increased MMP secretion into the ECM, and increased invasivity were found through these mechanisms in response to increased *Mllt11* transcript levels (Li et al., 2006). Consistent with this finding, integrin α3 was also found to be upregulated following *Mllt11* overexpression in breast cancer tissue. A3 acts as an adhesion receptor for extracellular matrix (ECM) proteins and its expression correlates with invasivity of tumors, likely through its ability to adhere to and form an anchor point through ECM interactions. Estrogen-responsive finger protein (EFP) also exhibited protein expression levels that correlated with overexpression or knockdown of *Mllt11*. High levels of *EFP*, an estrogen receptor target gene, are correlated with cancer development, mediated by subsequent downregulation of 14-3-38, a p53-

inducible protein that sequesters mitotic cyclin-dependent kinases (CDKs) to inhibit cell cycle progression, and is conversely involved in dysregulated cell cycle progression exhibited by cancer cells when CDKs are aberrantly released into the nucleus to promote mitosis (Chang et al., 2008).

Further insight into the role of Mllt11 in cancer progression was found through its interaction with cellular components in response to cancer treatment. Doxirubicin, a cancer drug which functions by blocking Topoisomerase 2 to interfere with release of DNA supercoiling, was found to have an increased impact on induction of apoptosis in resistant lines when *Mllt11* expression was artificially knocked down. Exogenous expression of *Mllt11* in A431 cells led to upregulation of BAD, a pro-apoptotic BCL-2 family protein. Targeting of *BAD* directly through siRNA mitigated the effect of *Mllt11* suggesting that *BAD* functions downstream of *Mllt11* activation, despite lack of any evidence for direct protein interaction. Lack of protein interaction coupled with the fact that transcriptional inhibitor actinomycin D suppressed Mllt11-mediated upregulation of *BAD* suggests that this regulatory interaction is likely occurring at the transcriptional level (Co et al., 2008). Mllt11 similarly plays a role in mediation of apoptosis in ovarian cancer cell lines treated with 4-HPR, a synthetic retinoid with antitumor and chemopreventive qualities (Tiberio et al., 2012). 4-HPR functions through generation of reactive oxygen species (ROS) which set off a signaling cascade of endoplasmic reticulum (ER) stress events culminating in JNK activation and induction of proapoptotic protein PLAB. Overexpression of *Mllt11* in A2780 ovarian cancer cells treated with 4-HPR exhibited increased apoptosis

compared to those expressing endogenous levels of *Mllt11*. Similarly, OVCAR-3 ovarian cancer cells, which naturally lack endogenous *Mllt11* expression, exhibit resistance to 4-HPR, became susceptible to its apoptotic effects when overexpressing *Mllt11* (Tiberio et al., 2012). As *Mllt11* has been identified as a retinoic acid target gene, it is likely that it interacts with the apoptotic pathway and mediates the effects of 4-HPR through retinoid signaling (Liu et al., 2005).

Though much remains unknown about the exact function and mechanism of this gene in tumorogenesis, there is much evidence through structural and functional analyses of its roles in other signaling pathways involved in cancer progression. Formation of a temporary MLLT11-TRIL complex increased each of their individual binding affinity to AKT, leading to its phosphorylation and inducing downstream signaling through the PI3K/AKT/mTOR signaling pathway (Hu et al., 2017; Liao et al., 2022). Through interaction with the Wnt signaling pathway, Mllt11 was found to enrich a stem-cell like population and enhance mammosphere formation of breast cells. Wnt signaling inhibitor Quercetin mitigated this effect of Mllt11-mediated Wnt signaling activation (Tse et al., 2017). The relation between *Mllt11* expression and Cdc42 signaling is evidenced by mutual regulation of Mllt11 and SPECs, small Cdc42 signaling molecules, through a shared promoter region. The *SPEC1* locus is aligned head to head with *Mllt11*, sharing the same promoter region, but are regulated uncoordinatedly and not active at the same time (Pirone et al., 2001). Wnt, Cdc42, and AKT signaling pathways are involved in cell cycle control and progression of mitosis,

which is commonly hijacked in development of cancer, providing insight into the mechanism through which *Mllt11* exerts its tumorogenic effects.

More recently, additional non-tumorogenic roles for *Mllt11* have been identified. Through analysis of subcellular localization and intracellular trafficking of Mllt11, it has been found that Mllt11 is exported from the nucleus followed by ubiquitin-mediated degradation at the centrosome (Li et al., 2014a; Parcelier et al., 2011a). This process is mediated by interactions between the KFERQ-like motif of Mllt11 and Hspa8 and LAMP-2A, two components of chaperone-mediated autophagy (Li et al., 2014b). One possible consequence of this regulation through degradation is to preferentially promote certain cell fates over others in development. Mllt11 has been implicated in regulation of prothymocytes by interacting with the Notch signaling pathway. Overexpression of *Mllt11* results in emergence of BM CD34+CD7+ prothymocytes which populate the developing thymus and accelerate the development of the T-cell fate lineage in the thymus, while silencing of *Mllt11* mimicking its endogenous degradation (Parcelier et al., 2011b).

Most relevant to the topics addressed herein, is the role for *Mllt11* in neural development. A study conducted by the Iulianella lab was the first to identify *Mllt11* expression in healthy, developing neural tissue, as well as its differential expression in maturing neurons during development (Yamada et al., 2014). Within the cortex, it is specifically highly expressed in maturing, migrating, post-mitotic neurons populating the developing cortical plate, while it exhibits little to no expression in progenitor pools constituting the ventricular and

subventricular zones at early developmental time points when these areas are densely populated with proliferating cells (Yamada et al., 2014). Investigation of the role of *Mllt11* in the developing cortex was first prompted as it was identified in several screens for novel neurogenic determinants of NDDs, such as ASD (Drozd et al., 2019; Xu et al., 2016), making it a potentially useful gene for modeling NDDs and enhancing our understanding of the genetic networks that underlie proper cortical development.

1.5. Hypothesis and Research Aims

Given that neural development requires the coordination of neuronal migration with the establishment of neuronal connections, characterizing novel regulators of these processes is essential to refine our knowledge of how brain networks are set up. The information stated herein suggests that *Mllt11* plays a regulatory role in the development of the cerebral cortex, and I therefore hypothesized that mutation of *Mllt11* contributes to morphological, pathological, and behavioral features associated with NDDs such as ASD. Moreover, as these processes may be altered in human NDDs like ASD, ID, and schizophrenia, identifying novel regulators of cortical development will shed light on possible molecular pathological mechanisms contributing to these congenital issues. To that end, the present thesis aims to address this question by characterizing the morphological, genetic, and behavioral phenotypes of the *Mllt11* mutant mouse. In doing so, this work aims to shed light on the regulatory roles of *Mllt11* in neurite outgrowth, maintenance of cortical layer-specific cell fate, neuronal

migration, as well as a variety of social behaviors that may be dysregulated in ASD.

CHAPTER 2. Materials and Methods

2.1. Generation of Experimental Animals

All animal experiments were done according to approved protocols (21-002, 21-003, 21-014, 22-038) from the IACUC at Dalhousie University. Mice (*Mus musculus*) carrying a null mutation in the *Mllt11* gene were generated using embryonic stem (ES) cell clones obtained from the mouse knock-out consortium project (UCDavis KOMP repository, *Mllt11tm1a(KOMP)Mbp*). The targeting construct is a “knock-out first, conditional second” approach, which inserts the gene encoding β-*galactosidase* (β-*gal*) into exon 2, the protein-coding sequence of the *Mllt11* gene. Two independently targeted clones were injected into blastocysts, and the resulting chimeras were mated to C57BL/6 females to achieve germ-line transmission. Offspring were genotyped by PCR using the following primers: wild-type forward (F) 5′-CGGTCCTGCCTTTGATTCTCAGC-3′ and reverse (R) 5′-GCCTACTGCACAAGGTTCTTCTTGG-3′ (expected product size: 379 bp), Mutant F 5′-GAGATGGCGCAACGCAATTAATG-3′ and R 5′-AAGCAGTATTTGCTTACTGGCCTGG-3′ (expected product size: 274 bp). Heterozygotes (*Mllt11tm1a(KOMP)Mbp/*+) were maintained on a C57BL/6 background and crossed with *FlpO*+/− (*B6.Cg-Tg(Pgk1-flpo)10Sykr/J*, 011065, The Jackson Laboratory) mice and converted to a conditional allele via germ line Flp recombinase expression. Resulting $Mllt11^{Flox/Flox}$ offspring were crossed with *Ai9* $Rosa26^{TdTomato}$ (B6.Cg-*Gt(ROSA)26Sortm9(CAG-tdTomato)Hze*/J, 007909, The Jackson Laboratory) reporter line to generate $Mllt11^{Flox/Flox}$; $Rosa26^{TdTomato+/-}$ or $Mllt11^{Flox/Flox}$; $Rosa26^{TdTomato+/+}$ offspring.

Cux2^{IREScre} mice used in this study to delete *Mllt11* in developing UL neurons were previously described (Gil-Sanz et al., 2015; Yamada et al., 2015) *Cux2*$^{IREScre+/-}$ mice (*B6(Cg)-Cux2<tm1.1(cre)Mull>/Mmmh*, Mutant Mouse Resource and Research Center). For all experiments other than DiI tracing, these mice were crossed with *Ai9* (B6.Cg-*Gt(ROSA)26Sortm9(CAG-tdTomato)Hze*/J, 007909, The Jackson Laboratory) mice. The resulting *Cux2*$^{IREScre+/-}$;*Rosa26*$^{TdTomato+/-}$ or *Cux2*$^{IREScre+/-}$;*Rosa26*$^{TdTomato+/+}$ offspring were crossed with the *Mllt11*$^{Flox/Flox}$; *Rosa26*$^{TdTomato+/+}$ line to conditionally knock out *Mllt11* and create *Mllt11* conditional knockout (cKO) mutants. Offspring of these crosses were genotyped using the following primers: wild-type F 5′-CGGTCCTGCCTTTGATTCTCAGC-3′ and R 5′-GCCTACTGCACAAGGTTCTTCTTGG-3′ (expected product size: 379 bp), Post Flp/Cre F 5′-CGGTCCTGCCTTTGATTCTCAGC-3′ and R 5′AAGCAGTATTTGCTTACTGGCCTGG-3′, and Cre F 5′-GTTATAAGCAATCCCCAGAAATG-3′ and R 5′-GGCAGTAAAAACTATCCAGCAA-3′. We genotyped for the presence of *TdTomato* using primers F 5′-TACGGCATGGACGAGCTGTACAAGTAA-3′ and R 5′-CAGGCGAGCAGCCAAGGAAA-3′ (expected product size: 500 bp) and allelism was determined with primers F 5′-TCAATGGGCGGGGGTCGTT-3′, R 5′-TTCTGGGAGTTCTCTGCTGCC-3′, and R 5′-CGAGGCGGATCACAAGCAATA-3′ (expected product size: 250 pb for wild-type and 300 bp for mutant). Similar numbers of C*ux2*$^{IREScre+/-}$;*Rosa26*$^{TdTomato+/-}$ or *Cux2*$^{IREScre+/-}$;*Rosa26*$^{TdTomato+/+}$ (control) and

Cux2$^{IREScre+/-}$;*Mllt11*$^{Flox/Flox}$;*Rosa26*$^{TdTomato+/+}$ or *Cux2*$^{IREScre+/-}$;*Mllt11*$^{Flox/Flox}$;*Rosa26*$^{TdTomato+/-}$ (cKO) male and female mouse embryos and neonates were used in the analysis (Moore, 2021). No sex differences in *Mllt11* cKO mutant phenotype were observed in histological pilot studies. Statistical analysis (see below) was conducted on combined numbers of male and female offspring for all histological studies, and behavioral analyses were conducted separately for males and females.

For behavioral experiments, sexes were segregated for analyses and testing. Littermates of all genotypes were tested, and grouped for analysis as follows:

1. Mllt11$^{Flox/Flox}$ or Mllt11$^{Flox/+}$ controls: *Mllt11*$^{Flox/Flox}$;*Rosa26*$^{TdTomato+/+}$, *Mllt11*$^{Flox/Flox}$;*Rosa26*$^{TdTomato+/-}$, *Mllt11*$^{Flox/+}$;*Rosa26*$^{TdTomato+/+}$, or *Mllt11*$^{Flox/+}$; *Rosa26*$^{TdTomato+/-}$.
2. Mllt11$^{Flox/+;Cre}$ controls: *Cux2*$^{IREScre+/-}$;*Mllt11*$^{Flox/+}$; *Rosa26*$^{TdTomato+/-}$, or *Cux2*$^{IREScre+/-}$;*Mllt11*$^{Flox/+}$; *Rosa26*$^{TdTomato+/-}$.
3. 3) Mllt11 cKOs: *Cux2*$^{IREScre+/-}$;*Mllt11*$^{Flox/Flox}$; *Rosa26*$^{TdTomato+/-}$, or *Cux2*$^{IREScre+/-}$;*Mllt11*$^{Flox/Flox}$; *Rosa26*$^{TdTomato+/+}$.

2.2. qPCR

To confirm the loss of *Mllt11* transcripts, RNA was extracted from cortices of three genotypic conditional knock-outs (cKOs) and four controls on embryonic day (E) 18.5 using the RNeasy Micro kit (QIAGEN). RNA was reverse transcribed to cDNA using the SuperScript II Reverse Transcriptase kit (Invitrogen). qPCRs were conducted using the SensiFAST SYBR No-ROX kit

(Bioline) with the following primers for Mllt11 and internal control GAPDH: Mllt11 F 5′-GAACTGGATCTGTCGGAGCT-3′ and R 5′-GCGCTCTCCAGAAGTTGAAG-3′, GAPDH F 5′-ACCACAGTCCATGCCATCAC-3′ and R 5′-TCCACCACCCTGTTGCTGTA-3′ (Weng et al., 2014) Reactions were performed in triplicates.

2.3. Histology

2.3.1. Dissection and Tissue Preparation

Pregnant dams were euthanized via cervical dislocation, and fetal brains were dissected out in phosphate buffered saline (PBS) and fixed in 4% paraformaldehyde (PFA) for 4–8 h, depending on embryonic stage, before being equilibrated in sucrose, embedded in Optimum Cutting Temperature (OCT) compound (Tissue-Tek), and cryosectioned at 12μm. Postnatal tissue was acquired following injection with ketamine hydrochloride (Ketaset, Bioniche Life Sciences) and xylazine (Rompun, Dechra Veterinary Products), or sodium pentobarbital (Dorminal, Rafter 8 Products) and perfusion with PBS followed by 4% PFA. Brains were dissected out and fixed in 4% PFA overnight. Cortex morphology was assessed by DAPI staining. β-Gal staining was performed on cryosectioned slides using the β-Gal Tissue Stain kit (Millipore).

2.3.2. Immunohistochemistry

Immunohistochemistry (IHC) was conducted on E14.5–E18.5 brains as described previously (Iulianella et al., 2008). IHC was conducted using the following antibodies: rabbit anti-CDP/Cux1 (1:100; Santa Cruz), mouse anti-Satb2 (1:250; Abcam), rat anti-Bcl11b/Ctip2 (1:500; Abcam), rabbit anti-Tbr1

(1:200; Abcam), rabbit anti-Cleaved Caspase 3 (CC3; 1:500; Cell Signaling Technology), rabbit anti-Pax6 (1:500; Abcam), goat anti-Sox2 (1:200; Santa Cruz Biotechnology), rat anti-Tbr2 (1:200; eBioscience), mouse anti-neurofilament 2H3 (1:200; DSHB, University of Iowa), rabbit anti-Tuj1 (Tubb3; 1:1000, Biolegend), mouse anti-acetylated α-tubulin (1:1000, Sigma-Aldrich), goat anti-Nestin (1:200, Santa Cruz Biotechnology), mouse anti-Reelin Alexa Fluor 488 Conjugate (1:500, Millipore), rabbit anti-GFAP (1:500, Abcam), anti-Ki67 (1:25, BD Pharmingen), DAPI (1:10,000, Stemcell Technologies), mouse anti-NeuN (1:200, Millipore), and rabbit anti-P73 (1:100, Bethyl Laboratories). Species-specific Alexa Fluor 488-, 568-, 594-, and/or 647-conjugated IgG (1:1500; Invitrogen) secondary antibodies were used to detect primary antibodies.

2.3.3. *In Situ* Hybridization

In situ hybridization (ISH) was performed on 30-mm frozen sections obtained from E18.5, postnatal day (P)7, P14, P21, and P28 Control and cKO brains fixed overnight as previously described (Yamada et al., 2014) using an Mllt11 riboprobe.

2.3.4. EdU Birth Dating

For EdU birth dating studies, dams were injected intraperitoneally with 30 mg/kg body weight of EdU (Invitrogen) at E14.5, E16.5, and E18.5 and sacrificed at E14.5 or E18.5. Sections were immunostained using the Click-It kit according to the manufacturer's protocol (Invitrogen).

2.3.5. Golgi Staining

For Golgi stains, brains were harvested from mice at P28 or P60 and subjected to the FD Rapid GolgiStain kit (FD Neurotechnologies) as per manufacturer instructions. Crude sections were cut and mounted on slides with Permount Mounting Medium (Fisher Scientific).

2.4. Microscopy

Histological and cytological mages were captured using a Zeiss AxioObserver fluorescence microscope equipped with an Apotome 2 structured illumination device, 10x, 20x, 40x, and a Hamamatsu Orca Flash v4.0 digital camera. β-Gal and *Mllt11 in situ* staining was captured using an upright Zeiss PrimoStar compound microscope with an ERc5s color camera. DiI tracing images were captured using a Zeiss V16 Axiozoom fluorescent stereomicroscope equipped with an Axiocam 506 mono digital camera (Zeiss). Images were processed using Zen software (Zeiss) and Photoshop CS6 (Adobe).

2.5. In Utero Electroporation and cDNA Constructs

In utero electroporation was conducted using standard methodology under sterile surgical conditions (Saito, 2006). Endotoxin-free DNA was prepared according to the instructions of the manufacturer (QIAGEN) and injected at 1.5 μg/μl into the telencephalic vesicles of embryos in time-staged pregnant females anesthetized under inhalable isoflurane (5 l/min). A small incision was made on the ventral midline of anesthetized pregnant FVB females under a sterile field

treatment. Single uteri containing the E13.5 fetuses were extruded and electric current was delivered across the fetal brains as five pulses for 50 ms at 900-ms intervals using tweezer-style electrodes linked to the pulse generator CUY21 Vivo SQ (Sonidel). The embryos were returned to the body cavity, the peritoneum was sutured and the skin was stapled. Experimental plasmids used were *Mllt11-ires-eGFP*, and control plasmids included *pIRES2-EGFP* (Clonetech) or pCIG (Addgene). To ensure comparable development staging, for each dam one uterus was electroporated with the experimental construct and the other with the control vector. Fetuses were allowed to survive for 2 days until E15.5 after which they were processed for cryosectioning to evaluate GFP expression and cortical layer development by immunostaining.

2.6. GST Protein Expression, Mass Spectrometry, and Immunoprecipitation

2.6.1. GST-Tagged Protein Expression

The entire *Mllt11* sequence was cloned into pGEX-4T-2 vector for GST pulldown assays. BL21 competent cells (Sigma) were transformed with pGEX-4T-2 (GST) and pGEX-4T-2-MLLT11 (GST-MLLT11). Colonies were picked and incubated overnight in 2-ml 2xYT media with ampicillin at 37°C with shaking. The following day, overnight culture was added to 150-ml 2xYT media with ampicillin and incubated at 37°C with shaking until OD600 reached 0.6. Protein expression was induced by adding IPTG (Invitrogen) to the culture to a final concentration of 0.1 mm and shaken at 28°C for ∼4 h. Cells were pelleted by centrifugation and resuspended in 8-ml NP-40 lysis buffer (50 mm Tris, pH 8.0, 150 mm NaCl, and

1% NP-40) with protease inhibitor cocktail (Sigma). Cells were nutated at 4°C for 10 min, sonicated on ice (30 s on/30 s off, for 3 min total, level 6 intensity), and again nutated at 4°C for 10 min. Lysed cells were pelleted and supernatant collected (protein lysate).

2.6.2. Immobilization of GST or GST-Mllt11 Bait Protein

GST or GST-Mllt11 proteins were immobilized to Glutathione Sepharose 4B beads (Pierce). GST or GST-Mllt11 protein lysates were added to equilibrated 50% bead slurry and nutated at 4°C for approximately 3 hours. Beads with immobilized protein were collected, washed, and resuspended in PBS to make a 50% slurry.

2.6.3. GST Pull-Downs and Mass Spectrometry

Whole embryonic mouse brains were harvested at E15.5 and lysed in NP-40 lysis buffer with protease inhibitor cocktail (Sigma). Whole-brain lysates from one embryo were added to either 6-µg GST or 6-µg GST-Mllt11 bead slurries and nutated overnight at 4°C. Beads with bound lysate were pelleted, washed, resuspended in sample buffer. Samples were heated for 15 minutes at 37°C and run on an SDS-PAGE gel, then stained with Coomassie Blue (Pierce). Bands were cut from the SDS-PAGE gel and processed by Dalhousie's Biological Mass Spectrometry Core Facility.

2.6.4. Co-Immunoprecipitation and Western Blottings

HEK293 cells were transfected with myc or myc-Mllt11 vectors using Lipofectamine 2000 (Invitrogen). 24 hours later, cells were lysed on ice with Tris-HCl lysis buffer containing 50 mM Tris-HCl, pH 7.4, 150 mm NaCl, 1 mM EDTA,

1% Triton X-100, and protease inhibitor cocktail (Sigma). Lysed cells were collected, centrifuged, and supernatant used for co-immunoprecipitation (co-IP). Anti-c-Myc Agarose resin (Pierce) was used, as per manufacturer's protocol, to co-immunoprecipitate myc or myc-Mllt11 and their binding partners. Proteins were eluted from the resin with 50 mM NaOH, neutralized with 1 M Tris, pH 9.5, and added to nonreducing sample buffer for Western blot analysis. For whole-brain lysates, E18.5 cortical protein samples were separated on 8% SDS-PAGE gels for 1 hour at 120 V and transferred overnight at 20 V on to PVDF membranes (Bio-Rad). Blots were probed with mouse anti-acetylated tubulin (1:20,000, Sigma), and rabbit anti-Mllt11 (1:2000, Abcam). Secondary antibodies were goat anti-rabbit HRP (1:5000, Invitrogen) and goat anti-mouse HRP (1:5000, Invitrogen). Blots were developed with Clarity Western ECL Substrate (Bio-Rad) and imaged on a ChemiDoc Touch Gel Imaging System (Bio-Rad). Band densitometry was done using Image Lab Software (Bio-Rad).

2.7. Primary Cortical Cell Culture and Immunocytochemistry

Cortices were microdissected from E18.5 embryos, digested in trypsin (Pierce), manually triturated and plated on 35-mm well onto poly-D-lysine coated coverslips at a density of 150,000 cells for the neurite outgrowth assay, 500,000 for cellular localization experiments and synaptic component colocalization experiments. Cells were plated in medium containing DMEM with 10% FBS and 1% penicillin/streptomycin and 4 h after plating, media was completely removed and replaced with Neurobasal media containing B-27+ (Gibco/Invitrogen), 1%

penicillin/streptomycin, and L-glutamine. Cells were cultured for 24 hours or one week in a 37°C incubator containing 5% CO_2, then fixed for 10 minutes in 4% PFA. Immunocytochemistry (ICC) was conducted using the following antibodies: mouse anti-Tau (1:200; Abcam), rabbit anti-MAP2 (1:1000; Abcam), rabbit anti-Mllt11 (1:300, Abcam), rabbit anti-Tuj1 (Tubb3; 1:1000, Biolegend), mouse anti-acetylated α-tubulin (1:1000, Sigma), rabbit anti-Synapsin I (1:500, Abcam), and mouse anti-PSD95 (1:1,000, Abcam). Species-specific Alexa Fluor 488-, 568-, 594-, and/or 647-conjugated IgG (1:1500; Invitrogen) secondary antibodies were used to detect primary antibodies.

2.8. Synaptic Colocalization Analysis

Following imaging, Z-stack images were deconvolved using AutoQuant software (v. X3.0.4, MediaCybernetics). The deconvolved output was imported into Imaris software (v. 8.1.2, Oxford Instruments) which was used to generate a 3-dimensional reconstruction of each imaged region. A surface was built around each grouping of cells using TdTomato innate fluorescence signal. A masked channel was generated using these surfaces, isolating the TdTomato signal from background. The masked channel was used to perform colocalization analysis between PSD95 and Synapsin I. To minimize background, threshold for the PSD95 channel was manually selected by acquisition of repeated measurements of unambiguous puncta of fluorescence on multiple optical slices, and an average was utilized for the final threshold. A new colocalization channel was

generated to calculate the percentage of the region of interest (ROI) containing colocalization of the PSD95 and Synapsin I channels.

2.9. DiI Tracing of Callosal Projections

Brains of E18.5 embryos were removed and embedded in 7% low gelling temperature agarose in DMEM medium with 1% penicillin/streptomycin. Embedded brains were crudely sectioned at a thickness of ~1–2 mm. Approximately 0.5 µl of DiI (Invitrogen) was injected into the cortical WM tracts at rostral and caudal axial levels and incubated for 8 h in Tyrode's solution. Tissues were then fixed overnight at 4°C in 4% PFA before incubating for two weeks at room temperature in PBS with 1% penicillin/streptomycin.

2.10. Image Sampling, Quantification, and Analysis

For analysis of immunostaining markers and EdU, counting frames (100 × 100µm) were placed in a vertical strip along the primary somatosensory (S1) cortex with the first counting frame along the edge of the ventricle. At least three histologic sections within S1 from three to eight different animals were analyzed for each immunostain, EdU or electroporated vector. Cells that were positively labeled for both DAPI and the marker were counted within each frame using ImageJ (FIJI; Schindelin et al., 2012). For analysis of primary cortical cell culture and Golgi stain, neurites were traced and measured and Sholl analyses were conducted using the “simple neurite tracer” plugin in FIJI. For analysis of radial glial parameters, E14.5, E16.5, and E18.5 control and *Mllt11* cKO mutant images

were captured with identical acquisition parameters and radial glial morphology was assessed using the “directionality” plugin in FIJI to calculate the percentage of fibres in the image aligned in the same direction. Automatic thresholds were then applied and the area covered by Nestin staining was measured and expressed as a percentage of the total image area.

To ensure consistency among samples, cell counts were restricted to the presumptive S1 of the embryonic brain. In all experiments, *Mllt11* cKO and control embryos were used for quantification analysis using the unbiased and systematic sampling method we described previously (Yamada et al., 2015). Counts for Ctip2, Tbr1, Cux1, Tbr2, Sox2, Pax6, CC3, Sox2, Ki67, and Satb2 are represented as line graphs, quantifying the proportion of DAPI stained cells expressing those markers. For EdU, TdTomato, and DAPI distribution analyses, proportion of total stained cells expressing markers within each cortical bin was quantified to ensure counting methods were consistent with previous studies (Chen et al., 2008; De León Reyes et al., 2019; Lawrenson et al., 2017). Image montages were assembled using Photoshop CS6 and Biorender.

2.11. Behavioral Testing and Analyses

2.11.1. Husbandry and Handling

All experimental timed mating crosses were housed singly or with one companion female of the same strain at the time of birth. Animals were ear clipped for genotyping tissue samples on P8, and weaned on P23. Whenever possible, animals were grouped at the time of weaning into home cages with

multiple littermates of various genotypes. All testing was performed between dawning and dusking in the same behavioral testing room under similar lighting and sound conditions unless otherwise stated. Tests were performed 7 days apart following a 7-8 day handling period beginning on day P22. Handling was performed in the testing room following a 10-minute acclimation period in the home cage. Animals were weighed and sexed at this time. Two experimenters performed each experiment with set roles that remained the same whenever possible. Animals were handled by and acclimatized to both experimenters. Experimenters were blinded to the genotypes of each mouse during testing.

2.11.2. Olfactory Habituation/Dishabituation

On P30, animals were placed into a new, clean cage and allowed to acclimate to the behavior room for 20 minutes. During this time, a dry cotton-tipped applicator was presented in the cage and held in place. Following the acclimation period, swabs were sequentially presented in triplicate 2-minute trials with 1-minute intertrial intervals between presentations. Swabs were presented in the following order: water, nonsocial odor 1 (lemon or vanilla extract in distilled water, 1:100 dilution), nonsocial odor 2 (lemon or vanilla extract in distilled water, 1:100 dilution), social odor 1 (swab of soiled bedding from a dirty cage of another group of mice of the same or opposite sex as test mouse), social odor 2 (swab of soiled bedding from a dirty cage of another group of mice of the same or opposite sex as test mouse). The order of presentation of each nonsocial and social odor was randomized. Following testing, animals were weighed and returned to their home cage or to a temporary cage to ensure that they were

segregated from littermates to be tested subsequently and eliminate the risk of scent transmission between littermates.

Analyses of behaviors were performed during and after the testing period by evaluating video footage. Time spent sniffing each swab was recorded, as well as time spent grooming, sleeping, and digging. Bouts of jumping, climbing, and rearing were also recorded.

2.11.3. Three-Chamber Social Test

On P37, animals were placed into a new, clean cage and placed into the center of a plexiglass container divided into three sections or “chambers” by two plexiglass dividers with removable doors. Two wire mesh pencil cups were placed in the center of the outermost chambers beneath water-filled plastic containers to keep them stationary. For 5 minutes, the animal was contained in the center chamber to allow them to acclimate to the chamber. During the following 5-minute period, the chamber doors were opened, and the animal was allowed to freely explore all three chambers. The time spent in each chamber was quantified by experimenters. Following this initial 10-minute habituation to the apparatus, the animal was then confined to the center chamber and the doors were closed. During this time, an unfamiliar, same-sex mouse (stranger mouse 1) was placed beneath the pencil cup in the chamber in which the test mouse spent the least amount of time during the habituation period. Dividing doors were lifted and the test mouse was allowed to freely explore for 10 minutes. During this time, the time spent in each chamber was quantified, as well as the time spent sniffing and directly interacting with stranger mouse 1.

Following the 10-minute trial, the test mouse was once again confined to the center chamber and a second stranger mouse (stranger mouse 2) was placed beneath the pencil cup in the empty chamber. The dividers were lifted, and the test mouse was given 10 minutes to freely explore all three chambers. During this time, the time spent directly interacting with each stranger mouse as well as the time spent in each chamber was quantified. Following testing, animals were weighed and returned to their home cage or to a temporary cage to ensure that they were segregated from littermates to be tested subsequently and eliminate the risk of scent transmission between littermates. Video footage was used to determine time spent in each chamber excluding time spent interacting with stranger mice, number of times a chamber barrier was crossed, and time spent grooming.

Stranger mice were habituated to the three-chamber apparatus prior to the testing day. Mice were placed beneath the wire pencil cups alternating between chambers for 3 10-minute habituation periods.

2.11.4. Social Transmission of Food Preference

On P44, the social transmission of food preference test was performed. Standard pellet chow was removed from the home cage 24 hours before the initiation of testing (P42) and replaced with powdered chow in a custom glass food jar with 6 holes of similar shape, size, and distribution for access to food while minimizing spillage. Each jar had a metal lid containing custom-sized holes, drilled and sanded to allow mice to reach their paws in without injury, and to prevent spillage for pre- and post-test weighing of jars. 2 hours after the pellet chow was replaced

with powdered chow, one mouse from each home cage of genotype *Mllt11*$^{Flox/+}$ or *Mllt11*$^{Flox/Flox}$ was removed and designated as the “demonstrator.” Demonstrator mice were deprived of food for 18 hours, but had access to water. 18 hours later (P43), demonstrator mice were presented with powdered chow in the same custom jar previously described, containing either 1% cinnamon (1mg/100mg powdered chow) or 2% cocoa (2mg/100mg powdered chow) prepared freshly and assigned to demonstrators on an alternating basis. For one hour, the demonstrator was able to freely explore the cage and consume the flavored chow while on a rack in the home room separated from the external environment by fabric barriers on either side of the cage and deprived of water and enrichment devices. Jars were weighed prior to and following testing, and demonstrators who did not consume at least 0.2 grams of food were excluded. The demonstrator was then returned to its home cage with its littermates and returned to the testing rack for 30 minutes, deprived of food and water. The demonstrator was then removed from the home cage and placed in a new cage with pellet chow, and plain powdered chow was replaced in the home cage. The remaining test mice in the home cage were deprived of food for 18 hours prior to testing. On P44, 18 hours after initiation of food deprivation, the test mice were separated into new, clean testing cages containing one jar of each flavor of food placed in opposite corners of the cage on an alternating basis. The test cages were placed on the test rack as previously described, and the test mice were allowed to freely explore and eat the flavored chow for one hour. Jars were weighed prior to and following testing and social transmission of food preference

was determined based on whether the test mouse ate more of the flavored chow presented to the demonstrator than the unfamiliar flavor. Following testing, demonstrators and test mice were placed into the same home cage and provided pellet chow and water.

2.11.5. Tests of Repetitive Behaviors: Marble Burying and Nestlet Shredding

On P51, mice were brought into the testing room in their home cages and separated into new, clean cages with only corn cob bedding. A single, pre-weighed Nestlet (Ancare) square was placed into the center of each cage. A single mouse was placed into the corner of each cage facing away from the Nestlet, and left undisturbed for 30 minutes. Mice were then removed, placed into the home cage, and the remaining unshredded Nestlet material was weighed. The home cage was returned to the home room for one hour before subsequent testing.

A clean, standard-sized rat cage with a 6 cm layer of fresh corn cob bedding was prepared for each test mouse. Glass marbles were placed on the surface of the bedding in a grid pattern of five rows of four marbles. Marbles were soaked in Peroxigard™ disinfectant (Virox Technologies Inc.) and dried thoroughly before each test trial. After one hour, mice were once again returned to the testing room in the home cage, and one test mouse was placed into the corner of each rat cage, facing away from the array of marbles, and left undisturbed for 30 minutes. Each mouse was then returned to the home cage,

and the condition of the marbles was assessed and photographed by the experimenters to determine how many had been buried and to what extent.

2.12. Statistical Analysis

For all data excluding behavioral testing and Sholl analyses, statistical differences were determined with Student's t-tests (two-tailed) with Welch's correction. Sholl analyses were performed with paired t-tests (two-tailed) to compare branch points within comparable radii. For behavioral testing, two-way repeated measures ANOVA was performed in comparisons of data between genotypes within sexes. One-way ANOVA was performed between comparisons of individual metrics within each genotype. Tukey's multiple comparisons test was utilized wherever statistical significance was found between means by genotype. Student's t-tests (two-tailed) with Welch's correction were used to compare behavioral testing where fewer than three conditions were compared. Bar charts, line graphs, and statistical testing were conducted using GraphPad Prism V5.0d software, with results shown as mean ± SD. In all quantification studies, significance level was set at $p \leq 0.05$ (*$p \leq 0.05$, **$p \leq 0.01$, ***$p \leq 0.001$, ****$p \leq 0.0001$).

CHAPTER 3. Conditional Knockout of *Mllt11* from UL2/3 CPNs: Initial Phenotypic Description and Identification of a Migratory Deficit

3.1. Introduction

In an effort to identify regulators of neural migration and differentiation, the Iulianella lab previously reported the expression of *Mllt11/Af1q* in the developing central nervous system, including the retina, hindbrain, midbrain, spinal cord and cortical plate (Blommers et al., 2023; Yamada et al., 2014). Mllt11 is a vertebrate-specific 90 amino acid protein that possesses a nuclear export signal but otherwise has poorly defined functional domains. *Mllt11* was first identified in an infant with acute myelomonocytic leukemia carrying the t(1;11)(q21;q23) translocation that creates an abnormal protein fused to Mll (W. Tse et al., 1995). *Mllt11* may play a normal role in neural differentiation, as its transcription is down-regulated by REST, a key factor involved in regulating terminal differentiation of neurons (Hu et al., 2015). However, functional studies addressing its role in neural development are currently lacking.

Mllt11 was first identified as a potential candidate for neuronally relevant genes through demonstration of its ability upon overexpression to promote extension of processes containing Tuj1/Tubb3, a neuronally-restricted β-tubulin isoform, in HEK293 cells (Lin et al., 2004a). Subsequently, it was identified in a short list of genes potentially important for neuronal differentiation in a proteomic screen in Hek293 cells (Iulianella lab, unpublished). Further investigation of its expression in the developing cerebral cortex revealed a large degree of overlap between its expression domain and that of *Cux2* (Stanton-Turcotte et al., 2022).

Cux2 is a transcription factor with many roles in neuronal development, particularly within the cortex. It exhibits widespread expression throughout pallial and subpallial regions. Subpalially, it is expressed in Reelin+ GABAergic interneurons born in the ganglionic eminences (Cubelos, Sebastián-Serrano, Kim, Redondo, et al., 2008a; Zhao et al., 2008). Palially, its expression is mainly restricted to hippocampal progenitors (Yamada et al., 2015) as well as Tbr2+ intermediate progenitors located in the SVZ and their neuronal progeny, which are mainly UL2/3 CPNs (Cubelos, Sebastián-Serrano, Kim, Moreno-Ortiz, et al., 2008; Gil-Sanz et al., 2015; Zimmer et al., 2004). Cux2 also exhibits limited, mosaic expression in DL CPNs but it is primarily an UL CPN marker (Gil-Sanz et al., 2015).

These UL2/3 CPNs face the most arduous migratory journey during cortical development, as they migrate through pre-existing layers of DL CPNs, employing dynamic modes of migration in order to alternate between crawling short distances through thick WM tracts and extend neurites basally to guide migration toward the pia, or migrating along tracts formed by preexisting radial glial fibres (Anton et al., 1997). In contrast, DL CPNs migrate only a short distance by virtue of being the earliest deposited layer, born just apical to the pia. Once in their laminar location, UL CPNs primarily form corticocortical projections, 80% of which are contralateral via the CC (Leone et al., 2015). This makes the CC an ideal model in which to study the neuritogenic potential of these UL neurons.

Given the temporal and spatial overlap between *Mllt11* expression and neurogenic regions of the cerebrum, I set out to investigate the role of *Mllt11* in the development of the cerebral cortex, and specifically in the formation of the UL2/3 callosally-projecting CPNs that bridge communication interhemispherically (Fame et al., 2011) where *Mllt11* expression appeared highest during corticogenesis (Figure 2.1. A).

3.2. Conditional Knockout of *Mllt11* From UL2/3

Mllt11 is expressed in developing neurons of the central nervous system, including the neocortex, but its role in cortical neurogenesis is unknown (Yamada et al, 2014). To investigate this, the Iulianella lab generated mice carrying a null mutation in the *Mllt11* gene using embryonic stem cell (ESC) clones obtained from the mouse knockout consortium project (UCDavis KOMP repository, Mllt11tm1a(KOMP)Mbp). We first used the targeted (unflipped) allele to visualize *Mllt11* expression domain through β-galactosidase (β-gal) staining through the LacZ gene inserted into the *Mllt11* locus (Figure 2.1. A). Initial *Mllt11* locus activity begins in the pallial MZ at E12.5, and its expression domain expands in the following days, showing stronger expression in the IZ of the fetal cortex at E14.5, coinciding with the birth of basal progenitors fated to become UL2/3 CPNs, and intensifying in the superficial cortical layers by E16.5- E18.5 (Figure 2.1. A). This confirms our previous report of Mllt11 mRNA and protein localization in these regions (Yamada et al., 2014). Subsequent in situ hybridization (ISH) revealed that cortical expression is maintained until postnatal day 21 (P21) when it begins to taper to levels indistinguishable from background at P28

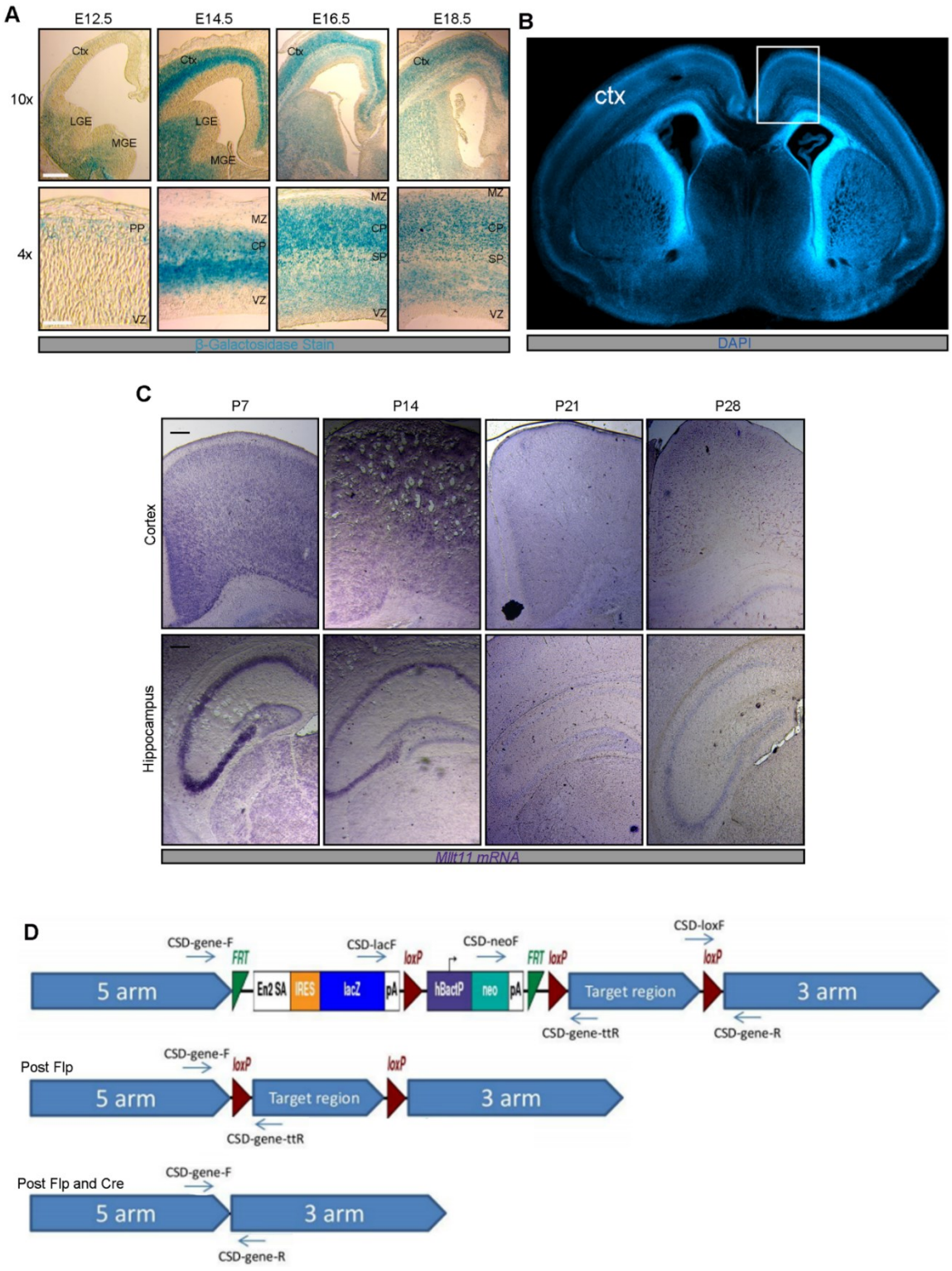
A
E12.5
E14.5
E16.5
E18.5
10x
4x
Ctx
LGE
MGE
PP
MZ
CP
SP
VZ
β-Galactosidase Stain
B
ctx
DAPI
C
P7
P14
P21
P28
Cortex
Hippocampus
Millt11 mRNA
D
CSD-gene-F
FRT
CSD-lacF
loxP
CSD-neoF
FRT loxP
CSD-loxF
loxP
5 arm
En2 SA
IRES
lacZ
pA
hBactP
neo
pA
Target region
3 arm
CSD-gene-ttR
CSD-gene-R
Post Flp
CSD-gene-F
loxP
loxP
5 arm
Target region
3 arm
CSD-gene-ttR
Post Flp and Cre
CSD-gene-F
5 arm
3 arm
CSD-gene-R

Figure 2.1.

Figure 2.1. *Mllt11* Targeting Strategy and Ontogenic Expression Profile. **A**, Coronal sections of the targeted *Mllt11* locus (with inserted a lacZ cDNA) showing *Mllt11* expression across four time points during cortical neurogenesis through β-Gal staining. At E14.5, β-Gal expression was most intense in the CP, corresponding to UL neurogenesis. By E16.5, β-Gal staining intensity shifted to the superficial cortex where UL CPNs were accumulating. **B**, Reference image of region captured in panel C. **C**, *Mllt11* expression in the cortex (top panel) and hippocampus (bottom panel) from P7 to P28. RNA levels declined in the cortex and were indistinguishable from background at P28. **D**, Graphic representation of the targeting construct inserted into the *Mllt11* locus before and after Flp and Cre recombinase activity. The entire protein-coding region of *Mllt11* is encoded by *exon 2* (Mllt11 ex2), which is flanked by loxP sites. *Mllt11* expression can be evaluated by β-Gal staining because of the insertion of lacZ cDNA in the targeted allele. A cKO allele can be generated by the removal of the lacZ and selection cassette by germline Flp recombination. Scale bar: 100μm. Ctx, cortex; CP, cortical plate; IZ, intermediate zone; LGE, lateral ganglionic eminence; MGE, medial ganglionic eminence; MZ, marginal zone; PP, preplate; SP, subplate; VZ, ventricular zone.

(Figure 2.1. B-C). *Mllt11* transcript levels decreased but remained detectable in the hippocampus through P28 (Figure 2.1. C).

The targeted *Mllt11* null allele was utilized to generate a conditional knockout (cKO) *Mllt11* allele in which the entire coding sequence in Exon 2 is flanked by *loxP* sites (Figure 2.1. D). To avoid non-specific effects of the selection cassette, mice encoding germline-expressing flp recombinase were crossed to mice harboring the *Mllt11* targeted allele, leaving only *loxP* sites used to excise the entire protein-coding exon and create a conditional allele (Figure 2.1. D). To inactivate *Mllt11* in UL2/3 of the cerebral cortex, I crossed the $Mllt11^{Flox/Flox}$ mice to the $Cux2^{IREScre}$ strain with the Ai9 *TdTomato* reporter mice to visualize recombined neurons through TdTomato fluorescence, creating fluorescently labeled *Mllt11* conditional mutants. *Cux2* is highly expressed in developing UL2/3 projections neurons, and mosaically expressed in the SVZ in the pallial cortex (Cubelos, Sebastián-Serrano, Kim, Moreno-Ortiz, et al., 2008; Cubelos, Sebastián-Serrano, Kim, Redondo, et al., 2008b; Nieto et al., 2004; Zimmer et al., 2004), and as such, the resulting $Cux2^{IREScre}$-driven Mllt11 cKO mice should lack *Mllt11* expression in UL2/3 of the neonatal cortex.

3.3. Loss of *Mllt11* from UL2/3 Leads to Progressive Decrease in Cortical Thickness

I first confirmed *Mllt11* loss in UL CPNs. qPCR performed on E18.5 cortical lysates confirmed decreased *Mllt11* transcript levels (Figure 2.2. A-B). As a secondary confirmation of *Mllt11* reduction, specifically in *Cux2*-expressing regions, ISH was performed at P7 and also revealed a reduction in *Mllt11*

specifically in the cortical ULs (Figure 2.2. C), as well as the hippocampus (Figure 2.2. D). Due to the genetic strategy employed, all cells exhibiting *Mllt11* loss were labeled by TdTomato fluorescence. TdTomato labeling was observed mostly in UL2/3 of the cortex (Figure 2.2. E) and commissural tracts at P7 (Figure 2.2. F), confirming that Cre-mediated excision was specific to the *Cux2* expression domain.

Brain and body weights were not found to differ significantly between *Mllt11* cKO mutants and controls at E18.5 (Figure 2.3. A-B), nor was the ratio of brain weight to body weight (Figure 2.3. C). Most notably, mutants displayed a thinning of the cortex. (Figure 2.3. D).

3.4. Total Cortical Cell Numbers are not Affected in *Mllt11* cKO

To explore the origin of this cortical thinning, I examined the morphology of the cortex beginning at E14.5 (Figure 2.3. E), when UL CPNs are born and begin to express *Cux2* (Cubelos, Sebastián-Serrano, Kim, Redondo, et al., 2008b; Zimmer et al., 2004). At this earliest stage of *Cux2* expression, no differences were found between control and cKO cortices. A slight thinning of the cKO cortex was observed beginning at E16.5 (Figure 2.3. F), increasing in severity by E18.5 (Figure 2.3. G). Though the total number of DAPI+ cortical cells in the *Mllt11* mutant cortex did not differ significantly (Figure 2.3. G), there were significant changes in the distribution of DAPI+ nuclei in deeper bins of the *Mllt11*

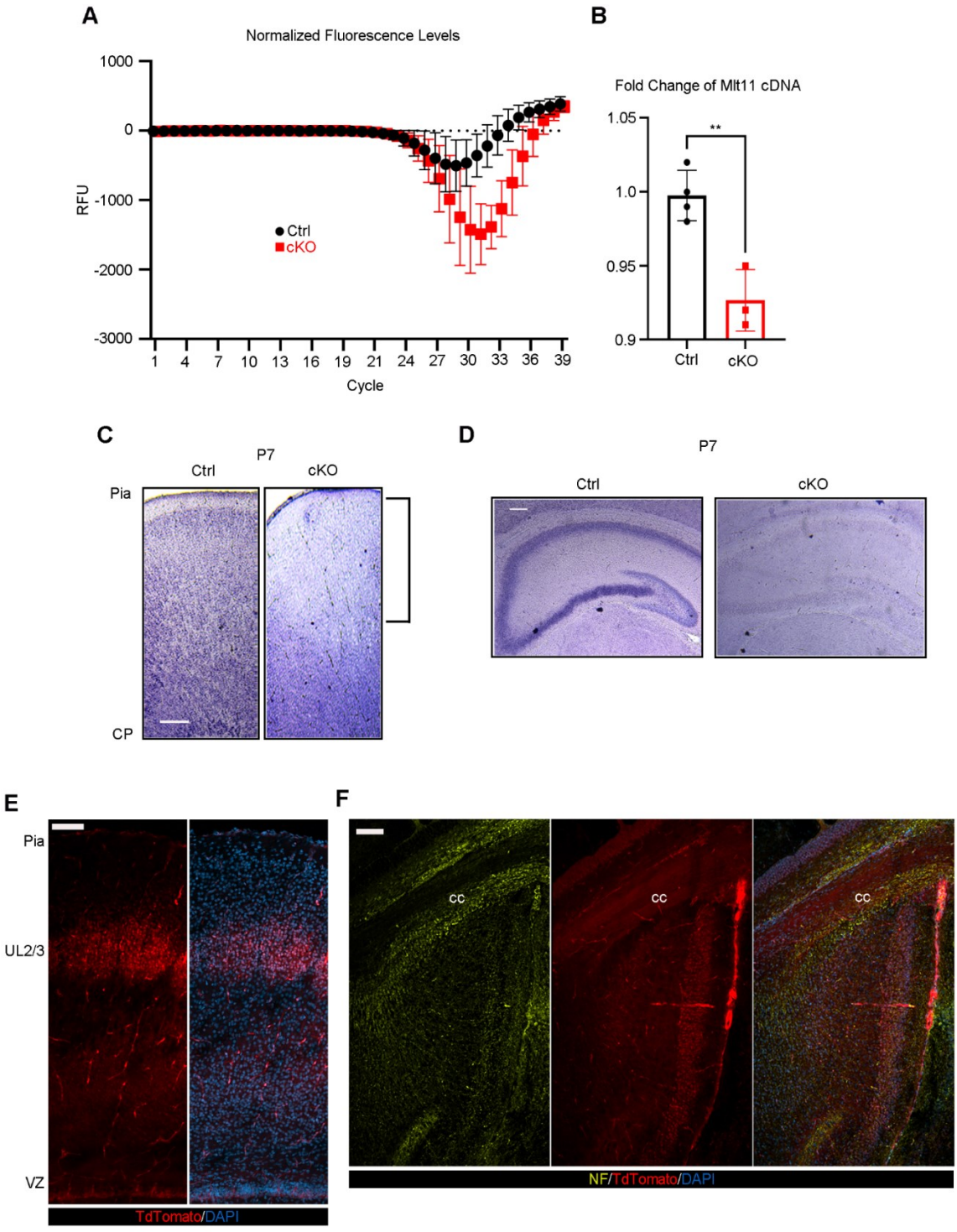
A
Normalized Fluorescence Levels
1000
0
-1000
-2000
-3000
RFU
Ctrl
cKO
1 4 7 10 13 16 19 21 24 27 30 33 36 39
Cycle
B
Fold Change of Mlt11 cDNA
1.05
1.0
0.95
0.9
**
Ctrl
cKO
C
P7
Ctrl
cKO
Pia
CP
D
P7
Ctrl
cKO
E
Pia
UL2/3
VZ
TdTomato/DAPI
F
cc
cc
cc
NF/TdTomato/DAPI

Figure 2.2.

Figure 2.2. *Mllt11* cKO Validation by qPCR and ISH. **A**, Quantification of qPCR fluorescence levels of control and cKO cortices normalized to internal control *GAPDH*. **B**, Fold change of *Mllt11* cDNA transcript levels was significantly decreased in cKO relative to control brains. **C**, **D**, Images of ISH of *Mllt11* riboprobe on P7 control and cKO cortices and (**D**) Hippocampi showed decreased labeling in the superficial cortex, corresponding to the *Cux2*-expressing region. **E**, **F**, Reference image of TdTomato expression in *Cux2*-expressing neurons of UL2/3 (**E**) as well as their projections comprising the corpus callosum (**F**) indicated by NF staining. (**A**, **B**) N=4 controls, 3 cKOs, (**C**, **D**) N=3. Data presented as mean ± SD; **p ≤ 0.01. Scale bar: 100μm. CP, cortical plate; RFU, relative fluorescence units; cc, corpus callosum.

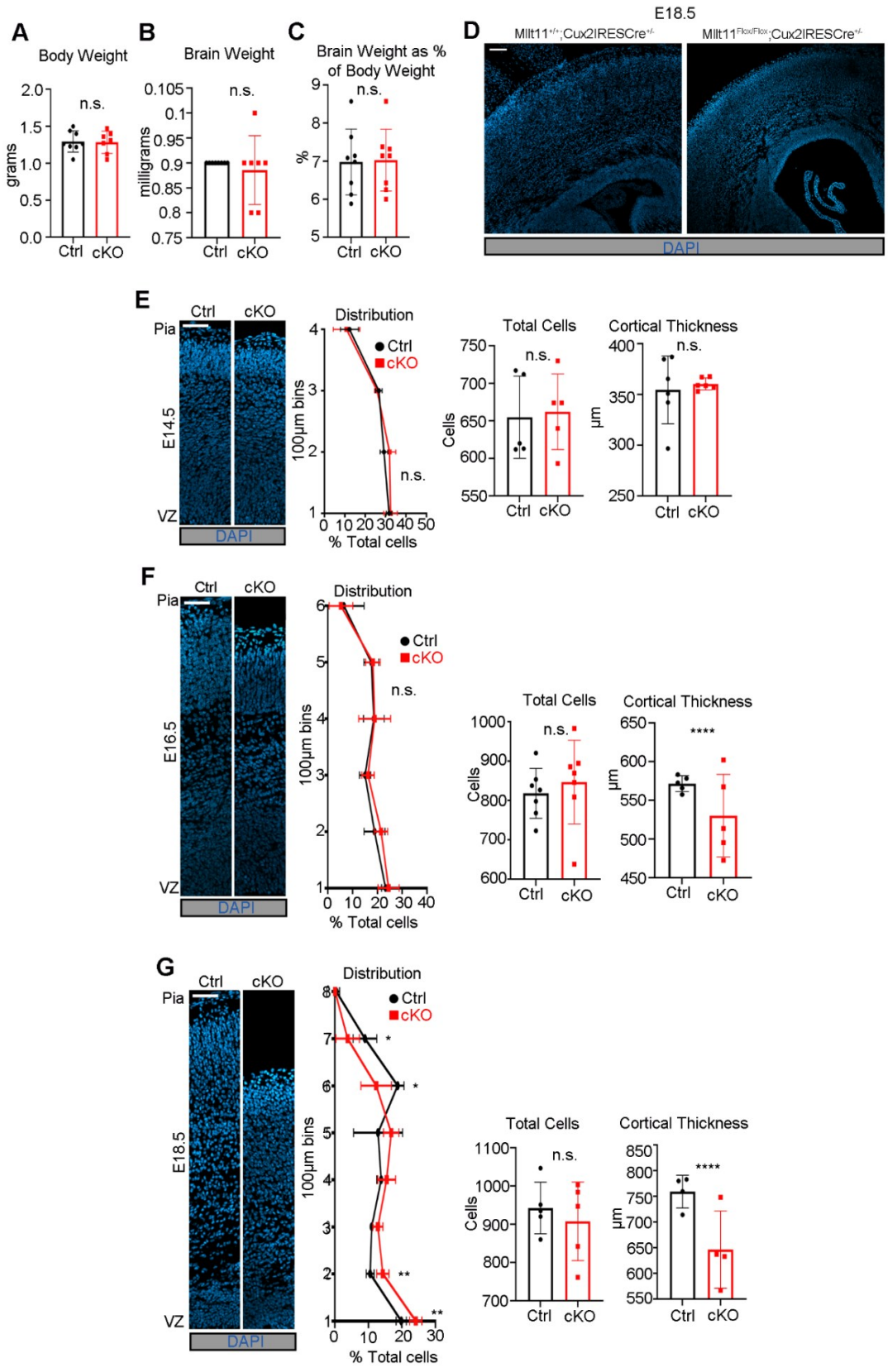
A
Body Weight
grams
n.s.
Ctrl cKO
B
Brain Weight
milligrams
n.s.
Ctrl cKO
C
Brain Weight as % of Body Weight
%
n.s.
Ctrl cKO
D
E18.5
Mllt11+/+;Cux2IRESCre+/-
Mllt11Flox/Flox;Cux2IRESCre+/-
DAPI
E
Ctrl cKO
Pia
E14.5
VZ
DAPI
Distribution
Ctrl
cKO
100µm bins
n.s.
% Total cells
Total Cells
Cells
n.s.
Cortical Thickness
µm
n.s.
F
Ctrl cKO
Pia
E16.5
VZ
DAPI
Distribution
Ctrl
cKO
100µm bins
n.s.
% Total cells
Total Cells
Cells
n.s.
Cortical Thickness
µm
****
G
Ctrl cKO
Pia
E18.5
VZ
DAPI
Distribution
Ctrl
cKO
100µm bins
*
*
**
**
% Total cells
Total Cells
Cells
n.s.
Cortical Thickness
µm
****

Figure 2.3.

Figure 2.3. *Mllt11* Loss Affects the Laminar Distribution of Cells. **A**-**C**, Body weight (**A**), brain weight (**B**), and brain weight as a percentage of body weight (**C**) showed no difference between control and cKOs at E18.5. **D**, cKO cortices were thinner than controls at E18.5. **E**-**G**, Thinning of the cKO cortex was progressive, with thicknesses being comparable to controls at E14.5 (**F**), but *Mllt11* mutants exhibited reduced thickness and reduced distribution of cells in the superficial cortex at E16.5 (**G**), which increased in severity by E18.5 (**H**). Total cell counts and cortical thickness measurements (μm) are shown as bar graphs. Cell count line charts represent percentage of positive cells normalized to DAPI+ nuclei per 100 × 100μm bin. (**A**-**C**) N=8, (**E**) N=5, (**F**) N=7 for total cells, N=5 for cortical thickness, (**G**) N=5 for total cells, N=4 for cortical thickness. Data presented as mean ± SD; n.s., not significant; *p ≤ 0.05, **p ≤ 0.01, ***p ≤ 0.001, ****p ≤ 0.0001. Scale bars: 100μm (**E**), 50μm (**F**-**H**).

cKOs, with a larger proportion of DAPI+ nuclei localized apically in E18.5 mutants relative to controls (Figure 2.3. G).

To rule out potential cell non-autonomous contributions from neural progenitors to the *Mllt11* mutant cortical phenotype, I quantified cells positive for progenitor markers from E14.5-18.5, corresponding to the period of UL neurogenesis. Pax6, a marker of radial glial cells (RGCs) and neural progenitors (Götz et al., 1998; Stoykova et al., 1996), was unaltered at all observed time points (Figure 2.4. A-C). Sox2, a less restrictive marker for neural progenitors and quiescent RGCs (D'Amour & Gage, 2003; Ellis et al., 2004), also exhibited no significant differences in expression (Figure 2.4. D-F). Tbr2+ IPs (basal), which also express Cux2 and give rise to UL2/3 CPNs, did not differ markedly between control and *Mllt11* cKO groups at E14.5 or E16.5 (Figure 2.4. G-H) but displayed fewer cells within deeper regions of the mutant cortex distinct from the progenitor domains, at E18.5 (Figure 2.4. I), suggesting alterations in the formation and/or migration of nascent neurons from the SVZ.

To further corroborate this finding, I explored whether amounts of proliferation varied between controls and *Mllt11* cKOs to account for the differences in cortical morphology and cellular distribution. Immunostaining for Ki67, a protein which aids in segregation of chromosomes into daughter cells during mitosis, indicating cells with proliferative potential (Cuylen et al., 2016; Scholzen & Gerdes, 2000), revealed no differences in numbers of proliferative progenitors in the VZ or SVZ at E14.5 (Figure 2.5. A) or E18.5 (Figure 2.5. B). To examine whether *Mllt11* loss affected the neurogenesis of UL neurons, I pulsed

dams with EdU for 2 hours at E14, which efficiently labeled nuclei within the BP region (Figure 2.5. C). I observed no difference in the numbers or distribution of EdU+ nuclei in *Mllt11* mutants vs. control cortices after a short pulse at E14 (Figure 2.5. C). I repeated this short pulse at E18, when UL neurogenesis is nearly complete, and noted no differences in EdU+ cells in the superficial cortex of *Mllt11* mutant brains compared to controls (Figure 2.5. D). I did observe a slight increase of EdU+ cells in the deepest 100μm bin of the *Mllt11* mutant cortex relative to controls, possibly reflecting aberrant migration of later born neurons (Figure 2.5. D). Overall, the EdU birth dating analysis, lack of impact on proliferating cell population size, and the fact that *Mllt11* expression was restricted to the developing cortical plate and not in the apical progenitors in the VZ of the cortex, suggested that *Mllt11* does not regulate neurogenesis of UL CPNs.

I next evaluated whether programmed cell death could account for the cortical thinning and alteration of cellular distribution, but did not find any cells positive for the apoptotic marker cleaved caspase-3 (CC3, Darmon et al., 1995) in the *Mllt11* mutant cortex at E14.5 (Figure 2.5. E) or E18.5 (Figure 2.5. F). Retrosplenial regions, which typically show enhanced apoptosis, showed comparable levels of CC3 staining in controls and mutants (Figure 2.5. G). Taken together, *Mllt11* loss does not impact the total number of cortical cells, does not alter proliferation or rates of cell death during cortical neurogenesis, but plays a determinant role in the distribution and packing of cells throughout the apicobasal axis of the cortex.

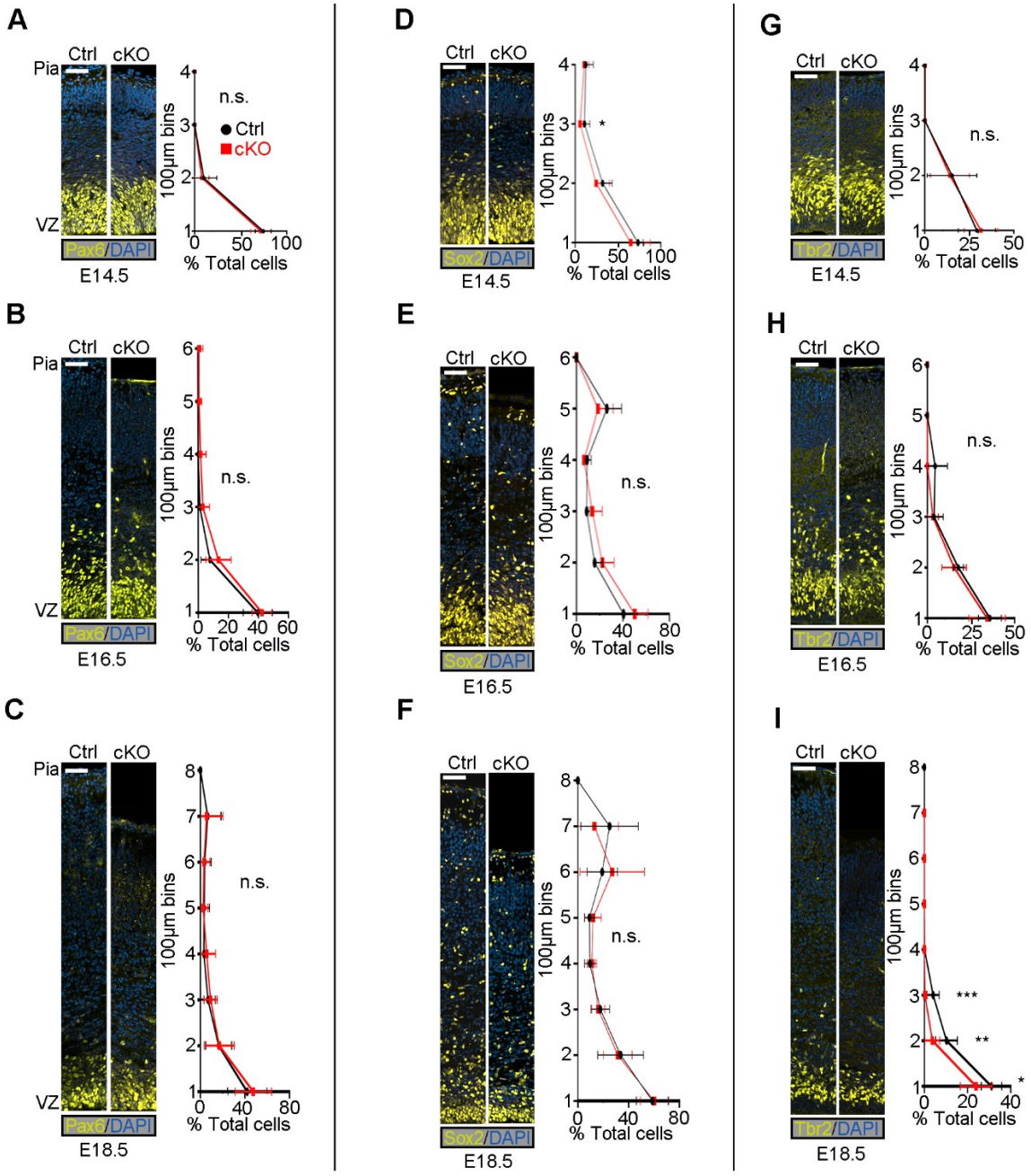
A
Ctrl
cKO
Pia
VZ
Pax6/DAPI
E14.5
n.s.
Ctrl
cKO
100μm bins
% Total cells
B
E16.5
C
E18.5
D
Sox2/DAPI
*
E
F
G
Tbr2/DAPI
H
I
***
**

Figure 2.4.

Figure 2.4. Neural Progenitor Populations Were Largely Unaffected in *Mllt11* cKO. **A**-**C**, Coronal cortical slices stained for Pax6 with IHC was unaltered in cKO cortices relative to controls at E14.5 (**A**), E16.5 (**B**), and E18.5 (**C**). **D**-**F**, Sox2 levels were largely similar between cKO and controls at E14.5 (**D**), E16.5 (**E**), and E18.5 (**F**). **G**-**I**, Tbr2 expression was also largely unaltered in cKOs at E14.5 (**G**) and E16.5 (**H**), but showed a significant trend toward decreased levels normalized to DAPI+ nuclei immediately basal to the Tbr2+ progenitor domain at E18.5 (**I**). Line charts represent percentage of positive cells normalized to DAPI+ nuclei per 100 × 100μm bin. (**A**-**C**, **F**-**I**) N = 4, (**D**, **E**) N = 3. Data presented as mean ± SD; n.s., not significant; *p ≤ 0.05, **p ≤ 0.01, ***p ≤ 0.001. Scale bar: 50μm (**A**-**I**). VZ, ventricular zone.

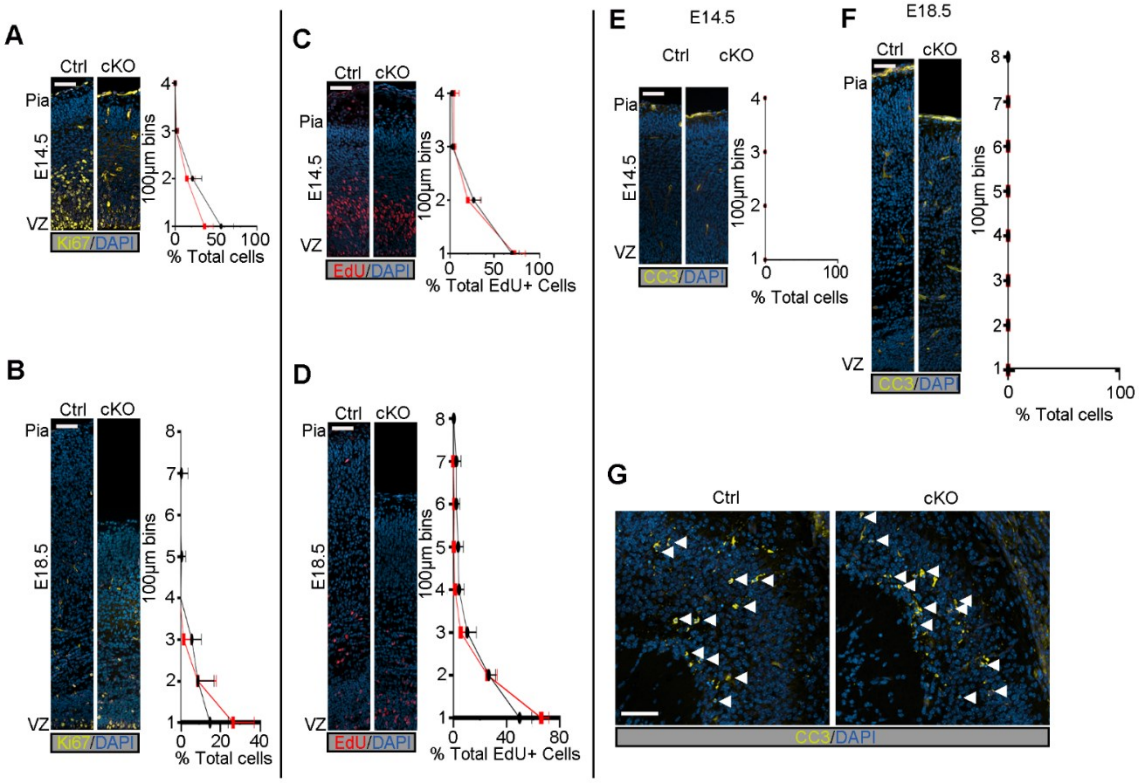

Figure 2.5. Loss of *Mllt11* Had No Impact on Proliferation or Programmed Cell Death. **A**, **B**, Ki67 staining in the cortex was unaltered in cKO cortices at E14.5 (**A**) and E18.5 (**B**). **C**, Proliferating cells labeled with a short pulse of EdU at E14 showed no significant differences in numbers or distribution between controls and cKOs. **D**, No significant difference was seen in numbers of nuclei labeled by a short pulse of EdU at E18 populating most bins in cKOs versus controls, but a greater proportion of cells were retained in the cKO VZ region. **E**, **F**, Cortical slices at E14.5 (**E**) and E18.5 (**F**) showed no differences in the levels of CC3 in cKOs relative to controls. **G**, CC3 staining in the retrosplenial area, which normally exhibits apoptosis, was included as an antibody control for CC3 staining. White arrowheads indicate positive labeling. Line charts represent percentage of positive cells per 100 × 100µm bin as a proportion of total EdU+ cells. Total co-labeled cells are shown as bar graphs. (**A-C**) N=4, (**D**) N=3, (**E-G**) N=3 controls, 5 cKOs. Data presented as mean ± SD; n.s., not significant; *p ≤ 0.05, **p ≤ 0.01, ***p ≤ 0.001, ****p ≤ 0.0001. Scale bar: 50µm (A-G). VZ, ventricular zone.

3.5. *Mllt11* is Required for the Maintenance of UL CPN Molecular Identity

The transcriptional de-repression loop that specifies cell types in discrete cortical laminae coincides with the birth and migration of projection neurons (Kumamoto et al., 2013; Toma et al., 2014). Thus, a loss of *Mllt11* in UL progenitors can potentially affect neuronal birth, migration, and/or specification. I therefore investigated whether *Mllt11* loss had any role in regulating the molecular identity of UL CPNs. Expression of Satb2 in CPNs of L2-4 exhibited a decrease at E18.5 (Figure 2.6. C) as did CDP/Cux1, another marker of UL CPNs (Figure 2.6. F). Investigation at earlier developmental time points revealed that this phenotype was progressive, displaying expression levels comparable to controls at E14.5 (Figure 2.6. A, D), becoming apparent at E16.5 (Figure 2.6. B, E), and increasing in severity by E18.5 (Figure 2.6. C, F). While the extent of CDP/Cux1 and Satb2 staining displayed variability across individual mutants, there was a consistent decrease in expression levels and apical shift in expression domain in all *Mllt11* cKOs, though it was unclear whether this was due to a lack of Satb2 expression, or an inability of Satb2+ cells to migrate properly. TdTomato labeling was used to identify Cux2+ cells as well as intermediate progenitors that give rise to UL2/3 CPNs, and while reporter levels were found to be unaltered at all time points (Figure 2.6. G-I), there was a consistent apical shift in expression domain at E18.5 (Figure 2.6. I). Collectively, these findings suggested that *Mllt11* loss in nascent UL neurons did not affect their neurogenesis, or fully hinder activation of UL gene expression programs, but may have affected the maintenance of these gene expression programs

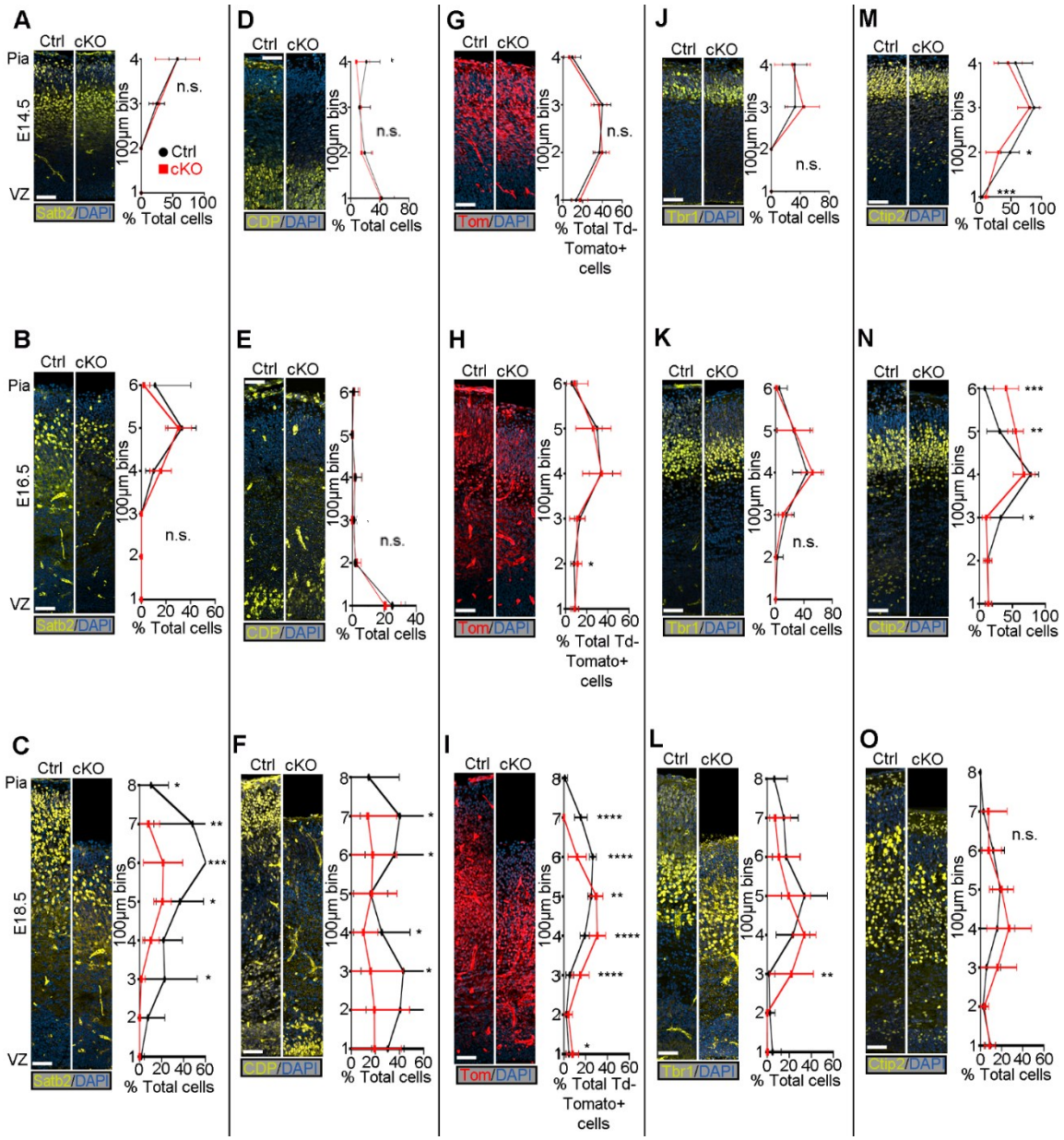
A
Ctrl cKO
Pia
E14.5
VZ
Satb2/DAPI
100μm bins
n.s.
Ctrl
cKO
% Total cells
D
CDP/DAPI
G
Tom/DAPI
% Total Td-Tomato+ cells
J
Tbr1/DAPI
M
Ctip2/DAPI
B
E16.5
E
H
K
N
C
E18.5
F
I
L
O
*
**
***
****

Figure 2.6.

Figure 2.6. *Mllt11* Loss Progressively Perturbed the Formation of UL CPNs. **A**-**O**, Coronal cortical slices stained for cortical layer markers. **A**, **B**, Coronal cortical slices stained for Satb2 were similar between *Mllt11* cKOs and controls at E14.5 (**A**) but displayed decreased numbers of Satb2+ cells in upper bins, and an apical shift at E16.5 (**B**). **C**, *Mllt11* cKO cortices displayed decreased Satb2+ cell numbers and apical shift at E18.5 compared with controls. **D**, **E**, CDP/Cux1+ cell numbers were largely normal at E14.5 (**D**), but began to decrease at E16.5 (**E**). **F**, CDP/Cux1 levels were severely decreased in *Mllt11* cKOs compared with controls at E18.5. **G**-**I,** Distribution of TdTomato expression in the cortex was comparable between controls and cKOs at E14.5 (**G**), E16.5 (**H**), and E18.5 (**I**). **J**-**L**, Tbr1 levels and localization were comparable between control and cKOs at E14.5 (**J**) and E16.5 (**K**), but its expression domain exhibited an apical shift at E18.5 (**L**). **M**-**O**, Ctip2+ cell numbers and localization were largely unaltered in cKO at E14.5 (**M**) and E16.5 (**N**) but exhibited an apical shift in expression domain at E18.5 (**O**). Line charts represent percentage of positive cells normalized to DAPI+ nuclei per 100 × 100μm bin (**A**-**F**, **J**-**O**) and percentage of total TdTomato+ cells per 100 × 100μm bin (**G**-**I**). (**A**, **E**, **J**, **L**-**O**) N=4, (**F, H**-**I**) N=5, (**G**) N=5 controls, 6 mutants, (***K***) N = 4 controls, 5 mutants. Data presented as mean ± SD; n.s., not significant; *p ≤ 0.05, **p ≤ 0.01, ***p ≤ 0.001, ****p ≤ 0.0001. Scale bar: 50μm (**A**-**O**). VZ, ventricular zone.

and/or their migration into UL2/3.

The cortical de-repression loop functions on a cellular level by alternately repressing DL and UL fate (Toma et al., 2014), so I wanted to determine if the loss of UL CPN fate was coupled with a complementary upregulation of DL CPN fates in these cells. I examined the localization of DL6- and DL5-specific markers Tbr1 (Figure 2.6. J-L) and Ctip2 (Figure 2.6. M-O) respectively, which both exhibited similar numbers and staining patterns between Mllt11 cKOs and controls at all time points. However, the mutants displayed a downward shift of the expression domains of both markers consistent with the decreased cortical thickness and UL formation (Figure 2.6. L, O).

Given that the *Mllt11* mutants failed to maintain UL-specific transcription factors over time, I wanted to understand whether the cortical de-repression loop and layer-specific cell type specification were de-coupled, such that CPNs born at the time of UL CPN birth could instead mis-express a DL-specific transcriptional regulator. Pregnant dams were injected with EdU at E14 or E16 to label UL neurogenesis, and embryos were harvested at E18.5 to examine the co-localization of the DL CPN marker Ctip2, and UL marker CDP/Cux1, with EdU. The proportion of Ctip2+ CPNs born at E14 did not differ significantly between controls and cKOs with the exception of the overall downward shift in the distribution of Ctip2+/EdU+ cells in the cKO cortex (Figure 2.7. A). Embryos pulsed with EdU at E16 and harvested at E18.5 displayed the same trend, exhibiting a downward shift but no significant differences in overall proportions of Ctip2+/EdU+ co-labeled cells (Figure 2.7. B). Colocalization of CDP/Cux1 and

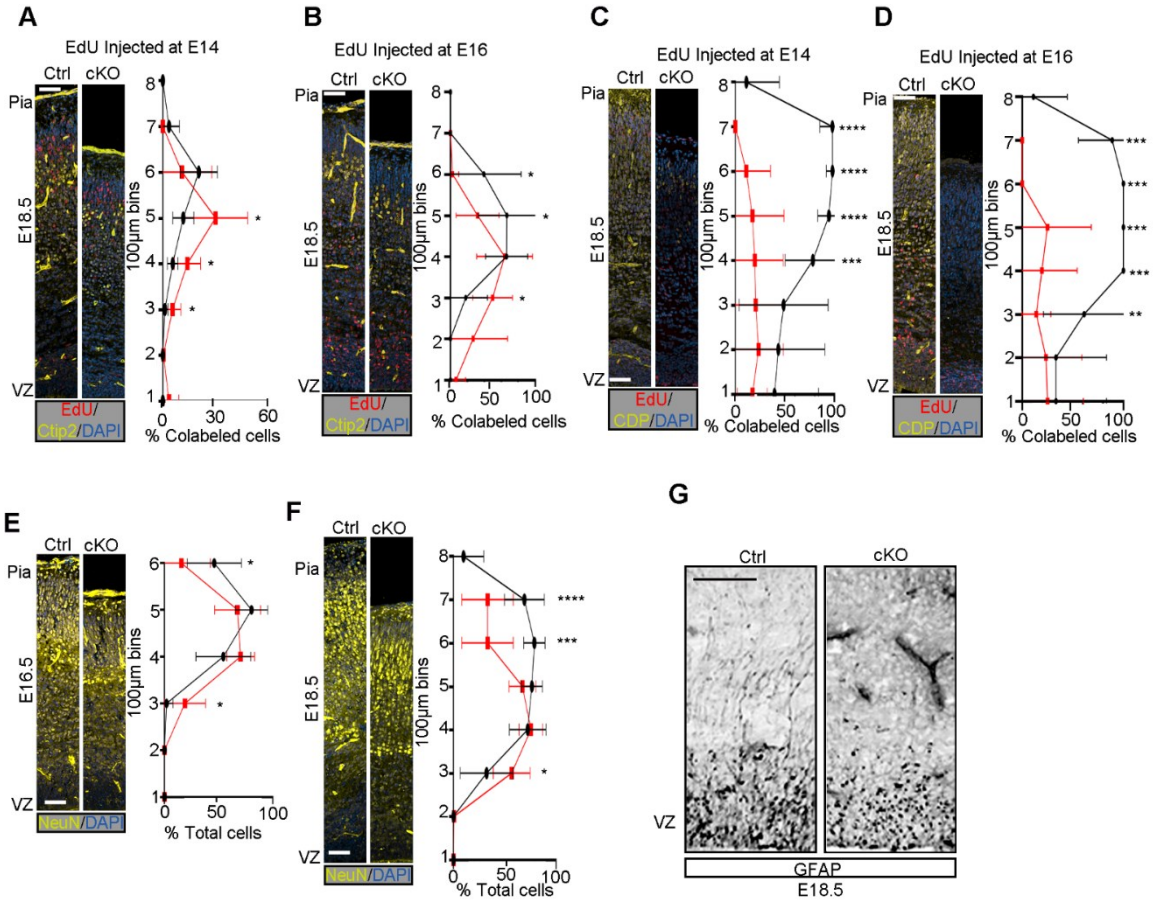

Figure 2.7. *Mllt11* Loss Impacts Maintenance of UL CPN Markers but Does Not Cause a Gliogenic Fate Change. **A**, **B**, Cortical slices from embryos injected with EdU at E14 (**A**) and E16 (**B**) showed comparable levels of cells co-stained for Ctip2 and EdU despite a downward shift in cKOs at E18.5. **C**, **D**, Cortical slices injected with EdU at E14 (**C**) and E16 (**D**) display a severe decrease in CDP+ cells and varied EdU+ cell localization, with a greater proportion retained in deeper bins of the CP and VZ, suggesting that UL CPNs are born, but do not express CDP/Cux1 in cKOs. **E**, **F**, Cortical slices at E16 (**E**) and E18 (**F**) displaying comparable staining for NeuN throughout the CP. (**G**) Radial glial fibers displaying GFAP staining in the VZ and SVZ. (**A-D**) N=4, (**E-G**) N=3. Data presented as mean ± SD n.s., not significant; *p ≤ 0.05, **p ≤ 0.01, ***p ≤ 0.001, ****p ≤ 0.0001. Scale bar: 50μm (**A-H**). VZ, ventricular zone.

EdU in cells born at E14.5 exhibited a decrease between cKO and controls in all bins (Figure 2.7. C). Subsequent visualization of cells born at E16.5 revealed a decrease in total co-labeled cells positive for CDP/Cux1 and EdU (Figure 2.7. D), suggesting that these newly born UL CPNs which initially express CDP/Cux1 at birth, may be unable to migrate out of the SVZ. Taken together, these data suggest that UL CPNs are not experiencing a fate change to DL CPNs, but initiate expression of proper layer-specific transcription factors which they fail to maintain over time, as well as a tendency to accumulate in the progenitor domains.

To determine whether the loss of CPN subtype-specific markers was indicative of loss of neuronal identity, I examined the localization of NeuN, a marker for maturing neurons (Mullen et al., 1992) and found no substantial alterations in *Mllt11* cKOs at E16.5 (Figure 2.7. E) or E18.5 (Figure 2.7. F). Consistent with the maintenance of NeuN expression, a qualitative view of staining for GFAP, a marker of radial glial fibres and astrocytes, (Bignami & Dahl, 1977; Kálmán & Hajós, 1989) revealed no apparent drastic changes, demonstrating that these *Mllt11* mutant cortical cells were not experiencing a shift from neuronal to glial identity (Figure 2.7. G). This finding is consistent with the neuronally restricted expression of *Mllt11* (Yamada et al., 2014).

3.6. *Mllt11* Affects the Migration of CPN Progenitors

Given the thinning of the cortex and downward shift of cortical layer markers throughout development, I hypothesized that *Mllt11* may regulate CPN

migration into the CP. To explore this, I pulsed pregnant dams with EdU to label UL CPNs at E14 or E16 and observed the localization of EdU at E18.5. CPNs labeled with EdU at E14 exhibited a severe downward shift of roughly 100μm, consistent with the decrease in cortical thickness. A greater proportion of E14-born CPNs remained restricted to the deeper bins of *Mllt11* cKO cortices relative to controls (Figure 2.8. A). As CPNs labeled with EdU at E16 were still in transit by E18, with only a few control CPNs reaching the outermost layers of the cortex, the discrepancy in UL cell migration was less pronounced in cKOs (Figure 2.8. B). Previously mentioned EdU short pulse experiments at E18.5 also revealed slight increase of EdU+ cells in the deepest 100μm bin of the *Mllt11* mutant cortex relative to controls, possibly reflecting aberrant migration of later born neurons (Figure 2.5. C-D). Overall, the EdU birth dating analysis suggested that *Mllt11* affects the migration, but not neurogenesis, of UL CPNs into the cortical plate.

A complementary approach to identify a role of *Mllt11* in the migration of CPN progenitors into the cortical plate is to observe the impact of its overexpression in the developing fetal brains. Dr. Makiko Yamada, a postdoctoral fellow in the Iulianella lab, therefore used *in utero* electroporation to express a bicistronic vector containing *Mllt11* and *eGFP* cDNAs, or control *eGFP* vector alone, in wild type mouse embryonic forebrains to examine whether overexpression of *Mllt11* is sufficient to promote migration to the superficial regions of the developing cortex. Electroporations were performed in anesthetized, pregnant dams at E13.5 by injecting a DNA solution containing

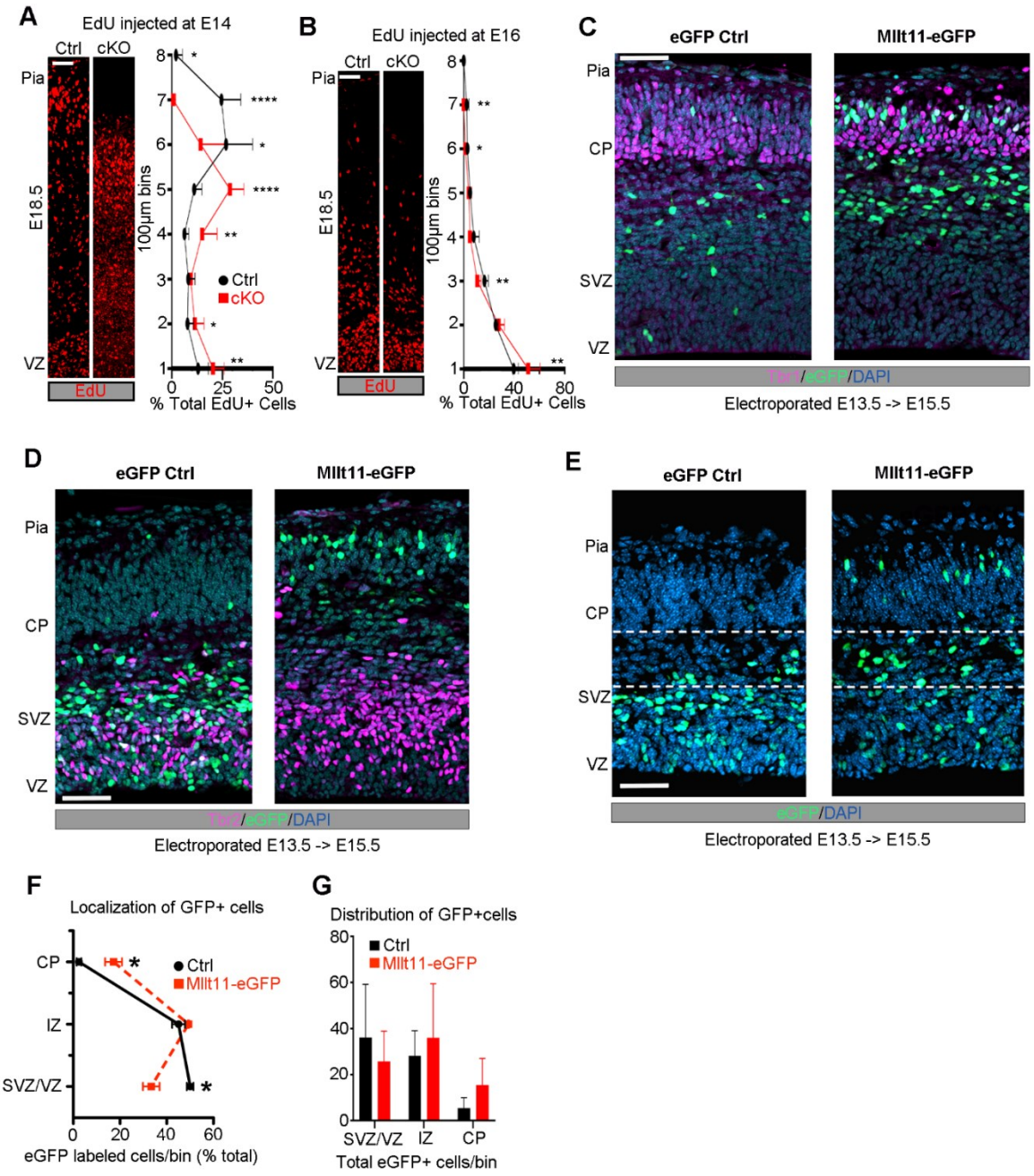
A
EdU injected at E14
Ctrl
cKO
Pia
E18.5
VZ
EdU
100μm bins
Ctrl
cKO
% Total EdU+ Cells
B
EdU injected at E16
C
eGFP Ctrl
Mllt11-eGFP
CP
SVZ
Tbr1/eGFP/DAPI
Electroporated E13.5 -> E15.5
D
E
eGFP/DAPI
F
Localization of GFP+ cells
IZ
SVZ/VZ
eGFP labeled cells/bin (% total)
G
Distribution of GFP+cells
Total eGFP+ cells/bin

Figure 2.8.

Figure 2.8. *Mllt11* Overexpression Promoted Migration into the CP. **A**, **B**, EdU birth dating of UL CPNs by injection at E14 (**A**) showed altered distribution in *Mllt11* cKOs at E18.5, reflecting an apical shift in expression correlating with the decreased cortical thickness. **B**, Apical shift in migrating CPNs in cKOs relative to controls following an EdU pulse at E16 (**B**). **C**, **D**, E15.5 coronal cortical sections after electroporation at E13.5 either with a control *eGFP* (left) or *Mllt11-ires-eGFP* (Mllt11-eGFP) bicistronic plasmid (right). **D**, *Mllt11-eGFP* electroporation promoted migration into the CP, identified by Tbr1 staining. **E**, Control *eGFP* (eGFP-control) electroporated cells remained mostly within the SVZ/VZ, identified by Tbr2 staining. **F**, **G**, Localization of eGFP-control and Mllt11-eGFP+ cells quantified as a percentage of total eGFP+ cells (**F**), and as the distribution of total eGFP+ cells per fetal cortical layer bin (**G**). (**A**) N=4, (**B**) N=3, (**C**-**G**) N=3 *Mllt11-eGFP*, N=4 *eGFP* controls. Data presented as mean ± SD; *p ≤ 0.05. Scale bars: 50μm (**A**-**B**), 25μm (**C**-**E**). CP, cortical plate; IZ intermediate zone; SVZ, subventricular zone; VZ, ventricular zone.

expression vectors unilaterally into forebrain ventricles. The resulting fetal brains were harvested 2 days after, at E15.5, when neurons are migrating into the cortical plate. At E15.5, CPNs overexpressing *Mllt11* localized to the CP, demarcated with staining of Tbr1, a marker of the preplate, an early-born structure which forms the precursor of DL6 (Figure 2.8. C, F, G). GFP-expressing control CPNs localized more closely with Tbr2+ basal progenitors near the IZ (Figure 2.8. D-G), demonstrating that *Mllt11* overexpression is sufficient to promote CPN migration into the developing CP.

Taken together, loss and gain-of-function analyses strongly support a role for *Mllt11* in promoting nascent UL neuronal migration in the developing cortical plate.

The migration of CPN progenitors is facilitated by a meshwork of glial fibres which extend from the VZ towards the pial surface (Campbell & Götz, 2002; Hartfuss et al., 2001; Miyata et al., 2001). These fibres act as tracks for extending neurites, guiding neuronal translocation, and contributing to the meshwork laid down by earlier born progenitors. As such, the orientation of Nestin+ fibres can indicate the direction of migration into the CP (Hartfuss et al., 2001; Miyata et al., 2001). To rule out any possible cell non-autonomous effects of *Mllt11* loss on the migrating scaffold in the developing cortex, analysis of the the Nestin+ glial scaffold of the cortex was performed (Figure 2.9. A-B, F-G, K-L). I found no significant alterations in representative angle (Figure 2.9. C, H, M), density (Figure 2.9. D, I, N, and dispersion (Figure 2.9. E, J, O) of RGC fibres in *Mllt11* cKOs during cortical development. These data suggest that alteration to

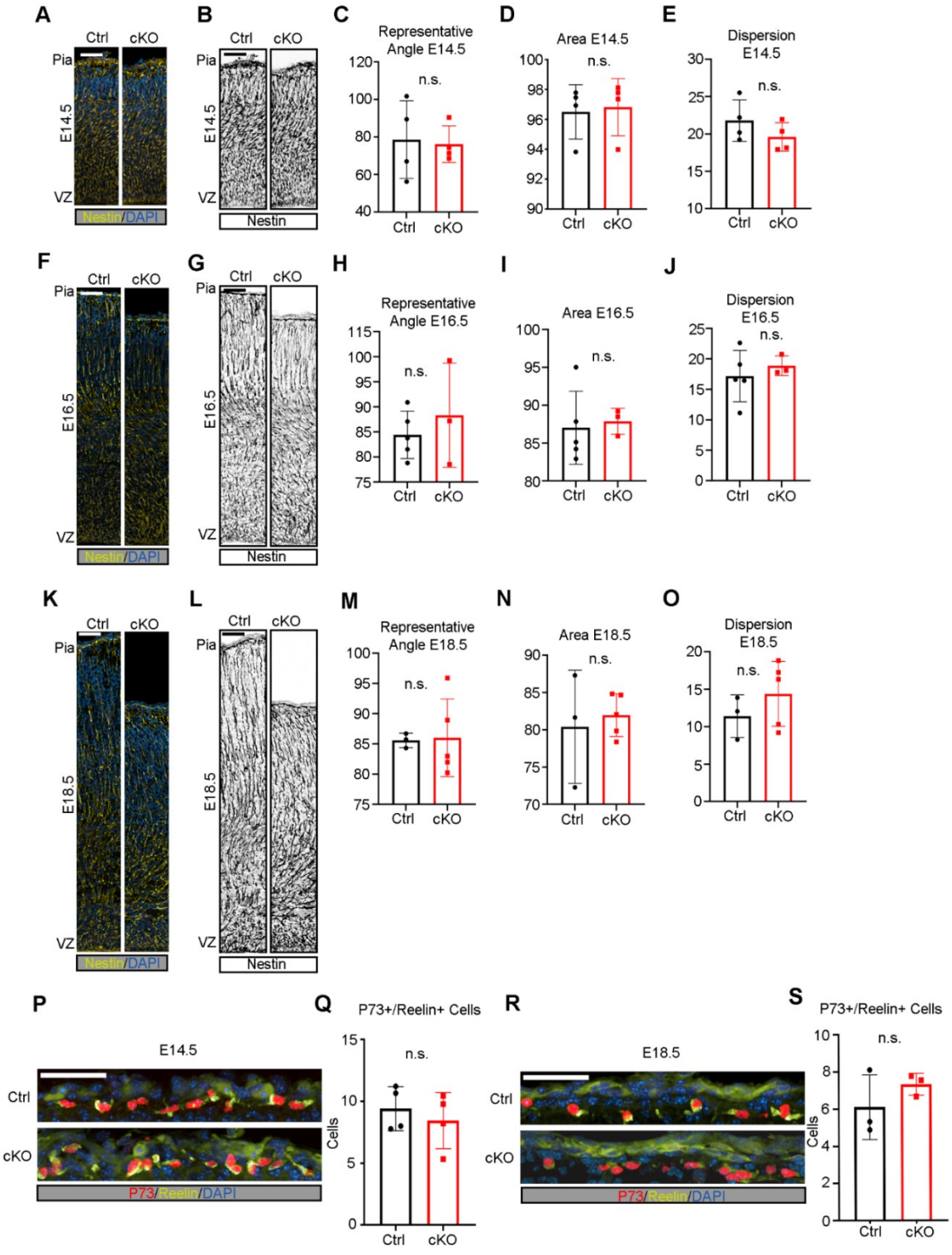
A
Ctrl
cKO
Pia
E14.5
VZ
Nestin/DAPI
B
Ctrl
cKO
Pia
E14.5
VZ
Nestin
C
Representative Angle E14.5
n.s.
120
100
80
60
40
Ctrl
cKO
D
Area E14.5
n.s.
100
98
96
94
92
90
Ctrl
cKO
E
Dispersion E14.5
n.s.
30
25
20
15
10
Ctrl
cKO
F
Ctrl
cKO
Pia
E16.5
VZ
Nestin/DAPI
G
Ctrl
cKO
Pia
E16.5
VZ
Nestin
H
Representative Angle E16.5
n.s.
115
100
95
90
85
80
75
Ctrl
cKO
I
Area E16.5
n.s.
100
95
90
85
80
Ctrl
cKO
J
Dispersion E16.5
n.s.
25
20
15
10
5
0
Ctrl
cKO
K
Ctrl
cKO
Pia
E18.5
VZ
Nestin/DAPI
L
Ctrl
cKO
Pia
E18.5
VZ
Nestin
M
Representative Angle E18.5
n.s.
100
95
90
85
80
75
Ctrl
cKO
N
Area E18.5
n.s.
90
85
80
75
70
Ctrl
cKO
O
Dispersion E18.5
n.s.
20
15
10
5
0
Ctrl
cKO
P
E14.5
Ctrl
cKO
P73/Reelin/DAPI
Q
P73+/Reelin+ Cells
n.s.
15
10
5
0
Cells
Ctrl
cKO
R
E18.5
Ctrl
cKO
P73/Reelin/DAPI
S
P73+/Reelin+ Cells
n.s.
10
8
6
4
2
0
Cells
Ctrl
cKO

Figure 2.9.

Figure 2.9. Cortical Radial Glia Were Unaltered in *Mllt11* cKOs. **A**, **B**, Cortical slices at E14.5 stained for Nestin (**A**) and black and white traces of Nestin fibres (**B**). **C**, **D**, **E**, analyses of Nestin staining in E14.5 cortical slices exhibit no significant differences in representative angle (**C**), area (**D**), and dispersion (**E**) in cKOs compared to controls. **F**, **G**, Cortical slices at E16.5 stained for Nestin (**F**) and black and white traces of Nestin fibres (**G**)**. H**, **I**, **J**, analyses of Nestin staining in E16.5 cortical slices exhibit no significant differences in representative angle (**H**), area (**I**), and dispersion (**J**) in cKOs compared to controls. **K**, **L**, Cortical slices at E16.5 stained for Nestin (**K**) and black and white traces of Nestin fibres (**L**)**. K**, **L**, **M**, analyses of Nestin staining in E16.5 cortical slices exhibit no significant differences in representative angle (**K**), area (**L**), and dispersion (**M**) in cKOs compared to controls. **P**, **Q**, Pial staining for P73 and Reelin at E14.5 (**P**) revealed no differences in CR cell numbers (**Q**). **R**, **S**, Pial staining for P73 and Reelin at E18.5 (**R**) revealed no differences in CR cell numbers (**S**). (**A**-**E**, **P**-**Q**) N=4, (**F**-**J**) N=5, (**K**-**O**, **R**-**S**) N=3. Data presented as mean ± SD; n.s., not significant. Scale bars: 50μm. VZ, ventricular zone.

the GFAP+ radial glial fibre meshwork does not underlie the migration deficienc exhibited by *Mllt11* cKOs.

In addition to the radial glial fibre substratum along which nascent neurons migrate, guidance of migratory CPNs is dependent on the earliest born CR cells of L1, which secrete Reelin to attract and halt neuronal migration at the pial interface (Hirota & Nakajima, 2017; Tueting et al., 1999). To determine if malformation of L1 of the cortex gave rise to this migration phenotype, analysis of CR cells was performed. However, there were no differences in the expression of CR markers p73 or Reelin at E14.5 (Figure 2.9. P-Q) or E18.5 (Figure 2.9. R-S) following *Mllt11* loss in UL progenitors and nascent neurons. Altogether, these findings demonstrate that the aberrant migration of UL CPNs in *Mllt11* mutants was not caused by alterations in the development of Reelin-secreting CR cells, nor abnormalities in radial glial fibre scaffold. Rather, *Mllt11* seems to be required cell autonomously to promote invasiveness of nascent neurons into the developing cortical plate.

3.7. Discussion

The main objectives of the experiments described in this section were to identify the spatiotemporal expression profile of *Mllt11*, generate a model in which to study its role in cortical development, provide an initial phenotypic description of the *Mllt11* cKO, and identify potential functions of *Mllt11* in cortical development through identification of developmental deficits in its absence. The expression pattern of β-gal in the targeted *Mllt11* allele confirmed that it is

normally expressed only within the developing CNS, with the highest levels reflecting UL cortical neurogenesis. Using the *Cux2*^{IREScre} driver to excise *Mllt11* in developing UL CPNs, I revealed a role for *Mllt11* in the development and maintenance of transcriptionally distinct cortical layers as well as their ability to migrate to their appropriate laminar location. Consistent with this expression profile and role in cortical lamination, I also showed that *Mllt11* is required for proper migration but not neurogenesis of UL CPNs. I also characterized a severe dysplasia of CPNs in *Mllt11* cKO mutant neonatal brains; a phenotype found in severe neurodevelopmental disorders such as ASD and Fragile X-associated tremor ataxia syndrome with which *Mllt11* dysregulation has been associated (Drozd et al., 2019; Xu et al., 2016). *Mllt11* cKOs appear largely normal during development and at birth. They exhibit a progressive thinning of cortex and altered distribution of CPNs, as well as improper segregation of cells expressing specific layer markers within the cortex. The observed cortical thinning seems to be largely due to a migratory defect, which limits the ability of CPNs lacking *Mllt11* to reach their proper laminar location. Furthermore, *Mllt11* conditional mutants did not largely affect the formation of Reelin+ CR cells nor radial glial scaffolding, both of which are crucial for guiding the migration of CPNs. Conversely, it has been shown that loss of *Mllt11* leads to a reduction of Reelin+/P73+ cells emanating from the cortical hem during embryogenesis, however this effect does not seem to impact the pial surface (unpublished, Iulianella lab). These results suggests that *Mllt11* loss acted cell-autonomously to hinder radial migration of CPN progenitors into the CP.

Additionally, *Mllt11* cKOs exhibited a decreased capacity to maintain expression of transcriptional programs characteristic of UL CPNs. The initiation of these programs was properly executed, evidenced by their expression at early developmental time points, but there was a marked decrease over the course of development. Loss of *Mllt11* from the superficial cortex altered levels of UL2/3-specific transcription factors Satb2 and CDP/Cux1, which function in establishment and maintenance of the CC as well as mature arborescent neuronal morphology and somal packing. Importantly, the loss of layer-specific identity has been demonstrated in postmortem brain tissue from autistic humans (Casanova et al., 2013; Fujimoto et al., 2021; Stoner et al., 2014). It is presently unclear whether the loss of UL-specific gene expression exhibited by *Mllt11* mutants, is primarily the result of uncharacterized gene expression pathways functioning downstream of *Mllt11*, or other reasons to be explored henceforth.

Consistent with the impact of *Mllt11* loss on radial migration of cortical neurons, I showed that the overexpression of *Mllt11* promotes increased migration into the CP. This finding is also consistent with *in vitro* studies demonstrating that the overexpression of *Mllt11* in cancer stem cell lines promotes proliferation and invasiveness (Tse et al., 2017), and an increased tendency to reorganize the microtubule skeleton to form Tuj1/Tubb3-enriched projections much like an axon, upon overexpression of *Mllt11* in Hek293 cells (Lin et al., 2004b). Taken together these data suggest that a cytoskeletal regulatory function involved in projection or maintenance of processes may be at play. This will be the topic of the subsequent chapter.

CHAPTER 4. Mllt11 Interacts With the Microtubule Cytoskeleton, and Regulates Formation of CPN Morphology and WM Tracts

4.1. Introduction

There is a vast body of evidence linking the role of the cytoskeleton to functional and morphological outcomes of developing cells, such as packing density, migration, and neurite extension (Dent et al., 2011; Ofek et al., 2009; Schaar & McConnell, 2005). The cytoskeleton underlies the morphology, motility, and function of a neuron in a number of ways, by providing scaffolding for signaling and regulatory components, anchoring and protection of organelles, structural integrity and support, and by providing a series of tracts along which intracellular cargo can be trafficked and transported as needed (Koizumi & Gleeson, 2009; Nirschl et al., 2017; Shafrir et al., 2000; Vessey & Karra, 2007). Among these cargos are mitochondria necessary to meet local energy demands, mRNA transcripts contained within RNP granules for local translation and protein synthesis, and additional cytoskeletal components required for growth, repair, or reinforcement (Cioni et al., 2019; Nabariya et al., 2022; Rangaraju et al., 2019). Additionally, more specialized, neuronal-specific components, such as synaptic machinery or signaling receptors that allow the cell to respond to growth or migration cues, also require trafficking to their respective cellular compartments (Cai & Sheng, 2009; Herbst & Martin, 2017). Each of these functions and processes is mediated by coordination and organization of the cytoskeleton.

In the context of a neuron, the cytoskeleton and its interacting associated proteins also serve to organize the cell into discrete functional domains; the

axonal compartment, comprised of the axon, and somatodendritic compartment, consisting of the soma and dendrites, (Kapitein & Hoogenraad, 2011). This bipolar organization allows for the spatial segregation of components required for the transmission of electrical signals in the form of an action potential, which occurs as postsynaptic structures in the dendritic or somatic compartments are stimulated by presynaptic components localized to the axon of the presynaptic cell, allowing for a propagation of information from one cell to the next (Barnett & Larkman, 2007; Magura, 1968). Axons project from the soma as tubulin dimers polymerize and link together to form microtubules; rigid yet flexible molecules which are the largest cytoskeletal structures and main source of structural integrity of the axon. Microtubules interact with numerous associated proteins to facilitate trafficking of materials to and from the soma, making long-range transport of cellular components possible. In the somatodendritic compartment, bidirectional polymerization of microtubules creates cellular protrusions which are typically shorter and more branched than the axonal compartment (Delandre et al., 2016; Dent, 2017). In both the axonal and somatodendritic compartments, microtubules interact with a host of region-specific scaffold and structural proteins which allow for the formation of actin complexes, enabling steering at the most peripheral region of the axon, the growth cone, during axonal development, as well as the development of dendritic spines (Dent, 2017; Kahn & Baas, 2016).

Within the greater context of the brain, individual axons fasciculate to form cohesive WM tracts which serve to connect various brain regions. Among the

most notable WM tracts of the cerebral cortex are the CC, EC, and IC. The CC bridges communication between the left and right hemispheres and is primarily comprised of connections between UL2/3 CPNs. The IC and EC, which infiltrate and surround the striatum respectively, are primarily comprised of connections between DL neurons and more basal structures, such as the basal ganglia and eventually the spinal cord, forming a conduit for connectivity between pallial and subpallial regions (Biswas et al., 2022).

As previously stated, *Mllt11* cKOs exhibited a decreased cortical thickness, which was apparently due in part to a decreased thickness of the WM tracts beneath the cortical plate formed by projections of CPNs within the developing cortex. Both the decreased thickness of the cortical plate and WM, as well as the apparent retention of UL CPNs and their progenitors in deeper layers of the CP was consistent with the migratory deficit exhibited by knockouts as they began to invade the developing CP. The commonality underlying both the formation of WM tracts and migration of neurons to invade the CP is the cytoskeleton. This chapter will focus primarily on exploring the underlying cytoskeletal mechanism through which *Mllt11* loss impacts CP thickness, WM thickness, and the migration of CPNs into the CP.

4.2. Mllt11 Interacts with Cytoskeletal Proteins

Birth dating analyses coupled with the observation that UL CPN-specific marker expression was properly initiated in cKOs, suggest that the migratory defects observed in *Mllt11* cKOs are likely independent of the maintenance of UL

transcriptional programs. To identify potential pathways through which Mllt11 might be exerting its effects on CPN migration, Karolynn Hsu, a member of the Iulianella lab, performed a GST pulldown assay to identify interacting proteins using cortical lysate from E18.5 brains. Potential Mllt11-interacting proteins are listed in Table 1 and include multiple α and β tubulin isoforms (> 70% coverage) as well several atypical myosins, such as Myosin 5a (Myo5a, 36%), Myosin 9 (Myh9, 24%) and Myosin 10 (Myh10, 8%). A potential association between Mllt11 and tubulin is consistent with a recent whole cell proteomic study, which identified Mllt11 as a likely interactor of both α- and β-tubulins (Go et al., 2021). Given that acetylation of α-tubulin is associated with stabilized microtubules and is crucial for outgrowth of stable neurites, I decided to focus on validating interactions between Mllt11 and acetylated α-tubulin by immunoprecipitation analysis. Myc-tagged *Mllt11* was overexpressed in Hek293 cells and co-IP experiments were performed. α-tubulin was pulled down (Figure 3.1. A) and probing the blots with anti-Mllt11 antibodies confirmed this interaction was dependent on heterologous Mllt11 expression in the cells (Figure 3.1. B), validating an association between Mllt11 and tubulin isoforms. This agrees with a study identifying possible microtubule interactions with Mllt11 (Go et al., 2021).

Because the microtubule cytoskeleton is crucial for neurite growth, development, and stability, I sought to evaluate whether Mllt11 localized to growing neurites. ICC was used to probe the subcellular distribution of Mllt11, Tuj1/Tubb3, and α-tubulin in cultures of primary fetal cortical neurons. Cortical neurons were extracted from wild type C57BL/6 embryos at E18.5 and cultured

Band	Accession	Description	Sum PEP Score	Coverage [%]	# Peptides	# PSMs	# AAs	MW [kDa]	Reference
7	D3Z4J3	Unconventional myosin-Va (Myo5a)	201.776	36	53	240	1855	215.4	
7	Q8VDD5	Myosin-9 (Myh9)	181.542	24	36	142	1960	226.2	
6	Q3UH59	Myosin-10 (Myh10)	31.272	8	10	22	2013	233.3	
5	P63017	Heat shock cognate 71 kDa protein OS=Mus musculus OX=10090 GN=Hspa8 PE=1 SV=1	199.247	59	32	303	646	70.8	Li et al., 2014
5	P38647	Stress-70 protein, mitochondrial (Hspa9)	20.395	12	6	12	679	73.4	
5	P20029	Endoplasmic reticulum chaperone BiP (Hspa5)	23.74	10	5	50	655	72.4	
5	Q3THK7	GMP synthase [glutamine-hydrolyzing] (Gmps)	8.67	5	3	6	693	76.7	
5	O08553	Dihydropyrimidinase-related protein 2 OS=Mus musculus OX=10090 GN=Dpysl2 PE=1 SV=2	12.297	15	4	7	572	62.2	
4	Q9CWF2	Tubulin beta-2B chain (Tubb2b)	381.396	74	29	1338	445	49.9	
4	Q7TMM9	Tubulin beta-2A chain (Tubb2a)	380.755	74	29	1340	445	49.9	
4	P99024	Tubulin beta-5 chain (Tubb5)	369.155	74	29	1232	444	49.6	
4	P68372	Tubulin beta-4B chain (Tubb4b)	365.578	74	29	1153	445	49.8	
4	Q9ERD7	Tubulin beta-3 chain (Tubb3)	347.246	72	28	970	450	50.4	
4	Q9D6F9	Tubulin beta-4A chain (Tubb4a)	324.979	73	27	993	444	49.6	Go et al., 2021
4	P68369	Tubulin alpha-1A chain (Tuba1a)	255.603	66	27	557	451	50.1	Go et al., 2021
4	P05213	Tubulin alpha-1B chain (Tuba1b)	241.479	66	26	519	451	50.1	
4	Q922F4	Tubulin beta-6 chain (Tubb6)	176.166	40	17	444	447	50.1	
4	P10126	Elongation factor 1-alpha 1 (Eef1a1)	74.451	37	10	62	462	50.1	
4	A2AQ07	Tubulin beta-1 chain (Tubb1)	54.274	13	7	202	451	50.4	
4	Q9D8N0	Elongation factor 1-gamma (Eef1g)	27.863	20	6	14	437	50	
4	Q3UX10	Tubulin alpha chain-like 3 (Tubal3)	30.405	8	4	89	446	50	
3	Q9CWF2	Tubulin beta-2B chain (Tubb2b)	239.301	71	24	304	445	49.9	
3	P99024	Tubulin beta-5 chain (Tubb5)	214.778	71	24	324	444	49.6	
3	Q9D8N0	Elongation factor 1-gamma (Eef1g)	193.321	65	23	324	437	50	
3	P10126	Elongation factor 1-alpha 1 (Eef1a1)	202.141	56	21	542	462	50.1	
3	Q9ERD7	Tubulin beta-3 chain (Tubb3)	158.874	64	21	199	450	50.4	
3	P68369	Tubulin alpha-1A chain (Tuba1a)	188.056	64	20	177	451	50.1	Go et al., 2021
3	P05213	Tubulin alpha-1B chain (Tuba1b)	178.724	64	20	169	451	50.1	
3	Q9D6F9	Tubulin beta-4A chain (Tubb4a)	170.961	54	19	253	444	49.6	Go et al., 2021
3	P62631	Elongation factor 1-alpha 2 (Eef1a2)	50.614	28	9	259	463	50.4	
3	Q8BFR5	Elongation factor Tu, mitochondrial (Tufm)	39.656	32	9	28	452	49.5	
3	P60710	Actin, cytoplasmic 1 (Actb)	41.856	31	7	24	375	41.7	
3	P17182	Alpha-enolase (Eno1)	27.891	24	7	12	434	47.1	
3	P62737	Actin, aortic smooth muscle (Acta2)	24.601	16	5	16	377	42	
3	Q3UX10	Tubulin alpha chain-like 3 (Tubal3)	19.056	8	4	36	446	50	
3	P10637-3	Isoform Tau-B of Microtubule-associated protein tau (Mapt)	14.659	14	4	17	364	38.2	
2	Custom-P97783	Protein AF1q (Mllt11)	298.867	89	35	1363	320	36.7	

Table 1.1. Potential Mllt11 Interaction Targets From GST Pulldowns in E18.5 Whole Brain Lysates

for 24 hours or 1 week, then immunostained to reveal the localization of Tuj1/Tubb3, acetylated α-tubulin, and Mllt11. After 24 hours *in vitro*, corresponding to the extension of a primary neurite, Mllt11/Tubb3 colocalized in discrete punctate patterns in varicosities along the distal portion of the developing neurite (Figure 3.1. C), as well as in the growth cone (Figure 3.1. c') with limited overlap in the soma (Figure 3.1. C). At this early stage of axonogenesis, the distal axon contains a plethora of machinery required to support the energetic, translational, signal-transductional, and structural needs of the growth cone as it steers axonal growth, indicating that Mllt11 may be involved in one or more of these processes.

After 1 week in culture, neurons displayed a more elaborate neurite arborization pattern, and acetylated α-tubulin and Mllt11 were both detected along the proximal portion of neurites (Figure 3.1. D). At this later stage of neurite development, axonal microtubules exhibit a higher degree of stabilization and increased structural integrity conferred by acetylation of α-tubulin. I next evaluated microtubule levels in the CC of Mllt11 mutants and found that both Tuj1/Tubb3 and acetylated α-tubulin staining was reduced in cKOs at E18.5, reflecting reduced axonal targeting to the midline in mutants (Figure 3.1. E). In summary, Mllt11 expression displayed a high degree of overlap with acetylated α- and β-tubulin isoforms differentially over neurite development, consistent with a role in neurite development that is potentially dynamic in its function over developmental time.

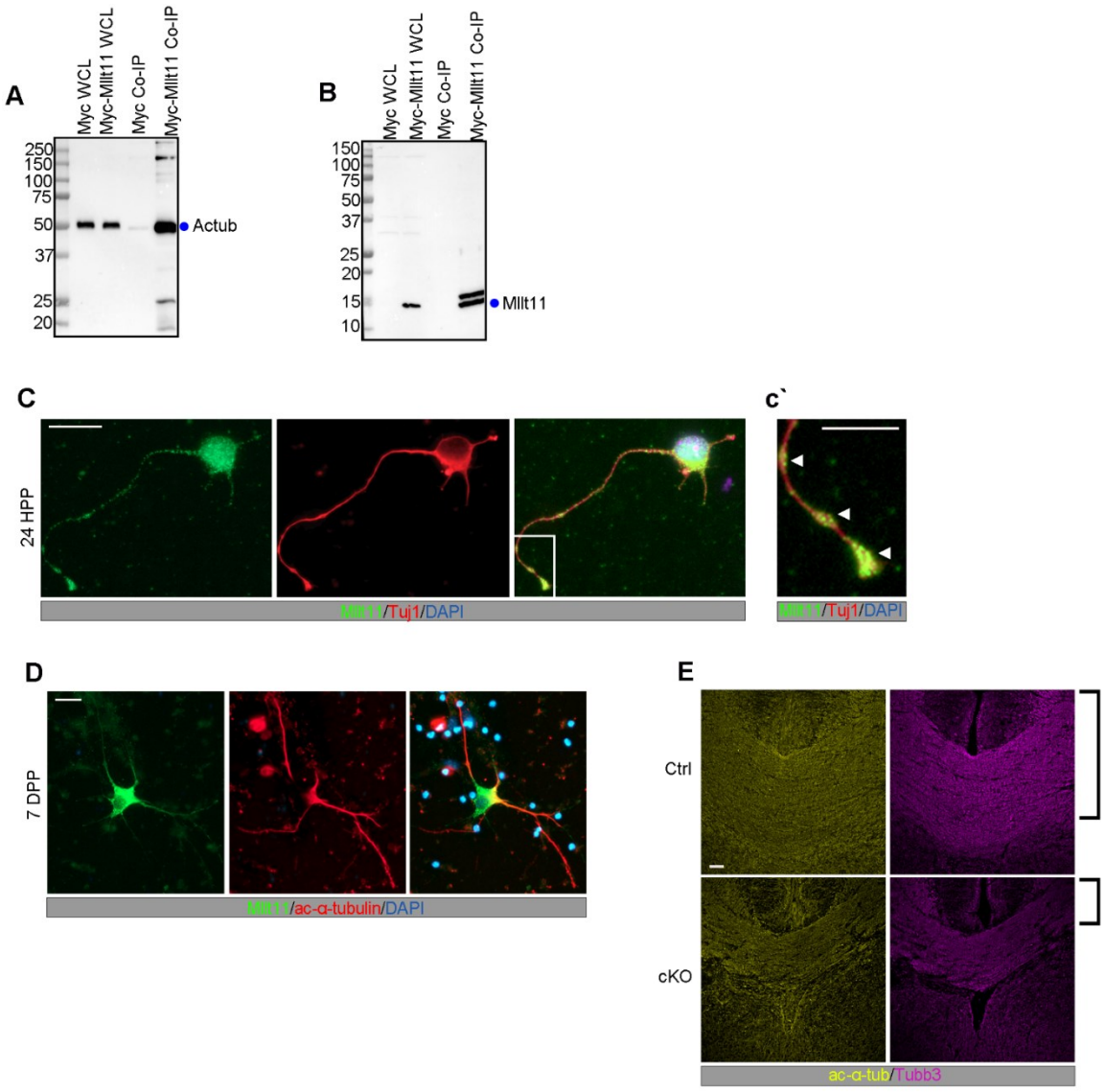
A
Myc WCL
Myc-Mllt11 WCL
Myc Co-IP
Myc-Mllt11 Co-IP
250
150
100
75
50
37
25
20
Actub
B
Myc WCL
Myc-Mllt11 WCL
Myc Co-IP
Myc-Mllt11 Co-IP
150
100
75
50
37
25
20
15
10
Mllt11
C
24 HPP
Mllt11/Tuj1/DAPI
c`
Mllt11/Tuj1/DAPI
D
7 DPP
Mllt11/ac-α-tubulin/DAPI
E
Ctrl
cKO
ac-α-tub/Tubb3

Figure 3.1.

Figure 3.1. Mllt11 Associated and Colocalized With Acetylated α-tubulin in Growing Neurites. **A**, Co-IP of acetylated α-tubulin (Actub) with Myc-tagged Mllt11 in whole cell lysates of HEK293 cells compared with a myc control. **B**, Co-IP probed with Mllt11 antibody showing immunoprecipitated (IP) signal restricted to lanes containing Mllt11. **C**, **D**, Primary cortical neurons cultured for 24 h (**C**) or 7 d (**D**) post-plating. **C**, After 24 h, Mllt11 colocalizes with Tuj1/Tubb3 in the growth cone and at swellings along the distal axon as indicated by arrowheads (**c'**), and in the soma (**C**). After 7 d, Mllt11 was primarily found along proximal portions of the axon where it colocalizes with acetylated α-tubulin (**D**). **E**, Coronal sections of the CC at E18.5 labeled with acetylated α-tubulin and Tubb3. Brackets show decreased thickness in cKO compared with control. (**A**-**B**) N=4. Scale bar: 20μm (**C**, **D**) and 50μm (**E**). cc; corpus callosum, WCL; whole cell lysate.

4.3. Mllt11 is Required for Neurite Outgrowth

The relationship between stabilized and dynamic forms of tubulin has been shown to regulate the migratory potential of neurons as well as neurite extension because of the cycling of microtubule severing during outgrowth (Wei et al., 2018; Lin & Smith, 2015; Sudo & Baas, 2010). If *Mllt11* loss affected the relative amounts of stabilized microtubules, one would expect to see significant changes in neurite morphogenesis of UL neurons. I therefore evaluated the morphology of cultured primary cortical neurons from *Mllt11* cKO mutants. I took advantage of the Ai9 *TdTomato* reporter introduced into the *Cux2*$^{IREScre/+}$*;Mllt11*$^{Flox/Flox}$ conditional mouse to efficiently label and isolate UL primary neurons in culture. Primary neurons were visualized at two stages, one early, and one late in neurite development to elucidate any trends in localization indicative of a particular regulatory role. Early in neuritogenesis, within the first 24 hours, neurons exhibit a uni- or bipolar morphology, with one primary neurite, likely a putative axon, extending from the soma, along with the presence of a number of shorter neurites extending dynamically. In the following days, the shorter neurites develop into more complex and arborescent dendrites (Dotti et al., 1988; Sahu et al., 2019). After 24 hours *in vitro*, the length of MAP2+ primary neurites was reduced in cKOs compared with controls (Figure 3.2. A-B), as was the total length of all neurites (Figure 3.2. C). Moreover, the proportion of total length of extended neurites represented by the primary neurite at 24 hours was slightly increased in cKOs (Figure 3.2. D). Quantification of the average number of neurites per neuron revealed a significant decrease in cKOs compared to

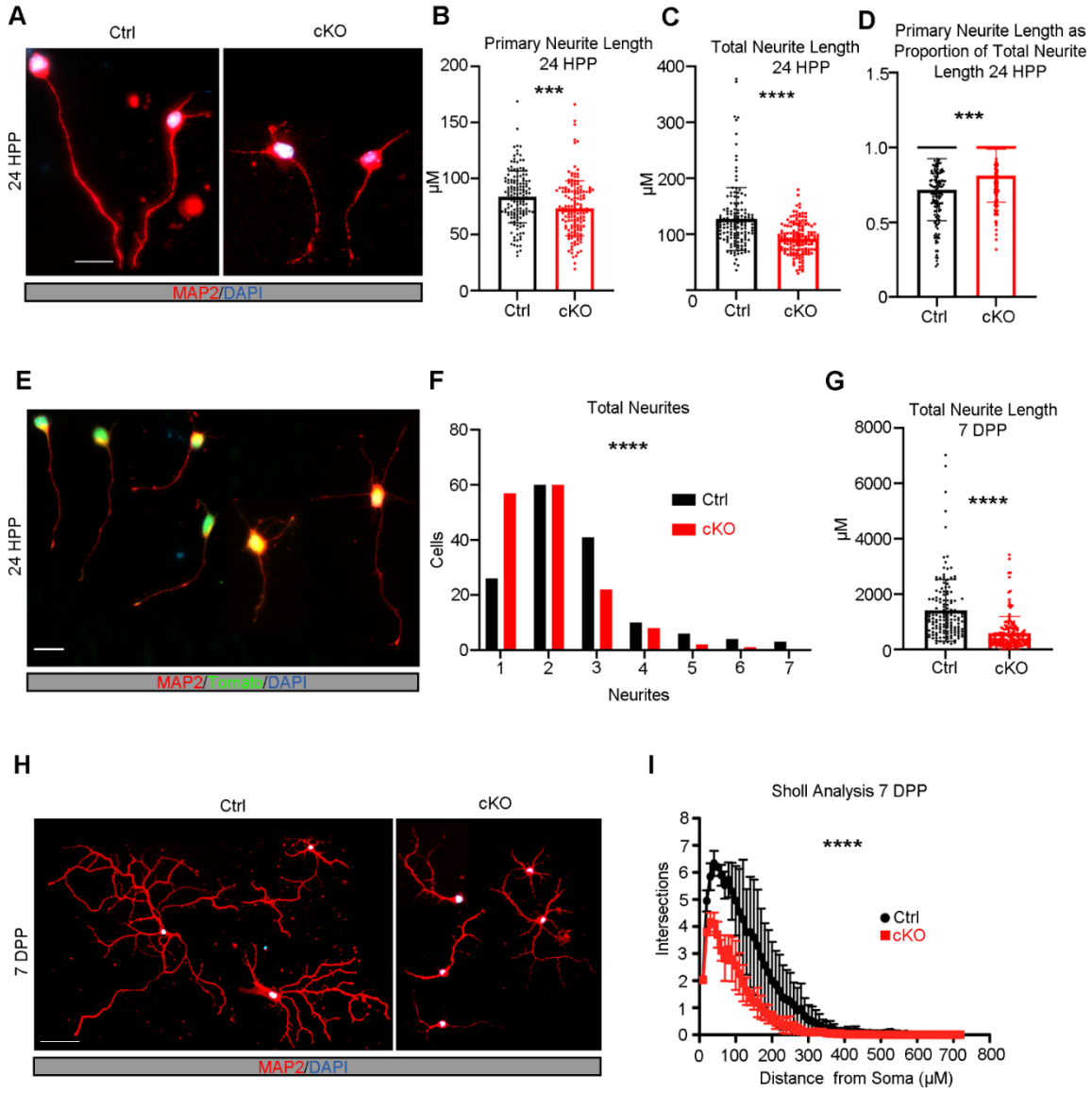
A
Ctrl
cKO
24 HPP
MAP2/DAPI
B
Primary Neurite Length
24 HPP
***
µM
Ctrl
cKO
C
Total Neurite Length
24 HPP
****
µM
Ctrl
cKO
D
Primary Neurite Length as
Proportion of Total Neurite
Length 24 HPP
***
Ctrl
cKO
E
24 HPP
MAP2/Tomato/DAPI
F
Total Neurites
****
Ctrl
cKO
Cells
Neurites
G
Total Neurite Length
7 DPP
****
µM
Ctrl
cKO
H
Ctrl
cKO
7 DPP
MAP2/DAPI
I
Sholl Analysis 7 DPP
****
Ctrl
cKO
Intersections
Distance from Soma (µM)

Figure 3.2.

Figure 3.2. *Mllt11* Loss Decreased Neurite Outgrowth and Branching Complexity *in vitro*. **A**, Primary cortical neurons derived from E18.5 brains cultured for 24 h post-plating. Neurites identified with MAP2 staining. **B**, **C**, 24 hours post-plating, primary neurite length (**B**) and total neurite length (**C**) were significantly decreased in cKO neurons relative to controls (**D**). The proportion of total primary neurite length was significantly increased in cKO neurons relative to controls. **E**, Examples of neuronal morphologies with varying numbers of neurites 24 hours post-plating. **F**, Quantification of number of neurites per neuron 24 hours post-plating, where cKO neurons had significantly fewer neurites compared with controls. **G**-**I**, Quantification of decreases in total neurite length (**G**) and branching complexity (**I**) of cKO relative to control primary cortical neurons cultured for 7 days post-plating (**H**). N=150 neurons (50 neurons/individual x 3 individuals). Data presented as mean ± SD; *p ≤ 0.05, **p ≤ 0.01, ***p ≤ 0.001, ****p ≤ 0.0001. Scale bar: 20μm (**A**, **E**) and 50μm (**H**). HPP, hours post-plating; DPP, days post-plating.

controls (Figure 3.2. E-F), further suggesting that neurite outgrowth was impaired on *Mllt11* loss.

After 1 week of culture *in vitro*, the total neurite length was drastically reduced in cKO CPNs (Figure 3.2. G-H). Since *Mllt11* loss progressively attenuated primary neurite outgrowth in cultured primary UL CPNs, I next evaluated a requirement for Mllt11 in the elaboration of dendritic arborization patterns in cultured CPNs. An advantage of using cultured neurons is that they are free of apical and basal contacts and their density and sparsity can be controlled, allowing for better visualization of neurites radiating uniformly from the soma and evaluation of dendritic complexity by Sholl analysis (O'Neill et al., 2015; van Niekerk et al., 2022). *Mllt11* mutant primary neurons displayed much less complexity in the branching of their neurites (Figure 3.2. H-I), thus *Mllt11* loss greatly impacted the arborization patterns of cultured UL CPNs.

Given the limitations of 2-dimensional *in vitro* culturing methods, as well as the vast array of morphological growth and pruning in early perinatal development, I wanted to assess the requirement of Mllt11 function in the morphology of UL CPNs *in vivo* at a time when mature arborization patterns have fully developed. Golgi staining was performed on *Mllt11* cKO and control brains harvested at P28 to capture mature CPN morphologies. While control UL CPNs displayed complex dendritic morphologies typical of cortical pyramidal neurons (Figure 3.3. a-d), UL CPNs of *Mllt11* cKOs displayed greatly attenuated dendritic morphologies (Figure 3.3. a'-d'). *Mllt11* cKOs also exhibited a severe decrease in total neurite length in UL2/3 CPNs relative to controls (Figure 3.3. B). The extent

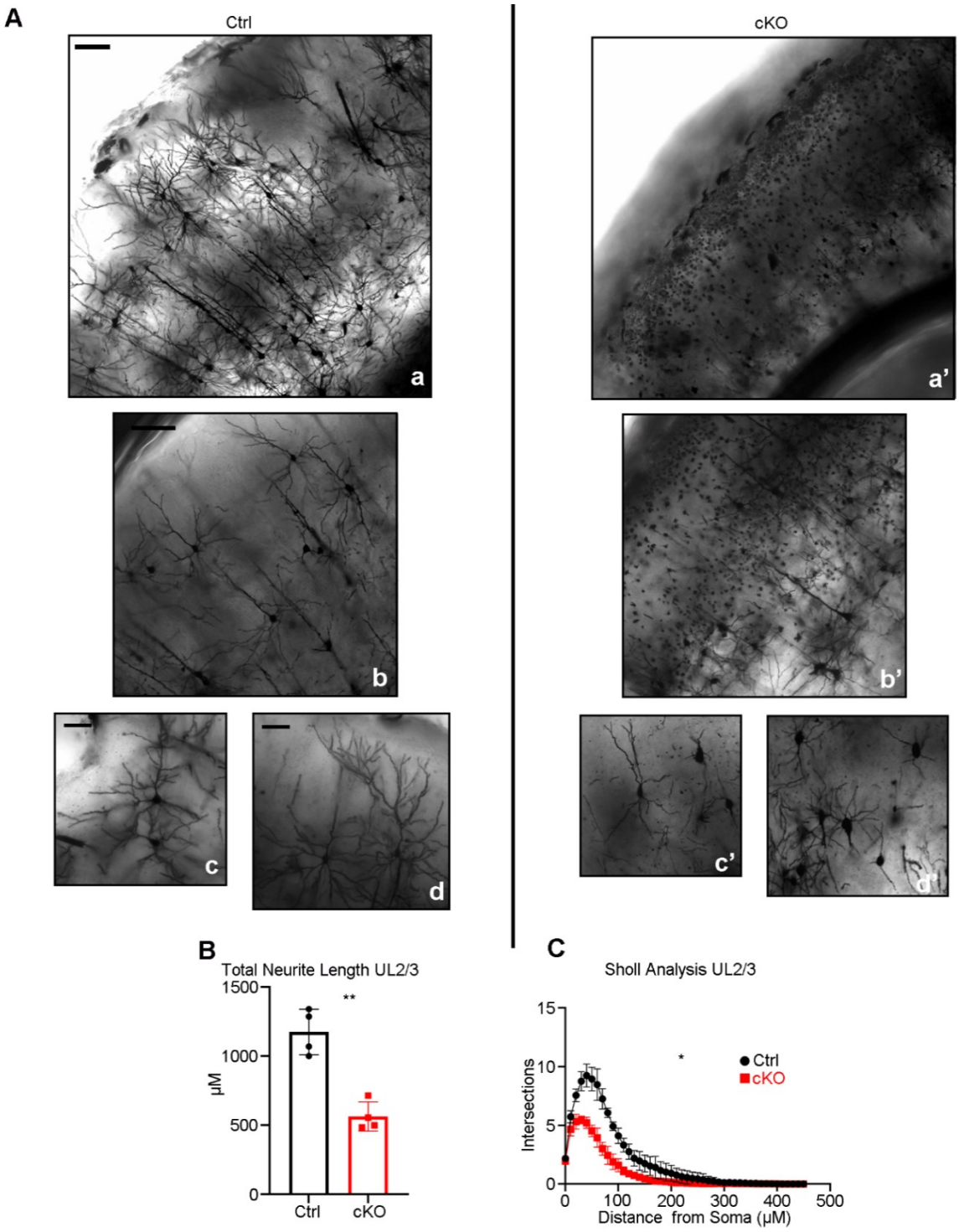
A
Ctrl
cKO
a
a'
b
b'
c
c'
d
d'
B
Total Neurite Length UL2/3
1500
1000
500
0
µM
**
Ctrl
cKO
C
Sholl Analysis UL2/3
15
10
5
0
Intersections
*
Ctrl
cKO
0
100
200
300
400
500
Distance from Soma (µM)

Figure 3.3.

Figure 3.3. Decreased Neurite Outgrowth and Branching Complexity in UL CPNs in the *Mllt11* cKO cortex. **A**, Corresponding 100× (**Aa**, **Aa'**) and 200× (**Ab–Ad'**) magnification images of coronal sections of P28 Golgi-stained control (**Aa–Ad**) and *Mllt11* cKO cortices (**Aa'–Ad'**). **B**, **C**, Quantification of neurite length (**B**) and branching complexity (**C**) within UL2/3 showed reduced neurite length and branching complexity in cKOs compared with controls. N=120 neurons (30 neurons/individual x four individuals). Data presented as mean ± SD; *p ≤ 0.05, **p ≤ 0.01. Scale bar: 100μm (**Aa**, **Aa'**) and 50μm (**Ab–Ad'**).

of the decrease of neurite arborization *in vivo* was similar to that observed in cultured primary neurons. Sholl analysis revealed that the overall neuronal morphology was also much less complex, with less elaborately-branched neurites in *Mllt11* cKO UL CPNs compared to controls (Figure 3.3. C). Taken together, these findings confirmed a critical requirement of Mllt11 in the growth of neurites and in the elaboration of the mature projection neuron morphology in the superficial cortex.

4.4. *Mllt11* Loss Leads to Reduced Callosal Crossing Fibres and Thinning of Cortical WM Tracts

Given that a reduction in UL CPNs and their altered morphology and decreased capacity to extend and develop arborescent neurites would largely affect interhemispheric projections (Aboitiz & Montiel, 2003; Alcamo et al., 2008; Fame et al., 2011), I next examined whether *Mllt11* loss impacted formation of projection fibres contributing to the cortical WM tracts by staining for Neurofilament (NF), a neuronally-restricted intermediate filament protein enriched in axons (Yuan et al., 2012), in coronal brain slices. I observed notable decreases in the thickness of NF+ axonal fibres in the cortical WM tract and in the proportion of the cortex containing WM between E16.5 (Figure 3.4. A-D) and E18.5 (Figure 3.4. E-H) following *Mllt11* loss. Importantly, while NF+ fibre staining in the CC was greatly reduced in *Mllt11* cKOs at E18.5, NF+ fibres in the IC, reflecting corticothalamic projections, remained unchanged in the mutant brains (Figure 3.4. I, Crespo et al., 2022). Taken together, our findings revealed a

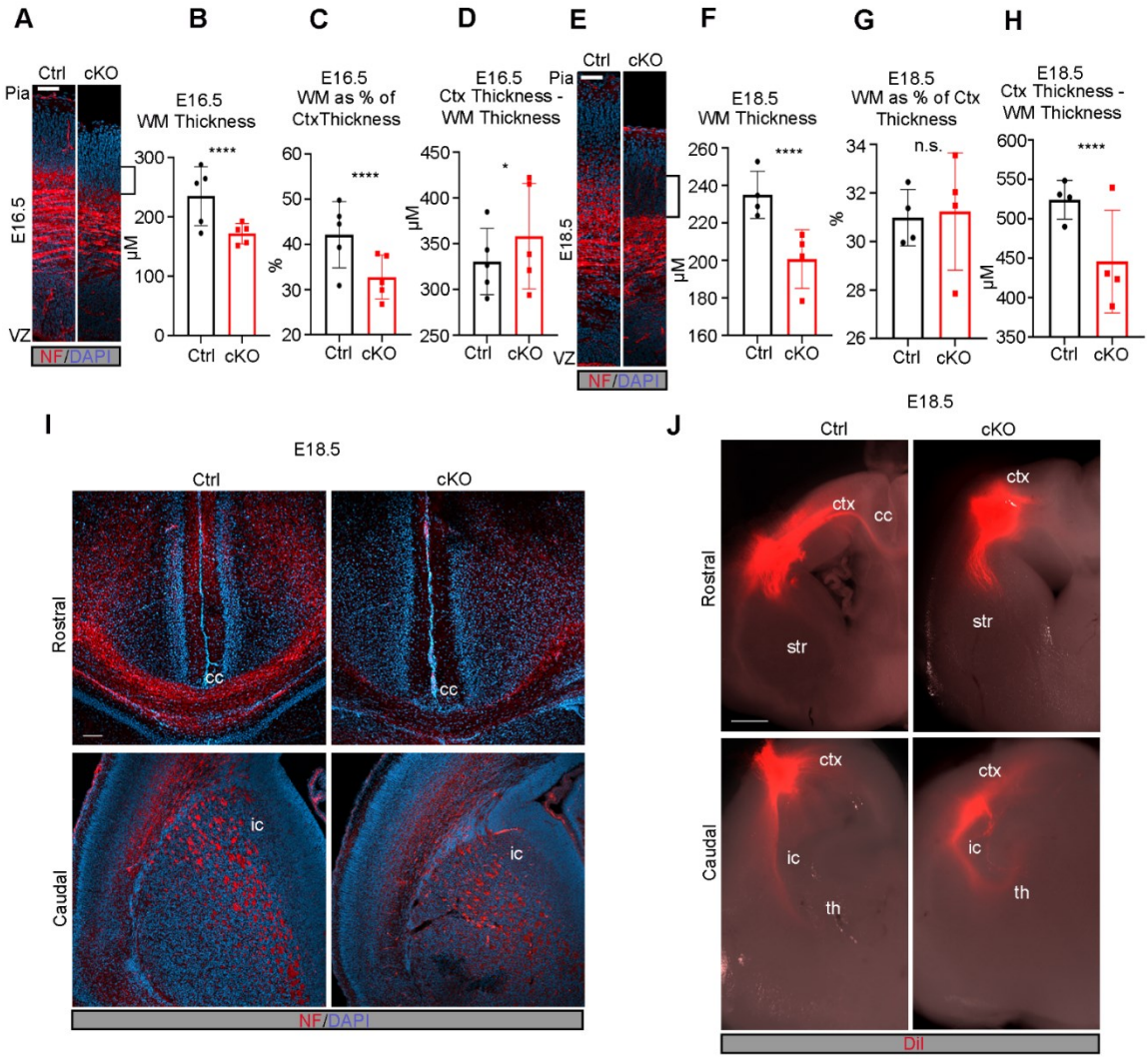
A
B
C
D
E
F
G
H
Ctrl
cKO
Pia
E16.5
VZ
NF/DAPI
E16.5
WM Thickness
E16.5
WM as % of
CtxThickness
E16.5
Ctx Thickness -
WM Thickness
E18.5
E18.5
WM Thickness
E18.5
WM as % of Ctx
Thickness
E18.5
Ctx Thickness -
WM Thickness
μM
%
****
*
n.s.
I
J
Rostral
Caudal
cc
ic
ctx
str
th
Dil

Figure 3.4.

Figure 3.4. Formation of WM Tracts and Callosal Projections is Impaired in the *Mllt11* cKO Cortex. **A**, Image of cortical WM tracts labeled with neurofilament at E16.5. Brackets indicate decreased WM. **B**, **C**, Quantification of cortical WM thickness (**B**) and WM thickness as a proportion of total cortical thickness (**C**) showed significant decrease in WM in cKOs relative to controls at E16.5. **D**, Quantification of cortical thickness subtracted from WM tract thickness showed a slight increase in *Mllt11* mutants compared with controls at E16.5. **E**, Image of cortical WM tracts labeled with neurofilament at E18.5. Brackets show decreased WM staining area. **F**-**H**, Quantification of cortical WM thickness (**F**), WM thickness as a proportion of total cortical thickness (**G**), and cortical thickness subtracted from WM tract thickness (**H**) all showed significant decreases in *Mllt11* mutants compared with controls at E18.5. **I**, **J**, Coronal sections of E18.5 cortices at rostral (upper panels) and caudal (lower panels) axial levels labeled with neurofilament (**I**) or traced with DiI (**J**). **I**, Neurofilament labeling of the CC was significantly decreased in cKO compared with controls but labeling of the internal capsule was unaffected. **J**, DiI labeling was absent in the CC of cKO slices while control cortices displayed crossing fibres labeled by DiI. Rostrally, the IC was traced comparably in control and cKO cortices. (**A**-**D**) N=5, (**E**-**H**) N=4, (**J**) N=3. Data presented as mean ± SD; ****$p \leq 0.0001$. Scale bar: 200μm (**A**) and 50μm (**B**). ctx, cortex; cc, corpus callosum; str, striatum; th, thalamus; ic, internal capsule; VZ, ventricular zone; WM, white matter.

critical role for *Mllt11* in UL CPN neurite morphology and axonogenesis of callosal fibres connecting the developing cerebral hemispheres.

The reduction of NF+ fibres crossing the CC in mutant brains suggested that *Mllt11* loss impacted the ability of UL2/3 CPNs to extend fibres across the telencephalic midline. To address this, I injected the lipophilic fluorescent dye DiI into the WM of cortical slices at E18.5 and allowed it to diffuse through the tissue for 2 weeks before visualization. DiI labeling was not detectable in the callosal fibres of *Mllt11* cKOs, while controls exhibited clearly labeled crossing fibres (Figure 3.4. J). In contrast, the corticothalamic projections of the IC were intact and traced by the DiI in both controls and cKOs, demonstrating that corticothalamic projections from DL6 of the cortex were unaffected by the *Cux2*^{IREScre} driven *Mllt11* cKO strategy (Figure 3.4. J). Altogether, our findings demonstrated that *Mllt11* loss in UL neurons specifically impacted the development of callosal projections.

4.5. *Mllt11* Loss Does Not Affect Colocalization of Pre- and Postsynaptic Markers *In Vitro*

Given the impact of *Mllt11* loss on morphology of developing neurons, I wanted to determine if the development of synapses would be altered in *Mllt11* cKOs. In collaboration with Dr. Emily Witt, a postdoctoral fellow in the Iulianella lab, primary neurons from E18.5 embryos were cultured for 1 week then stained for PSD95 and Synapsin I, markers of the postsynaptic density and presynaptic machinery involved in neurotransmitter release, respectively (Rosahl et al., 1993;

Walters & Matus, 1975). *Mllt11* cKOs exhibited reduced colocalization between pre- and post-synaptic markers (Figure 3.5. A-C), however, this effect disappeared when the number of colocalized voxels was normalized to surface area (Figure 3.5. D). It was also apparent that the average number of cells per image differed between controls and cKOs despite identical plating densities (Figure 3.5. E), so data were also normalized to the surface area of each individual cell, revealing no statistically significant difference in colocalized voxels (Figure 3.5. F). Taken together, this implies that, *in vitro*, cKOs exhibited the ability to organize synaptic machinery such that pre- and postsynaptic machinery overlap in a capacity similar to that seen in controls, despite an overall decrease in cell surface area and density.

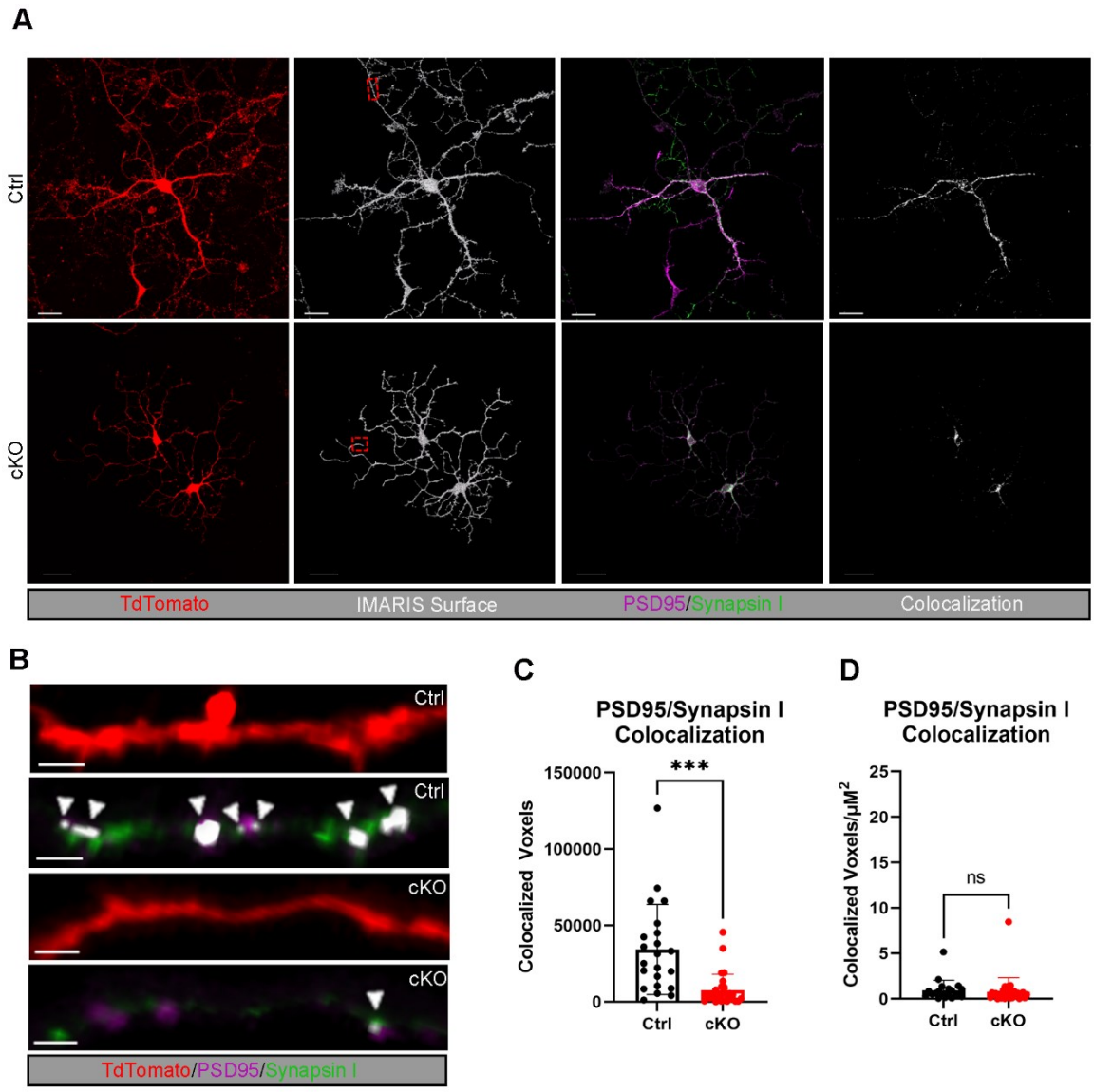
A
Ctrl
cKO
TdTomato
IMARIS Surface
PSD95/Synapsin I
Colocalization
B
Ctrl
Ctrl
cKO
cKO
TdTomato/PSD95/Synapsin I
C
PSD95/Synapsin I Colocalization
***
Colocalized Voxels
150000
100000
50000
0
Ctrl
cKO
D
PSD95/Synapsin I Colocalization
ns
Colocalized Voxels/µM²
25
20
15
10
5
0
Ctrl
cKO
E
Cells/Image
**
Cells
25
20
15
10
5
0
Ctrl
cKO
F
PSD95/Synapsin I Colocalization
ns
(Colocalized Voxels/µM²)/Cell
25
20
15
10
5
0
Ctrl
cKO

Figure 3.5.

Figure 3.5. *Mllt11* Loss Does Not Impact Overlap of Pre- and Post-Synaptic Markers. **A**, Primary UL2/3 cortical neurons obtained from E18.5 brains of *Cu2^{IREScre}; Ai9; Mllt11$^{flox/+}$* (control) and *Cux2^{IREScre}; Ai9; Mllt11$^{flox/flox}$* (cKO) and mice cultured for 14 days. Colocalization analysis was performed using masked channels following IMARIS surface construction. Red dashed boxes indicate areas scaled up in (**B**) for colocalization visualization. **B**, Representative colocalization. (**i**) cKO TdTomato expression (**ii**) cKO PSD95 and Synapsin signal, colocalization indicated by arrow (**iii**) control TdTomato expression (**iv**) control PSD95 and Synapsin I signal, colocalization indicated by arrowhead. **C**, Quantification of the colocalization of PSD95/Synapsin I, n=2, 12-15 images per individual. **D**, Quantification of the colocalization of PSD95/Synapsin I normalized to surface area showed no differences between controls and cKOs. **E**, Quantification of total number of cells in each image analyzed, in which cKO cells displayed a lower density despite being plated at a similar density to controls. **F**, Quantification of the colocalization of PSD95/Synapsin I normalized to surface area per individual cell, showed no differences between controls and cKOs. Data presented as mean ± SD; *p ≤0.05. Data points represent an average number of colocalized voxels per image per individual. Scale bar: 30μm (**A**) and 1μm (**B**).

4.6. Discussion

I described the role of a novel vertebrate-specific and neuronally restricted protein, Mllt11, in the regulation of neurite extension and migration of superficial CPNs. Using the *Cux2*^{IREScre} driver to excise *Mllt11* in developing UL CPNs, I revealed that conditional *Mllt11* loss decreased cortical WM tracts and callosal fibres, and abrogated extension and maintenance of mature arborescent dendrites. The inefficient migration of UL CPNs in *Mllt11* mutant brains likely reflected a role for Mllt11 in regulating the cytoskeleton, as it associated with stabilized microtubules. Neurons lacking *Mllt11* displayed deficits in neurite complexity both *in vivo* and *in vitro*, demonstrating that Mllt11 is a critical regulator of neurite outgrowth.

Mllt11 was initially identified in an infant patient with acute myelomonocytic leukemia (Tse et al., 2017) and expression of its protein product fused to MLL in t(1;11) (q21;q23), is specifically expressed in leukemic and immature hematopoietic cells (So et al., 2000). Over subsequent years, it was implicated in increasing invasiveness of other cancers as well, by both enhancing the ability to grow projections required for migration and invasion, and through increased secretion of enzymes that promote migration. However, evidence for its role in neural differentiation was shown in later years (Hu et al., 2015; Yamada et al., 2014), and work from the Iulianella lab first showed that its expression in the nervous system is restricted to developing neurons, and is active in multiple regions of the CNS, where a requirement for its function in migration has been demonstrated (Blommers et al., 2023; Stanton-Turcotte et al., 2022; Yamada et

al., 2014). During development, CPNs undergo vast morphological changes as they distort their shape, migrate into the CP, and acquire bipolarity to extend an axon apically to form WM tracts, allowing for formation of functional circuitry with other intra- and extra-cortical brain regions. I show that Mllt11 interacts with tubulin isoforms, confirming a recent proteomic screen (Go et al., 2021), which provides a molecular rationale for the basis of the *Mllt11* mutant phenotype. Cortical thinning and increased ventricular lumen surface area are common phenotypes associated with neurodevelopmental disorders, and were observed in *Mllt11* mutant brains, suggesting cytoskeletal dysregulation may underlie a subset of these disorders (Bahi-Buisson et al., 2014; Li et al., 2019; Mensen et al., 2017).

The microtubule cytoskeleton generates polarized force and provides a functional railway along which motor proteins migrate, whether to drive actin polymerization in generating protrusive forces at the leading edge of the growth cone or integrate extracellular cues into regulation of microtubule activity (Buck & Zheng, 2002; Dent & Kalil, 2001; Lee et al., 2004; Zhou et al., 2004). Tubulin mutations have been shown to impair neuronal migration into the cortex (Aiken et al., 2017), and specifically affect UL CPNs (Keays et al., 2007) reliant on dynamic, multipolar cytoskeletal reorganization to extend short processes, “crawling” through established DL CPNs (Miyata et al., 2001; Sakakibara et al., 2014). The dynamic expression of *Mllt11* during UL CPN development also supports its role as a critical regulator of UL CPN migration. Interestingly, mutations in α-tubulin have been shown to cause axonal trafficking defects that

impair synaptic stability and function without impacting axonal degeneration or neuronal survival (Buscaglia et al., 2020). The interaction of Mllt11 with microtubules could therefore provide a mechanistic explanation for the impaired migration and reduced CPN dendritic complexity seen in *Mllt11* mutants. Specifically, I showed that Mllt11 associates with acetylated α-tubulin in fetal brain lysates, suggesting that it may be required for the stabilization of the cytoskeleton in growing neurites, and account for the similarities between the *Mllt11* mutant phenotype with those targeting tubulin isoforms. Alternatively, the interaction between Mllt11 and tubulin as well as several motor proteins, may indicate a role in axonal trafficking.

The loss of *Mllt11* led to a reduction of interhemispheric connectivity via reduced crossing callosal fibres, a result of decreased neurite extension. The inefficient extension of neurites may also be attributed to impaired trafficking of organelles and ribosomes for local protein synthesis, or vesicles carrying secreted cues and growth cone machinery to the axonal periphery (González et al., 2016; Kennedy & Ehlers, 2006). Specifically, a potential Mllt11 interactor Myosin 10 (Table 1) is known to regulate radial migration of CPNs through its effect on the localization of N-cadherin (Lai et al., 2015), and has been implicated in tumor invasion by regulating process extension (Ropars et al., 2016). It is tempting to speculate that altered neuronal trafficking may underlie morphologic and transcriptional deficits of *Mllt11* mutant CPNs. Myh10 is crucial in neuronal migration as well as the proper formation and function of dendritic spines (Hodges et al., 2011; Rex et al., 2010; Zhang et al., 2005) and has been

associated with ASD (Fromer et al., 2014). Other interacting MAPs included Myh5a, a transporter of cargo bound for the synaptic scaffold of the dendritic spine (Yoshii et al., 2013), and mRNAs incorporated into RNP granules to be translated locally at the synapse (Fujii et al., 2005; Marchani et al., 2012). Finally, Mllt11 was found to potentially interact with Myh9 which was also identified as a protein implicated in ASD (Iossifov et al., 2014; Marchani et al., 2012; Rauch et al., 2012; Wang et al., 2020). I speculate that Mllt11 may stabilize interactions between cargo-trafficking complexes consisting of aforementioned myosins and the microtubule cytoskeleton along which they migrate.

Our exploration of potential Mllt11 interacting targets indicated interactions with several tubulins including: Tubb2b, Tubb2a, Tubb5, Tubb4b, Tubb3, Tubb4a, Tubb1a, & Tubb6. Of these interactions, three of these tubulin genes (Tubb2a, Tubb2b, Tubb4a) have been associated with tubulinopathy pathology in humans (Bonini et al., 2017; Garduno-Robles et al., 2020). Microtubule associating proteins are equally important as they contribute to normal neuronal function by regulating cytoskeletal organization and dendritic arborization (Bonini et al., 2017). Myh10 and Myh5A, two interacting proteins with Mllt11, are also indicated as microtubule associated proteins (Cao et al., 2004; Weber et al., 2004).

Very little is known regarding how microtubules are regulated and stabilized in the development of synapses and neurite terminals. It is known that some non-muscle myosins play a role in this process, some of which were pulled out as Mllt11-interactors. MYH10, is required for neuronal migration, dendritic

spine formation and function (Hodges et al., 2011b; Rex et al., 2010b; Zhang et al., 2005b) and has been associated with both ASD and schizophrenia (Fromer et al., 2014). Other potentially interacting myosins included Myh5a, which transports cargo to the synaptic scaffold of the dendritic spine (Yoshii et al., 2013), and mRNAs to be translated at the synapse (Fujii et al., 2005; Yoshimura et al., 2006). Finally, Mllt11 was found to interact with Myosin 9, which has been implicated in ASD (Iossifov et al., 2014; Marchani et al., 2012; Rauch et al., 2012; Wang et al., 2020) potentially through its involvement in processes such as the translocation of the actin cytoskeleton (Pecci et al., 2018). Given all aspects of this phenotype explored thus far, it is tempting to speculate that Mllt11 may mediate interactions between axonal microtubules, motor proteins such as the non-muscle myosins previously mentioned, and their cargo directed to neurite termini and developing synapses.

Mllt11 expression begins in early embryogenesis as soon as neurons are born at E9.5 (Pecci et al., 2018), with mRNA levels in the cortex declining to undetectable by P30, however expression continues in the postnatal mouse hippocampus and remains detectable at P28, suggesting a role in plasticity. At E14.5, *Mllt11* locus activity displays greatest expression in the IZ. This coincides spatially and temporally with the birth of BPs fated to become UL2/3 CPNs. This expression profile also coincides with the period of synapse formation in the mouse brain (Cizeron et al., 2020) and immunostaining with Mllt11 antibodies reveals primarily cytoplasmic staining in primary cortical neurons, with puncta distributed along the length of the growing neurite and concentrated in

varicosities and growth cones. I hypothesized that *Mllt11* could have a role in neurite outgrowth and synaptogenesis. Consistent with a role in neuritogenesis, loss of *Mllt11* resulted in abrogated neuronal morphology, featuring reduced axonal length and dendritic arborization.

Importantly, the loss of layer-specific morphology and identity has been demonstrated in postmortem brains from autistic humans (Casanova et al., 2013; Fujimoto et al., 2021; Stoner et al., 2014). These clinical data are reminiscent of the severe dysplasia in the cortex of our conditional *Mllt11* mutants, revealed by the Golgi staining method. It is presently unclear whether the loss of UL-specific gene expression observed in the *Mllt11* mutants is primarily due to cytoskeletal dysregulation, or other uncharacterized gene expression pathways functioning downstream of *Mllt11*. Some neuronal subtypes exhibit altered expression of subpopulation-specific markers when cytoskeletal regulation is altered such that connections to target regions cannot be established (Hippenmeyer et al., 2005), implying that there may be uncharacterized feedback mechanisms between establishment of connectivity and maintenance of expression of CPN subtype-specific transcription factors.

Moreover, changes in microtubule dynamics can affect the generation of functional connections in the brain. These are processes whose dysfunction may underlie a wide spectrum of neurodevelopmental disorders. Given that *Mllt11* mutant mice displayed both migratory and neurite outgrowth defects, they are an appropriate model to study brain disorders arising from aberrant regulation of the neuronal cytoskeletal during development. An appropriate next step is to

investigate whether these morphological changes and synapse deficiencies have any effect on behavior. Behavioral outcomes of conditional *Mllt11* loss will be the focus of the subsequent chapter of this thesis.

CHAPTER 5. Behavioral Phenotyping of *Mllt11* Loss

5.1. Introduction

Formation of the cerebral cortex relies on precise coordination of molecular processes occurring independently such that distinct cells in physically segregated regions are able to project to other regions to establish functional connections. The intricate nature of this process relies on the regulation of cytoskeletal proteins, which promote development by directing neuronal migration as well as axonogenesis and dendritogenesis, resulting in a functional network of neurons interconnected through synapses (Parato & Bartolini, 2021; Sainath & Gallo, 2015). Axonal and dendritic structures are supported by a network of microtubules, actin, intermediate filaments, and associated proteins that change dynamically to facilitate the growth of neurites and formation of synapses. It therefore follows logically that mutations in microtubules and MAPs have been linked to neurodevelopmental disorders known as tubulinopathies. Significantly, some individuals with tubulinopathies exhibit both anatomical and behavioral characteristics consistent with those seen in NDDs such as ASD and Intellectual Deficiency (ID) (Moreno-De-Luca et al., 2013; Schmidt et al., 2021).

Human NDDs encompass a range of disorders that are linked to various genetic mutations all affecting brain development and function. Although many genetic mutations associated with NDDs have been identified, the precise functions of the majority of these genes in neuronal development remain unclear. A significant number of implicated genes have been shown to disrupt synaptic formation and function when mutated, which are essential to proper neurological

development. Some genes are involved in migration and projection of neurons during development, which may lead to a reduction in cortical thickness as observed in NDDs like ASD (Mensen et al., 2017). Among the most notable findings is that the molecular mechanisms underlying neurodevelopmental processes that go awry in cases of NDDs, are often pleiotropic. The transcription factors, cell adhesion molecules, ECM proteins, axon guidance cues, and neurotrophins that participate in establishing connections in the brain are typically integral to multiple processes and play many roles (Kazdoba et al., 2016; Mensen et al., 2017; Rylaarsdam & Guemez-Gamboa, 2019). In neurodevelopmental disorders, the spatial and temporal context of gene expression, as well as the extent of the disruption, determines the characteristics of the disorder (Geschwind & Levitt, 2007a)

As such, ASD presents as a diverse range of symptoms and severity levels, commonly co-occurring with other NDDs. Among the core symptoms are atypical social communication or communication deficits, and restricted or repetitive behaviors (Lai et al., 2014). Similarly, there are various genes associated with ASD sharing substantial overlap with other NDDs. Due to variability between individuals with ASD, creating effective treatment interventions is challenging, highlighting the need to understand the function of the mechanisms perturbed in cases of NDDs in a neurotypical context in which there is a lack of neurologically atypical behavioral or thought patterns, as well as the behavioral consequences of each genetic mutation individually. Development of therapeutics is aided by the combination of gene-specific manipulations in

animal models and behavioral assays that are designed to test for symptoms that are clinically relevant to specific genes. Developing a working model is complicated by the fact that no one specific gene is linked to the majority of ASD cases, with even the most common mutations accounting for a small percentage of cases (Bucan et al., 2009a).

As previously shown, the protein Mllt11 is a cytoskeletal-interacting protein that contributes to proper migration of UL2/3 CPNs to their designated cortical laminae. Conditional knockout of *Mllt11* in UL2/3 results in a morphological and molecular phenotype with features exhibiting overlap with ASD and other NDDs, such as altered cortical thickness and morphology, altered synaptogenesis, and cortical heterotopias. It is unknown, however, if *Mllt11* cKO mice share behavioral phenotypes with models of ASD and other NDDs. Behavioral characterization of *Mllt11* cKO may be instrumental in revealing future diagnostic and treatment pathways for ASD and other NDDs, as comorbidity of two or more NDDs is common (van Bokhoven, 2011).

To investigate any potential overlap between ASD behavioral symptomology and *Mllt11* mutant behavioral phenotypes, it is necessary to perform a battery of behavioral tests for mouse models of ASD designed to maximize face validity to the core ASD symptoms, including social abnormalities, repetitive behaviors, and communication deficits, described in detail by Silverman and colleagues (Silverman et al., 2010a). Behavioral testing includes one test for each core symptom with a seven-day break allotted between testing assays.

Tests, testing timeline (Figure 4.1. A), and rationale will be described briefly herein.

P30: Olfactory Habituation/Dishabituation Test

This test aims to quantify the level of interest in social stimuli through introduction of social odors as well as nonsocial odors for comparison. Given the fact that olfaction is a major component of social communication among mice, deficits in olfactory ability have been reported across various neurodevelopmental disorders in humans (Crow et al., 2020; Lyons-Warren et al., 2021), and the limited expression of cux2 in the olfactory bulb (Lein, 2007), it is also necessary to examine whether olfactory discrimination deficits are present in *Mllt11* cKO mice to determine if any social deficits are attributable to impaired olfaction. The test involves presenting novel nonsocial and social odors, such as vanilla and lemon extract and soiled bedding respectively, introduced via a cotton-tipped applicator with which the mice may freely interact during 3 subsequent 2-minute intervals of odor presentation with 1-minute intertrial interval. During this time, the time spent sniffing the swab is recorded (Figure 4.1. B). It is expected that, if the animal's olfactory processes are functioning normally, the animal will sniff the first presentation of a new odor for the greatest amount of time, and each subsequent presentation of the same odor should elicit less time spent sniffing, as the animal becomes habituated to the odor. Dishabituation should occur with presentation of each novel odor, meaning the animal should sniff the applicator for a longer period of time upon the initial presentation of a novel odor than the final trial of the previous odor. It is also

expected that the animals should sniff the social odors significantly more than any of the nonsocial odors (Crawley et al., 2007; Ryan et al., 2008; Yang & Crawley, 2009).

P37: Three-Chamber Social Test

This test allows for identification of deficits in sociability as well as responsiveness to social novelty, both of which are early markers for various neurodevelopmental disorders. The test involves allowing the mouse to explore a three-chamber apparatus in which both peripheral chambers contain mice of varying novelty and unfamiliarity to the test subject. Following a habituation period in the center chamber (Figure 4.1. C), the mouse is allowed to freely explore the open apparatus (Figure 4.1. D), after which the mouse is initially presented with one stranger in either of the peripheral chambers (Figure 4.1. E), spending the desired amount of time in the presence of and interacting with the stranger. Following this trial, a second, presently less familiar mouse is presented in the previously empty chamber (Figure 4.1. F), and the test subject is once again allowed to freely explore, spending the desired amount of time with both mice. This test aims to interrogate the animal's preference for sociability, as a wild type mouse is expected to investigate and spend the greatest amount of time with a novel, or stranger, mouse due to the social nature of mice and their inherent curiosity for novel social interaction (Kaidanovich-Beilin et al., 2011; Moy et al., 2004). It is expected that an animal recognizes the most recently presented stranger as novel, and will shift from a greater investment of time spent with stranger 1 to increased time spent with stranger 2 upon presentation.

P44: Social Transmission of Food Preference

This task evaluates communication between animals as in their natural habitat, rodents learn whether foods are safe for consumption through social interactions with animals who have previously consumed a particular food. The test involves habituating mice to powdered chow, then presenting cage mates deemed “demonstrators” with powdered chow supplemented with cocoa or cinnamon flavoring. Demonstrators are reintroduced for a demonstration period with their cage mates, who are then presented with a choice between the cued, or demonstrated food flavor, and a non-cued, or unfamiliar food flavor (Figure 4.1. G). The amount of each flavor eaten is compared to determine whether a preference was communicated by the demonstrator and accurately interpreted as safe by the test subjects. Social communication and/or learning is disrupted in several neurodevelopmental disorders; therefore, this test will provide a model for examining social communication (Galef, 2003; Wrenn, 2004; Wrenn et al., 2003).

P51: Repetitive Behaviors: Marble Burying and Nestlet Shredding

Repetitive behaviors are used as diagnostic criteria for autism and are commonly reported in other NDDs. The following tasks are widely used to evaluate the occurrence of repetitive, compulsive-like behaviors in rodent models of psychiatric conditions (McFarlane et al., 2008; Silverman et al., 2010b; Yang et al., 2009; Yang, Scattoni, et al., 2007; Yang, Zhodzishsky, et al., 2007).

The Nestlet shredding test evaluates the tendency of rodents to engage in repetitive behaviors such as shredding of bedding material to construct a nest for

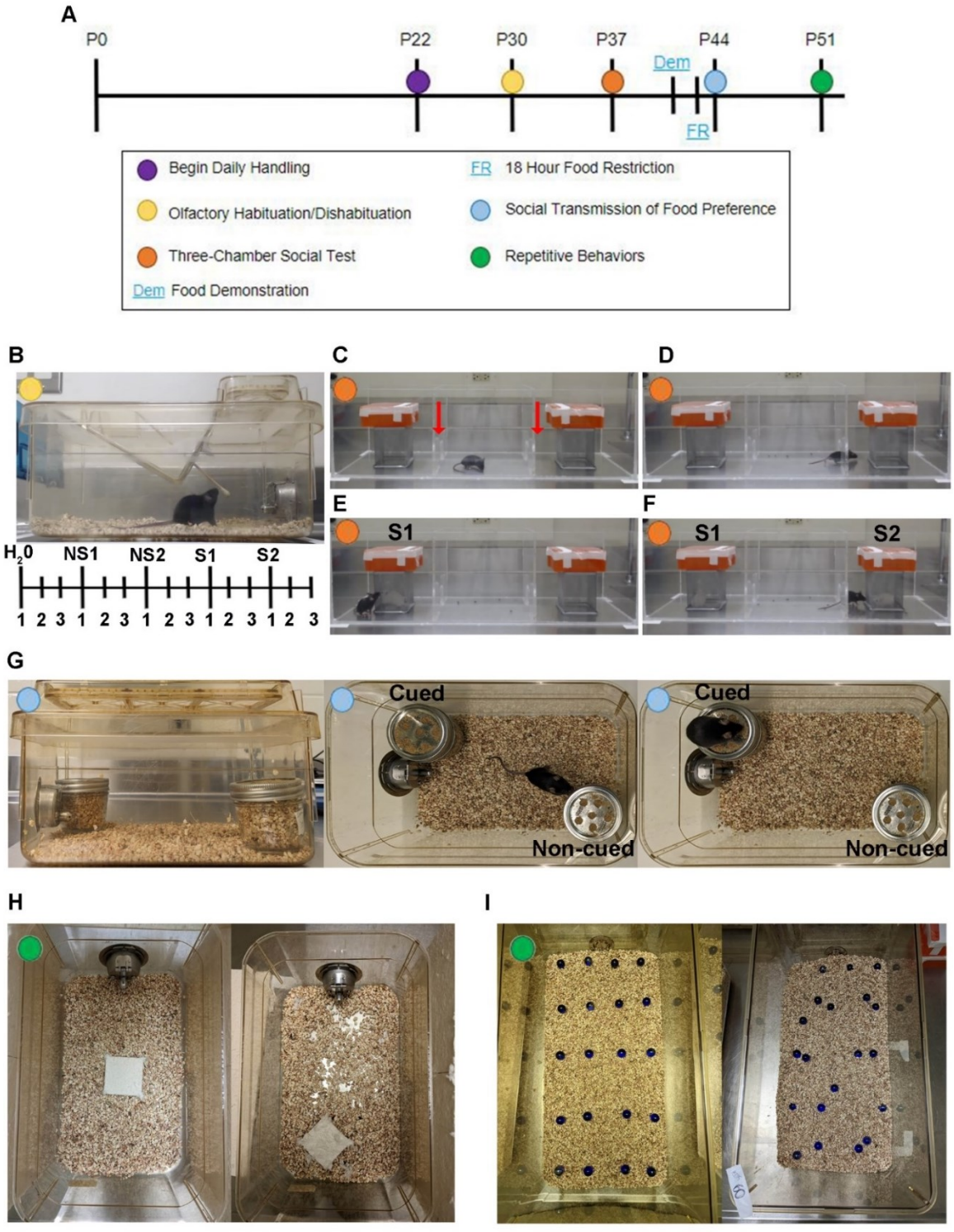
A
P0
P22
P30
P37
Dem
P44
FR
P51
Begin Daily Handling
Olfactory Habituation/Dishabituation
Three-Chamber Social Test
Dem Food Demonstration
FR 18 Hour Food Restriction
Social Transmission of Food Preference
Repetitive Behaviors
B
C
D
E
F
S1
S1
S2
H20
NS1
NS2
S1
S2
1 2 3 1 2 3 1 2 3 1 2 3 1 2 3
G
Cued
Cued
Non-cued
Non-cued
H
I

Figure 4.1.

Figure 4.1. Experimental Timeline and Behavioral Test Battery. **A**, Timeline of behavioral testing. Colored circles correspond to colored icons in the text with a description of testing procedures and rationale as well as sample images in panels **B**-**I**. **B**, Test mouse interacting with a scented swab during the olfactory habituation/dishabituation testing on P30 (top panel). Schematic (bottom panel) depicting the experimental design in which each scent is presented over three consecutive trials. **C**, Test mouse in center chamber during initial 5-minute habituation period in the three-chamber apparatus. Red arrows indicate closed doors confining the mouse to the center chamber. **D**, Test mouse freely roaming about the three-chamber apparatus during the second 5-minute habituation period. **E**, Test mouse interacting with stranger 1 during the first 10-minute stranger social approach period. **F**, Test mouse interacting with stranger 2 during the second 10-minute social approach period. **G**, Experimental setup for the conditioned taste preference test. **H**, Nestlet shredding test setup (left) and shredded Nestlet post-test (right). **I**, Marble burying test setup (left) and marble distribution post-test (right).

protection from their environment. The test involves placing a single mouse into a cage with a pre-weighed square of Nestlet bedding material for a period of 30 minutes. Following the test period, the portion of Nestlet material that remains unshredded is weighed to determine the degree of shredding behavior (Figure 4.1. H, Angoa-Pérez et al., 2013).

Similarly, the marble burying test capitalizes on the proclivity of rodents to dig under natural circumstances in order to create tunnels and burrows for shelter and storage of resources. The test involves placing a mouse into a standard sized rat sized cage with a quantity of fresh mouse bedding sufficient for digging, burrowing, and burying of resources, containing glass marbles on the surface of the bedding in a grid pattern of 5 rows of 4 marbles. Following the 30-minute test period, the degree of marble burying behavior is determined by the proportion of total marbles buried (Figure 4.1. I, Angoa-Pérez et al., 2013).

5.2. *Mllt11* Loss Impacts Social Odor Interaction in a Sex- and Copy Number-Dependent Manner

Given the overlap in the molecular and morphological phenotype of *Mllt11* cKO mice and those exhibited in ASD, such as such as migratory and neurite outgrowth defects, altered cortical morphology, and improper maintenance of gene expression, we sought to investigate the impact of loss of *Mllt11* on behavior. To assess this, we performed several tests to evaluate sociability, social communication, and tendency toward repetitive behaviors. Behavioral experimentation began on P22 with handling of pups. Pups were handled daily

leading up to behavioral experimentation to acclimatize them to the experimenters and testing facility. During the handling period, pups were also weighed, revealing a slightly decreased body weight in both male and female cKOs, an effect which disappeared following weaning (Figure 4.2. A-B). Male cKOs weighed significantly less than *Mllt11*$^{flox/+;cre}$ and *Mllt11*$^{flox/+}$ mice on P22, and continued to display a significantly decreased weight compared to *Mllt11*$^{flox/+}$ with a nonsignificant trend toward decreased weight compared to *Mllt11*$^{flox/+;cre}$ mice on P23 and P24 (Figure 4.2. A). Female cKOs weighed significantly less than *Mllt11*$^{flox/+;cre}$ littermates and showed a non-significant trend toward reduced weight compared to *Mllt11*$^{flox/+}$ controls on P22 and P23 compared to littermate controls (Figure 4.2. B). Pups were weaned on P23 to ensure that they would be large enough to have the greatest chance of survival.

Following weaning and handling, behavioral testing began on P30 with the olfactory habituation/dishabituation testing paradigm. It was established that both males and females of all genotypes demonstrated functional olfactory sensation as well as the ability to habituate to odors following repeated presentations, and dishabituate in response to presentation of a novel odor to some, though they did this to varying degrees (Figure 4.3. A-D). An olfactory habituation score was calculated by subtracting the amount of time spent sniffing on trial 1 from trial 3 for each scent. If this value was negative, the animal was considered to have habituated. All sexes and genotypes were able to habituate (Figure 4.3. A-B), however *Mllt11*$^{flox/+;cre}$ females exhibited a lower habituation score compared to female cKOs upon presentation of the second social odor, though neither differed

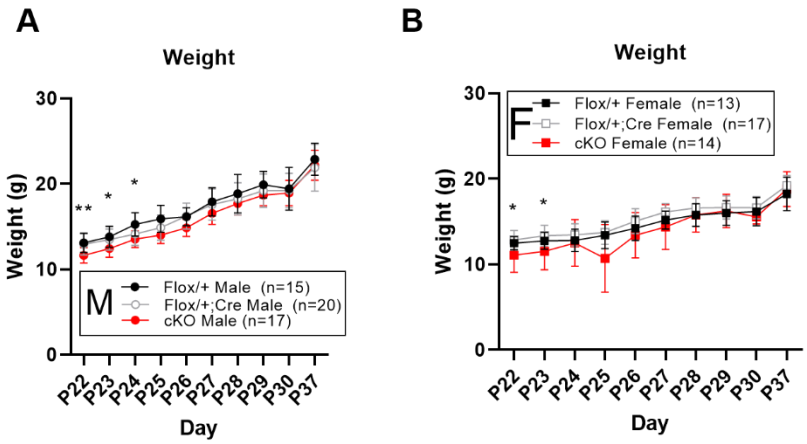

Figure 4.2. *Mllt11* cKOs Exhibit Delayed Weight Gain Postnatally. **A**, **B**, Both male (**A**) and female (**B**) cKO mice exhibit decreased weight compared to littermates until P25 (**A**) and P24 (**B**) respectively. Data presented as mean ± SD; *p ≤0.05, **p ≤ 0.01. Flox/+; *Mllt11*$^{flox/+}$; Flox/+;Cre, *Mllt11*$^{flox/+;cre;}$ cKO, conditional knockout.

significantly from *Mllt11*$^{flox/+}$ littermates (Figure 4.3. B). The dishabituation score was calculated by subtracting the time spent sniffing the swab on trial 3 of a given scent from the time spent sniffing on trial 1 of the subsequent odor presentation. All sexes and genotypes also displayed dishabituation (Figure 4.3. C-D). Taken together, these data suggest that loss of *Mllt11* does not impair olfaction, olfactory habituation, or olfactory dishabituation, however *Mllt11*$^{flox/+;cre}$ females have a slightly increased tendency to habituate to a social odor following presentation of a different social odor.

In order to control for the effects of the order of presentation of odors as well as any characteristic behavioral trends specific to particular odors, analyses were performed separately for each scent compared between genotypes within sexes, as well as based on order of presentation of each nonsocial and social odor, and whether each social odor was from the same or opposite sex of each experimental mouse. Upon presentation of the first odor, which was water regardless of the presentation order of the test odors, cKO males exhibited significantly reduced time spent sniffing on the first presentation, compared to *Mllt11*$^{flox/+}$ males (Figure 4.4. A), while female *Mllt11*$^{flox/+;cre}$ mice spent significantly more time sniffing the swab upon initial presentation when compared to *Mllt11*$^{flox/+}$ and cKO females (Figure 4.4. B). Cumulatively, male cKOs spent significantly less time sniffing the swab than *Mllt11*$^{flox/+}$ males (Figure 4.4. C), and *Mllt11*$^{flox/+;cre}$ females spent significantly more time sniffing the swab than cKOs,

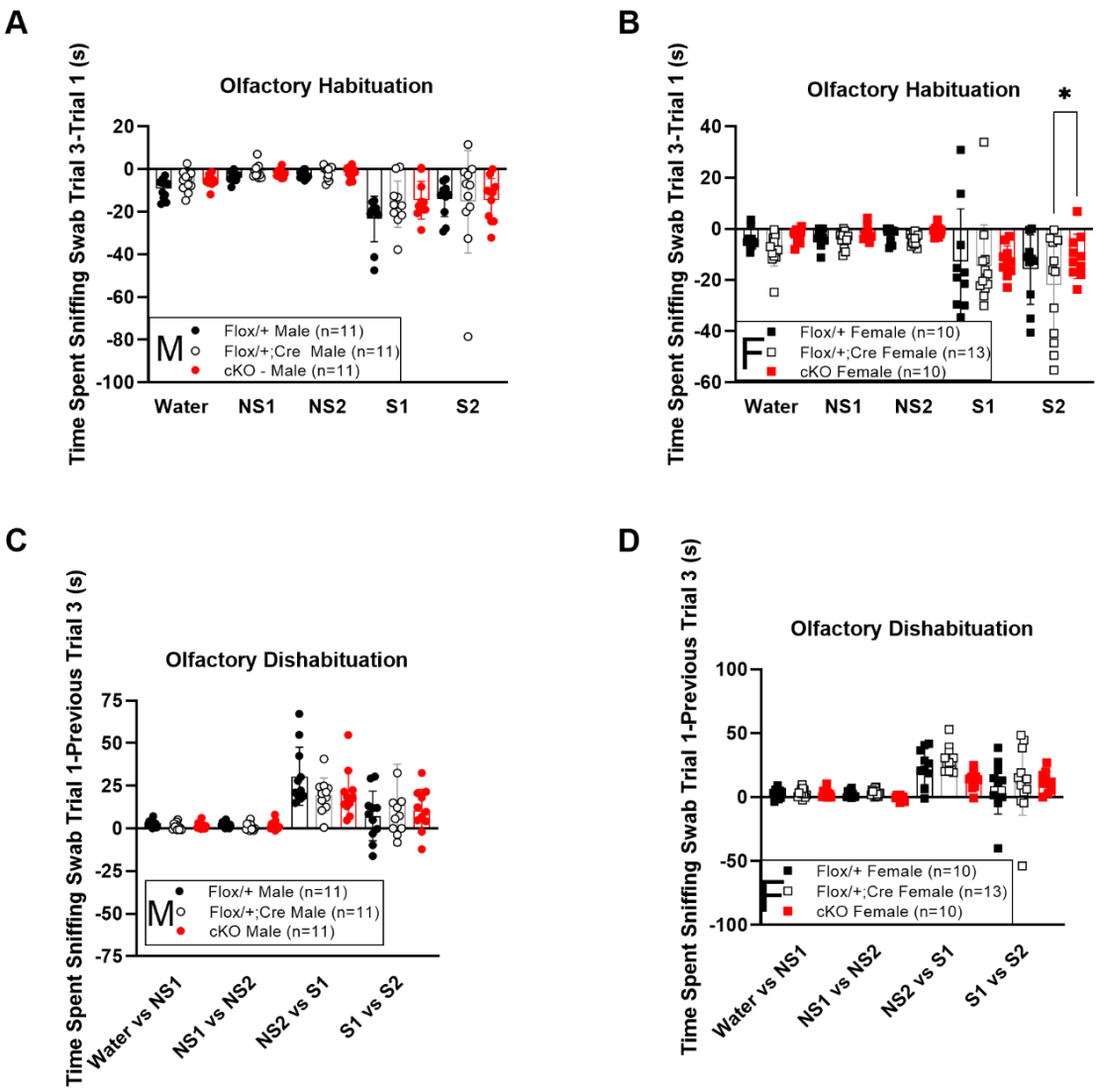

Figure 4.3. *Mllt11* cKOs Exhibit Olfactory Sensation, Habituation, and Dishabituation. **A**, **B**, Olfactory habituation scores for males (**A**) and females (**B**) calculated by subtracting the sniffing time of the first presentation of each swab from the sniffing time from the third trial of the previous swab. *Mllt11*$^{flox/+;cre}$ females displayed an increased rate of habituation to the second social odor compared to cKO females. **C**, **D**, Olfactory dishabituation scores for males (**C**) and females (**D**) calculated by subtracting the sniffing time of the third presentation of each swab from the sniffing time from the first presentation of the following swab. No differences were seen. Data presented as mean ± SD; *p ≤0.05. NS1, Nonsocial odor 1; NS2, Nonsocial odor 2; S1, Social odor 1; S2, Social odor 2; Flox/+; *Mllt11*$^{flox/+}$; Flox/+;Cre, *Mllt11*$^{flox/+;cre}$; cKO, conditional knockout.

though neither differed markedly from *Mllt11*$^{flox/+}$ female littermates (Figure 4.4. D).

Despite these slight differences in interest in interacting with the water swab, which served as an odorless, nonsocial control, there were minimal differences in time spent sniffing the other nonsocial odors. There were no significant differences seen in any genotype of either sex when presented with lemon extract (Figure 4.4. E-H), and upon presentation of vanilla extract, *Mllt11*$^{flox/+;cre}$ males spent significantly less time sniffing during the first presentation than *Mllt11*$^{flox/+}$ males (Figure 4.4. I) but all other genotypes showed no differences (Figure 4.4. J-L). To control for any potential preferences or aversions to each odor that could account for these slight differences in sniffing time of each nonsocial odor, the data were also analyzed by presentation order of each nonsocial odor, revealing no significant differences in sniffing time, by trial or cumulatively, for any sex or genotype (Figure 4.5. A-H).

Following presentation of the nonsocial odors, mice were presented with a swab scented with soiled bedding from a cage of male or female mice. Upon presentation of the male social odor, males showed no significant differences across genotypes (Figure 4.6. A). Female cKOs, however, spent significantly less time sniffing than *Mllt11*$^{flox/+;cre}$ females upon the first presentation of the male social odor, though neither differed significantly from *Mllt11*$^{flox/+}$ littermates (Figure 4.6. B). Cumulatively across all trials, males exhibited no differences in time spent sniffing the male social odor (Figure 4.6. C), a trend which was also displayed by the females (Figure 4.6. D). When presented with a female social

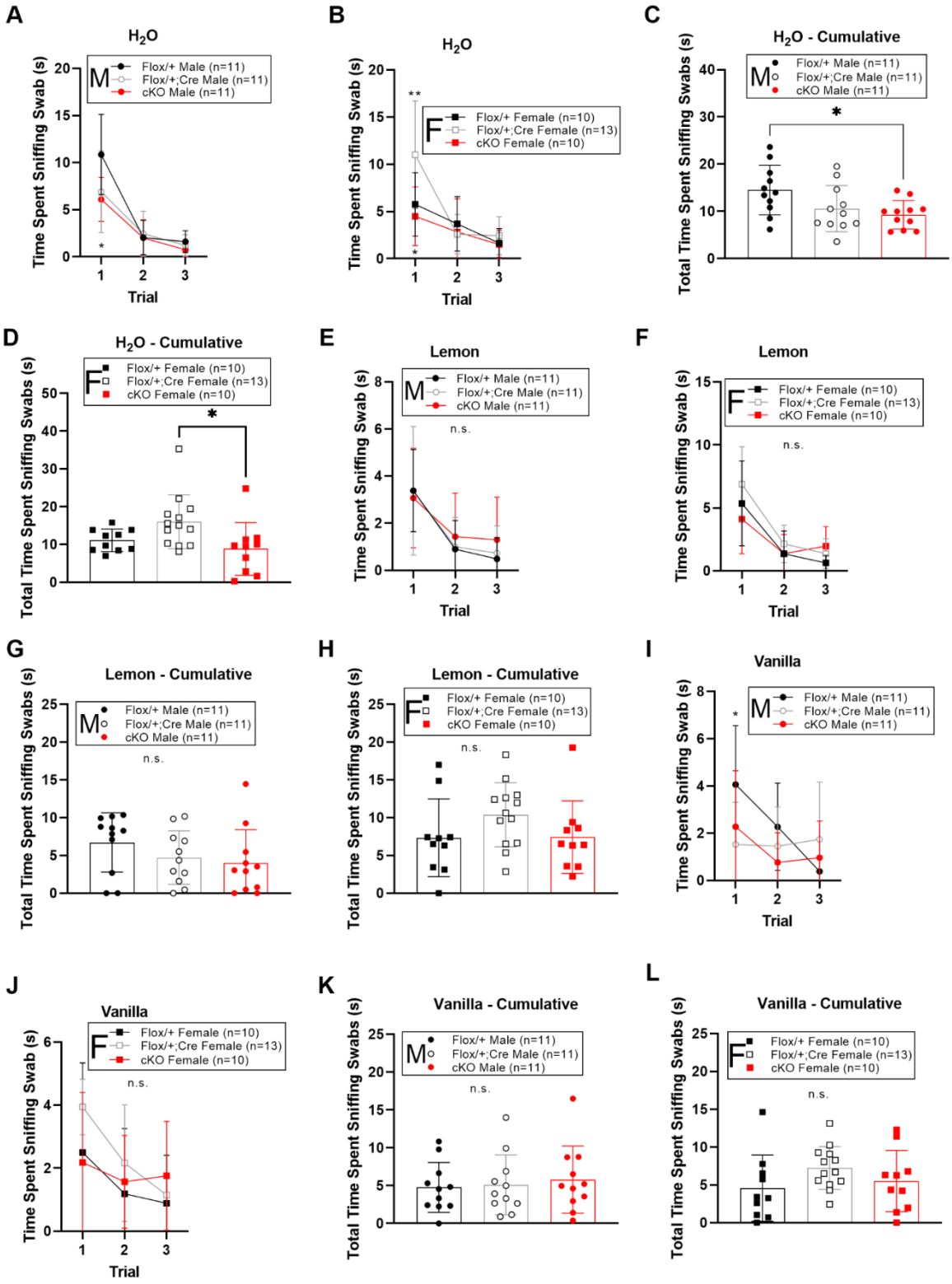
A
H2O
Flox/+ Male (n=11)
Flox/+;Cre Male (n=11)
cKO Male (n=11)
Time Spent Sniffing Swab (s)
Trial
B
H2O
Flox/+ Female (n=10)
Flox/+;Cre Female (n=13)
cKO Female (n=10)
C
H2O - Cumulative
Total Time Spent Sniffing Swabs (s)
D
H2O - Cumulative
E
Lemon
n.s.
F
Lemon
G
Lemon - Cumulative
H
Lemon - Cumulative
I
Vanilla
J
Vanilla
K
Vanilla - Cumulative
L
Vanilla - Cumulative

Figure 4.4.

Figure 4.4. Loss of *Mllt11* Has Limited Effect on Interaction With Nonsocial Odors. **A**, **B**, Time spent sniffing the water control swab over each trial for males (**A**) and females (**B**). cKO males exhibited significantly reduced time spent sniffing on the first presentation, compared to *Mllt11*$^{flox/+}$ males. Female *Mllt11*$^{flox/+;cre}$ mice spent significantly more time sniffing the swab upon initial presentation when compared to *Mllt11*$^{flox/+}$ and cKO females. **C**, **D**, Cumulative time spent sniffing the water control swab over all trials for males (**C**) and females (**D**). Male cKOs spent significantly less time sniffing the swab compared to *Mllt11*$^{flox/+}$ males. *Mllt11*$^{flox/+;cre}$ females spent significantly more time sniffing the swab than cKO females, though neither differed significantly from *Mllt11*$^{flox/+}$ littermates. **E**, **F**, Time spent sniffing the lemon-scented swab over each trial for males (**E**) and females (**F**). No differences were seen. **G**, **H**, Cumulative time spent sniffing the lemon-scented swab over all trials for males (**G**) and females (**H**). No differences were seen. **I**, **J**, Time spent sniffing the vanilla-scented swab over each trial for males (**I**) and females (**J**). *Mllt11*$^{flox/+;cre}$ males spent significantly less time sniffing during the first presentation than *Mllt11*$^{flox/+}$ males. No differences were seen in females. **K**, **L**, Cumulative time spent sniffing the vanilla-scented swab over all trials for males (**K**) and females (**L**). No differences were seen. Data presented as mean ± SD; n.s., not significant; *p ≤0.05. Flox/+; *Mllt11*$^{flox/+}$; Flox/+;Cre, *Mllt11*$^{flox/+;cre}$; cKO, conditional knockout.

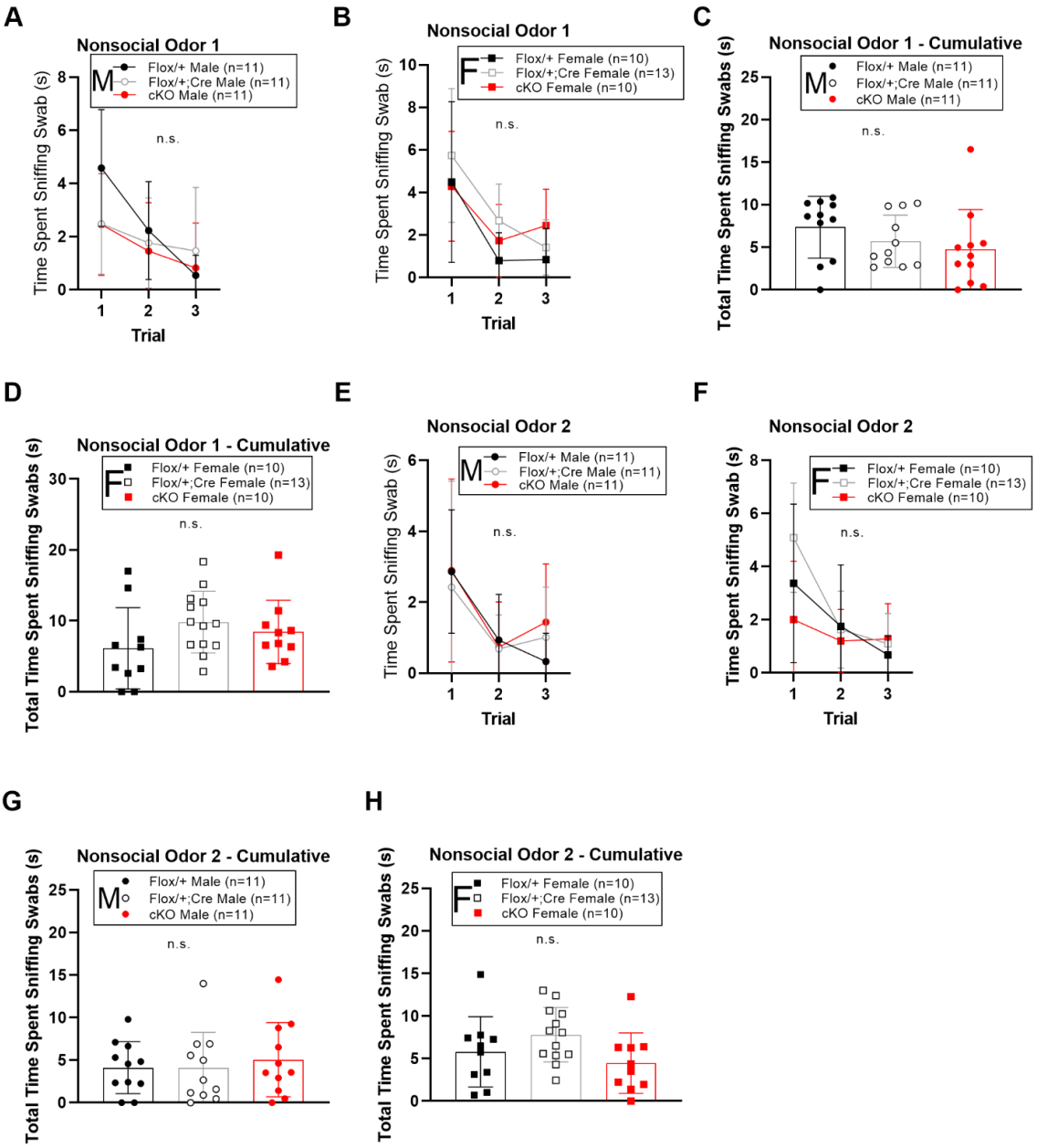

Figure 4.5. Loss of *Mllt11* Has No Effect on Interaction With Nonsocial Odors Regardless of Presentation Order. **A**, **B**, Time spent sniffing the first nonsocial odor over each trial for males (**A**) and females (**B**). No differences were seen. **C**, **D**, Cumulative time spent sniffing the first nonsocial odor over all trials for males (**C**) and females (**D**). No differences were seen. **E**, **F**, Time spent sniffing the second nonsocial odor over each trial for males (**E**) and females (**F**). No differences were seen. **G**, **H**, Cumulative time spent sniffing the second nonsocial odor over all trials for males (**G**) and females (**H**). No differences were seen. Data presented as mean ± SD; n.s., not significant. Flox/+; *Mllt11*$^{flox/+}$; Flox/+;Cre, *Mllt11*$^{flox/+;cre}$; cKO, conditional knockout.

odor, males showed no differences across trials (Figure 4.6. E), or cumulatively (Figure 4.6. G). *Mllt11*$^{flox/+;cre}$ females, however, spent significantly more time sniffing than cKO females upon the second presentation of the female social odor, though neither differed significantly from *Mllt11*$^{flox/+}$ littermates (Figure 4.6. F), a trend which was also seen cumulatively across all trials (Figure 4.6. G).

Given these slight differences, I sought to investigate the potential role of presentation order, so the data were analyzed by order of presentation of the social odors, regardless of sex. No significant differences were observed between genotypes in males (Figure 4.7. A, C, E, G), however some differences were observed in females. Upon presentation of the first social odor, cKOs spent significantly less time sniffing the swab compared to *Mllt11*$^{flox/+;cre}$ females during the first trial, though neither differed significantly from *Mllt11*$^{flox/+}$ littermates (Figure 4.7. B). During the second trial, cKO females spent significantly less time sniffing compared to *Mllt11*$^{flox/+;cre}$ and *Mllt11*$^{flox/+}$ females (Figure 4.7. B). Cumulatively across trials of social odor 1, female cKOs sniffed significantly less than *Mllt11*$^{flox/+;cre}$ females (Figure 4.7. D). Upon presentation of the second social odor, these effects were no longer apparent (Figure 4.7. F, H).

In order to identify any discrepancies in sniffing time between genotypes that may be dependent on presentation order or impact of previous odor interactions, the data were next compared across the entire experimental regime. When analyzed by non-scent-specific presentation order, no differences were observed between genotypes in males (Figure 4.8. A), however, *Mllt11*$^{flox/+;cre}$ females exhibited an increased amount of time sniffing upon the first presentation

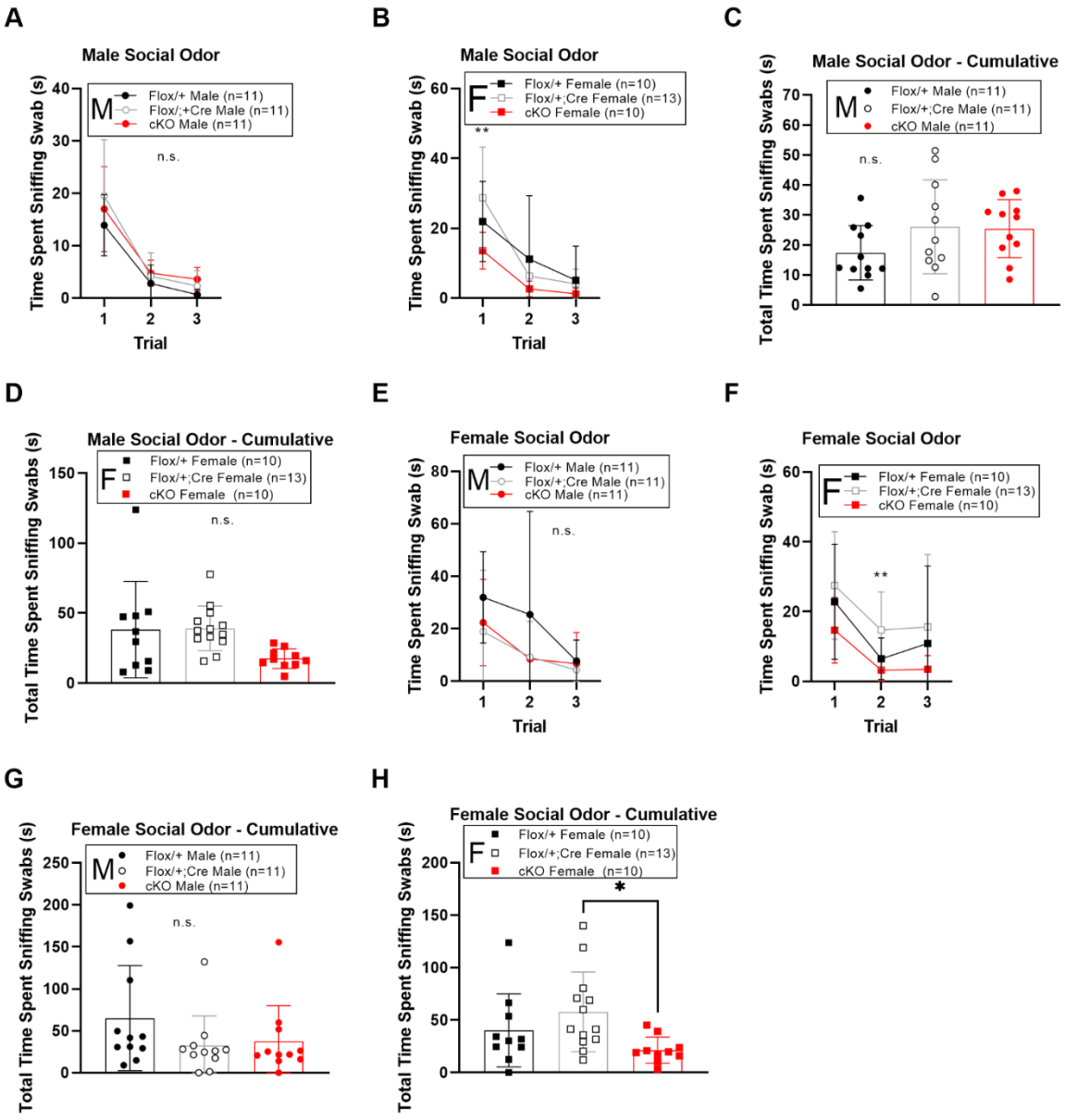
A
Male Social Odor
Time Spent Sniffing Swab (s)
M
Flox/+ Male (n=11)
Flox/;+Cre Male (n=11)
cKO Male (n=11)
n.s.
Trial
B
Male Social Odor
Time Spent Sniffing Swab (s)
F
Flox/+ Female (n=10)
Flox/+;Cre Female (n=13)
cKO Female (n=10)
**
Trial
C
Male Social Odor - Cumulative
Total Time Spent Sniffing Swabs (s)
M
Flox/+ Male (n=11)
Flox/+;Cre Male (n=11)
cKO Male (n=11)
n.s.
D
Male Social Odor - Cumulative
Total Time Spent Sniffing Swabs (s)
F
Flox/+ Female (n=10)
Flox/+;Cre Female (n=13)
cKO Female (n=10)
n.s.
E
Female Social Odor
Time Spent Sniffing Swab (s)
M
Flox/+ Male (n=11)
Flox/+;Cre Male (n=11)
cKO Male (n=11)
n.s.
Trial
F
Female Social Odor
Time Spent Sniffing Swab (s)
F
Flox/+ Female (n=10)
Flox/+;Cre Female (n=13)
cKO Female (n=10)
**
Trial
G
Female Social Odor - Cumulative
Total Time Spent Sniffing Swabs (s)
M
Flox/+ Male (n=11)
Flox/+;Cre Male (n=11)
cKO Male (n=11)
n.s.
H
Female Social Odor - Cumulative
Total Time Spent Sniffing Swabs (s)
F
Flox/+ Female (n=10)
Flox/+;Cre Female (n=13)
cKO Female (n=10)
*

Figure 4.6.

Figure 4.6. *Mllt11* Loss Impacts Interaction With Social Odors in a Sex-Specific and Copy Number-Dependent Manner. **A**, **B**, Time spent sniffing the male social odor over each trial for males (**A**) and females (**B**). No differences were seen in males. Female cKOs spent significantly less time sniffing than *Mllt11*$^{flox/+;cre}$ females upon the first presentation of the male social odor, though neither differed markedly from *Mllt11*$^{flox/+}$ littermates. **C**, **D**, Cumulative time spent sniffing the male social odor over all trials for males (**C**) and females (**D**). No differences were seen. **E**, **F**, Time spent sniffing the female social odor over each trial for males (**E**) and females (**F**). No differences were seen in males. *Mllt11*$^{flox/+;cre}$ females spent significantly more time sniffing than cKO females upon the second presentation of the female social odor, though neither differed significantly from *Mllt11*$^{flox/+}$ littermates **G**, **H**, Cumulative time spent sniffing the female social odor over all trials for males (**G**) and females (**H**). Males showed no differences in sniffing time. Female cKOs spent significantly less time sniffing than *Mllt11*$^{flox/+;cre}$ females cumulatively across all trials, though neither differed significantly from *Mllt11*$^{flox/+}$ littermates. Data presented as mean ± SD; n.s., not significant, *p ≤0.05, **p ≤ 0.01. Flox/+; *Mllt11*$^{flox/+}$; Flox/+;Cre, *Mllt11*$^{flox/+;cre}$; cKO, conditional knockout.

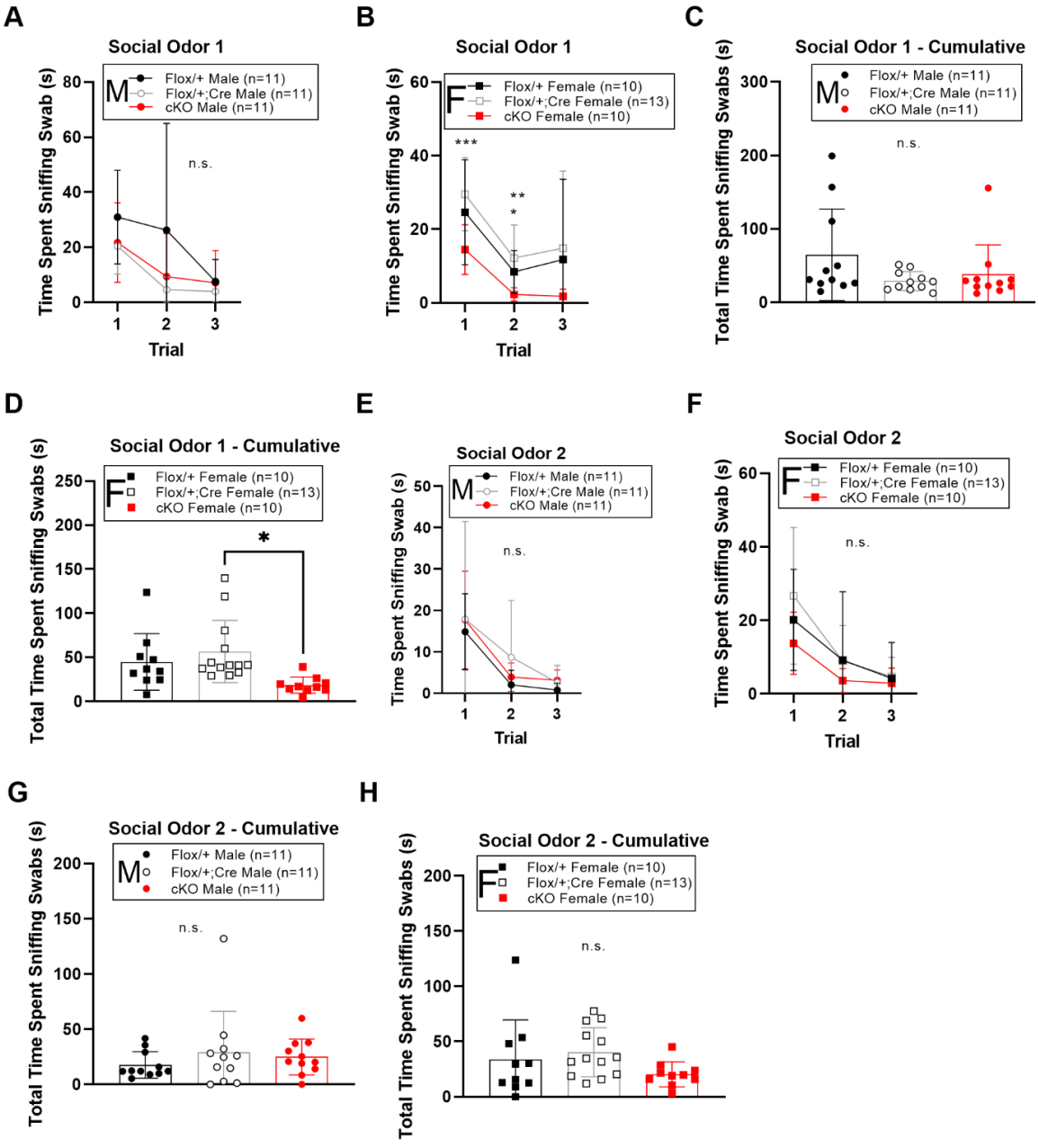
A
Social Odor 1
Flox/+ Male (n=11)
Flox/+;Cre Male (n=11)
cKO Male (n=11)
n.s.
Time Spent Sniffing Swab (s)
Trial
B
Social Odor 1
Flox/+ Female (n=10)
Flox/+;Cre Female (n=13)
cKO Female (n=10)
***
**
*
Time Spent Sniffing Swab (s)
Trial
C
Social Odor 1 - Cumulative
Flox/+ Male (n=11)
Flox/+;Cre Male (n=11)
cKO Male (n=11)
n.s.
Total Time Spent Sniffing Swabs (s)
D
Social Odor 1 - Cumulative
Flox/+ Female (n=10)
Flox/+;Cre Female (n=13)
cKO Female (n=10)
*
Total Time Spent Sniffing Swabs (s)
E
Social Odor 2
Flox/+ Male (n=11)
Flox/+;Cre Male (n=11)
cKO Male (n=11)
n.s.
Time Spent Sniffing Swab (s)
Trial
F
Social Odor 2
Flox/+ Female (n=10)
Flox/+;Cre Female (n=13)
cKO Female (n=10)
n.s.
Time Spent Sniffing Swab (s)
Trial
G
Social Odor 2 - Cumulative
Flox/+ Male (n=11)
Flox/+;Cre Male (n=11)
cKO Male (n=11)
n.s.
Total Time Spent Sniffing Swabs (s)
H
Social Odor 2 - Cumulative
Flox/+ Female (n=10)
Flox/+;Cre Female (n=13)
cKO Female (n=10)
n.s.
Total Time Spent Sniffing Swabs (s)

Figure 4.7.

Figure 4.7. *Mllt11* Loss Impacts Interaction With Social Odors Differentially by Presentation Order in a Sex-Specific and Copy Number-Dependent Manner. **A**, **B**, Time spent sniffing the first social odor over each trial for males (**A**) and females (**B**). No differences were seen in males. cKO females spent significantly less time sniffing the swab compared to *Mllt11*$^{flox/+;cre}$ females during the first trial, though no differences were seen between either genotype and *Mllt11*$^{flox/+}$ littermates. Female cKOs spent less time sniffing compared to *Mllt11*$^{flox/+;cre}$ and *Mllt11*$^{flox/+}$ females during the second trial. **C**, **D**, Cumulative time spent sniffing the first social odor over all trials for males (**C**) and females (**D**). No differences were seen in males. Female cKOs sniffed significantly less than *Mllt11*$^{flox/+;cre}$ females cumulatively across all trials, though neither differed significantly from *Mllt11*$^{flox/+}$littermates. **E**, **F**, Time spent sniffing the second social odor over each trial for males (**E**) and females (**F**). No differences were seen. **G**, **H**, Cumulative time spent sniffing the second social odor over all trials for males (**G**) and females (**H**). No differences were seen. Data presented as mean ± SD; n.s., not significant, *p ≤0.05, **p ≤ 0.01, ***p ≤ 0.001. Flox/+; *Mllt11*$^{flox/+}$; Flox/+;Cre, *Mllt11*$^{flox/+;cre}$; cKO, conditional knockout.

of the unscented water swab compared to both cKO and *Mllt11*$^{flox/+}$ females, as well as increased time sniffing the second presentation of nonsocial odor 1 compared to *Mllt11*$^{flox/+}$ females (Figure 4.8. B). *Mllt11*$^{flox/+;cre}$ females also spent significantly more time sniffing upon the first presentation of nonsocial odor 2 than cKO females, though neither differed significantly from *Mllt11*$^{flox/+}$ littermates (Figure 4.8. B). This trend was also seen upon the first presentation of social odor 1, and upon the second presentation of the same social odor, cKO females spent significantly less time sniffing than both *Mllt11*$^{flox/+;cre}$ and *Mllt11*$^{flox/+}$ individuals (Figure 4.8. B). Cumulatively, no differences were observed in males (Figure 4.8. C), but *Mllt11*$^{flox/+;cre}$ females displayed increased sniffing of social odor 1 compared to *Mllt11*$^{flox/+}$ and cKO littermates (Figure 4.8. D). *Mllt11*$^{flox/+;cre}$ females also displayed increased sniffing of social odor 2 compared to female cKOs, although neither differed significantly from *Mllt11*$^{flox/+}$ littermates (Figure 4.8. D).

When the data were organized by whether each social odor was from the same or opposite sex of the test mouse, males once again showed no significant differences (Figure 4.8. E), however, differences were observed in females. *Mllt11*$^{flox/+;cre}$ females displayed increased sniffing upon the second presentation of the first nonsocial odor compared to *Mllt11*$^{flox/+}$ females, as well as the initial presentation of the second nonsocial odor compared to cKO females, though neither differed significantly from *Mllt11*$^{flox/+}$ littermates. An increase in sniffing behavior in *Mllt11*$^{flox/+;cre}$ females compared to cKO females was also observed upon the second presentation of same sex odor, as well as the first presentation

of the opposite sex odor, though there was no significant differences between either genotype and *Mllt11*$^{flox/+}$ littermates (Figure 4.8. F). Cumulatively, both *Mllt11*$^{flox/+;cre}$ and cKOs *Mllt11*$^{flox/+}$ males displayed a decrease in time spent sniffing the opposite sex social scent compared to *Mllt11*$^{flox/+}$ littermates (Figure 4.8. G), while female cKOs spent less time sniffing the same sex odor compared to *Mllt11*$^{flox/+;cre}$ and *Mllt11*$^{flox/+}$ females (Figure 4.8. H). Female cKOs also spent less time sniffing the opposite sex odor compared to *Mllt11*$^{flox/+;cre}$ females, though neither differed significantly from *Mllt11*$^{flox/+}$ littermates (Figure 4.8. H).

Analysis of the data based on specific scent presentation revealed no differences in males (Figure 4.8. I), while females displayed differences in sniffing behaviors. Female cKOs spent significantly less time sniffing upon initial presentation of the male social odor compared to *Mllt11*$^{flox/+;cre}$ individuals as well as the second presentation of the female social odor (Figure 4.8. J). Cumulatively, males also showed no differences in overall sniffing time (Figure 4.8. K), while cKO females spent less time sniffing both male and female social odors than *Mllt11*$^{flox/+;cre}$ females, though in both cases neither differed from *Mllt11*$^{flox/+}$ littermates. (Figure 4.8. L).

It is expected that a wild-type mouse will spend significantly more time interacting with social odors compared to nonsocial odors. To determine if this phenomenon was observable in mice lacking one or both copies of *Mllt11*, the cumulative time spent sniffing both nonsocial odors was compared to the cumulative time spent sniffing social odors within each sex and genotype separately. In both males and females, all genotypes were found to have spent

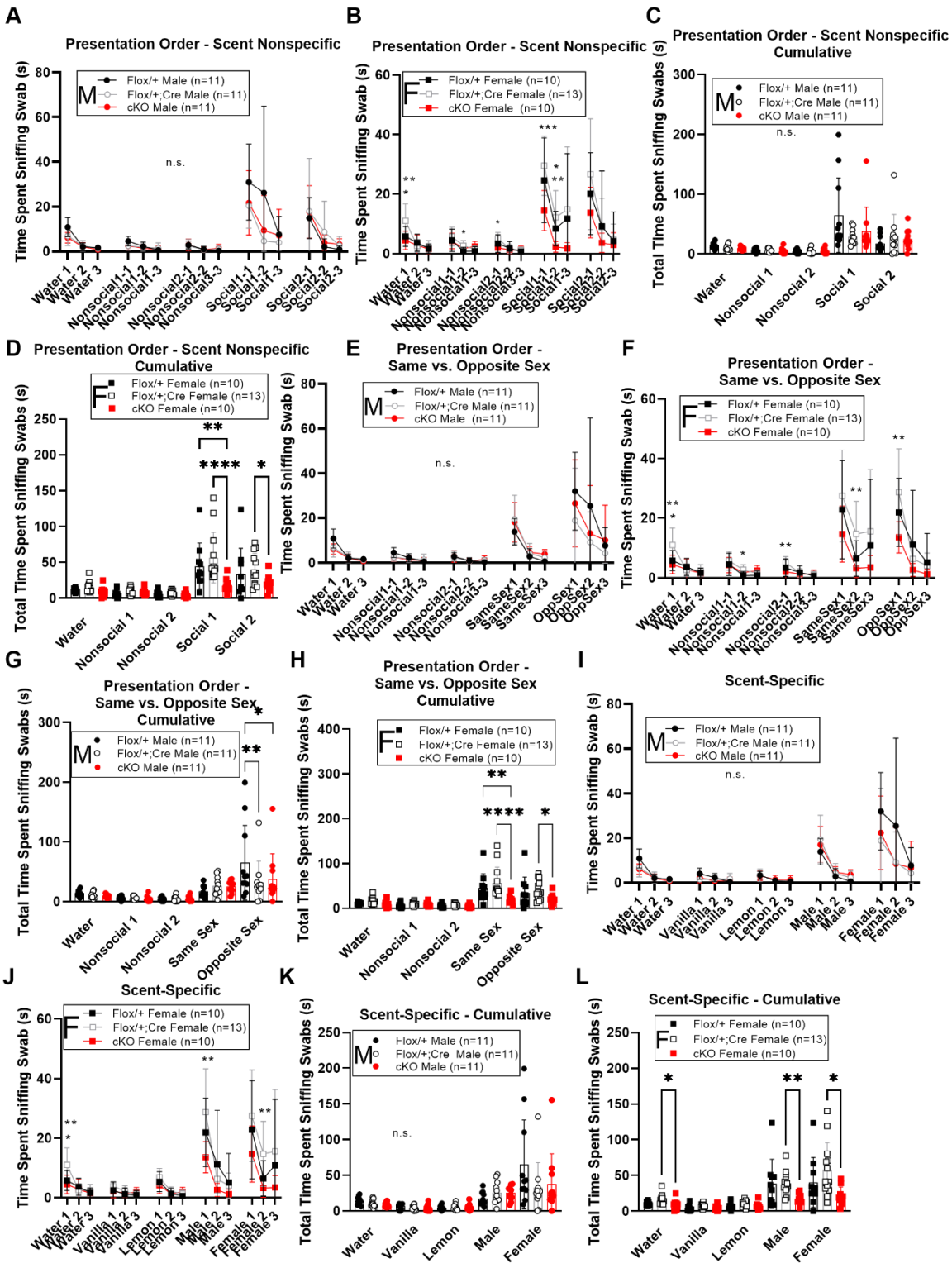
A
Presentation Order - Scent Nonspecific
Time Spent Sniffing Swab (s)
M
Flox/+ Male (n=11)
Flox/+;Cre Male (n=11)
cKO Male (n=11)
n.s.
Water 1
Water 2
Water 3
Nonsocial1-1
Nonsocial1-2
Nonsocial1-3
Nonsocial2-1
Nonsocial2-2
Nonsocial3-3
Social1-1
Social1-2
Social1-3
Social2-1
Social2-2
Social2-3
B
Presentation Order - Scent Nonspecific
Time Spent Sniffing Swab (s)
F
Flox/+ Female (n=10)
Flox/+;Cre Female (n=13)
cKO Female (n=10)
C
Presentation Order - Scent Nonspecific Cumulative
Total Time Spent Sniffing Swabs (s)
M
Flox/+ Male (n=11)
Flox/+;Cre Male (n=11)
cKO Male (n=11)
n.s.
Water
Nonsocial 1
Nonsocial 2
Social 1
Social 2
D
Presentation Order - Scent Nonspecific Cumulative
Total Time Spent Sniffing Swabs (s)
F
Flox/+ Female (n=10)
Flox/+;Cre Female (n=13)
cKO Female (n=10)
E
Presentation Order - Same vs. Opposite Sex
Time Spent Sniffing Swab (s)
M
Flox/+ Male (n=11)
Flox/+;Cre Male (n=11)
cKO Male (n=11)
n.s.
SameSex1
SameSex2
SameSex3
OppSex1
OppSex2
OppSex3
F
Presentation Order - Same vs. Opposite Sex
Time Spent Sniffing Swab (s)
F
Flox/+ Female (n=10)
Flox/+;Cre Female (n=13)
cKO Female (n=10)
G
Presentation Order - Same vs. Opposite Sex Cumulative
Total Time Spent Sniffing Swabs (s)
M
Flox/+ Male (n=11)
Flox/+;Cre Male (n=11)
cKO Male (n=11)
Water
Nonsocial 1
Nonsocial 2
Same Sex
Opposite Sex
H
Presentation Order - Same vs. Opposite Sex Cumulative
Total Time Spent Sniffing Swabs (s)
F
Flox/+ Female (n=10)
Flox/+;Cre Female (n=13)
cKO Female (n=10)
I
Scent-Specific
Time Spent Sniffing Swab (s)
M
Flox/+ Male (n=11)
Flox/+;Cre Male (n=11)
cKO Male (n=11)
n.s.
Vanilla 1
Vanilla 2
Vanilla 3
Lemon 1
Lemon 2
Lemon 3
Male 1
Male 2
Male 3
Female 1
Female 2
Female 3
J
Scent-Specific
Time Spent Sniffing Swab (s)
F
Flox/+ Female (n=10)
Flox/+;Cre Female (n=13)
cKO Female (n=10)
K
Scent-Specific - Cumulative
Total Time Spent Sniffing Swabs (s)
M
Flox/+ Male (n=11)
Flox/+;Cre Male (n=11)
cKO Male (n=11)
n.s.
Water
Vanilla
Lemon
Male
Female
L
Scent-Specific - Cumulative
Total Time Spent Sniffing Swabs (s)
F
Flox/+ Female (n=10)
Flox/+;Cre Female (n=13)
cKO Female (n=10)

Figure 4.8.

Figure 4.8. *Mllt11* Loss Impacts Interaction With Social Odors Differentially by Presentation Order in a Sex-Specific and Copy Number-Dependent Manner. **A**, **B**, Time spent sniffing each odor over all trials combined, controlling for scent nonspecific presentation order for males (**A**) and females (**B**). No differences were seen in males. *Mllt11*$^{flox/+;cre}$ females spent an increased amount of time sniffing upon the first presentation of the unscented water swab compared to both cKO and *Mllt11*$^{flox/+}$ females, and an increased time sniffing the second presentation of nonsocial odor 1 compared to *Mllt11*$^{flox/+}$ females. *Mllt11*$^{flox/+;cre}$ females spent significantly more time sniffing the first presentation of nonsocial odor 2 than cKO females, though neither differed significantly from *Mllt11*$^{flox/+}$ littermates. *Mllt11*$^{flox/+;cre}$ females spent significantly more time sniffing the first presentation of social odor 1 than cKO females, though neither differed significantly from *Mllt11*$^{flox/+}$ littermates. Female cKOs spent significantly less time sniffing than both *Mllt11*$^{flox/+;cre}$ and *Mllt11*$^{flox/+}$ individuals on the second trial of the same odor. **C**, **D**, Cumulative time spent sniffing each odor over all trials combined, controlling for scent nonspecific presentation order for males (**C**) and females (**D**). No differences were seen in males. *Mllt11*$^{flox/+;cre}$ females spent more time sniffing social odor 1 compared to *Mllt11*$^{flox/+}$ and cKO females. *Mllt11*$^{flox/+;cre}$ females also spent more time sniffing social odor 2 compared to female cKOs, though neither differed significantly from *Mllt11*$^{flox/+}$ littermates. **E**, **F**, Time spent sniffing each odor over all trials combined, controlling for sex of each social scent relative to the test mouse, for males (**E**) and females (**F**). No differences were seen in males. *Mllt11*$^{flox/+;cre}$ females spent more time sniffing in the second trial of nonsocial odor 1 compared to *Mllt11*$^{flox/+}$ females. *Mllt11*$^{flox/+;cre}$ females spent more time sniffing trial 1 of nonsocial odor 2 compared to cKO females, though neither differed significantly from *Mllt11*$^{flox/+}$ littermates. This trend was also seen in the second presentation of same sex odor, as well as the first presentation of the opposite sex odor, though there was no significant differences between either genotype and *Mllt11*$^{flox/+}$ littermates. **G**, **H**, Cumulative time spent sniffing each odor over all trials combined, controlling for sex of each social scent relative to the test mouse, for males (**G**) and females (**H**). Both *Mllt11*$^{flox/+;cre}$ and cKOs. males spent less time sniffing the opposite sex social scent compared to *Mllt11*$^{flox/+}$ littermates. Female cKOs spent less time sniffing the same sex odor compared to *Mllt11*$^{flox/+;cre}$ and *Mllt11*$^{flox/+}$ females, and less time sniffing opposite sex, compared to *Mllt11*$^{flox/+;cre}$ females, though no differences were seen between either genotype and *Mllt11*$^{flox/+}$ females. **I**, **J**, Time spent sniffing each odor over all trials combined, controlling for scent, for males (**I**) and females (**J**). Males showed no differences in sniffing. Female cKOs spent significantly less time sniffing on trial one of the male social odor as well as the second trial of the female social odor compared to *Mllt11*$^{flox/+;cre}$ females, though neither differed significantly from *Mllt11*$^{flox/+}$ littermates. **K**, **L**, Cumulative time spent sniffing each odor over all trials combined, controlling for scent, for males (**K**) and females (**L**). No differences were seen in males. cKO females spent less time sniffing both male and female social odors than *Mllt11*$^{flox/+;cre}$ females. Data presented as mean ± SD; n.s., not significant, *p ≤0.05, **p ≤ 0.01, ***p ≤ 0.001, ****p ≤ 0.0001. Flox/+; *Mllt11*$^{flox/+}$; Flox/+;Cre, *Mllt11*$^{flox/+;cre}$; cKO, conditional knockout.

significantly more time sniffing social odors than nonsocial odors (Figure 4.9. A-F), however, when these differences were compared between genotypes within sexes, no differences were seen in males (Figure 4.9. G), while female cKOs displayed reduced cumulative social odor sniffing compared to both *Mllt11*$^{flox/+}$ and *Mllt11*$^{flox/+;cre}$ females (Figure 4.9. H).

Taken together, these data suggest that loss of *Mllt11* may have a slight impact on social behaviors. Both *Mllt11*$^{flox/+;cre}$ and cKOs. males spent less time sniffing the opposite sex social scent compared to *Mllt11*$^{flox/+}$ littermates, but otherwise did not vary significantly in cumulative interaction with odors. Female cKOs exhibited decreased sniffing compared to *Mllt11*$^{flox/+;cre}$ and *Mllt11*$^{flox/+}$ littermates with regard to cumulative sniffing of same sex odors, social odor 1 regardless of sex, as well as cumulative social odor sniffing across all trials. Interestingly, a trend was also observed among some social odors in which *Mllt11*$^{flox/+;cre}$ and cKO females displayed opposite trends when compared to *Mllt11*$^{flox/+}$ littermates. In cumulative sniffing of water as well as all social odors regardless of sex and presentation order, *Mllt11*$^{flox/+;cre}$ females exhibited increased sniffing while cKO females exhibited decreased sniffing. Although the differences observed between *Mllt11*$^{flox/+;cre}$ and cKOs were significantly different from each other, they did not differ significantly from littermates *Mllt11*$^{flox/+}$. As loss of one or both copies of *Mllt11* in females gives rise to opposing and variable phenotypes, while loss of one or both copies in males gave rise to similar phenotypes or lack thereof entirely, it is tempting to speculate that *Mllt11* may play different roles or have a variable degree of impact between sexes with

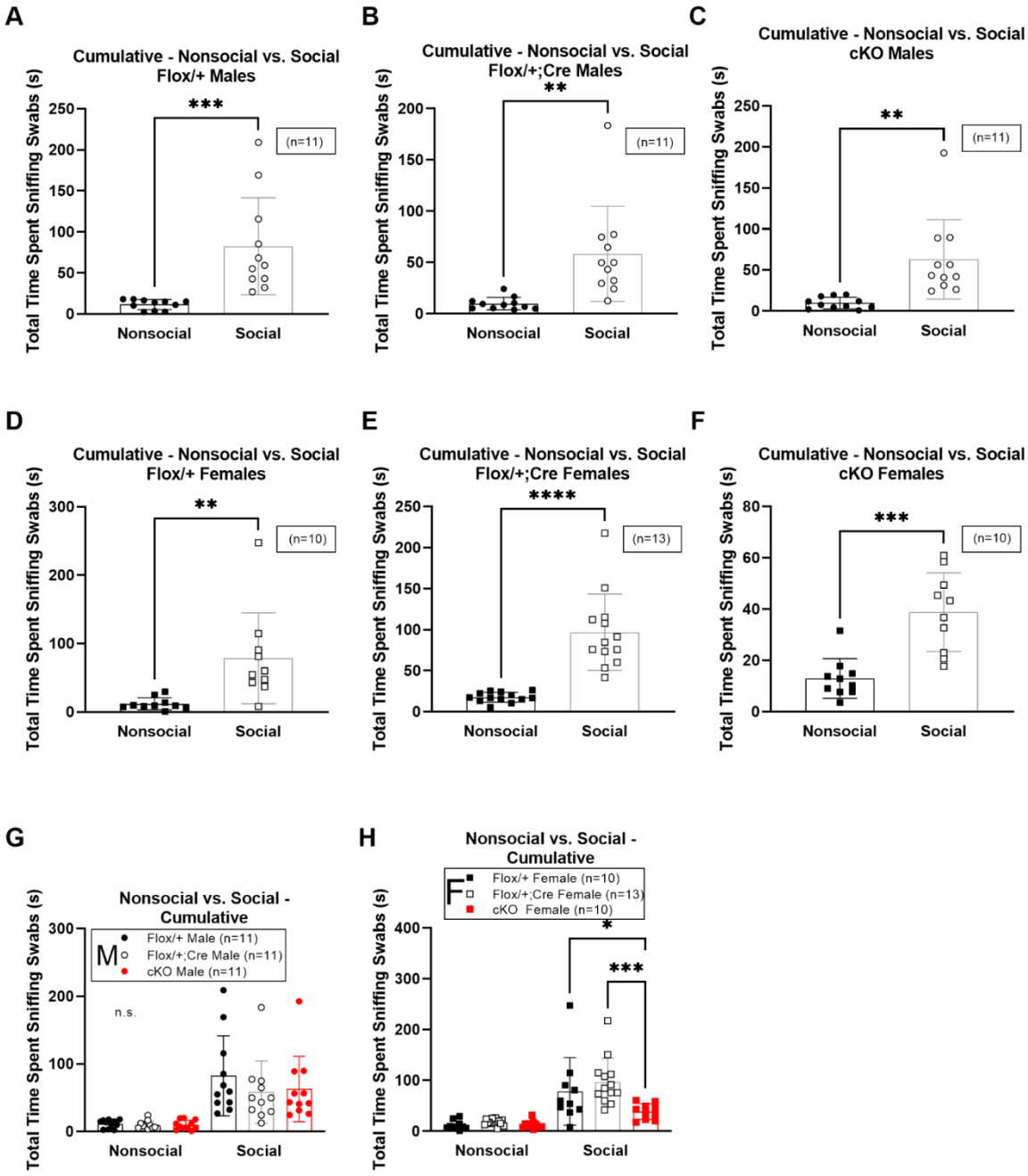
A
Cumulative - Nonsocial vs. Social
Flox/+ Males
***
(n=11)
Total Time Spent Sniffing Swabs (s)
Nonsocial
Social
B
Cumulative - Nonsocial vs. Social
Flox/+;Cre Males
**
(n=11)
C
Cumulative - Nonsocial vs. Social
cKO Males
**
(n=11)
D
Cumulative - Nonsocial vs. Social
Flox/+ Females
**
(n=10)
E
Cumulative - Nonsocial vs. Social
Flox/+;Cre Females
****
(n=13)
F
Cumulative - Nonsocial vs. Social
cKO Females
***
(n=10)
G
Nonsocial vs. Social -
Cumulative
M
Flox/+ Male (n=11)
Flox/+;Cre Male (n=11)
cKO Male (n=11)
n.s.
H
Nonsocial vs. Social -
Cumulative
F
Flox/+ Female (n=10)
Flox/+;Cre Female (n=13)
cKO Female (n=10)
*
***

Figure 4.9.

Figure 4.9. Loss of *Mllt11* Impacts Preference for Social vs. Nonsocial Odors in a Sex-Dependent Manner. **A**-**F**, Cumulative time spent sniffing nonsocial vs. social odors across all trials for males (**A**-**C**) and females (**D**-**F**) of each genotype. All showed a significant preference for social compared to nonsocial scents. **G**, **H**, Cumulative time spent sniffing nonsocial vs. social odors across all trials compared between genotypes within sexes for males (**G**) and females (**H**). Males showed no differences. Female cKOs displayed reduced cumulative social odor sniffing compared to both *Mllt11*$^{flox/+}$ and *Mllt11*$^{flox/+;cre}$ females. Data presented as mean ± SD; n.s., not significant, *p ≤0.05, **p ≤ 0.01, ***p ≤ 0.001, ****p ≤ 0.0001. Flox/+; *Mllt11*$^{flox/+}$; Flox/+;Cre, *Mllt11*$^{flox/+;cre}$; cKO, conditional knockout.

regard to social behaviors. Importantly, discerning that animals of all genotypes and sexes have the ability to sense and perceive olfactory stimuli is crucial to interpreting results of other social tests which will be discussed herein.

5.3. Loss of *Mllt11* Has Minimal Impact on Novel Social Approach Task in a Sex- and Copy Number-Dependent Manner

Given slight differences in social preference revealed in the olfactory habituation/dishabituation test, we wanted to look more closely at social behaviors by directly observing social interaction. On P37, sociability of mice was assessed through a three-chamber social approach test. Mice were placed into the center of a closed three-chamber apparatus for an initial habituation period of 5 minutes. Following this period, the chamber doors were opened, allowing mice to freely explore each chamber for an additional 5-minute period. Following this habituation and free exploration period, a stranger mouse was placed beneath a wire mesh pencil cup in one of the peripheral chambers. The experimental mouse was once again given free roam of the apparatus, and the time spent in each chamber was quantified. *Mllt11*$^{flox/+}$ males spent significantly more time in the presence of the stranger than in both the center and empty chambers, and significantly more time in the empty chamber compared to the center chamber (Figure 4.10. A). This distribution of time spent between the chambers is reflective of stereotypical social behavior in which mice choose to engage in novel social situations preferentially over a nonsocial object, or empty chamber (Silverman et al., 2010a). *Mllt11*$^{flox/+;cre}$ and cKO males both spent significantly

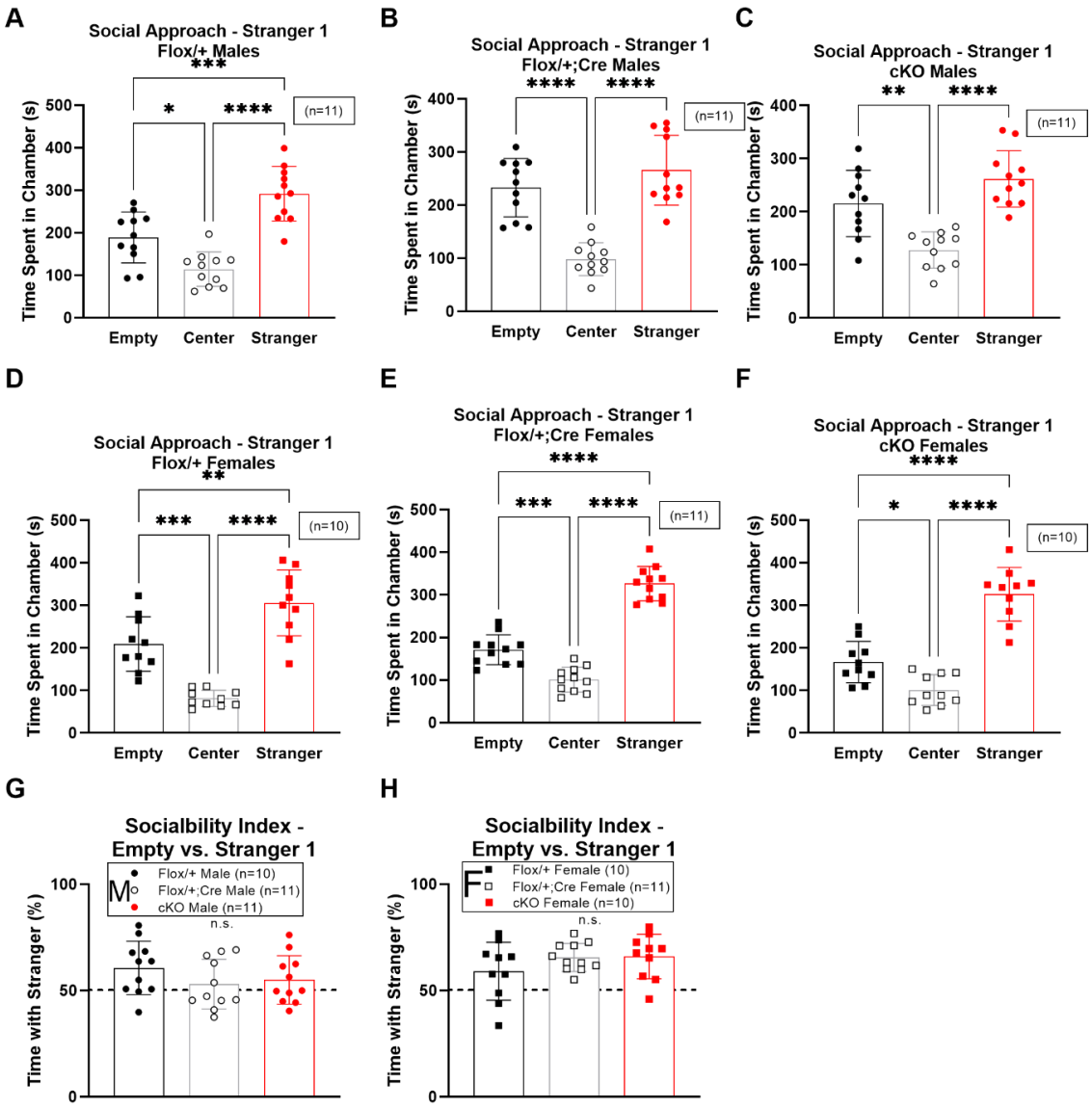

Figure 4.10. Loss of *Mllt11* Impacts Sociability in a Sex- and Copy Number-Dependent Manner. **A**-**F**, Time spent in each chamber during the first stranger presentation trial for males (**A**-**C**) and females (**D**-**F**) of each genotype. All genotypes spent more time in the presence of the stranger than all other chambers with the exception of *Mllt11*$^{flox/+;cre}$ and cKO males, which did not display a significant difference between time spent in the stranger and empty peripheral chambers. **G**, **H**, Sociability index, calculated as the percentage of total time spent in the stranger chamber compared to the empty peripheral chamber for males (**G**) and females (**H**). No differences were seen. Data presented as mean ± SD; n.s., not significant, *p ≤0.05, **p ≤ 0.01, ***p ≤ 0.001, ****p ≤ 0.0001. Flox/+; *Mllt11*$^{flox/+}$; Flox/+;Cre, *Mllt11*$^{flox/+;cre}$; cKO, conditional knockout.

more time in the presence of the stranger than the center chamber, though there was no statistically significant difference between time spent in the stranger chamber and empty chamber (Figure 4.10. B-C). Females, however, displayed a similar distribution of time spent in each chamber across genotypes, in which there was a significant difference between time spent in the stranger and center chambers as well as the stranger and empty chamber, with the greatest amount of time spent in the presence of the stranger (Figure 4.10. D-F).

A social preference index was calculated as the percentage of total time between peripheral chambers spent with the stranger, versus the empty chamber. All genotypes and sexes displayed an average social preference index of at least 50%, and no significant differences were exhibited between genotypes (Figure 4.10. G-H). As an additional measure of sociability, I sought to quantify the time spent interacting with the stranger mouse. No differences were found in time spent interacting with the stranger between genotypes within sexes (Figure 4.11. A-B). There was also no significant difference in time investment ratio, calculated by the percentage of total time spent in the stranger chamber that was spent interacting with the stranger (Figure 4.11. C-D). Taken together, these data suggest that loss of one or both copies of *Mllt11* in males may impact their preference for sociability, yet this effect does not seem to be apparent in females.

Following the presentation of the stranger (S1), a second stranger (S2) was added to the empty chamber in the manner previously described, and experimental mice were once again allowed to freely roam the apparatus and

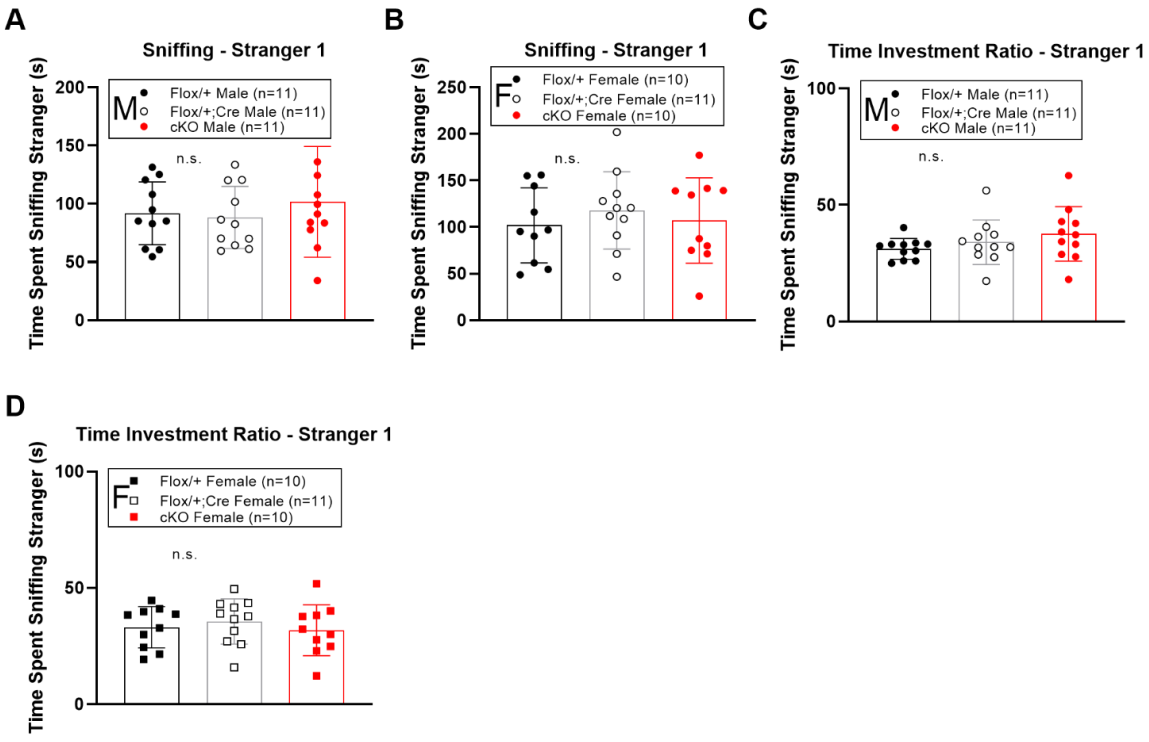

Figure 4.11. Time Investment With a Single Novel Stranger is Unaffected by Loss of *Mllt11*. **A**, **B**, Time spent directly interacting with, or sniffing, the stranger mouse in stranger presentation trial one, for males (**A**) and females (**B**). Sniffing levels were comparable across genotypes and sexes. **C**, **D**, Time investment ratio, calculated as the percentage of total time spent in the stranger chamber spent interacting with the stranger, for males (**C**) and females (**D**). Ratios were comparable across sexes and genotypes. Data presented as mean ± SD; n.s., not significant. Flox/+; *Mllt11*$^{flox/+}$; Flox/+;Cre, *Mllt11*$^{flox/+;cre}$; cKO, conditional knockout.

interact with the strangers. The time spent in each chamber was once again quantified, as well as the time spent specifically interacting with or sniffing each stranger mouse. Quantification of total time spent in each chamber revealed slight variations in distribution across genotypes and sexes. *Mllt11*$^{flox/+}$ and cKO males displayed no significant differences between time spent with S1 and S2, but spent significantly more time in both stranger chambers than in the center (Figure 4.12. A, C), while *Mllt11*$^{flox/+;cre}$ males spent significantly more time with S2 than S1 and the center chamber, and also spent significantly more time with S1 than in the center chamber (Figure 4.12. B). Females of all genotypes did not differ significantly in the amount of time spent between S1 and S2, but spent more time in both S1 and S2 than the center chamber (Figure 4.12. D-F).

Time spent interacting with each stranger was also quantified, revealing slight differences in some genotypes. *Mllt11*$^{flox/+}$ males exhibited no differences in interaction time between strangers (Figure 4.13. A), while *Mllt11*$^{flox/+;cre}$ and cKO males both spent significantly more time interacting with S2 than S1 (Figure 4.13. B-C). Quantification of interaction time amongst females of all genotypes revealed no differences in preference for either stranger (Figure 4.13. D-F). No significant differences were observed when time investment ratios were compared between S1 and S2 among genotypes of either sex (Figure 4.14. A-F). There were also no differences in the social novelty index, calculated as the percentage of total interaction time with both strangers spent interacting with S2 (Figure 4.14. G-H). Taken together, these data suggest that loss of one or

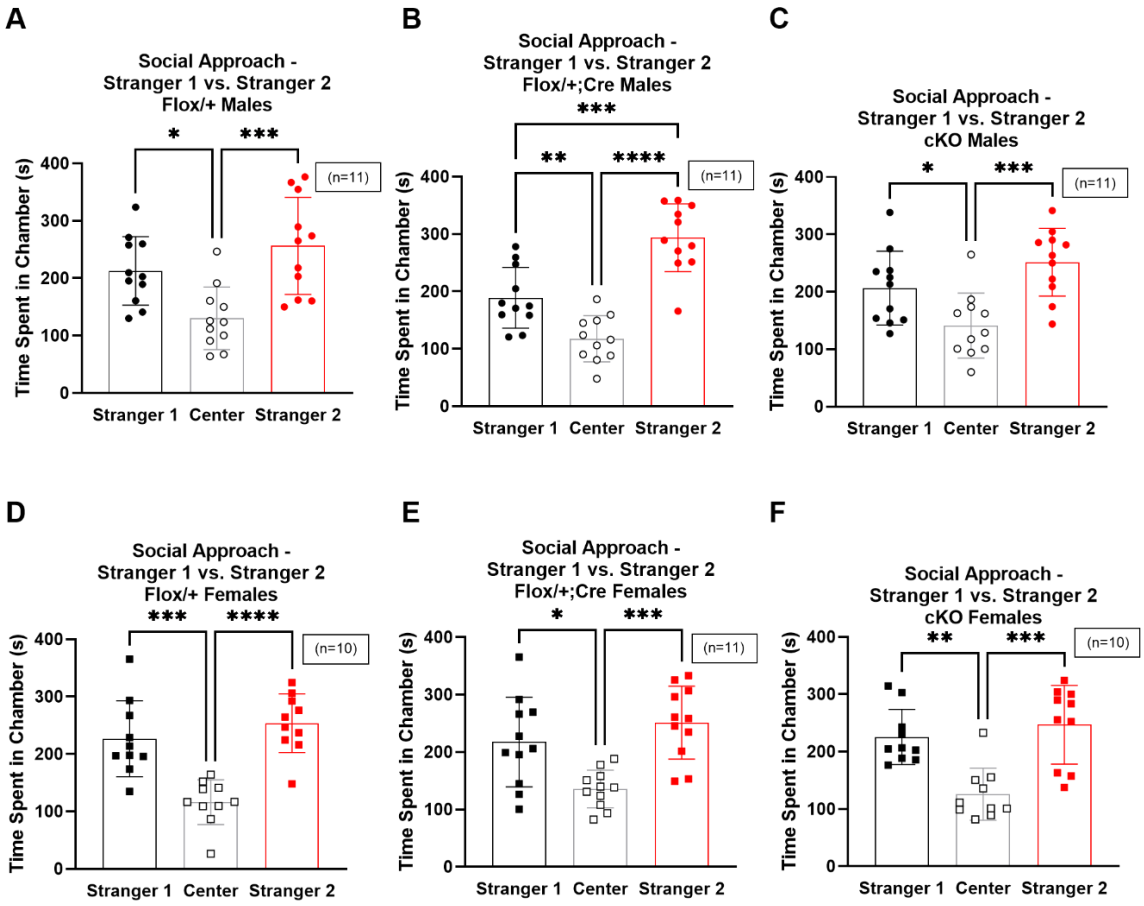

Figure 4.12. *Mllt11* Loss Has Minimal Effect on Time Spent in the Presence of Novel Compared to Familiar Mice in a Sex- and Copy Number-Dependent Manner. **A-F**, Distribution of time spent across all chambers during the second stranger presentation trial, for males (**A-C**) and females (**D-F**) of all genotypes. All sexes and genotypes displayed a significant preference for both stranger chambers compared to the center chamber, and *Mllt11*$^{flox/+;cre}$ males also spent more time in the second stranger chamber compared to the presence of stranger 1. Data presented as mean ± SD; *p ≤0.05, **p ≤ 0.01, ***p ≤ 0.001, ****p ≤ 0.0001. Flox/+; *Mllt11*$^{flox/+}$; Flox/+;Cre, *Mllt11*$^{flox/+;cre}$; cKO, conditional knockout.

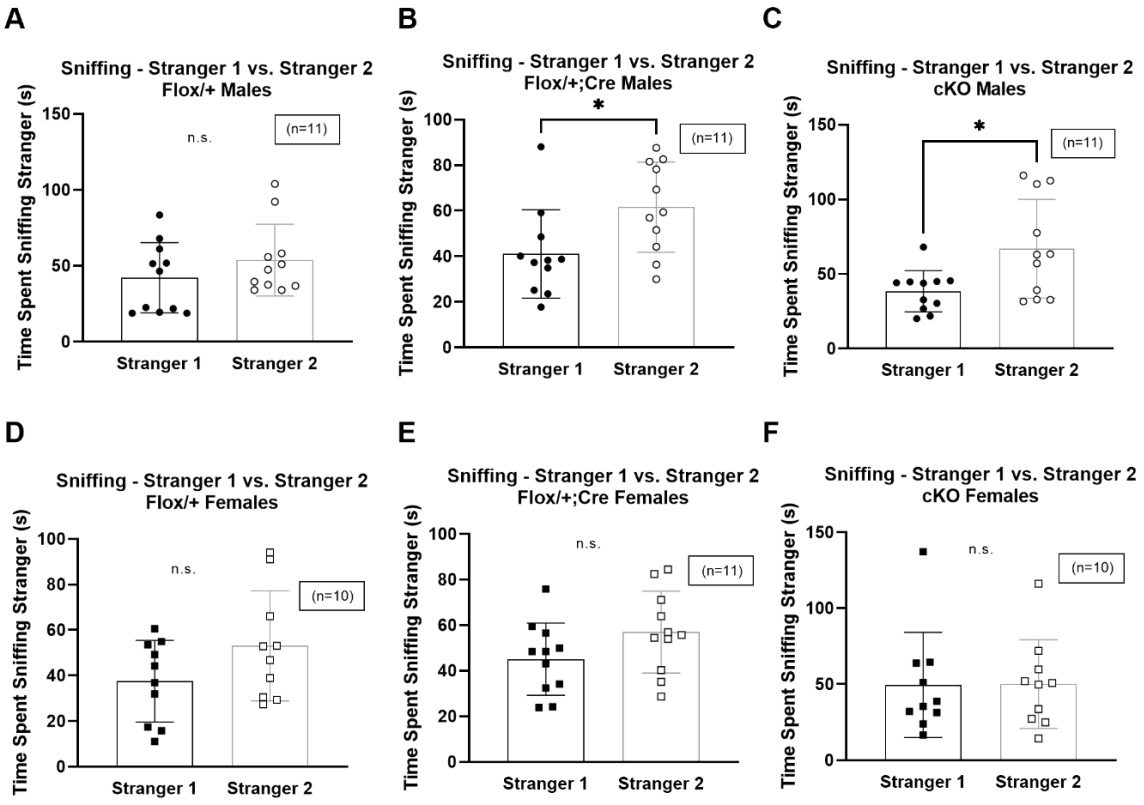

Figure 4.13. Loss of *Mllt11* Has a Moderate Effect on Time Spent Interacting With Novel Compared to Familiar Mice in a Sex-Dependent Manner. **A**-**F**, Distribution of time spent interacting with both stranger mice during the second stranger presentation trial, for males (**A**-**C**) and females (**D**-**F**) of all genotypes. *Mllt11*$^{flox/+;cre}$ and cKO males exhibited a preference for interacting with stranger 2 while all others showed no significant difference in time spent interacting with each stranger. Data presented as mean ± SD; n.s., not significant, *p ≤0.05. Flox/+; *Mllt11*$^{flox/+}$; Flox/+;Cre, *Mllt11*$^{flox/+;cre}$; cKO, conditional knockout.

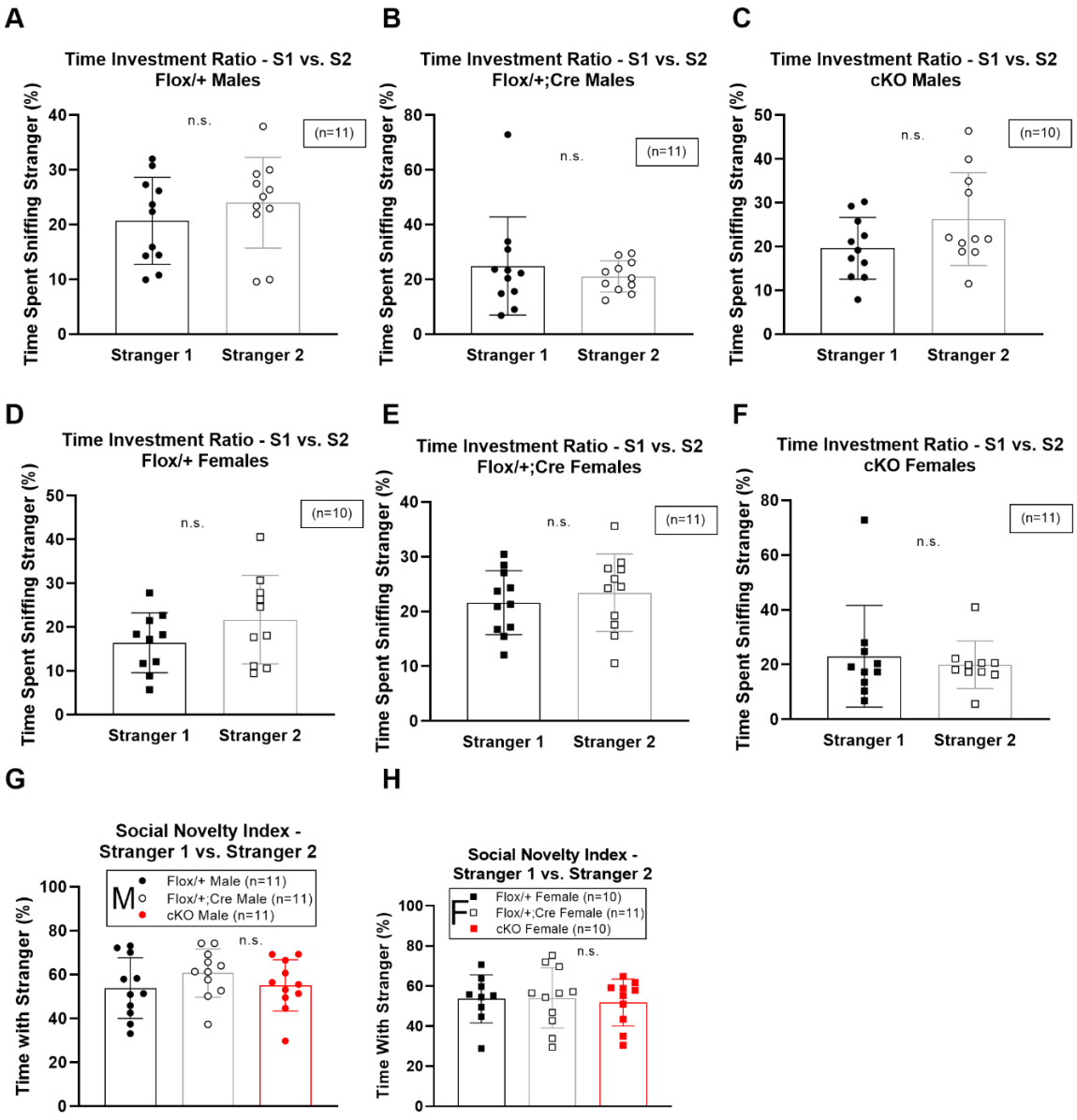

Figure 4.14. Loss of *Mllt11* Has No Notable Effect on Time Investment Ratios Between Novel and Familiar Mice. **A**-**F**, Time investment ratios for stranger 1 and stranger 2 across all genotypes for males (**A**-**C**) and females (**D**-**F**). Time investment ratios between strangers were comparable across all sexes and genotypes. **G**, **H**, Social novelty index, calculated by the percentage of total time spent interacting with strangers occupied by interaction with stranger 2, for males (**G**) and females (**H**). Social novelty indexes were comparable across genotypes and sexes. Data presented as mean ± SD; n.s., not significant, *p ≤0.05. Flox/+; *Mllt11*$^{flox/+}$; Flox/+;Cre, *Mllt11*$^{flox/+;cre}$; cKO, conditional knockout.

both copies of *Mllt11* in males may minimally impact their socialization in a manner that increases pursuit of novel social interaction over interaction with familiar individuals, while females are unaffected.

5.4. Impact of *Mllt11* Loss on Transmission of Food Preference is Negligible

The ability to infer information via communication through odors is a crucial behavior in mice, allowing them to gauge safety of food supply based on transmission of cues that a given food supply has been safely consumed by others (Forestier et al., 2019). Given the slight variations in sociability seen in the previously reported tests, we tested the ability of mice to communicate a food preference specifically, on P44. *Mllt11*$^{flox/+}$ or *Mllt11*$^{flox/flox}$ control cage mates were isolated and exposed to cocoa or cinnamon flavored chow for one hour, then placed with cage mates for 30 minutes to allow for demonstration and communication of flavored chow consumption. The following day, experimental cage mates, or observers, were offered the choice of cinnamon and cocoa flavored chow, one of which had previously been presented to the demonstrator cage mate, and one of which hadn't, cued and non-cued respectively.

Food receptacles were weighed before and after testing to determine which flavor was preferentially consumed during this time. Among males, no significant difference in food preference was observed across genotypes (Figure 4.15. A-C). Though no differences were observed in *Mllt11*$^{flox/+}$ or cKO females, *Mllt11*$^{flox/+;cre}$ females exhibited a preference for the cued food (Figure 4.15. D-F). A social transmission index was acquired by calculating the percentage of total

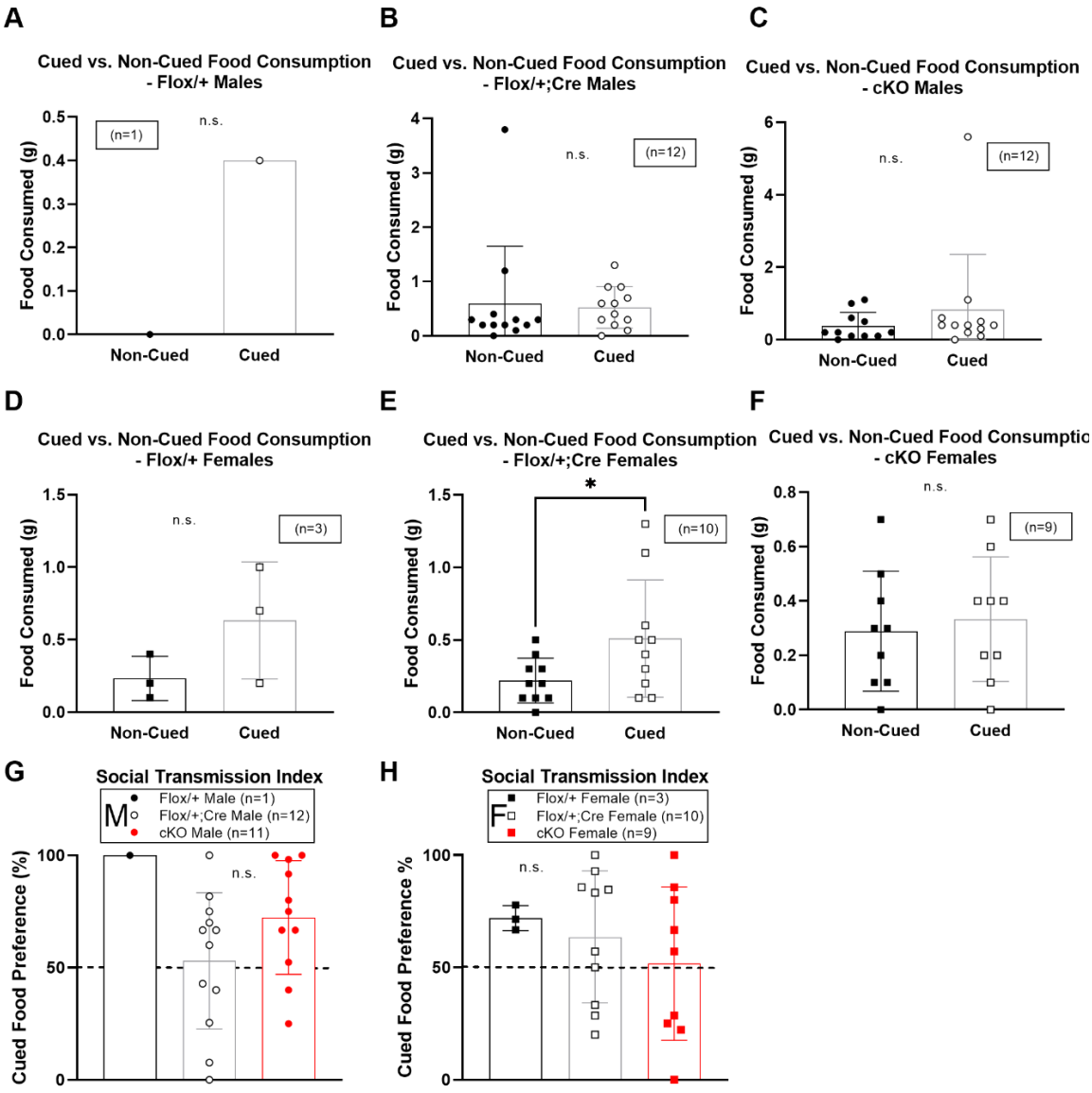

Figure 4.15. *Mllt11* Loss Impacts Transmission of a Conditioned Food Preference in a Manner That is Sex- and Copy Number-Dependent. **A-F**, Consumption of non-cued vs. cued food across all genotypes for males (**A-C**) and females (**D-F**). All genotpypes and sexes showed no statistically significant preference for either food with the exception of *Mllt11*$^{flox/+;cre}$ females which displayed a preference for the cued food. **G**, **H**, Social transmission index, calculated as the percentage of total consumed food that was cued for males (**G**) and females (**H**). All social transmission indices were comparable. Data presented as mean ± SD; n.s., not significant, *p ≤0.05. Flox/+; *Mllt11*$^{flox/+}$; Flox/+;Cre, *Mllt11*$^{flox/+;cre}$; cKO, conditional knockout.

food consumed that was cued, and consistent with previous results, no significant differences were observed between genotypes, however *Mllt11*$^{flox/+;cre}$ males (Figure 4.15. G) and cKO females (Figure 4.15. H) had the lowest scores of all genotypes within each sex.

Taken together, these data suggest that *Mllt11* likely does not play a major role in communication of food preference. It should be noted, however, that comparisons made between *Mllt11*$^{flox/+}$ individuals and others should be taken lightly, as the sample size of *Mllt11*$^{flox/+}$ or *Mllt11*$^{flox/flox}$ individuals achieved was low, due to the fact that mice of this genotype were designated demonstrators and only tested when there were excess born in a litter sufficient to permit separate mice of the desired genotypes for both demonstration and testing. A higher n of *Mllt11*$^{flox/+}$ or *Mllt11*$^{flox/flox}$ individuals is required to further parse out the extent to which *Mllt11* plays a role in this behavior.

5.5. Loss of *Mllt11* Results in Minimal Variation in Repetitive Behaviors in a Sex-Dependent Manner

In addition to social deficits and altered social behaviors, another hallmark feature of ASD is hyper fixation on a task or interest and increased tendency to engage in repetitive behaviors. These are also common features of OCD and ADHD, which exhibit a high degree of comorbidity with ASD (Abramovitch et al., 2015). As such, we elected to examine these behaviors on P51 through the marble burying and Nestlet shredding tests. First, mice were placed in an empty cage with a square of Nestlet bedding material for 30 minutes and allowed to

freely explore the open field and shred the Nestlet, which was weighed prior to and following testing to assess the degree of shredding behavior exhibited. Males did not display any significant differences in shredding behavior across genotypes (Figure 4.16. A), however female cKOs shredded significantly less nestlet than both *Mllt11*$^{flox/+}$ and *Mllt11*$^{flox/+;cre}$ individuals (Figure 4.16. B).

Following the Nestlet shredding, animals were returned to their home cage for one hour, then placed in a new rat cage with 3 inches of corncob bedding upon which sat a grid-like array of marbles. Mice were allowed to interact with the marbles and dig or burrow in the bedding for 30 minutes, at which time the number of buried marbles was quantified. No significant differences were found in the number of marbles buried across sexes and genotypes (Figure 4.16. C-D). Taken together, the slight variations in tendency toward engaging in repetitive behaviors suggest that loss of *Mllt11* may have a slight impact on repetitive behavior in a manner that is dependent on sex and type of behavior.

5.6. Loss of *Mllt11* May Impact Tendency Toward Anxiety-like Behaviors in a Sex- and Copy Number-Dependent Manner

Repetitive behaviors such as grooming (Figure 4.17. A), digging (Figure 4.17. B-C), climbing (Figure 4.17. D-F), jumping (Figure 4.17. G), sleeping (Figure 4.17. H), and bouts of rearing (Figure 4.17. I) can also be used as a proxy for anxiety-like or compulsive behaviors, and as such these were measured during olfactory habituation/dishabituation and social preference testing to determine if any notable changes in anxiety occurred in cKO mice, as

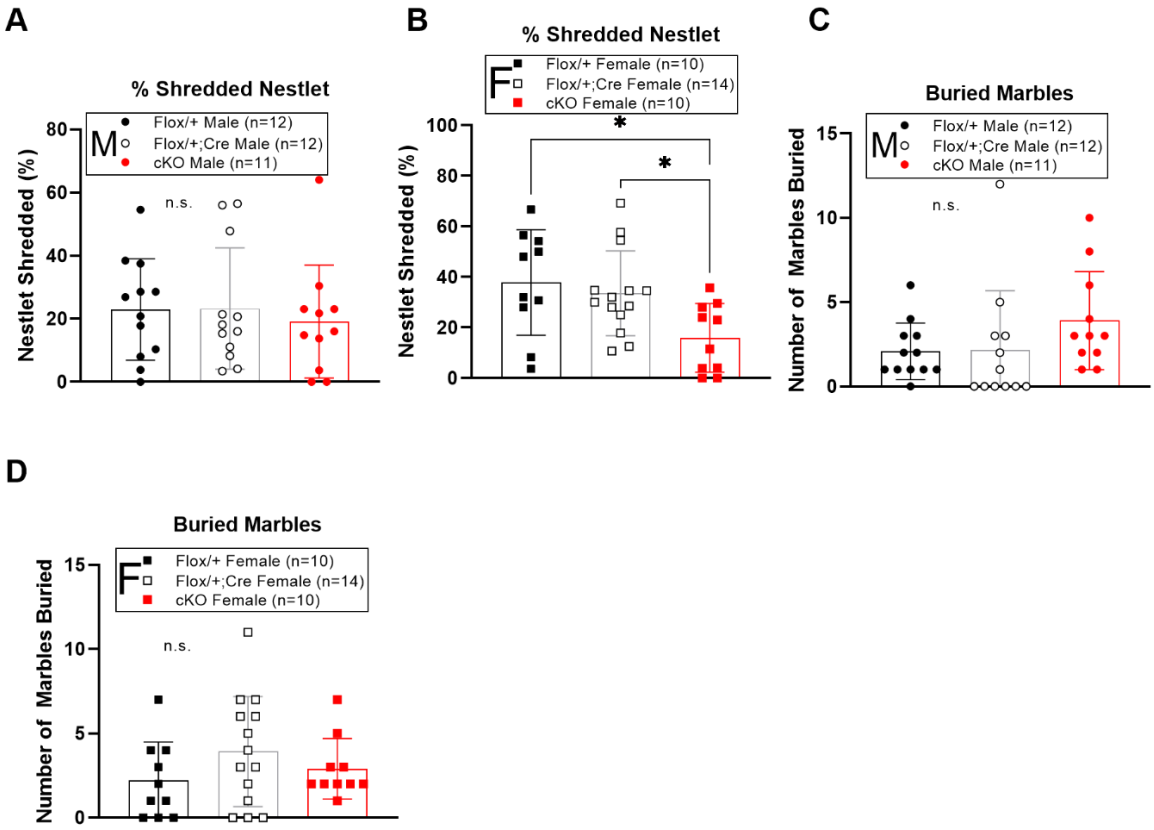

Figure 4.16. *Mllt11* Loss Impacted Tendency Toward Repetitive Behaviors in a Sex-Dependent Manner. **A**, **B**, Percentage of total Nestlet shredded by males (**A**) and females (**B**). Males displayed no significant difference in shredded Nestlet. cKO females shredded less than *Mllt11*$^{flox/+}$ and *Mllt11*$^{flox/+;cre}$ females. **C**, **D**, Number of marbled buried by males (**C**) and females (**D**). No significant differences were seen. Data presented as mean ± SD; n.s., not significant, *p ≤0.05. Flox/+; *Mllt11*$^{flox/+}$; Flox/+;Cre, *Mllt11*$^{flox/+;cre}$; cKO, conditional knockout.

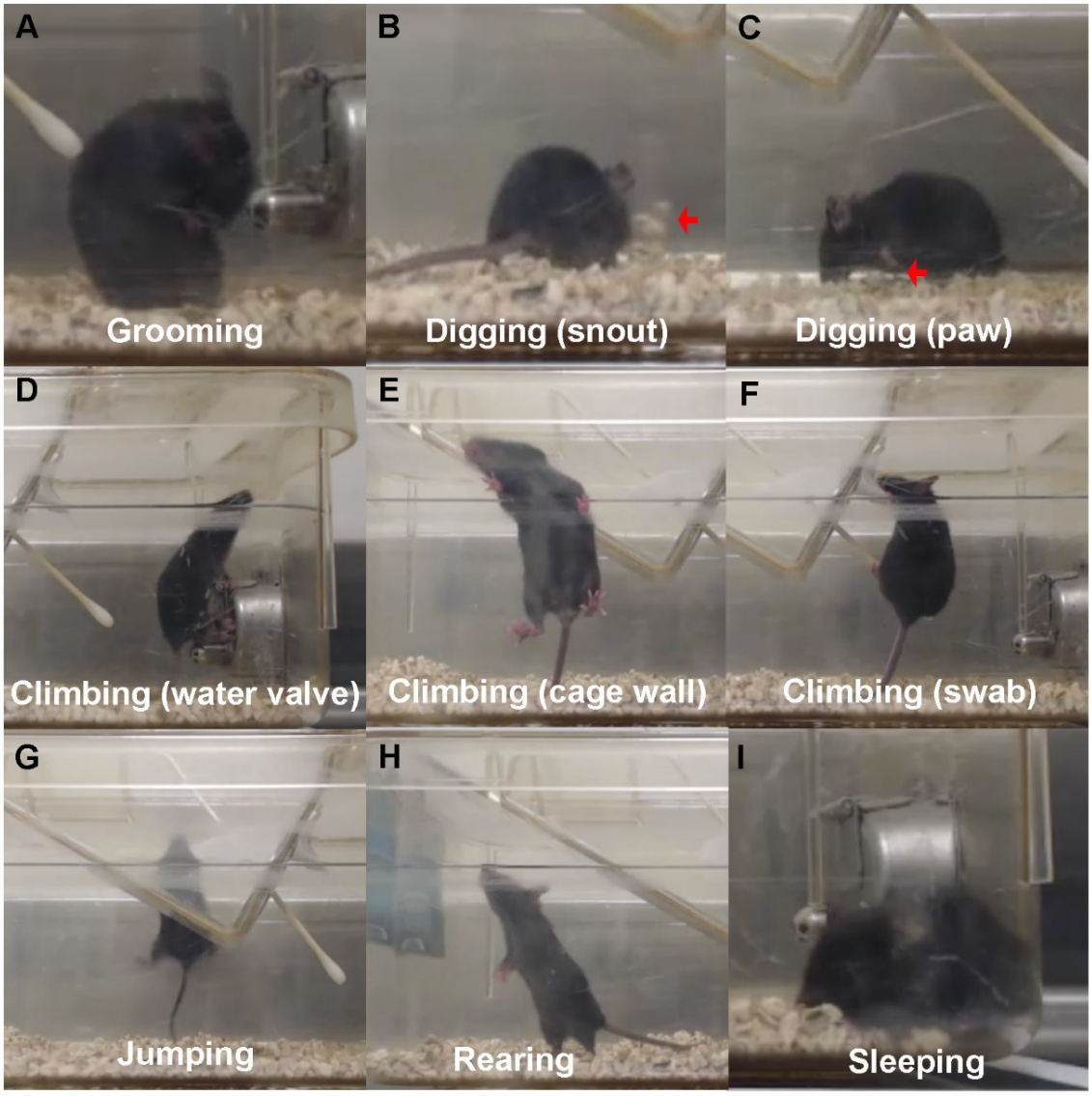

Figure 4.17. Sample Images of Repetitive and Anxiety-Like Behaviors. **A**, An example of grooming behavior in which a mouse licks its torso. **B**, **C**, Examples of digging in which a mouse moves corncob bedding (red arrows) with its snout (**B**) or paw (**C**). **D**-**F**, Examples of climbing in which a mouse is completely elevated with all four paws off of the ground and contacting another surface, specifically the water valve (**D**), cage wall (**E**), or swab (**F**). **G**, Jumping behavior in which the mouse is in midair with all four paws free of contacts with the ground or any other surface. **H**, Rearing behavior in which the mouse is elevated on its hind limbs. **I**, Sleeping behavior in which the eyes are closed and the mouse is still.

these behaviors are often comorbid with ASD, and variability in the form of an increase or decrease compared to controls may be indicative of anxiety (Zaboski & Storch, 2018). No significant differences were seen between genotypes across measures of any anxiety-like behaviors; however variability was seen between sexes and genotypes (Figure 4.18.A-L).

Though the assessment of anxiety-like behaviors at P30 did not reveal statistically significant variations between genotypes, it is important to note that each test animal was in isolation for the duration of the test. To assess the impact of social interaction on levels of anxiety-like behaviors, I sought to assess the differences in grooming behavior over each trial of the social approach task on P37. The percentage of time spent grooming during each period was quantified, and no significant differences were seen across genotypes within sexes (Figure 4.19. A-F). When percentage of time spent grooming was compared between the habituation trial and each of the stranger presentation trials, all genotypes and sexes displayed a significantly increased amount of time spent grooming upon presentation of S2 compared to S1 and habituation (Figure 4.20. A-F), while *Mllt11*$^{flox/+}$ females also exhibited a significant increase in grooming between the presentation of S1 and habituation (Figure 4.20. D). No differences in total grooming summed across all trials were observed (Figure 4.20. G-H).

Additionally, alterations in levels of locomotion can be indicative of anxiety. As such, we quantified numbers of entries into each chamber in the three-chamber apparatus on testing P37 while the test mouse was alone and in the

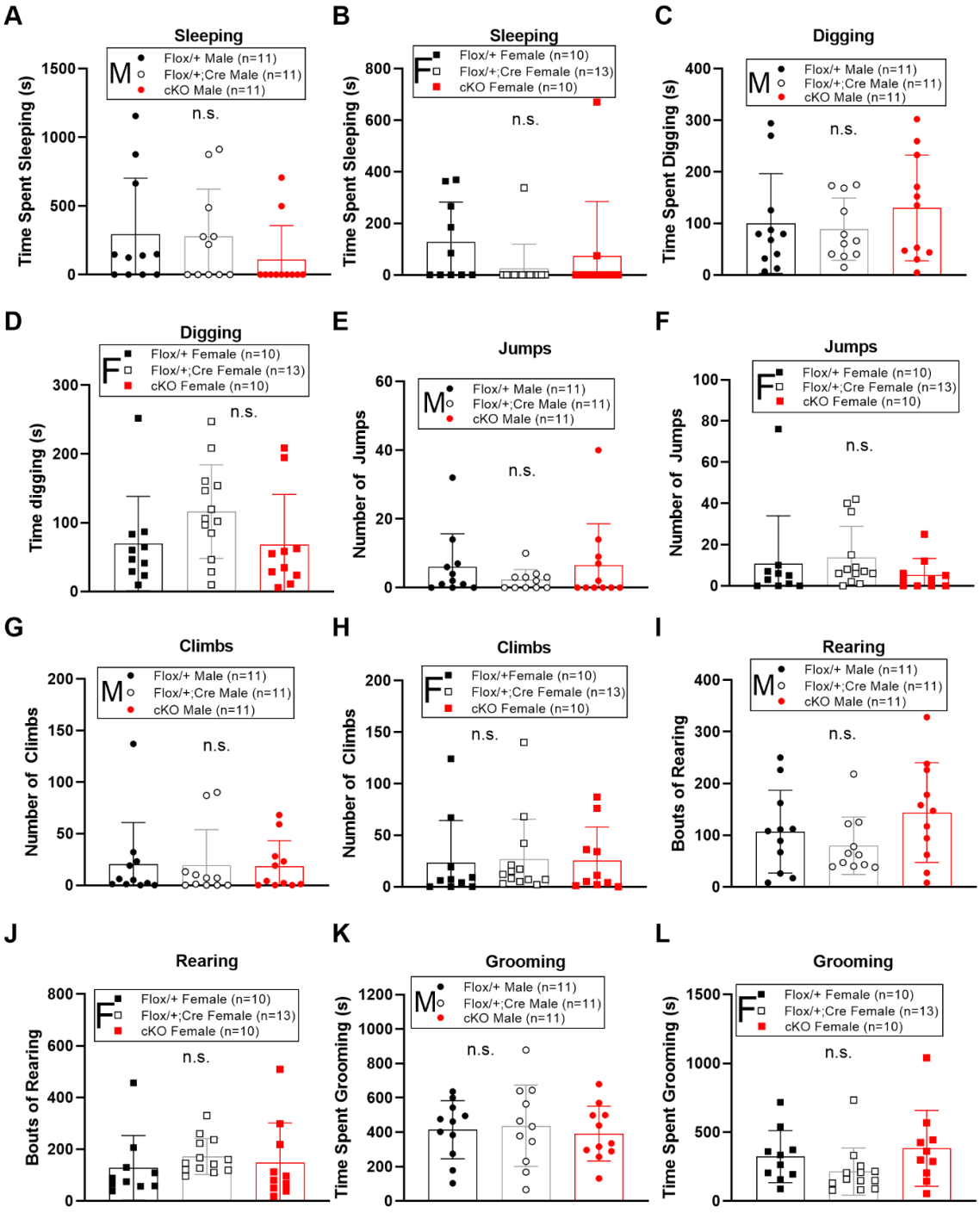
A
Sleeping
M
Flox/+ Male (n=11)
Flox/+;Cre Male (n=11)
cKO Male (n=11)
n.s.
Time Spent Sleeping (s)
B
Sleeping
F
Flox/+ Female (n=10)
Flox/+;Cre Female (n=13)
cKO Female (n=10)
n.s.
Time Spent Sleeping (s)
C
Digging
M
Flox/+ Male (n=11)
Flox/+;Cre Male (n=11)
cKO Male (n=11)
n.s.
Time Spent Digging (s)
D
Digging
F
Flox/+ Female (n=10)
Flox/+;Cre Female (n=13)
cKO Female (n=10)
n.s.
Time digging (s)
E
Jumps
M
Flox/+ Male (n=11)
Flox/+;Cre Male (n=11)
cKO Male (n=11)
n.s.
Number of Jumps
F
Jumps
F
Flox/+ Female (n=10)
Flox/+;Cre Female (n=13)
cKO Female (n=10)
n.s.
Number of Jumps
G
Climbs
M
Flox/+ Male (n=11)
Flox/+;Cre Male (n=11)
cKO Male (n=11)
n.s.
Number of Climbs
H
Climbs
F
Flox/+Female (n=10)
Flox/+;Cre Female (n=13)
cKO Female (n=10)
n.s.
Number of Climbs
I
Rearing
M
Flox/+ Male (n=11)
Flox/+;Cre Male (n=11)
cKO Male (n=11)
n.s.
Bouts of Rearing
J
Rearing
F
Flox/+ Female (n=10)
Flox/+;Cre Female (n=13)
cKO Female (n=10)
n.s.
Bouts of Rearing
K
Grooming
M
Flox/+ Male (n=11)
Flox/+;Cre Male (n=11)
cKO Male (n=11)
n.s.
Time Spent Grooming (s)
L
Grooming
F
Flox/+ Female (n=10)
Flox/+;Cre Female (n=13)
cKO Female (n=10)
n.s.
Time Spent Grooming (s)

Figure 4.18.

Figure 4.18. Impact of *Mllt11 L*oss on Repetitive Behaviors in Solitude is Minimal, Variable, and Sex-and Copy Number-Dependent. **A**, **B**, Time spent sleeping during P30 testing in males (**A**) and females (**B**). No significant differences were observed. **C**, **D**, Time spent digging during P30 testing in males (**C**) and females (**D**). No significant differences were observed. **E**, **F**, Bouts of jumping during P30 testing in males (**E**) and females (**F**). No significant differences were observed. **G**, **H**, Bouts of climbing during P30 testing in males (**G**) and females (**H**). No differences were seen. **I**, **J**, Bouts of rearing during P30 testing in males (**I**) and females (**J**). No significant differences were observed. **K**, **L**, Time spent grooming during P30 testing in males (**K**) and females (**L**). No significant differences were observed. Data presented as mean ± SD; n.s. Flox/+; *Mllt11*$^{flox/+}$; Flox/+;Cre, *Mllt11*$^{flox/+;cre}$; cKO, conditional knockout.

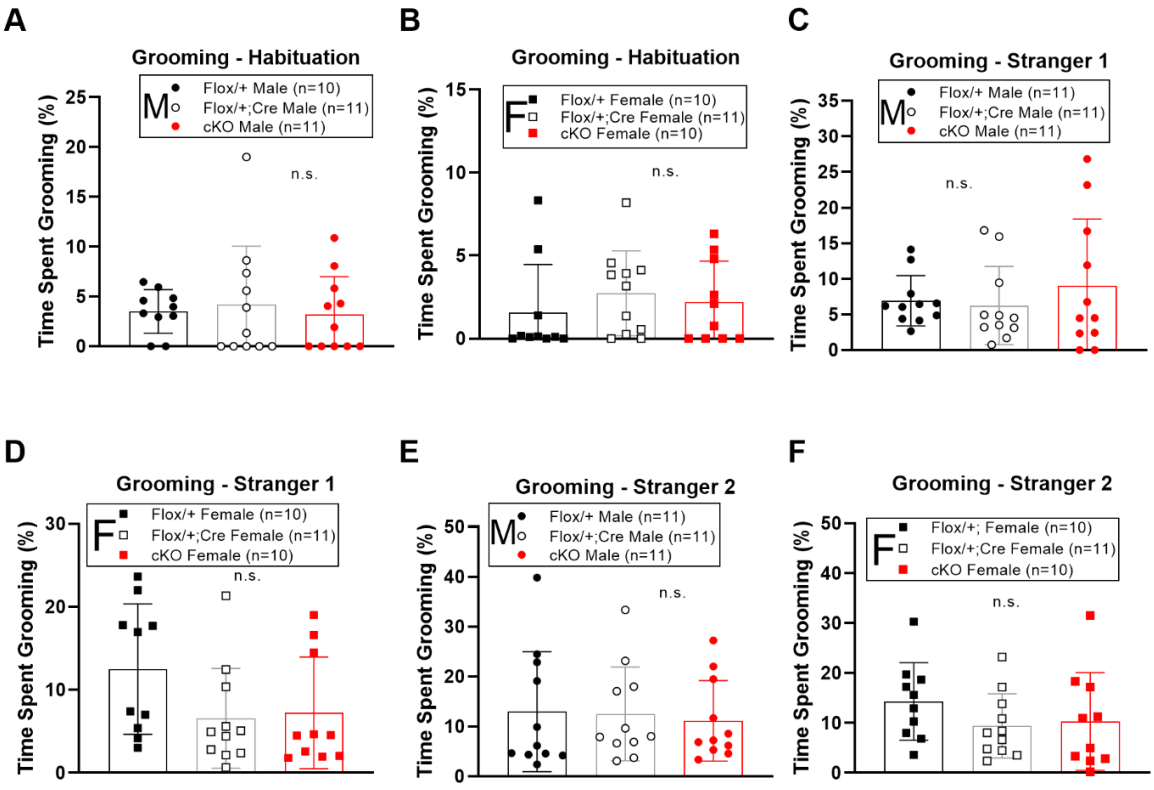

Figure 4.19. Impact of *Mllt11* Loss on Repetitive Behaviors in a Social Environment is Minimal, Variable, and Sex- and Copy Number-Dependent. **A**, **B**, Time spent grooming during P37 habituation in males (**A**) and females (**B**). No significant differences were seen. **C**, **D**, Time spent grooming during first stranger presentation trial during P37 testing in males (**C**) and females (**D**). No significant differences were observed. **E**, **F**, Time spent grooming during second stranger presentation trial during P37 testing in males (**E**) and females (**F**). No differences were observed. Data presented as mean ± SD; n.s. Flox/+; *Mllt11*$^{flox/+}$; Flox/+;Cre, *Mllt11*$^{flox/+;cre}$; cKO, conditional knockout.

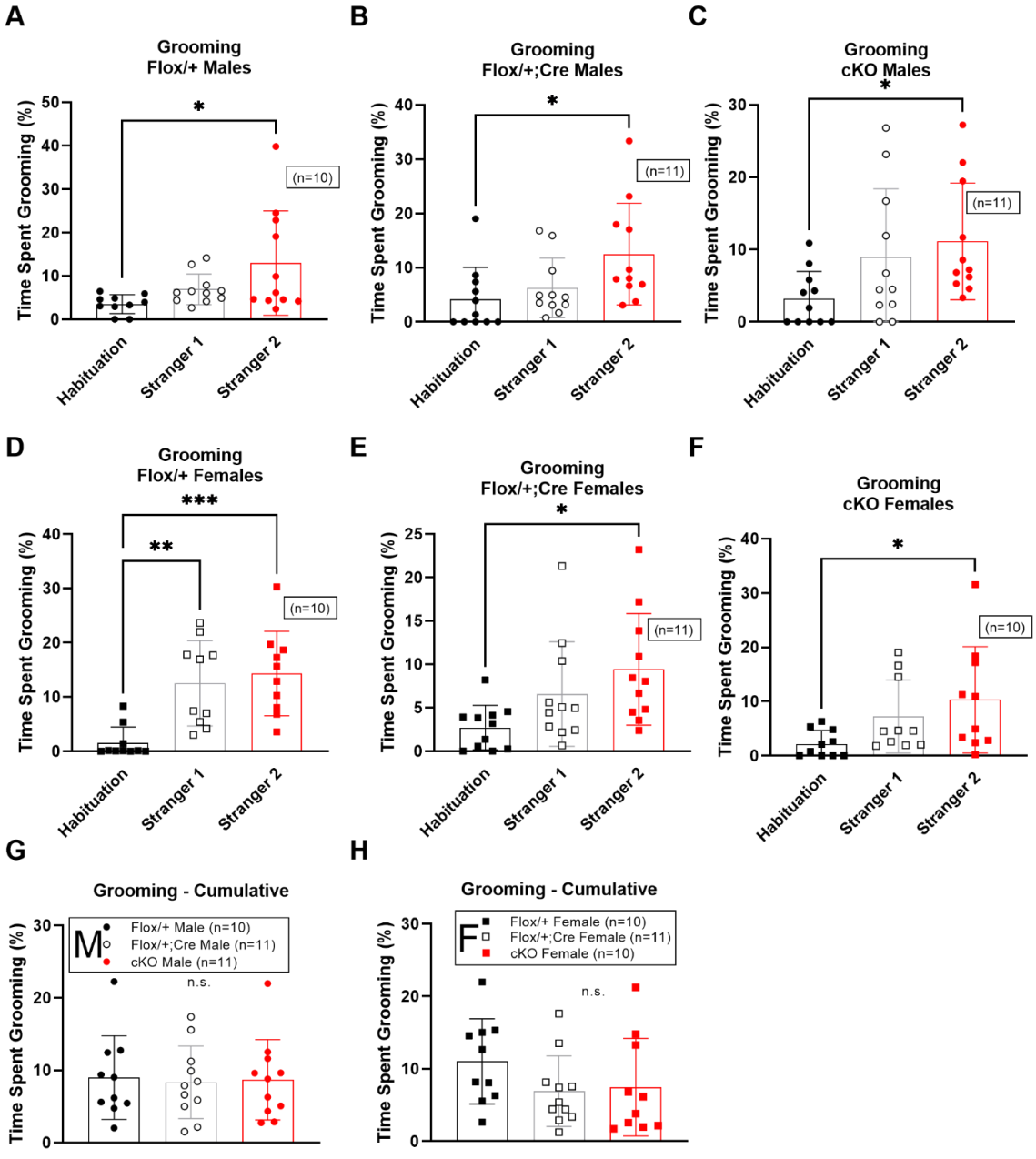
A
Grooming
Flox/+ Males
Time Spent Grooming (%)
(n=10)
Habituation
Stranger 1
Stranger 2
B
Grooming
Flox/+;Cre Males
(n=11)
C
Grooming
cKO Males
(n=11)
D
Grooming
Flox/+ Females
(n=10)
E
Grooming
Flox/+;Cre Females
(n=11)
F
Grooming
cKO Females
(n=10)
G
Grooming - Cumulative
M
Flox/+ Male (n=10)
Flox/+;Cre Male (n=11)
cKO Male (n=11)
n.s.
H
Grooming - Cumulative
F
Flox/+ Female (n=10)
Flox/+;Cre Female (n=11)
cKO Female (n=10)
n.s.

Figure 4.20.

Figure 4.20. Loss of *Mllt11 D*oes Not Impact Grooming Behavior Across Social Contexts. **A**-**F**, Distribution of time spent grooming across habituation, first stranger presentation, and second stranger presentation trials during P37 testing for males (**A**-**C**) and females (**D**-**F**). All sexes and genotypes spent significantly more time grooming in the presence of two strangers than during the habituation period, and *Mllt11*$^{flox/+}$ females also spent significantly more time grooming in the presence of one stranger than during the habituation period. **G**, **H**, Time spent grooming cumulatively across all trials during P37 testing for males (**G**) and females (**H**). No significant differences were seen. Data presented as mean ± SD; n.s., not significant, *p ≤0.05, **p ≤ 0.01, ***p ≤ 0.001. Flox/+; *Mllt11*$^{flox/+}$; Flox/+;Cre, *Mllt11*$^{flox/+;cre}$; cKO, conditional knockout.

presence of one or both stranger mice in order to assess any impact of *Mllt11* loss on this measure of locomotion as a proxy for anxiety-like behavior in various social contexts. During habituation, no differences in total entries were observed (Figure 4.21. A-B). Following habituation, upon presentation of S1, entries into the empty chamber and S1 were compared, and no differences were seen across genotypes or sexes (Figure 4.21. C-H), nor were there differences in total entries (Figure 4.21. I-J).

In the second stranger presentation trial, entries into the chamber containing S1 and S2 were quantified and compared across genotypes, and all were again relatively equal, with no statistically significant differences (Figure 4.22. A-F), nor were there differences in total entries (Figure 4.22. G-H). Total entries summed across all trials also revealed no differences (Figure 4.23. A-B). When comparing total entries during the habituation, S1, and S1 vs. S2 trials, significant increases in entries were seen across all genotypes and sexes correlating to the number of mice involved in the trial (Figure 4.23. C-H).

Taken together, quantification of measures of anxiety-like behaviors suggests the potential of a slight and highly variable impact of *Mllt11* loss across sexes and genotypes. These data and the variability among them are consistent with variability seen in the vast spectrum of symptoms with which ASD presents. However, the impact of *Mllt11* loss on these behaviors is minimal and not statistically significant in most cases, consistent with a potential role for *Mllt11* as one of many regulators of molecular determinants of ASD-like behavior.

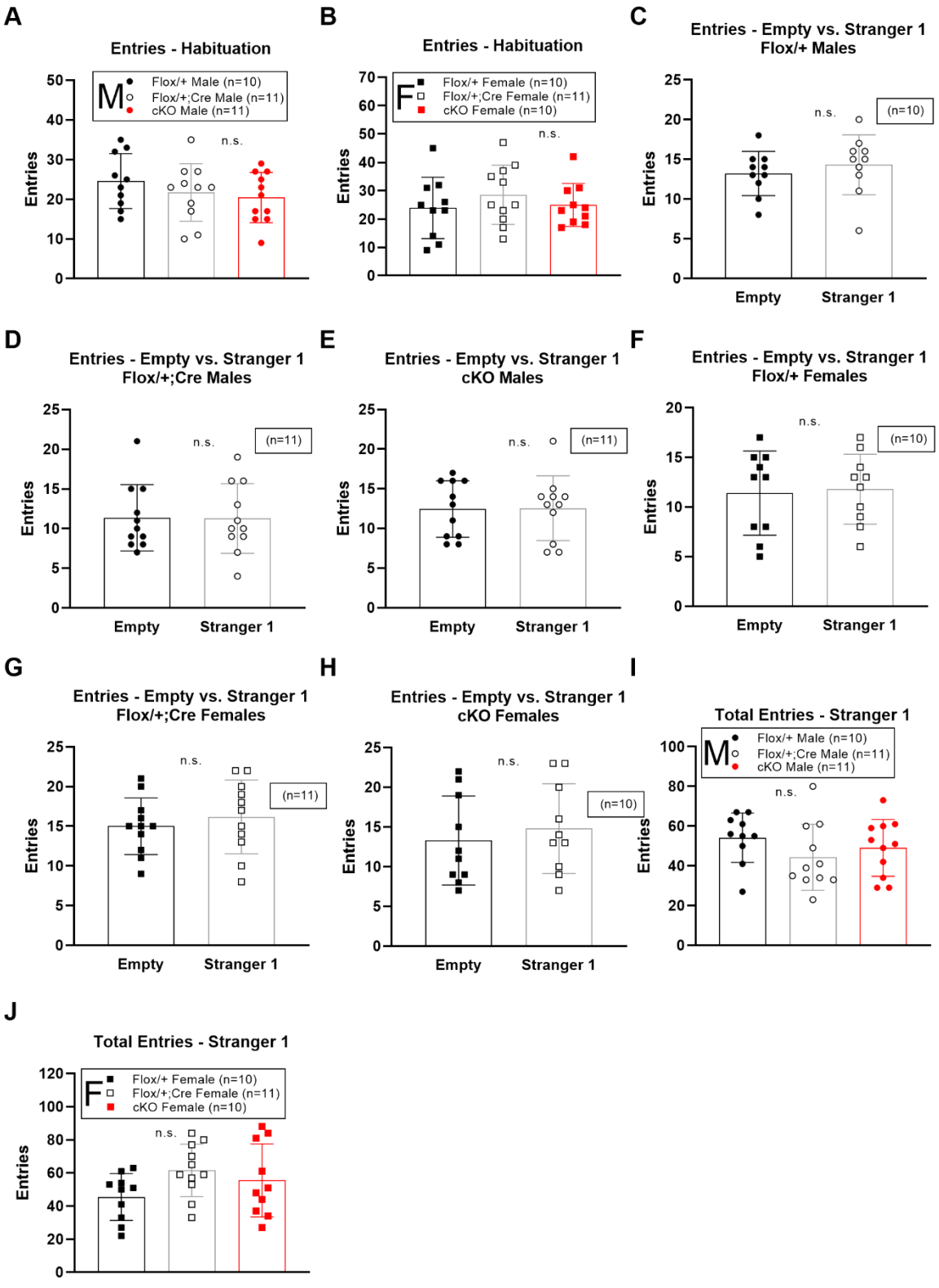
A
Entries - Habituation
M
Flox/+ Male (n=10)
Flox/+;Cre Male (n=11)
cKO Male (n=11)
Entries
n.s.
B
Entries - Habituation
F
Flox/+ Female (n=10)
Flox/+;Cre Female (n=11)
cKO Female (n=10)
Entries
n.s.
C
Entries - Empty vs. Stranger 1
Flox/+ Males
Entries
n.s.
(n=10)
Empty
Stranger 1
D
Entries - Empty vs. Stranger 1
Flox/+;Cre Males
Entries
n.s.
(n=11)
Empty
Stranger 1
E
Entries - Empty vs. Stranger 1
cKO Males
Entries
n.s.
(n=11)
Empty
Stranger 1
F
Entries - Empty vs. Stranger 1
Flox/+ Females
Entries
n.s.
(n=10)
Empty
Stranger 1
G
Entries - Empty vs. Stranger 1
Flox/+;Cre Females
Entries
n.s.
(n=11)
Empty
Stranger 1
H
Entries - Empty vs. Stranger 1
cKO Females
Entries
n.s.
(n=10)
Empty
Stranger 1
I
Total Entries - Stranger 1
M
Flox/+ Male (n=10)
Flox/+;Cre Male (n=11)
cKO Male (n=11)
Entries
n.s.
J
Total Entries - Stranger 1
F
Flox/+ Female (n=10)
Flox/+;Cre Female (n=11)
cKO Female (n=10)
Entries
n.s.

Figure 4.21.

Figure 4.21. *Mllt11* Loss Has No Impact on Locomotor Activity Between Isolation and a Novel Social Context. **A**, **B**, Entries from one chamber into another during the habituation period during P37 testing in males (**A**) and females (**B**). No significant differences were observed. (**C**-**H**) Entries into the empty peripheral or stranger 1 chamber during the first stranger presentation trial during P37 testing for males (**C**-**E**) and females (**F**-**H**). Entries were comparable across sexes and genotypes. **I**, **J**, Total entries during the first stranger presentation trial during P37 testing in males (**I**) and females (**J**). No significant differences were observed. Data presented as mean ± SD; n.s. Flox/+; *Mllt11*$^{flox/+}$; Flox/+;Cre, *Mllt11*$^{flox/+;cre}$; cKO, conditional knockout.

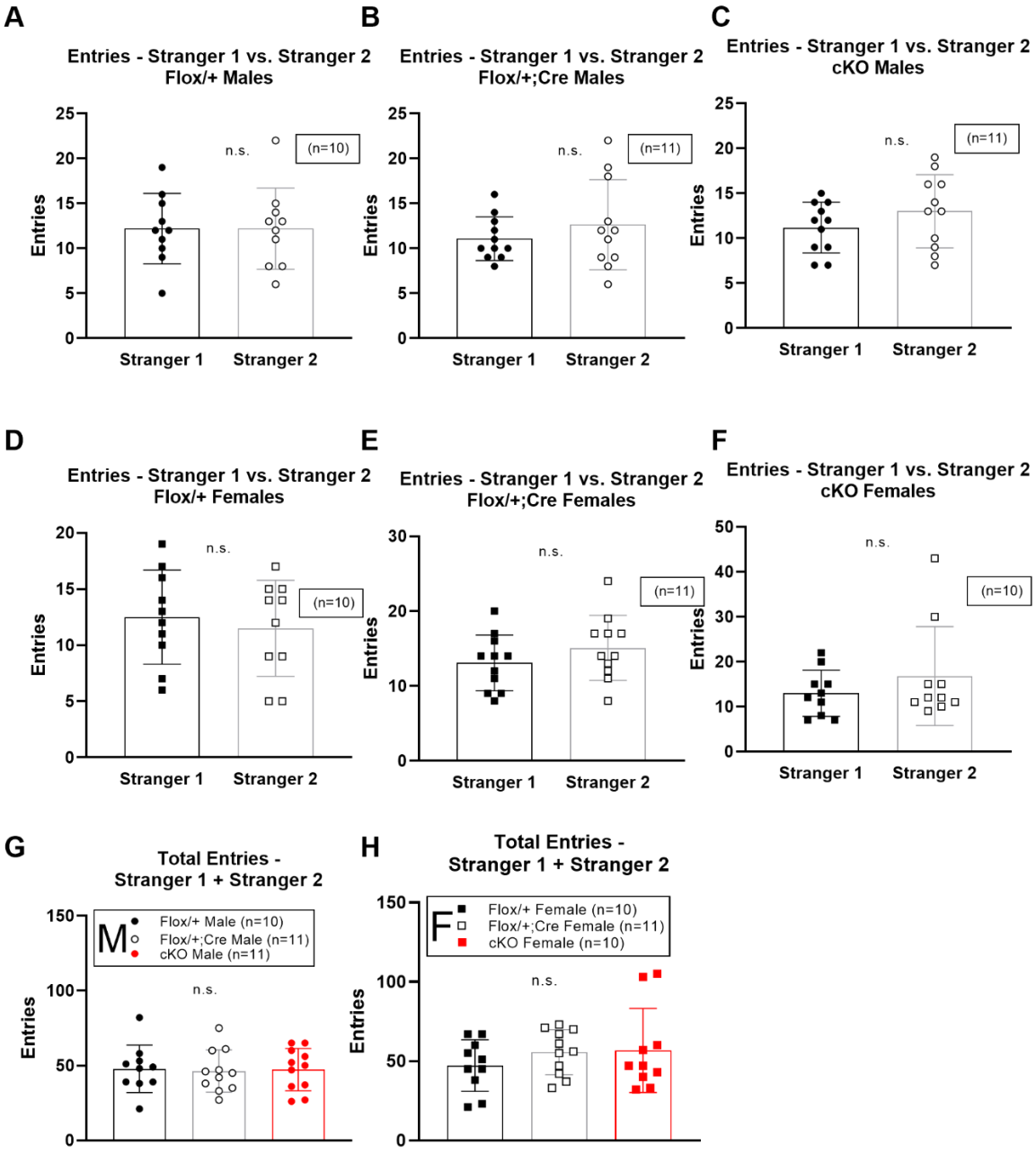

Figure 4.22. *Mllt11* Loss Has No Impact on Locomotor Activity in Two Novel Social Contexts. **A**-**F**, Entries into the chamber containing stranger 1 or 2 during the second stranger presentation trial during P37 testing in males (**A**-**C**) and females (**D**-**F**). No significant differences were observed. **G**, **H**, Total entries during the second stranger presentation trial during P37 testing compared across genotypes and within sexes for males (**G**) and females (**H**) No significant differences were seen. Data presented as mean ± SD; n.s. Flox/+; *Mllt11*$^{flox/+}$; Flox/+;Cre, *Mllt11*$^{flox/+;cre}$; cKO, conditional knockout.

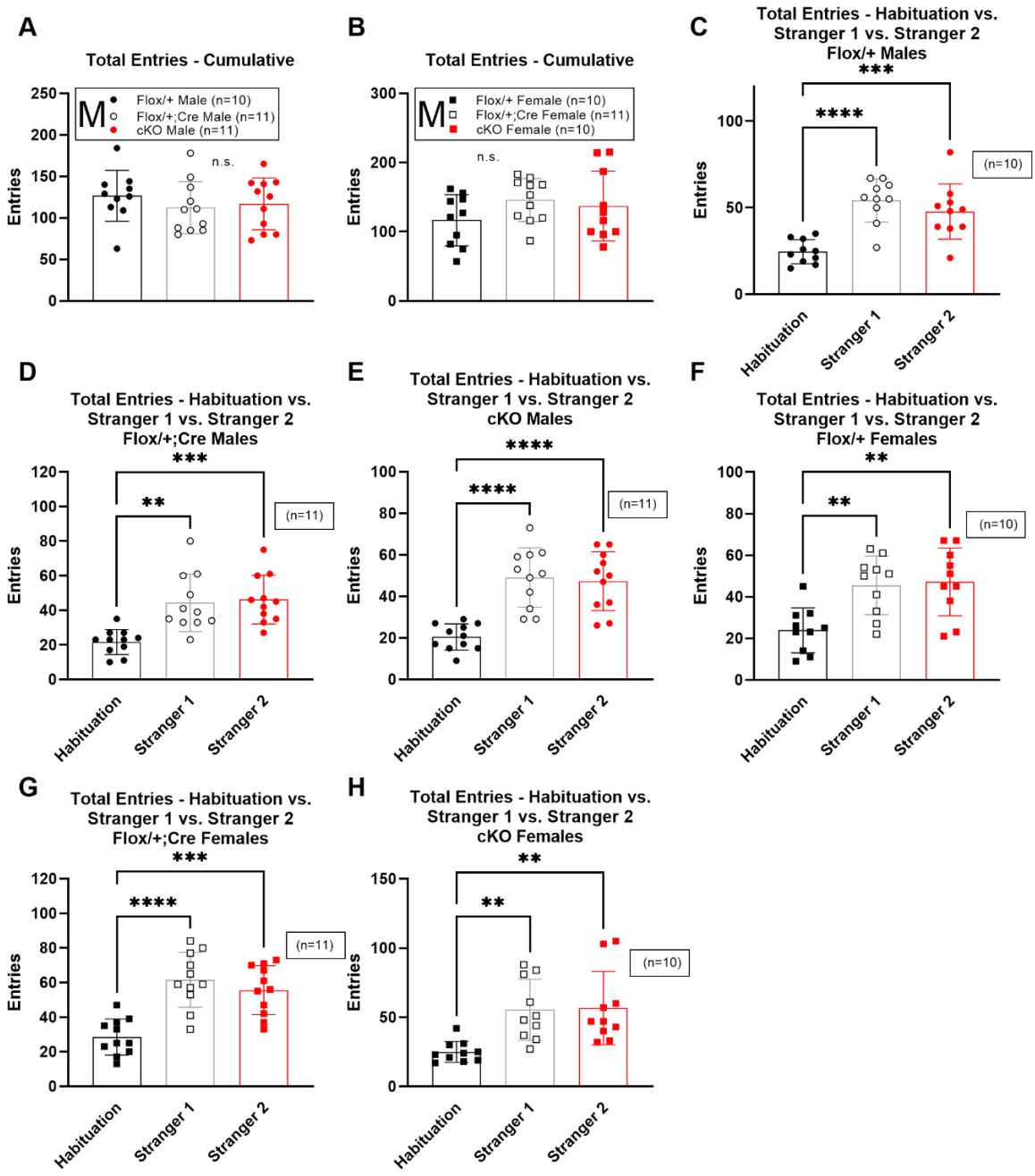

Figure 4.23. *Mllt11* Loss Has No Impact on Locomotor Activity Between Isolation and Social Contexts. **A**, **B**, Total cumulative entries across all habituation and stranger presentation trials during P37 testing in males (**A**) and females (**B**). Entries were comparable between all conditions. **C**-**H**, Distribution of entries within each trial compared across trials for males (**C**-**E**) and females (**F**-**H**). All sexes and genotypes moved between chambers a significantly greater number of times in the presence of one or two strangers than during the habituation period. Data presented as mean ± SD; n.s., **p ≤ 0.01, ***p ≤ 0.001, ****p ≤ 0.0001. Flox/+; *Mllt11*$^{flox/+}$; Flox/+;Cre, *Mllt11*$^{flox/+;cre}$; cKO, conditional knockout.

5.7. Discussion

Based on the reduced complexity of arborization patterns in the UL CPNs, and reduced projections across the CC, both of which are phenotypes reflected in human ASD, we performed behavioral tests on our *Cux2*^{IREScre}-driven *Mllt11* cKO mice to determine if this mutation gave rise to any behavioral phenotypes consistent with autism. Five behavioral tasks were chosen to reflect human ASD symptomology, including olfaction habituation/dishabituation, three-chamber social approach, social transmission of food preference, marble burying, and Nestlet shredding, as well as several quantifications of repetitive and anxiety-like behaviors. Much like the presentation of ASD, a disorder with a broad and diverse range of symptoms across a spectrum, the results were highly variable across sex and genotype.

Specifically *Mllt11*$^{flox/+;cre}$ females demonstrated an increased rate of habituation to social odors and showed opposing behavioral trends to cKO females with regard to time spent sniffing control and social odors. Female cKOs displayed a significant reduction compared to both other genotypes with regard to time spent interacting with social odors. Male cKOs also demonstrated reduced interaction with social odors from females specifically, and both cKO and *Mllt11*$^{flox/+;cre}$ males displayed a slightly disrupted social approach, evidenced by a non-significant difference between time spent in the chamber containing the stranger mouse and the empty peripheral chamber. Somewhat paradoxically, cKO and *Mllt11*$^{flox/+;cre}$ males also displayed an increased preference for novel social approach evidenced by increased time spent interacting with a novel

stranger mouse compared to a less novel mouse, when compared to *Mllt11*$^{flox/+}$ littermates. No significant disruptions were exhibited in social transmission of food preference, though this is likely due to an insufficient sample size of *Mllt11*$^{flox/+}$ controls. Additionally, female cKOs exhibited significantly reduced Nestlet shredding.

With regard to other measures of anxiety-like or compulsive behaviors, a large degree of variability was seen across sexes and genotypes, however none of these trends were statistically significant. Given the high degree variability in symptoms of ASD as well as comorbidity between ASD and other disorders like OCD, ADHD, and anxiety, it is tempting to speculate that the variability in these behaviors demonstrated across sexes and genotypes may be indicative a minor, but not inconsequential, role of *Mllt11* in these behaviors. Variation in symptoms and presentation of ASD across sexes has been explored extensively, and it is known that males present with more visible, external behaviors such as increased repetitive or restricted behaviors coupled with reduced pro-social behaviors (Werling & Geschwind, 2013). Conversely, females with ASD typically present with more inwardly observable behaviors such as increased anxiety and communication difficulties but reduced outwardly apparent social deficits compared to males (Werling & Geschwind, 2013). Rates of diagnosis among females are lower than males, and data suggests that females considered to be higher-functioning are diagnosed later in life than males (Baron-Cohen et al., 2011; Begeer et al., 2013; Giarelli et al., 2010). Some of these sex-correlated differences may be due to genetic mechanisms, however there is much evidence

that social and societal confounds contribute at least partially to inconsistencies in diagnostic criteria and clinical interpretations of ASD symptoms across sexes.

The discrepancy in diagnostic rates and presentations could be partially attributed to inherent biases in diagnostic criteria skewed toward identifying traits more common among males due to societal standards and norms, necessitating that females display a greater number of simultaneous behavioral or cognitive deficits to receive a clinical diagnosis (Dworzynski et al., 2012; Russell et al., 2011). Alternatively, this diagnostic disparity between sexes could stem from an inherent ability of females to better compensate for or conceal their symptoms through a phenomenon referred to as “camouflage” or “masking” (Cheslack-Postava & Jordan-Young, 2012; Lai et al., 2011). The use of mouse models to study these phenomena is advantageous in that they eliminate the impact of the human-specific societal framework which could potentially impact the presentation of these behaviors differently across sexes, allowing for targeted research into specific genetic contributions to behavior. Regardless of the contributions of societally-imposed interpretations of sex-specific traits and behaviors, strong evidence suggests that genetic mechanisms underlie the disorder. The fact that the *Cux2*^{IREScre}-driven *Mllt11* cKO model has given rise to some phenotypes characteristic of ASD is consistent with our current understanding of the molecular origins of ASD.

Diagnosis of ASD and other NDDs is often possible early in life, as behavioral manifestations often appear prior to age three, a critical period for formation and development of synapses (Guang et al., 2018; Hadders-Algra,

2021; Huttenlocher & Dabholkar, 1997). Given the high degree of temporal overlap between emergence of behavioral phenotypes and significant synaptogenic events, it is unsurprising that many known genetic causes of ASD specifically impact various aspects of synaptogenesis. Such implicated genes include neurexins and neuroligins, cadherins and contactins, shanks, integrins, and reelin (Abrahams & Geschwind, 2008; Buxbaum, 2009; Lintas & Persico, 2009; Südhof, 2008; Wang et al., 2009). Many known mutations also impact developmental events prior to synaptogenesis, such as transcription and posttranslational modification of components of signaling cascades which inform migration and differentiation of neurons as well as the ion channels which allow the cell to respond to such cascades (Bassell & Warren, 2008; Benayed et al., 2005; Bucan et al., 2009b; Hashimoto et al., 2006; Kelleher & Bear, 2008; Levitt & Campbell, 2009; Nishimura et al., 2007; Sadakata et al., 2007). Though the number of genetic factors associated with ASD is ever-increasing, contributing to the wide range of behavioral manifestations of the disorder, substantial evidence indicates correlations between specific genetic mutations or genotypes with particular behavioral phenotypes (Bruining et al., 2014; Pollak et al., 2019; Tammimies et al., 2019).

A shared feature between the manifestation of the various mutations that give rise to ASD behavioral phenotypes is their contribution to abnormal neural connectivity, and therefore activity. As such, a newer approach to understanding ASD combines synaptic and connectivity models along with genetic mutation models, and centers developmental disconnection between cortical regions

(Belmonte et al., 2004; Brock et al., 2002; Geschwind & Levitt, 2007b). In doing so, it employs a behavior-based neurological framework to incorporate multiple possible levels of molecular dysfunction, such as disordered synaptogenesis, vesicle transport, signaling, defective migration, axonogenesis, and dendritogenesis, all of which are highly interrelated and contribute to functional disconnection. *Mllt11* has been shown to play a role in regulation of many of these aspects of cortical development, with potential involvement in others which have not yet been overtly proven. It is therefore tempting to speculate that some of these processes may underlie the variable behavioral phenotypes observed in the *Cux2*^{IREScre}-driven *Mllt11* cKO model, which share features with ASD symptomology. Taken together, these behavioral results suggest that partial or complete loss of *Mllt11* elicits mild behavioral phenotypes characteristic of core ASD traits. It is apparent that *Mllt11* loss impacts these behavioral outcomes in a slight and variable manner dependent upon sex, and it likely does so through its roles in neuronal migration and regulation of cortical WM formation and connectivity.

CHAPTER 6. Discussion

Herein, I report a role for *Mllt11* in cortical development. *Mllt11* exhibits high levels of expression during cortical development, coinciding spatially and temporally with the genesis of postmitotic neurons and formation of the cortical plate. Expression of *Mllt11* is dynamic in the cortical plate, coinciding with migration and differentiation of neurons, and fades coinciding with termination of neuronal migration during the period where synaptogenesis and activity-dependent pruning occur. Excision of *Mllt11* from Cux2+ UL CPNs and their progenitors revealed functional roles of *Mllt11* in development of the cortex. *Mllt11* was found to play a role in radial migration from the progenitor domains to the proper cortical laminae, as its loss altered the cortical thickness and distribution of cortical cells such that a greater proportion was retained in deeper cortical layers as well as progenitor domains, and its overexpression enhanced migration into the CP. Consistent with this, *Mllt11* loss also led to reduced connectivity between the hemispheres via the CC, the major WM tract linking UL2/3 CPNs contralaterally, while other WM tracts appeared largely undisturbed. Cortical WM beneath the CP was also reduced, consistent with the reduction in callosal fibres. Additionally, maintenance of transcriptionally and morphologically discrete cortical layers was shown to be in part dependent on normal *Mllt11* expression, as there was a large reduction in UL2/3 CPN-specific transcription factor expression over time following *Mllt11* loss, though proper expression was initiated. *Mllt11* cKO mice exhibited behavioral phenotypes that varied by sex and

number of intact copies by across behavioral tasks but shared some overlapping features of those characteristic of ASD.

6.1. Evidence of a Role for *Mllt11* in Regulation of Neuronal Morphology, and Cortical Morphology and Connectivity

Following specification of CPNs and lamination of the cortex, loss of *Mllt11* led to aberrant neuronal morphology. Neurons lacking *Mllt11* displayed reduced axonal length and dendritic arborization complexity in vivo and in vitro. Mllt11 was also found to be localized throughout the soma and neurites, displaying high expression in a punctate pattern in varicosities along the distal axon and in the growth cone. The swellings along the axon shaft to which *Mllt11* localization seems to be highly targeted, called varicosities, may become what are referred to as *en passant* synapses that form along the axon trunk as opposed to 'terminal synapses' which form at the end of axonal projections. Interestingly, these *en passant* synapses are determined independently from the mechanisms which guide axonal terminals (Sabo et al., 2006). While contact with dendrites typically initiates the development of a functional synapse, these sites are unique in that synaptic vesicle precursors pause at them preceding any dendritic contact and effectively attracting it (Sabo et al., 2006). Based on the present findings, it is unknown if *Mllt11* cKO disrupts varicosity formation or proper synaptic formation and function. Disrupted varicosity presentation is seen in ASD individuals (Azmitia et al., 2011) and in other NDDs such as epilepsy (Goikolea-Vives & Stolp, 2021).

En passant synapses can significantly affect conduction and synaptic transmission and are present to varying degrees in normal, diseased, and injured brains (Gu, 2021). Given the present results, it is possible that downstream effects of Mllt11-dependent cytoskeletal reorganization may influence trafficking of organelles such as mitochondria. When mitochondria accumulate at *en passant* synapses, their synaptic stability is increased (Sabo et al., 2006). Though the mechanism for this phenomenon is unknown, it could be due to the ability of mitochondria to influence local signaling events such as Ca^{2+}-dependent signaling (Lees et al., 2019; Smit-Rigter et al., 2016). Additionally, the developmental regulation of dendritic spine morphology is a dynamic process also linked to synaptic function and cognition, and as such, changes in spine shape, size, and density are hallmarks of many NDDs (Nishiyama, 2019). Though further investigation of this aspect of the *Mllt11* mutant phenotype was beyond the scope of this project, it will be the objective of future studies.

A proteomic screen for potential Mllt11-interacting proteins revealed numerous possible mechanisms for Mllt11 function. We show that Mllt11 interacts with tubulin isoforms, confirming a recent proteomic screen (Go et al., 2021), which provides a molecular rationale for the basis of the *Mllt11* mutant phenotype. Cortical thinning and increased ventricular lumen surface area are common phenotypes associated with NDDs, and were observed in *Mllt11* mutant brains, suggesting cytoskeletal dysregulation may underlie a subset of these disorders (Bahi-Buisson et al., 2014; L. Li et al., 2019; Mensen et al., 2017). The increased packing density seen in the cortex as a result of inefficient invasion of

the CP in cKOs is also characteristic of NDDs such as ASD (Bailey et al., 1998; Courchesne et al., 2011; Kemper & Bauman, 1998; Schumann & Amaral, 2006). Moreover, changes in microtubule dynamics can affect neuronal migration and the generation of functional connections in the brain. These are processes whose dysfunction may underlie a wide spectrum of neurodevelopmental disorders.

The microtubule cytoskeleton generates polarized force and provides a functional railway along which motor proteins migrate, whether to drive actin polymerization in generating protrusive forces at the leading edge of the growth cone, or integrate extracellular cues into regulation of microtubule activity (Buck & Zheng, 2002; Dent, 2017; Dent & Kalil, 2001; Lee et al., 2004; Zhou et al., 2004). Tubulin mutations have been shown to impair neuronal migration into the cortex (Aiken et al., 2017), and specifically affect UL CPNs (Keays et al., 2007) reliant on dynamic, multipolar cytoskeletal reorganization to extend short processes, “crawling” through established DL CPNs (Miyata et al., 2001; Sakakibara et al., 2014). The dynamic expression of *Mllt11* during UL CPN development also supports its role as a critical regulator of UL migration.

Interestingly, mutations in α-tubulin have been shown to cause axonal trafficking defects that impair synaptic stability and function without impacting axonal degeneration or neuronal survival (Buscaglia et al., 2020). The interaction of Mllt11 with microtubules could therefore provide a mechanistic explanation for the impaired migration and reduced CPN dendritic complexity seen in *Mllt11* mutants. Specifically, we showed that Mllt11 associates with acetylated α-tubulin in fetal brain lysates, suggesting that it may be required for the stabilization of the

cytoskeleton in growing neurites, and account for the similarities between the *Mllt11* mutant phenotype with those targeting tubulin isoforms, as alpha tubulin mutations have been associated with NDD pathology (IC, Bahi-Buisson et al., 2008; Jansen et al., 2011; Keays et al., 2007; Kumar et al., 2010; Poirier et al., 2007; Tian et al., 2010).

In addition to the previously confirmed interaction with tubulin isoforms, other potential interactors were identified, shedding light on other mechanisms for these molecular and anatomical phenotypic features. Other identified potential interactors, such as Hspa8 have been previously confirmed in the literature, suggesting that other potential regulatory roles of Mllt11 may depend on binding to chaperon protein Hspa8 and regulating protein export from the nucleus required for protein degradation (P. Li et al., 2014). Yet another possible function for Mllt11 may include regulating the Wnt signaling cascade via T cell factor 7, which in turn regulates CD44 to promote cell migration and metastasis (Li et al., 2018; Park et al., 2015). As ours is the first study to explore *Mllt11* function in the developing brain, additional studies are needed to determine whether *Mllt11* could be exerting its effect on transcriptional regulation directly or indirectly via cytoskeletal interactions, or both.

The inefficient extension of neurites may also be attributed to impaired trafficking of organelles and ribosomes for local protein synthesis, or vesicles carrying secreted cues and growth cone machinery to the axonal periphery (González et al., 2016; Kennedy & Ehlers, 2006). Specifically, a potential Mllt11 interactor, Myosin 10, which is essential for growth cone formation and cell

motility (Yu et al., 2012, 2015), may be involved. One mechanism through which Myosin 10 exerts its regulatory effect on radial migration of CPNs is through its role in the localization of N-cadherin (Yu et al., 2015), and it has also been implicated in tumor invasion by regulating process extension (Ropars et al., 2016). Additionally, Myh5a, another potential interactor, is known to transport cargo to the synaptic scaffold of the dendritic spine (Yoshii et al., 2013), as well as mRNAs to be translated at the synapse (Fujii et al., 2005; Yoshimura et al., 2006). MYH9 has also been identified previously as a variant in ASD (Iossifov et al., 2014a, 2014b; Rauch et al., 2012; Wang et al., 2020). It is tempting to speculate that altered neuronal trafficking through aberrant function of any of these molecular motors in the absence of Mllt11 may underlie morphologic and transcriptional deficits of *Mllt11* mutant CPNs.

In light of this, we showed that the overexpression of *Mllt11* promoted migration into the CP, consistent with a cytoskeletal regulatory function. This finding is also consistent with *in vitro* studies, which showed that the overexpression of *Mllt11* in cancer stem cell lines promotes proliferation and invasiveness (Tse et al., 2017). It is possible that Mllt11-dependent cytoskeleton reorganization may favor symmetric divisions of organelles, nuclear components, and polarity protein complexes, therefore enhancing invasiveness of cells (Nance & Zallen, 2011; Piroli et al., 2019). On the other hand, the transcriptional regulation of *Mllt11* by REST has been associated with promoting neuronal differentiation, with high *REST* and low *Mllt11* expression in undifferentiated neuronal tissue, and increasing *Mllt11* levels correlated with decreased REST

activity during terminal neuronal differentiation (Hu et al., 2015). These previously published findings, in conjunction with the complexity of the *Mllt11* mutant phenotype reported here, imply that there are potentially two discrete pathways through which *Mllt11* regulates neuronal development: a cytoskeletal regulatory mechanism, and a transcriptional regulatory mechanism.

Much of what is known about *Mllt11* has been discerned from overexpression studies in immortalized cell lines and oncogenic clinical case studies, revealing pathogenic roles in cell process extension, invasiveness, and secretion of factors that promote efficient cellular motility (Chang et al., 2008; D.-Q. Li et al., 2006; Lin et al., 2004; Park et al., 2019; Tiberio et al., 2017; W. Tse et al., 2004). Oncogenesis and neurogenesis share commonalities at the level of cytoskeletal regulation of somatic and nuclear morphology, as well as extension of and trafficking along cytoplasmic processes, allowing for invasion of and migration through tissues. However, it is important to make the distinction between pathologic studies and our current findings on the role of *Mllt11*. Until the current study, which was the first to examine a role for Mllt11 *in vivo*, the physiological role for *Mllt11* was unclear. In all the published *in vitro* and oncogenic case studies, Mllt11 is aberrantly overexpressed in non-neuronal tissues, either by itself or as a fusion with the chromatin remodeling protein Mll. We previously reported that Mllt11 protein and mRNA was exclusively localized to the developing CNS embryonically, and not in any other tissues, though its expression is more widespread postnatally (Yamada et al., 2014). The expression pattern of β-gal in the targeted *Mllt11* allele confirmed that it is

normally expressed only within the developing CNS, with the highest levels reflecting UL cortical neurogenesis. Consistent with this expression profile, we now show that *Mllt11* is required for proper migration but not neurogenesis of UL CPNs. Furthermore, we also revealed that *Mllt11* regulates neurite outgrowth and the maintenance of UL gene expression programs. The loss of *Mllt11* led to a reduction of interhemispheric connectivity via reduced callosal fibres. We also characterized a severe dysplasia of CPNs in *Mllt11* cKO mutant neonatal brains; a phenotype found in severe neurodevelopmental disorders such as ASD and Fragile X-associated tremor ataxia syndrome with which *Mllt11* dysregulation has been associated (Drozd et al., 2019; Xu et al., 2016).

Importantly, the loss of layer-specific morphology and identity have also been demonstrated in postmortem brains from autistic humans (Casanova et al., 2013; Fujimoto et al., 2021; Stoner et al., 2014). These clinical data are reminiscent of the severe dysplasia in the cortex of our conditional *Mllt11* mutants, revealed by the Golgi staining method as well as the altered levels of UL2/3-specific transcription factors Satb2 and CDP/Cux1, which function in establishment and maintenance of the CC as well as mature arborescent neuronal morphology and somal packing (Alcamo et al., 2008; Cubelos et al., 2015; He et al., 2022; Rodríguez-Tornos et al., 2016). It is presently unclear whether the loss of UL-specific gene expression we observed in our *Mllt11* mutants, is primarily because of cytoskeletal dysregulation, or other uncharacterized gene expression pathways functioning downstream of *Mllt11*, as

both of these explanations could account for aspects of the altered morphology seen in *Mllt11* mutants.

Some neuronal subtypes exhibit altered expression of subpopulation-specific markers when cytoskeletal regulation is altered such that connections to target regions cannot be established (Hippenmeyer et al., 2005), implying that there may be uncharacterized feedback mechanisms between establishment of connectivity and maintenance of expression of CPN subtype-specific transcription factors. Additionally, although much remains to be elucidated about the structure of Mllt11, the presence of a nuclear export sequence and its demonstrated ability to bind to and traffic Hspa8 into the cytoplasm for lyosomal degradation further bolsters this implication of a role for Mllt11 in the nucleus.

6.2. Evidence of a Role for *Mllt11* in Behaviors Characteristic of ASD

Given the complexity of the molecular and morphological phenotype resultant from excision of *Mllt11* from UL CPNs and their overlap with clinical pathology of NDDs as well as NDD-like phenotypes from other rodent mutant models such as migratory and neurite outgrowth defects, they provide a model with which to study brain disorders arising from aberrant regulation of the neuronal cytoskeletal during development. From a behavioral standpoint, the role of *Mllt11* in ASD-like presentation seems to vary in severity across tasks. Additionally, these behavioral phenotypes display differences across sexes and also vary with the number of intact copies of the *Mllt11* allele in the genome. *Mllt11* cKOs displayed alterations to numerous behaviors, including sociability,

social preferences, interest in novelty, and some anxiety-like behaviors, and in some cases, mice heterozygous for *Mllt11* also displayed altered behaviors.

With regard to social behaviors, variability was seen across sexes and genotypes. Specifically, female cKOs exhibited reduced sniffing of social odors compared to littermates, while male cKOs exhibited reduced sniffing of female social odors specifically. In some cases, trends were observed wherein females lacking both copies of *Mllt11* exhibited opposing trends from heterozygous females when compared to *Mllt11*$^{flox/+}$ littermates with regard to social odor sniffing. *Mllt11*$^{flox/+;cre}$ and cKO males both exhibited an atypical approach behavior compared to *Mllt11*$^{flox/}$ littermates evidenced by the absence of a preference for spending time in the presence of a stranger mouse over an empty chamber. Paradoxically, *Mllt11*$^{flox/+;cre}$ and cKO males also displayed a stereotypical preference for social novelty when presented with a choice between the two stranger mice while no other genotypes of either sex displayed this behavior. The social transmission of a food preference task also revealed no major differences in social communication behaviors, with the exception of *Mllt11*$^{flox/+;cre}$ females as the only genotype of either sex who showed evidence of successful transmission of a preference for the cued food.

To rule out sensory defects as underlying causes for these altered social behaviors, olfaction was assessed, and it was found that *Mllt11* loss did not impact olfactory capabilities, nor did it majorly impact the ability to habituate or dishabituate to odors, though some differences were seen. *Mllt11*$^{flox/+;cre}$ females displayed an increased tendency to habituate to a social odor following

presentation of a different social odor compared to cKO littermates, though neither differed significantly from *Mllt11*$^{flox/+}$ littermates. Male cKOs were minimally impacted and spent less time interacting with the control nonsocial odor, while loss of one copy of *Mllt11* in females resulted in the opposite behavior compared to cKOs and *Mllt11*$^{flox/+}$ females. Taken together, these results indicate a slight and variable role for *Mllt11* in modulation of some social behaviors.

Another feature of ASD-like behavior is altered preference for or interest in novelty, in the form of situations, social interactions, or objects. This behavior was exhibited to varying degrees across tasks in males and females, and varied in severity and presentation with the number of intact copies of *Mllt11*. *Mllt11*$^{flox/+;cre}$ and cKO males displayed a preference for social novelty in the presence of two stranger mice, while no other genotypes of either sex showed this preference. *Mllt11*$^{flox/+;cre}$ and cKO males also exhibited decreased time spent interacting with opposite sex odors. Females, however, showed opposing trends with cKOs interacting with opposite sex odors less than *Mllt11*$^{flox/+;cre}$ females. Additionally, though the Nestlet shredding task is used as a measure of repetitive behaviors often seen in OCD and ADHD, disorders with a high degree of comorbidity with NDDs, it can also be indicative of interest in novel objects. Female cKOs exhibited reduced interaction with the Nestlet material, indicating a potentially reduced interest in this novel object compared to other genotypes, an effect not seen in males. Contrary to this interpretation, however, is the fact that no statistically significant differences were seen in marble-burying behavior

across genotypes and sexes, as the marbles used in this test were also novel objects.

A tendency to engage in restrictive or repetitive or anxiety-like behaviors is also a hallmark feature of ASD. The potential impact of *Mllt11* on these behaviors was the most variable of all behavioral modalities assessed. Though some trends were seen in a manner that varied across sexes and number of intact copies of *Mllt11*, none of these differences were statistically significant. Given this high degree of variability, it is difficult to make an argument for an obvious, clear-cut role for *Mllt11* in repetitive or anxiety-like behaviors. *Mllt11* cKO females did display a significantly decreased tendency toward shredding of nesting materials, however, as previously stated, this test could also indicate preference for interacting with a novel object, making it difficult to parse the exact role of *Mllt11* in modulating this behavior.

Well-documented cases exist in the literature of mutations that impact one or more of the behavioral modalities explored herein. Many of these mutations are also implicated in regulation of synaptogenesis or synaptic function in some way. For instance, *Neuroligins*, *Neurexins*, and *Shank3* complex mutations have been shown to account for some cases of autism, but paradoxically also occur in asymptomatic family members, suggesting that some mutations may underlie a genetic predisposition to ASD symptomology, increasing risk but not creating a phenotype severe enough to be classified clinically (Südhof, 2008). Specifically, *Nlgn3* and *Nlgn4* mutations give rise to a mild phenotype in humans but caused altered sociability in mice as well as varied preference for social novelty

(Chadman et al., 2008; Radyushkin et al., 2009a, 2009b; Tabuchi et al., 2007). Mutation of *Neurexin-1-alpha*, a presynaptic terminal component, gives rise to no notable social phenotype, but reduced nest-building activity as well as altering grooming behavior (Etherton et al., 2009). Postsynaptically, mutation of *Neuroligin1* also had little effect on social outcomes but impaired nest-building behavior (Blundell et al., 2010). In addition to the synaptic scaffolding components mentioned here, mutation to ion channels has been shown to impact behaviors in a manner that mimics NDDs. For instance, mutation of *Gabrb3*, a subunit of a ligand-gated ion channel, has been shown to impair social behaviors, and alter preference for social novelty, repetitive behaviors, and nest building (DeLorey et al., 2008). Much like *Mllt11*, *Gabrb3* plays a particularly important role specifically within contralaterally-projecting CPNs comprising the ULs of the somatosensory cortex (Babij et al., 2023).

There are also well-documented precedents in which mutation to genes with a regulatory role in local translation give rise to NDD-like phenotypes. Such is the case for fragile x mental retardation protein (FMRP), an RBP which functions in the regulation of local sequestration and translation of RNAs differentially in opposing regions of a progenitor cell, enabling asymmetrical division of daughter cells which inherit unique genetic components required for further differentiation. Similar to Mllt11, which demonstrates the capacity to bind both ribonucleoprotein and cytoskeletal components, FMRP enacts its regulatory role by occupying the opposing basal region to CyclinD2 apically, where it complexes with the cytoskeleton, signaling factors, and RNA to be translated in

basal endfeet of dividing cells (Zahr et al., 2019). Conditional mutation of *Pten*, a regulator of local protein synthesis, in the cortex and hippocampus also gives rise to autism-like phenotypes in the form of altered sociability, impaired nest-building behavior, and social recognition (Kwon et al., 2006). Interestingly, similar to *Mllt11* mutants, which vary in severity and presentation of behavioral phenotype in a sex- and copy number-specific manner, females heterozygous for this conditional *Pten* mutation also exhibit a distinct phenotype in the form of low sociability compared to controls (Kelleher & Bear, 2008; Page et al., 2009). It is possible that Mllt11 is exerting a regulatory role such that, in its absence, local translation of crucial axon guidance, signaling, and/or synaptic machinery is limited and proceeds less efficiently. These processes may be modulated in a sex-dependent manner, giving rise to unique phenotypes across sexes.

The impact of *Mllt11* on maintenance of UL2/3-specific markers may also provide a possible mechanism through which *Mllt11* may play a role in modulation of behavior. *CDP/Cux1* has been shown to play a role in regulating neurite outgrowth and overall neuronal morphology (Cubelos et al., 2010a), and loss or mutation of *CDP/Cux1* gives rise to neurons with shorter, less arborescent neurites (Cubelos et al., 2010b). Neuronal morphology altered in this manner has been established as a hallmark feature of both human and mouse ASD or ASD-like pathology (Barón-Mendoza et al., 2021; Nagy et al., 2017). Additionally, *Satb2* mutation in humans gives rise to SATB2 syndrome, an NDD characterized by intellectual disability, language and communication deficits, some ASD-like behaviors such as repetitive or restrictive movements and

interests, as well as hyperactivity and aggression (Cotton et al., 2020). Although there were no notable alterations to Tbr1 expression in the present model, likely due to the fact that *Mllt11* was specifically inactivated in Cux2+ cells of the cortical upper layers, it is known that mutation to *Tbr1* can give rise to autism through its activation of *Auts2*, an autism-associated gene. Tbr1 activates *Auts2*, whose protein product functions through regulation of cytoskeletal reorganization to regulate CPN development and migration, demonstrating a role for cortical layer marker malfunction in autism pathology through both transcriptional regulation and cytoskeletal organization (Bedogni et al., 2010; Hori et al., 2021).

Another issue that requires consideration when interpreting the behavioral phenotypes of mutant mouse models of NDDs is the background of the strain in which the mutation is maintained. C57Bl/6 mice have been shown, in some cases, to display various autism-like behaviors under wild type conditions. This phenomenon is likely due to the level of inbreeding required in maintaining the genetic purity characteristic of this strain (Ryan et al., 2010). Alternatively, genetic outbreeding and the genetic variability enhanced when crossing strains may also be a source of variability in behaviors. As the mice used in the experiments reported herein were derived from outbred C57Bl/6/FVB hybrid crosses, this requires careful consideration when parsing the impact of *Mllt11* loss from other potential sources of variation. To try to mitigate the effects of this variability, littermates of all genotypes were used as behavioral controls. Additionally, the slight difference in body weight seen in cKOs of both sexes compared to all other littermates, an effect that disappeared following weaning,

could potentially suggest that maternal behaviors, such as nursing of pups, were altered in response to abnormalities evident in cKO pups independent of other strain-related variability.

6.3. Conclusion

In summary, the results of this thesis provide insight into the role of *Mllt11* in cortical development as well as its function in modulation of certain behaviors which present atypically in NDDs. Mllt11 is a neuronally-restricted, cytoskeletal-interacting protein that exhibits high levels of expression during corticogenesis. *Mllt11* regulates neuronal morphology, neurite outgrowth, and therefore overall cortical morphology and connectivity, as well as the maintenance of layer-specific markers of CPN subtypes. Though the exact mechanism through which it exerts its regulatory role is not fully understood, I have provided evidence of interactions with multiple tubulin isoforms, MAPs, molecular motors, and machinery for local protein synthesis, seeming to suggest a role in trafficking of molecular cargo crucial for neurite elongation to the axonal periphery. Many features of the *Mllt11* mutant phenotype are reminiscent of pathologies seen in human cases of ASD. The behavioral phenotype of *Mllt11* cKO from UL2/3 of the cortex is highly variable across sex and number of intact copies of *Mllt11* in the genome, but the spectrum of behavioral outcomes displayed shares some overlap with human ASD as well as behaviors demonstrated in rodent models of ASD informed by mutations found commonly underlying or associated with human ASD pathology. Increasing our understanding of the molecular processes that govern proper

cortical development, as well as the pathological and behavioral relevance of individual genes could improve accuracy and ease of diagnosis of NDDs and provide insight into more individualized treatments to improve the quality of lives of those living with NDDs. *Mllt11* may be a potential target of treatment or diagnostic marker used to indicate susceptibility to particular pathological and behavioral outcomes common to ASD.

REFERENCES

1 Aboitiz, F. & Montiel, J. One hundred million years of interhemispheric communication: the history of the corpus callosum. *Brazilian journal of medical and biological research = Revista brasileira de pesquisas medicas e biologicas* **36**, 409-420, doi:10.1590/s0100-879x2003000400002 (2003).

2 Abrahams, B. S. & Geschwind, D. H. Advances in autism genetics: on the threshold of a new neurobiology. *Nature reviews. Genetics* **9**, 341-355, doi:10.1038/nrg2346 (2008).

3 Abramovitch, A., Dar, R., Mittelman, A. & Wilhelm, S. Comorbidity Between Attention Deficit/Hyperactivity Disorder and Obsessive-Compulsive Disorder Across the Lifespan: A Systematic and Critical Review. *Harvard review of psychiatry* **23**, 245-262, doi:10.1097/HRP.0000000000000050 (2015).

4 Adam Mp, M. G. M. P. R. A. e. & et al. *DCX-Related Disorders*. ((online), 2007).

5 Ahmad, F. J., Pienkowski, T. P. & Baas, P. W. Regional differences in microtubule dynamics in the axon. *The Journal of neuroscience : the official journal of the Society for Neuroscience* **13**, 856-866, doi:10.1523/JNEUROSCI.13-02-00856.1993 (1993).

6 Aiken, J., Buscaglia, G., Bates, E. A. & Moore, J. K. The α-Tubulin gene TUBA1A in Brain Development: A Key Ingredient in the Neuronal Isotype Blend. *Journal of Developmental Biology* **5**, 8-8, doi:10.3390/jdb5030008 (2017).

7 Al-Beltagi, M. Autism medical comorbidities. *World journal of clinical pediatrics* **10**, 15-28, doi:10.5409/wjcp.v10.i3.15 (2021).

8 Alcamo, E. A. *et al.* Satb2 regulates callosal projection neuron identity in the developing cerebral cortex. *Neuron* **57**, 364-377, doi:10.1016/j.neuron.2007.12.012 (2008).

9 Andrews, G. L. & Mastick, G. S. R-cadherin is a Pax6-regulated, growth-promoting cue for pioneer axons. *The Journal of neuroscience : the official journal of the Society for Neuroscience* **23**, 9873-9880, doi:10.1523/JNEUROSCI.23-30-09873.2003 (2003).

10 Angoa-Pérez, M., Kane, M. J., Briggs, D. I., Francescutti, D. M. & Kuhn, D. M. Marble burying and Nestlet shredding as tests of repetitive, compulsive-like behaviors in mice. *Journal of visualized experiments : JoVE*, 50978-50978, doi:10.3791/50978 (2013).

11 Anton, E. S., Marchionni, M. A., Lee, K. F. & Rakic, P. Role of GGF/neuregulin signaling in interactions between migrating neurons and radial glia in the developing cerebral cortex. *Development (Cambridge, England)* **124**, 3501-3510, doi:10.1242/dev.124.18.3501 (1997).

12 Argiro, V., Bunge, M. B. & Johnson, M. I. Correlation between growth form and movement and their dependence on neuronal age. *The Journal of neuroscience : the official journal of the Society for Neuroscience* **4**, 3051-3062, doi:10.1523/JNEUROSCI.04-12-03051.1984 (1984).

13 Argiro, V., Bunge, M. B. & Johnson, M. I. A quantitative study of growth cone filopodial extension. *Journal of neuroscience research* **13**, 149-162, doi:10.1002/jnr.490130111 (1985).

14 Arlotta, P. *et al.* Neuronal subtype-specific genes that control corticospinal motor neuron development in vivo. *Neuron* **45**, 207-221, doi:10.1016/j.neuron.2004.12.036 (2005).

15 Ayala, R., Shu, T. & Tsai, L.-H. Trekking across the brain: the journey of neuronal migration. *Cell* **128**, 29-43, doi:10.1016/j.cell.2006.12.021 (2007).

16 Azmitia, E. C., Singh, J. S., Hou, X. P. & Wegiel, J. Dystrophic Serotonin Axons in Postmortem Brains from Young Autism Patients. *The Anatomical Record: Advances in Integrative Anatomy and Evolutionary Biology* **294**, 1653-1662, doi:10.1002/ar.21243 (2011).

17 Babij, R. *et al.* Gabrb3 is required for the functional integration of pyramidal neuron subtypes in the somatosensory cortex. *Neuron* **111**, 256-274.e210, doi:10.1016/j.neuron.2022.10.037 (2023).

18 Bahi-Buisson, N. *et al.* Refinement of cortical dysgeneses spectrum associated with TUBA1A mutations. *Journal of medical genetics* **45**, 647-653, doi:10.1136/jmg.2008.058073 (2008).

19 Bahi-Buisson, N. *et al.* The wide spectrum of tubulinopathies: what are the key features for the diagnosis? *Brain* **137**, 1676-1700, doi:10.1093/brain/awu082 (2014).

20 Bailey, A. *et al.* A clinicopathological study of autism. *Brain : a journal of neurology* **121 (Pt 5)**, 889-905, doi:10.1093/brain/121.5.889 (1998).

21 Barlan, K., Lu, W. & Gelfand, V. I. The microtubule-binding protein ensconsin is an essential cofactor of kinesin-1. *Current biology : CB* **23**, 317-322, doi:10.1016/j.cub.2013.01.008 (2013).

22 Barnett, M. W. & Larkman, P. M. The action potential. *Practical neurology* **7**, 192-197 (2007).

23 Baron-Cohen, S. *et al.* Why are autism spectrum conditions more prevalent in males? *PLoS biology* **9**, e1001081-e1001081, doi:10.1371/journal.pbio.1001081 (2011).

24 Barón-Mendoza, I. *et al.* Changes in the Number and Morphology of Dendritic Spines in the Hippocampus and Prefrontal Cortex of the C58/J Mouse Model of Autism. *Frontiers in Cellular Neuroscience* **15**, doi:10.3389/fncel.2021.726501 (2021).

25 Bassell, G. J. & Warren, S. T. Fragile X syndrome: loss of local mRNA regulation alters synaptic development and function. *Neuron* **60**, 201-214, doi:10.1016/j.neuron.2008.10.004 (2008).

26 Bedogni, F. *et al.* Tbr1 regulates regional and laminar identity of postmitotic neurons in developing neocortex. *Proceedings of the National Academy of Sciences of the United States of America* **107**, 13129-13134, doi:10.1073/pnas.1002285107 (2010).

27 Begeer, S. *et al.* Sex differences in the timing of identification among children and adults with autism spectrum disorders. *Journal of autism and developmental disorders* **43**, 1151-1156, doi:10.1007/s10803-012-1656-z (2013).

28 Bellion, A., Baudoin, J.-P., Alvarez, C., Bornens, M. & Métin, C. Nucleokinesis in tangentially migrating neurons comprises two alternating phases: forward migration of the Golgi/centrosome associated with centrosome splitting and myosin contraction at the rear. *The Journal of neuroscience : the official journal of the Society for Neuroscience* **25**, 5691-5699, doi:10.1523/JNEUROSCI.1030-05.2005 (2005).

29 Belmonte, M. K. *et al.* Autism and abnormal development of brain connectivity. *The Journal of neuroscience : the official journal of the Society for Neuroscience* **24**, 9228-9231, doi:10.1523/JNEUROSCI.3340-04.2004 (2004).

30 Benayed, R. *et al.* Support for the homeobox transcription factor gene ENGRAILED 2 as an autism spectrum disorder susceptibility locus. *American journal of human genetics* **77**, 851-868, doi:10.1086/497705 (2005).

31 Bhabha, G., Johnson, G. T., Schroeder, C. M. & Vale, R. D. How Dynein Moves Along Microtubules. *Trends in biochemical sciences* **41**, 94-105, doi:10.1016/j.tibs.2015.11.004 (2016).

32 Bignami, A. & Dahl, D. Specificity of the glial fibrillary acidic protein for astroglia. *Journal of Histochemistry & Cytochemistry* **25**, 466-469, doi:10.1177/25.6.69656 (1977).

33 Biswas, A., Krishnan, P., Vidarsson, L. & Shroff, M. Cerebral White Matter Tract Anatomy. *Neuroimaging clinics of North America* **32**, 507-528, doi:10.1016/j.nic.2022.05.001 (2022).

34 Blommers, M., Stanton-Turcotte, D. & Iulianella, A. Retinal neuroblast migration and ganglion cell layer organization require the cytoskeletal-interacting protein Mllt11. *Developmental dynamics : an official publication of the American Association of Anatomists* **252**, 305-319, doi:10.1002/dvdy.540 (2023).

35 Blundell, J. *et al.* Neuroligin-1 deletion results in impaired spatial memory and increased repetitive behavior. *The Journal of neuroscience : the official journal of the Society for Neuroscience* **30**, 2115-2129, doi:10.1523/JNEUROSCI.4517-09.2010 (2010).

36 Bodakuntla, S., Jijumon, A. S., Villablanca, C., Gonzalez-Billault, C. & Janke, C. Microtubule-Associated Proteins: Structuring the Cytoskeleton. *Trends in cell biology* **29**, 804-819, doi:10.1016/j.tcb.2019.07.004 (2019).

37 Bonini, S. A., Mastinu, A., Ferrari-Toninelli, G. & Memo, M. Potential Role of Microtubule Stabilizing Agents in Neurodevelopmental Disorders. *International Journal of Molecular Sciences* **18**, 1627-1627, doi:10.3390/ijms18081627 (2017).

38 Bray, D. & Chapman, K. Analysis of microspike movements on the neuronal growth cone. *The Journal of neuroscience : the official journal of the Society for Neuroscience* **5**, 3204-3213, doi:10.1523/JNEUROSCI.05-12-03204.1985 (1985).

39 Breuss, M. *et al.* Mutations in the β-tubulin gene TUBB5 cause microcephaly with structural brain abnormalities. *Cell reports* **2**, 1554-1562, doi:10.1016/j.celrep.2012.11.017 (2012).

40 Breuss, M. W. *et al.* Uner Tan syndrome caused by a homozygous TUBB2B mutation affecting microtubule stability. *Human molecular genetics* **26**, 258-269, doi:10.1093/hmg/ddw383 (2017).

41 Bridgman, P. C. Myosin Va movements in normal and dilute-lethal axons provide support for a dual filament motor complex. *The Journal of cell biology* **146**, 1045-1060, doi:10.1083/jcb.146.5.1045 (1999).

42 Britanova, O. *et al.* Satb2 is a postmitotic determinant for upper-layer neuron specification in the neocortex. *Neuron* **57**, 378-392, doi:10.1016/j.neuron.2007.12.028 (2008).

43 Brock, J., Brown, C. C., Boucher, J. & Rippon, G. The temporal binding deficit hypothesis of autism. *Development and psychopathology* **14**, 209-224, doi:10.1017/s0954579402002018 (2002).

44 Brock, S. *et al.* Tubulinopathies continued: refining the phenotypic spectrum associated with variants in TUBG1. *European journal of human genetics : EJHG* **26**, 1132-1142, doi:10.1038/s41431-018-0146-y (2018).

45 Brown, A., Li, Y., Slaughter, T. & Black, M. M. Composite microtubules of the axon: quantitative analysis of tyrosinated and acetylated tubulin along individual axonal microtubules. *Journal of cell science* **104 (Pt 2)**, 339-352, doi:10.1242/jcs.104.2.339 (1993).

46 Bruining, H. *et al.* Behavioral signatures related to genetic disorders in autism. *Molecular Autism* **5**, 11-11, doi:10.1186/2040-2392-5-11 (2014).

47 Bucan, M. *et al.* Genome-wide analyses of exonic copy number variants in a family-based study point to novel autism susceptibility genes. *PLoS genetics* **5**, e1000536-e1000536, doi:10.1371/journal.pgen.1000536 (2009).

48 Buck, K. B. & Zheng, J. Q. Growth cone turning induced by direct local modification of microtubule dynamics. *The Journal of neuroscience : the official journal of the Society for Neuroscience* **22**, 9358-9367, doi:10.1523/JNEUROSCI.22-21-09358.2002 (2002).

49 Burden, S. J. Wnts as retrograde signals for axon and growth cone differentiation. *Cell* **100**, 495-497, doi:10.1016/s0092-8674(00)80685-6 (2000).

50 Buscaglia, G., Northington, K. R., Moore, J. K. & Bates, E. A. Reduced TUBA1A Tubulin Causes Defects in Trafficking and Impaired Adult Motor Behavior. *eneuro* **7**, ENEURO.0045-0020.2020, doi:10.1523/ENEURO.0045-20.2020 (2020).

51 Busson-Le Coniat, M., Salomon-Nguyen, F., Hillion, J., Bernard, O. A. & Berger, R. MLL-AF1q fusion resulting from t(1;11) in acute leukemia. *Leukemia* **13**, 302-306, doi:10.1038/sj.leu.2401299 (1999).

52 Buxbaum, J. D. Multiple rare variants in the etiology of autism spectrum disorders. *Dialogues in clinical neuroscience* **11**, 35-43, doi:10.31887/DCNS.2009.11.1/jdbuxbaum (2009).

53 Cai, D., McEwen, D. P., Martens, J. R., Meyhofer, E. & Verhey, K. J. Single molecule imaging reveals differences in microtubule track selection between Kinesin motors. *PLoS biology* **7**, e1000216-e1000216, doi:10.1371/journal.pbio.1000216 (2009).

54 Cai, Q. & Sheng, Z.-H. Molecular motors and synaptic assembly. *The Neuroscientist : a review journal bringing neurobiology, neurology and psychiatry* **15**, 78-89, doi:10.1177/1073858408329511 (2009).

55 Campbell, K. & Götz, M. Radial glia: multi-purpose cells for vertebrate brain development. *Trends in neurosciences* **25**, 235-238, doi:10.1016/s0166-2236(02)02156-2 (2002).

56 Campellone, K. G. & Welch, M. D. A nucleator arms race: cellular control of actin assembly. *Nature reviews. Molecular cell biology* **11**, 237-251, doi:10.1038/nrm2867 (2010).

57 Cao, T. T., Chang, W., Masters, S. E. & Mooseker, M. S. Myosin-Va binds to and mechanochemically couples microtubules to actin filaments. *Molecular biology of the cell* **15**, 151-161, doi:10.1091/mbc.e03-07-0504 (2004).

58 Casanova, M. F. *et al.* Focal cortical dysplasias in autism spectrum disorders. *Acta neuropathologica communications* **1**, 67-67, doi:10.1186/2051-5960-1-67 (2013).

59 Chadman, K. K. *et al.* Minimal aberrant behavioral phenotypes of neuroligin-3 R451C knockin mice. *Autism research : official journal of the International Society for Autism Research* **1**, 147-158, doi:10.1002/aur.22 (2008).

60 Chai, X., Förster, E., Zhao, S., Bock, H. H. & Frotscher, M. Reelin stabilizes the actin cytoskeleton of neuronal processes by inducing n-cofilin phosphorylation at serine3. *The Journal of neuroscience : the official journal of the Society for Neuroscience* **29**, 288-299, doi:10.1523/JNEUROSCI.2934-08.2009 (2009).

61 Chai, X. *et al.* Reelin and cofilin cooperate during the migration of cortical neurons: A quantitative morphological analysis. *Development*, doi:10.1242/dev.134163 (2016).

62 Chang, X.-Z. *et al.* Identification of the functional role of AF1Q in the progression of breast cancer. *Breast cancer research and treatment* **111**, 65-78, doi:10.1007/s10549-007-9761-y (2008).

63 Chen, B. *et al.* The Fezf2-Ctip2 genetic pathway regulates the fate choice of subcortical projection neurons in the developing cerebral cortex. *Proceedings of the National Academy of Sciences of the United States of America* **105**, 11382-11387, doi:10.1073/pnas.0804918105 (2008).

64 Cheslack-Postava, K. & Jordan-Young, R. M. Autism spectrum disorders: toward a gendered embodiment model. *Social science & medicine (1982)* **74**, 1667-1674, doi:10.1016/j.socscimed.2011.06.013 (2012).

65 Cioni, J.-M. *et al.* Late Endosomes Act as mRNA Translation Platforms and Sustain Mitochondria in Axons. *Cell* **176**, 56-72.e15, doi:10.1016/j.cell.2018.11.030 (2019).

66 Cizeron, M. *et al.* A brainwide atlas of synapses across the mouse life span. *Science* **369**, 270-275, doi:10.1126/science.aba3163 (2020).

67 Clark, D., Dedova, I., Cordwell, S. & Matsumoto, I. Altered proteins of the anterior cingulate cortex white matter proteome in schizophrenia. *Proteomics. Clinical applications* **1**, 157-166, doi:10.1002/prca.200600541 (2007).

68 Co, N. N. *et al.* Oncogene AF1q enhances doxorubicin-induced apoptosis through BAD-mediated mitochondrial apoptotic pathway. *Molecular cancer therapeutics* **7**, 3160-3168, doi:10.1158/1535-7163.MCT-08-0416 (2008).

69 Cotton, A. P., Gokarakonda, S., Caffrey, A. R., Zarate, Y. A. & Kumar, N. Behavioral phenotype and sleep problems in SATB2-associated syndrome. *Developmental medicine and child neurology* **62**, 827-832, doi:10.1111/dmcn.14330 (2020).

70 Courchesne, E. *et al.* Neuron Number and Size in Prefrontal Cortex of Children With Autism. *JAMA* **306**, 2001-2001, doi:10.1001/jama.2011.1638 (2011).

71 Crawley, J. N. *et al.* Social approach behaviors in oxytocin knockout mice: comparison of two independent lines tested in different laboratory environments. *Neuropeptides* **41**, 145-163, doi:10.1016/j.npep.2007.02.002 (2007).

72 Crespo, I. *et al.* Tbr1 Misexpression Alters Neuronal Development in the Cerebral Cortex. *Molecular neurobiology* **59**, 5750-5765, doi:10.1007/s12035-022-02936-x (2022).

73 Crow, A. J. D. *et al.* Olfactory Dysfunction in Neurodevelopmental Disorders: A Meta-analytic Review of Autism Spectrum Disorders, Attention Deficit/Hyperactivity Disorder and Obsessive-Compulsive Disorder. *Journal of autism and developmental disorders* **50**, 2685-2697, doi:10.1007/s10803-020-04376-9 (2020).

74 Cubelos, B., Briz, C. G., Esteban-Ortega, G. M. & Nieto, M. Cux1 and Cux2 selectively target basal and apical dendritic compartments of layer II-III cortical neurons. *Developmental neurobiology* **75**, 163-172, doi:10.1002/dneu.22215 (2015).

75 Cubelos, B. *et al.* Cux1 and Cux2 regulate dendritic branching, spine morphology, and synapses of the upper layer neurons of the cortex. *Neuron* **66**, 523-535, doi:10.1016/j.neuron.2010.04.038 (2010).

76 Cubelos, B. *et al.* Cux-2 controls the proliferation of neuronal intermediate precursors of the cortical subventricular zone. *Cerebral cortex (New York, N.Y. : 1991)* **18**, 1758-1770, doi:10.1093/cercor/bhm199 (2008).

77 Cubelos, B. *et al.* Cux-1 and Cux-2 control the development of Reelin expressing cortical interneurons. *Developmental neurobiology* **68**, 917-925, doi:10.1002/dneu.20626 (2008).

78 Cushion, T. D. *et al.* De novo mutations in the beta-tubulin gene TUBB2A cause simplified gyral patterning and infantile-onset epilepsy. *American*

journal of human genetics **94**, 634-641, doi:10.1016/j.ajhg.2014.03.009 (2014).

79 Cuylen, S. *et al.* Ki-67 acts as a biological surfactant to disperse mitotic chromosomes. *Nature* **535**, 308-312, doi:10.1038/nature18610 (2016).

80 D'Amour, K. A. & Gage, F. H. Genetic and functional differences between multipotent neural and pluripotent embryonic stem cells. *Proceedings of the National Academy of Sciences* **100**, 11866-11872, doi:10.1073/pnas.1834200100 (2003).

81 D'Arcangelo, G. *et al.* A protein related to extracellular matrix proteins deleted in the mouse mutant reeler. *Nature* **374**, 719-723, doi:10.1038/374719a0 (1995).

82 Dan, W. *et al.* α-Tubulin Acetylation Restricts Axon Overbranching by Dampening Microtubule Plus-End Dynamics in Neurons. *Cerebral cortex (New York, N.Y. : 1991)* **28**, 3332-3346, doi:10.1093/cercor/bhx225 (2018).

83 Darmon, A. J., Nicholson, D. W. & Bleackley, R. C. Activation of the apoptotic protease CPP32 by cytotoxic T-cell-derived granzyme B. *Nature* **377**, 446-448, doi:10.1038/377446a0 (1995).

84 De La Cruz, E. M. & Pollard, T. D. Nucleotide-free actin: stabilization by sucrose and nucleotide binding kinetics. *Biochemistry* **34**, 5452-5461, doi:10.1021/bi00016a016 (1995).

85 De León Reyes, N. S. *et al.* Transient callosal projections of L4 neurons are eliminated for the acquisition of local connectivity. *Nature communications* **10**, 4549-4549, doi:10.1038/s41467-019-12495-w (2019).

86 Delandre, C., Amikura, R. & Moore, A. W. Microtubule nucleation and organization in dendrites. *Cell cycle (Georgetown, Tex.)* **15**, 1685-1692, doi:10.1080/15384101.2016.1172158 (2016).

87 DeLorey, T. M., Sahbaie, P., Hashemi, E., Homanics, G. E. & Clark, J. D. Gabrb3 gene deficient mice exhibit impaired social and exploratory behaviors, deficits in non-selective attention and hypoplasia of cerebellar vermal lobules: a potential model of autism spectrum disorder. *Behavioural brain research* **187**, 207-220, doi:10.1016/j.bbr.2007.09.009 (2008).

88 Dent, E. W. Of microtubules and memory: implications for microtubule dynamics in dendrites and spines. *Molecular biology of the cell* **28**, 1-8, doi:10.1091/mbc.E15-11-0769 (2017).

89 Dent, E. W. & Gertler, F. B. Cytoskeletal dynamics and transport in growth cone motility and axon guidance. *Neuron* **40**, 209-227, doi:10.1016/s0896-6273(03)00633-0 (2003).

90 Dent, E. W., Gupton, S. L. & Gertler, F. B. The growth cone cytoskeleton in axon outgrowth and guidance. *Cold Spring Harbor perspectives in biology* **3**, doi:10.1101/cshperspect.a001800 (2011).

91 Dent, E. W. & Kalil, K. Axon branching requires interactions between dynamic microtubules and actin filaments. *The Journal of neuroscience : the official journal of the Society for Neuroscience* **21**, 9757-9769, doi:10.1523/JNEUROSCI.21-24-09757.2001 (2001).

92 Diefenbach, T. J. *et al.* Myosin 1c and myosin IIB serve opposing roles in lamellipodial dynamics of the neuronal growth cone. *The Journal of cell biology* **158**, 1207-1217, doi:10.1083/jcb.200202028 (2002).

93 Dominguez, R. & Holmes, K. C. Actin structure and function. *Annual review of biophysics* **40**, 169-186, doi:10.1146/annurev-biophys-042910-155359 (2011).

94 Dotti, C. G., Sullivan, C. A. & Banker, G. A. The establishment of polarity by hippocampal neurons in culture. *The Journal of neuroscience : the official journal of the Society for Neuroscience* **8**, 1454-1468, doi:10.1523/JNEUROSCI.08-04-01454.1988 (1988).

95 Dráberová, E. *et al.* Differential expression of human γ-tubulin isotypes during neuronal development and oxidative stress points to a γ-tubulin-2 prosurvival function. *FASEB journal : official publication of the Federation of American Societies for Experimental Biology* **31**, 1828-1846, doi:10.1096/fj.201600846RR (2017).

96 Drozd, M. *et al.* Reduction of Fmr1 mRNA Levels Rescues Pathological Features in Cortical Neurons in a Model of FXTAS. *Molecular therapy. Nucleic acids* **18**, 546-553, doi:10.1016/j.omtn.2019.09.018 (2019).

97 Duit, S., Mayer, H., Blake, S. M., Schneider, W. J. & Nimpf, J. Differential functions of ApoER2 and very low density lipoprotein receptor in Reelin signaling depend on differential sorting of the receptors. *The Journal of*

biological chemistry **285**, 4896-4908, doi:10.1074/jbc.M109.025973 (2010).

98 Dworzynski, K., Ronald, A., Bolton, P. & Happé, F. How different are girls and boys above and below the diagnostic threshold for autism spectrum disorders? *Journal of the American Academy of Child and Adolescent Psychiatry* **51**, 788-797, doi:10.1016/j.jaac.2012.05.018 (2012).

99 Ejaz, R. *et al.* De novo pathogenic variant in TUBB2A presenting with arthrogryposis multiplex congenita, brain abnormalities, and severe developmental delay. *American journal of medical genetics. Part A* **173**, 2725-2730, doi:10.1002/ajmg.a.38352 (2017).

100 Ellis, P. *et al.* SOX2, a persistent marker for multipotential neural stem cells derived from embryonic stem cells, the embryo or the adult. *Developmental neuroscience* **26**, 148-165, doi:10.1159/000082134 (2004).

101 English, J. A., Dicker, P., Föcking, M., Dunn, M. J. & Cotter, D. R. 2-D DIGE analysis implicates cytoskeletal abnormalities in psychiatric disease. *Proteomics* **9**, 3368-3382, doi:10.1002/pmic.200900015 (2009).

102 Etherton, M. R., Blaiss, C. A., Powell, C. M. & Südhof, T. C. Mouse neurexin-1alpha deletion causes correlated electrophysiological and behavioral changes consistent with cognitive impairments. *Proceedings of the National Academy of Sciences of the United States of America* **106**, 17998-18003, doi:10.1073/pnas.0910297106 (2009).

103 Even, A. *et al.* ATAT1-enriched vesicles promote microtubule acetylation via axonal transport. *Science advances* **5**, eaax2705-eaax2705, doi:10.1126/sciadv.aax2705 (2019).

104 Fame, R. M., MacDonald, J. L. & Macklis, J. D. Development, specification, and diversity of callosal projection neurons. *Trends in neurosciences* **34**, 41-50, doi:10.1016/j.tins.2010.10.002 (2011).

105 Fingar, D. C. *et al.* mTOR controls cell cycle progression through its cell growth effectors S6K1 and 4E-BP1/eukaryotic translation initiation factor 4E. *Molecular and cellular biology* **24**, 200-216, doi:10.1128/MCB.24.1.200-216.2004 (2004).

106 Forestier, T., Féron, C., Leroy, C., D'Ettorre, P. & Gouat, P. Necessary Conditions for Social Transmission of Food Preference Through Feces in the House Mouse, Mus musculus domesticus. *Chemical Senses* **44**, 113-121, doi:10.1093/chemse/bjy080 (2019).

107 Franco, S. J. *et al.* Fate-restricted neural progenitors in the mammalian cerebral cortex. *Science (New York, N.Y.)* **337**, 746-749, doi:10.1126/science.1223616 (2012).

108 Fromer, M. *et al.* De novo mutations in schizophrenia implicate synaptic networks. *Nature* **506**, 179-184, doi:10.1038/nature12929 (2014).

109 Frotscher, M. Cajal-Retzius cells, Reelin, and the formation of layers. *Current opinion in neurobiology* **8**, 570-575, doi:10.1016/s0959-4388(98)80082-2 (1998).

110 Fujii, R. *et al.* The RNA Binding Protein TLS Is Translocated to Dendritic Spines by mGluR5 Activation and Regulates Spine Morphology. *Current Biology* **15**, 587-593, doi:10.1016/j.cub.2005.01.058 (2005).

111 Fujimoto, A. *et al.* Epilepsy in patients with focal cortical dysplasia may be associated with autism spectrum disorder. *Epilepsy & behavior : E&B* **120**, 107990-107990, doi:10.1016/j.yebeh.2021.107990 (2021).

112 Fujiwara, I., Vavylonis, D. & Pollard, T. D. Polymerization kinetics of ADP- and ADP-Pi-actin determined by fluorescence microscopy. *Proceedings of the National Academy of Sciences of the United States of America* **104**, 8827-8832, doi:10.1073/pnas.0702510104 (2007).

113 Galef, B. G. Social learning of food preferences in rodents: rapid appetitive learning. *Current protocols in neuroscience* **Chapter 8**, Unit 8.5D-Unit 8.5D, doi:10.1002/0471142301.ns0805ds21 (2003).

114 Gao, P. *et al.* Deterministic progenitor behavior and unitary production of neurons in the neocortex. *Cell* **159**, 775-788, doi:10.1016/j.cell.2014.10.027 (2014).

115 Garduno-Robles, A. *et al.* MRI Features in a Rat Model of H-ABC Tubulinopathy. *Frontiers in neuroscience* **14**, 555-555, doi:10.3389/fnins.2020.00555 (2020).

116 Geschwind, D. H. & Levitt, P. Autism spectrum disorders: developmental disconnection syndromes. *Current opinion in neurobiology* **17**, 103-111, doi:10.1016/j.conb.2007.01.009 (2007).

117 Giarelli, E. *et al.* Sex differences in the evaluation and diagnosis of autism spectrum disorders among children. *Disability and health journal* **3**, 107-116, doi:10.1016/j.dhjo.2009.07.001 (2010).

118 Gil-Sanz, C. *et al.* Lineage Tracing Using Cux2-Cre and Cux2-CreERT2 Mice. *Neuron* **86**, 1091-1099, doi:10.1016/j.neuron.2015.04.019 (2015).

119 Gil-Sanz, C. *et al.* Cajal-Retzius cells instruct neuronal migration by coincidence signaling between secreted and contact-dependent guidance cues. *Neuron* **79**, 461-477, doi:10.1016/j.neuron.2013.06.040 (2013).

120 Gilman, Sarah R. *et al.* Rare De Novo Variants Associated with Autism Implicate a Large Functional Network of Genes Involved in Formation and Function of Synapses. *Neuron* **70**, 898-907, doi:10.1016/j.neuron.2011.05.021 (2011).

121 Glaser, S. *et al.* The histone 3 lysine 4 methyltransferase, Mll2, is only required briefly in development and spermatogenesis. *Epigenetics & chromatin* **2**, 5-5, doi:10.1186/1756-8935-2-5 (2009).

122 Go, C. D. *et al.* A proximity-dependent biotinylation map of a human cell. *Nature* **595**, 120-124, doi:10.1038/s41586-021-03592-2 (2021).

123 Goedert, M. Tau gene mutations and their effects. *Movement disorders : official journal of the Movement Disorder Society* **20 Suppl 12**, S45-52, doi:10.1002/mds.20539 (2005).

124 Goikolea-Vives, A. & Stolp, H. B. Connecting the Neurobiology of Developmental Brain Injury: Neuronal Arborisation as a Regulator of Dysfunction and Potential Therapeutic Target. *International Journal of Molecular Sciences* **22**, 8220-8220, doi:10.3390/ijms22158220 (2021).

125 Goldberg, D. J. & Burmeister, D. W. Stages in axon formation: observations of growth of Aplysia axons in culture using video-enhanced contrast-differential interference contrast microscopy. *The Journal of cell biology* **103**, 1921-1931, doi:10.1083/jcb.103.5.1921 (1986).

126 González, C. *et al.* Axons provide the secretory machinery for trafficking of voltage-gated sodium channels in peripheral nerve. *Proceedings of the National Academy of Sciences of the United States of America* **113**, 1823-1828, doi:10.1073/pnas.1514943113 (2016).

127 Götz, M., Stoykova, A. & Gruss, P. Pax6 controls radial glia differentiation in the cerebral cortex. *Neuron* **21**, 1031-1044, doi:10.1016/s0896-6273(00)80621-2 (1998).

128 Gregory, T. K. *et al.* Molecular prognostic markers for adult acute myeloid leukemia with normal cytogenetics. *Journal of hematology & oncology* **2**, 23-23, doi:10.1186/1756-8722-2-23 (2009).

129 Gu, C. Rapid and Reversible Development of Axonal Varicosities: A New Form of Neural Plasticity. *Frontiers in Molecular Neuroscience* **14**, doi:10.3389/fnmol.2021.610857 (2021).

130 Guang, S. *et al.* Synaptopathology Involved in Autism Spectrum Disorder. *Frontiers in cellular neuroscience* **12**, 470-470, doi:10.3389/fncel.2018.00470 (2018).

131 Gumy, L. F. *et al.* MAP2 Defines a Pre-axonal Filtering Zone to Regulate KIF1- versus KIF5-Dependent Cargo Transport in Sensory Neurons. *Neuron* **94**, 347-362.e347, doi:10.1016/j.neuron.2017.03.046 (2017).

132 Hadders-Algra, M. Early Diagnostics and Early Intervention in Neurodevelopmental Disorders-Age-Dependent Challenges and Opportunities. *Journal of clinical medicine* **10**, doi:10.3390/jcm10040861 (2021).

133 Han, W. *et al.* TBR1 directly represses Fezf2 to control the laminar origin and development of the corticospinal tract. *Proceedings of the National Academy of Sciences of the United States of America* **108**, 3041-3046, doi:10.1073/pnas.1016723108 (2011).

134 Hargreaves, A. J., Wandosell, F. & Avila, J. Phosphorylation of tubulin enhances its interaction with membranes. *Nature* **323**, 827-828, doi:10.1038/323827a0.

135 Hartfuss, E., Galli, R., Heins, N. & Götz, M. Characterization of CNS precursor subtypes and radial glia. *Developmental biology* **229**, 15-30, doi:10.1006/dbio.2000.9962 (2001).

136 Hashimoto, K. *et al.* Reduced serum levels of brain-derived neurotrophic factor in adult male patients with autism. *Progress in neuro-psychopharmacology & biological psychiatry* **30**, 1529-1531, doi:10.1016/j.pnpbp.2006.06.018 (2006).

137 He, C.-H. *et al.* Satb2 Regulates EphA7 to Control Soma Spacing and Self-Avoidance of Cortical Pyramidal Neurons. *Cerebral Cortex* **32**, 2321-2331, doi:10.1093/cercor/bhab321 (2022).

138 He, C.-W., Liao, C.-P. & Pan, C.-L. Wnt signalling in the development of axon, dendrites and synapses. *Open biology* **8**, doi:10.1098/rsob.180116 (2018).

139 Heavner, W. E. *et al.* Transcription factor expression defines subclasses of developing projection neurons highly similar to single-cell RNA-seq subtypes. *Proceedings of the National Academy of Sciences of the United States of America* **117**, 25074-25084, doi:10.1073/pnas.2008013117 (2020).

140 Herbst, W. A. & Martin, K. C. Regulated transport of signaling proteins from synapse to nucleus. *Current opinion in neurobiology* **45**, 78-84, doi:10.1016/j.conb.2017.04.006 (2017).

141 Hersheson, J. *et al.* Mutations in the autoregulatory domain of β-tubulin 4a cause hereditary dystonia. *Annals of neurology* **73**, 546-553, doi:10.1002/ana.23832 (2013).

142 Hevner, R. F. *et al.* Tbr1 regulates differentiation of the preplate and layer 6. *Neuron* **29**, 353-366, doi:10.1016/s0896-6273(01)00211-2 (2001).

143 Hippenmeyer, S. *et al.* A Developmental Switch in the Response of DRG Neurons to ETS Transcription Factor Signaling. *PLoS Biology* **3**, e159-e159, doi:10.1371/journal.pbio.0030159 (2005).

144 Hirata, T. *et al.* Zinc finger gene fez-like functions in the formation of subplate neurons and thalamocortical axons. *Developmental dynamics : an official publication of the American Association of Anatomists* **230**, 546-556, doi:10.1002/dvdy.20068 (2004).

145 Hirokawa, N., Noda, Y., Tanaka, Y. & Niwa, S. Kinesin superfamily motor proteins and intracellular transport. *Nature reviews. Molecular cell biology* **10**, 682-696, doi:10.1038/nrm2774 (2009).

146 Hirokawa, N. & Takemura, R. Molecular motors in neuronal development, intracellular transport and diseases. *Current Opinion in Neurobiology* **14**, 564-573, doi:10.1016/j.conb.2004.08.011 (2004).

147 Hirota, Y. & Nakajima, K. Control of Neuronal Migration and Aggregation by Reelin Signaling in the Developing Cerebral Cortex. *Frontiers in cell and developmental biology* **5**, 40-40, doi:10.3389/fcell.2017.00040 (2017).

148 Hisaoka, T., Nakamura, Y., Senba, E. & Morikawa, Y. The forkhead transcription factors, Foxp1 and Foxp2, identify different subpopulations of projection neurons in the mouse cerebral cortex. *Neuroscience* **166**, 551-563, doi:10.1016/j.neuroscience.2009.12.055 (2010).

149 Hlushchenko, I., Khanal, P., Abouelezz, A., Paavilainen, V. O. & Hotulainen, P. ASD-Associated De Novo Mutations in Five Actin Regulators Show Both Shared and Distinct Defects in Dendritic Spines and Inhibitory Synapses in Cultured Hippocampal Neurons. *Frontiers in Cellular Neuroscience* **12**, doi:10.3389/fncel.2018.00217 (2018).

150 Hodges, H., Fealko, C. & Soares, N. Autism spectrum disorder: definition, epidemiology, causes, and clinical evaluation. *Translational pediatrics* **9**, S55-S65, doi:10.21037/tp.2019.09.09 (2020).

151 Hodges, J. L., Newell-Litwa, K., Asmussen, H., Vicente-Manzanares, M. & Horwitz, A. R. Myosin IIB Activity and Phosphorylation Status Determines Dendritic Spine and Post-Synaptic Density Morphology. *PLoS ONE* **6**, e24149-e24149, doi:10.1371/journal.pone.0024149 (2011).

152 Hong, S.-J., Hyung, B., Paquola, C. & Bernhardt, B. C. The Superficial White Matter in Autism and Its Role in Connectivity Anomalies and Symptom Severity. *Cerebral cortex (New York, N.Y. : 1991)* **29**, 4415-4425, doi:10.1093/cercor/bhy321 (2019).

153 Hori, K., Shimaoka, K. & Hoshino, M. AUTS2 Gene: Keys to Understanding the Pathogenesis of Neurodevelopmental Disorders. *Cells* **11**, doi:10.3390/cells11010011 (2021).

154 Hu, J. *et al.* AF1q Mediates Tumor Progression in Colorectal Cancer by Regulating AKT Signaling. *International journal of molecular sciences* **18**, doi:10.3390/ijms18050987 (2017).

155 Hu, Y., Sun, Q., Zhang, C., Sha, Q. & Sun, X. RE1 silencing transcription factor (REST) negatively regulates ALL1-fused from chromosome 1q (AF1q) gene transcription. *BMC molecular biology* **16**, 15-15, doi:10.1186/s12867-015-0043-7 (2015).

156 Huttenlocher, P. R. & Dabholkar, A. S. Regional differences in synaptogenesis in human cerebral cortex. *The Journal of comparative neurology* **387**, 167-178, doi:10.1002/(sici)1096-9861(19971020)387:2<167::aid-cne1>3.0.co;2-z (1997).

157 Iossifov, I. *et al.* The contribution of de novo coding mutations to autism spectrum disorder. *Nature* **515**, 216-221, doi:10.1038/nature13908 (2014).

158 Iulianella, A., Sharma, M., Durnin, M., Vanden Heuvel, G. B. & Trainor, P. A. Cux2 (Cutl2) integrates neural progenitor development with cell-cycle progression during spinal cord neurogenesis. *Development (Cambridge, England)* **135**, 729-741, doi:10.1242/dev.013276 (2008).

159 Ivanova, E. L. *et al.* TUBG1 missense variants underlying cortical malformations disrupt neuronal locomotion and microtubule dynamics but not neurogenesis. *Nature communications* **10**, 2129-2129, doi:10.1038/s41467-019-10081-8 (2019).

160 Jacques, C. *et al.* Two-Step Differential Expression Analysis Reveals a New Set of Genes Involved in Thyroid Oncocytic Tumors. *The Journal of Clinical Endocrinology & Metabolism* **90**, 2314-2320, doi:10.1210/jc.2004-1337 (2005).

161 Jaglin, X. H. *et al.* Mutations in the beta-tubulin gene TUBB2B result in asymmetrical polymicrogyria. *Nature genetics* **41**, 746-752, doi:10.1038/ng.380 (2009).

162 Jamuar, S. S. & Walsh, C. A. Somatic mutations in cerebral cortical malformations. *The New England journal of medicine* **371**, 2038-2038, doi:10.1056/NEJMc1411784 (2014).

163 Jansen, A. C. *et al.* TUBA1A mutations: from isolated lissencephaly to familial polymicrogyria. *Neurology* **76**, 988-992, doi:10.1212/WNL.0b013e31821043f5 (2011).

164 Jude, C. D. *et al.* Unique and independent roles for MLL in adult hematopoietic stem cells and progenitors. *Cell stem cell* **1**, 324-337, doi:10.1016/j.stem.2007.05.019 (2007).

165 Kahn, O. I. & Baas, P. W. Microtubules and Growth Cones: Motors Drive the Turn. *Trends in neurosciences* **39**, 433-440, doi:10.1016/j.tins.2016.04.009 (2016).

166 Kaidanovich-Beilin, O., Lipina, T., Vukobradovic, I., Roder, J. & Woodgett, J. R. Assessment of social interaction behaviors. *Journal of visualized experiments : JoVE*, doi:10.3791/2473 (2011).

167 Kálmán, M. & Hajós, F. Distribution of glial fibrillary acidic protein (GFAP)-immunoreactive astrocytes in the rat brain. I. Forebrain. *Experimental brain research* **78**, 147-163, doi:10.1007/BF00230694 (1989).

168 Kang, H., Bradley, M. J., Elam, W. A. & De La Cruz, E. M. Regulation of actin by ion-linked equilibria. *Biophysical journal* **105**, 2621-2628, doi:10.1016/j.bpj.2013.10.032 (2013).

169 Kapitein, L. C. & Hoogenraad, C. C. Which way to go? Cytoskeletal organization and polarized transport in neurons. *Molecular and cellular neurosciences* **46**, 9-20, doi:10.1016/j.mcn.2010.08.015 (2011).

170 Kasper, E. M., Lübke, J., Larkman, A. U. & Blakemore, C. Pyramidal neurons in layer 5 of the rat visual cortex. III. Differential maturation of axon targeting, dendritic morphology, and electrophysiological properties. *The Journal of comparative neurology* **339**, 495-518, doi:10.1002/cne.903390404 (1994).

171 Kazdoba, T. M., Leach, P. T. & Crawley, J. N. Behavioral phenotypes of genetic mouse models of autism. *Genes, brain, and behavior* **15**, 7-26, doi:10.1111/gbb.12256 (2016).

172 Keays, D. A. *et al.* Mutations in α-Tubulin Cause Abnormal Neuronal Migration in Mice and Lissencephaly in Humans. *Cell* **128**, 45-57, doi:10.1016/j.cell.2006.12.017 (2007).

173 Keays, D. A. *et al.* Mutations in alpha-tubulin cause abnormal neuronal migration in mice and lissencephaly in humans. *Cell* **128**, 45-57, doi:10.1016/j.cell.2006.12.017 (2007).

174 Kelleher, R. J. & Bear, M. F. The Autistic Neuron: Troubled Translation? *Cell* **135**, 401-406, doi:10.1016/j.cell.2008.10.017 (2008).

175 Kemper, T. L. & Bauman, M. Neuropathology of infantile autism. *Journal of neuropathology and experimental neurology* **57**, 645-652, doi:10.1097/00005072-199807000-00001 (1998).

176 Kennedy, M. J. & Ehlers, M. D. Organelles and trafficking machinery for postsynaptic plasticity. *Annual review of neuroscience* **29**, 325-362, doi:10.1146/annurev.neuro.29.051605.112808 (2006).

177 Keshava, C., Whipkey, D. & Weston, A. Transcriptional signatures of environmentally relevant exposures in normal human mammary epithelial

cells: benzo[a]pyrene. *Cancer Letters* **221**, 201-211, doi:10.1016/j.canlet.2004.08.037 (2005).

178 Koizumi, H. & Gleeson, J. G. Sun proteins enlighten nuclear movement in development. *Neuron* **64**, 147-149, doi:10.1016/j.neuron.2009.10.010 (2009).

179 Kristiansen, L. V., Beneyto, M., Haroutunian, V. & Meador-Woodruff, J. H. Changes in NMDA receptor subunits and interacting PSD proteins in dorsolateral prefrontal and anterior cingulate cortex indicate abnormal regional expression in schizophrenia. *Molecular psychiatry* **11**, 737-747, 705, doi:10.1038/sj.mp.4001844 (2006).

180 Kumamoto, T. *et al.* Foxg1 coordinates the switch from nonradially to radially migrating glutamatergic subtypes in the neocortex through spatiotemporal repression. *Cell reports* **3**, 931-945, doi:10.1016/j.celrep.2013.02.023 (2013).

181 Kumar, R. A. *et al.* TUBA1A mutations cause wide spectrum lissencephaly (smooth brain) and suggest that multiple neuronal migration pathways converge on alpha tubulins. *Human molecular genetics* **19**, 2817-2827, doi:10.1093/hmg/ddq182 (2010).

182 Kwan, K. Y. *et al.* SOX5 postmitotically regulates migration, postmigratory differentiation, and projections of subplate and deep-layer neocortical neurons. *Proceedings of the National Academy of Sciences of the United States of America* **105**, 16021-16026, doi:10.1073/pnas.0806791105 (2008).

183 Kwon, C.-H. *et al.* Pten regulates neuronal arborization and social interaction in mice. *Neuron* **50**, 377-388, doi:10.1016/j.neuron.2006.03.023 (2006).

184 Lai, M. *et al.* Myosin X regulates neuronal radial migration through interacting with N-cadherin. *Frontiers in cellular neuroscience* **9**, 326-326, doi:10.3389/fncel.2015.00326 (2015).

185 Lai, M.-C., Lombardo, M. V. & Baron-Cohen, S. Autism. *The Lancet* **383**, 896-910, doi:10.1016/S0140-6736(13)61539-1 (2014).

186 Lai, M.-C. *et al.* A behavioral comparison of male and female adults with high functioning autism spectrum conditions. *PloS one* **6**, e20835-e20835, doi:10.1371/journal.pone.0020835 (2011).

187 Lai, T. *et al.* SOX5 controls the sequential generation of distinct corticofugal neuron subtypes. *Neuron* **57**, 232-247, doi:10.1016/j.neuron.2007.12.023 (2008).

188 Langford, G. M. Myosin-V, a versatile motor for short-range vesicle transport. *Traffic (Copenhagen, Denmark)* **3**, 859-865, doi:10.1034/j.1600-0854.2002.31202.x (2002).

189 Lawrenson, I. D. *et al.* Cortical Layer Inversion and Deregulation of Reelin Signaling in the Absence of SOCS6 and SOCS7. *Cerebral cortex (New York, N.Y. : 1991)* **27**, 576-588, doi:10.1093/cercor/bhv253 (2017).

190 LeDizet, M. & Piperno, G. Identification of an acetylation site of Chlamydomonas alpha-tubulin. *Proceedings of the National Academy of Sciences of the United States of America* **84**, 5720-5724, doi:10.1073/pnas.84.16.5720 (1987).

191 Lee, H. *et al.* The microtubule plus end tracking protein Orbit/MAST/CLASP acts downstream of the tyrosine kinase Abl in mediating axon guidance. *Neuron* **42**, 913-926, doi:10.1016/j.neuron.2004.05.020 (2004).

192 Lees, R. M., Johnson, J. D. & Ashby, M. C. Presynaptic Boutons That Contain Mitochondria Are More Stable. *Frontiers in synaptic neuroscience* **11**, 37-37, doi:10.3389/fnsyn.2019.00037 (2019).

Lein, E.S. et al. Genome-wide atlas of gene expression in the adult mouse brain, *Nature* **445**, 168-176, https://doi:10.1038/nature05453 (2007).

193 Leone, D. P. *et al.* Satb2 Regulates the Differentiation of Both Callosal and Subcerebral Projection Neurons in the Developing Cerebral Cortex. *Cerebral Cortex* **25**, 3406-3419, doi:10.1093/cercor/bhu156 (2015).

194 Lestou, V. S. *et al.* Characterization of the recurrent translocation t(1;1)(p36.3;q21.1-2) in non-Hodgkin lymphoma by multicolor banding and fluorescence in situ hybridization analysis. *Genes, chromosomes & cancer* **36**, 375-381, doi:10.1002/gcc.10181 (2003).

195 Levitt, P. & Campbell, D. B. The genetic and neurobiologic compass points toward common signaling dysfunctions in autism spectrum disorders. *The Journal of clinical investigation* **119**, 747-754, doi:10.1172/JCI37934 (2009).

196 Li, D.-Q. *et al.* Gene expression profile analysis of an isogenic tumour metastasis model reveals a functional role for oncogene AF1Q in breast cancer metastasis. *European Journal of Cancer* **42**, 3274-3286, doi:10.1016/j.ejca.2006.07.008 (2006).

197 Li, J. *et al.* Integrated systems analysis reveals a molecular network underlying autism spectrum disorders. *Molecular Systems Biology* **10**, doi:10.15252/msb.20145487 (2014).

198 Li, L. *et al.* ATAT1 regulates forebrain development and stress-induced tubulin hyperacetylation. *Cellular and molecular life sciences : CMLS* **76**, 3621-3640, doi:10.1007/s00018-019-03088-3 (2019).

199 Li, P. *et al.* Degradation of AF1Q by chaperone-mediated autophagy. *Experimental cell research* **327**, 48-56, doi:10.1016/j.yexcr.2014.05.013 (2014).

200 Li, W. *et al.* Novel AF1q/MLLT11 favorably affects imatinib resistance and cell survival in chronic myeloid leukemia. *Cell death & disease* **9**, 855-855, doi:10.1038/s41419-018-0900-7 (2018).

201 Li, Z.-g. *et al.* [Detection of 29 types of fusion gene in leukemia by multiplex RT-PCR]. *Zhonghua xue ye xue za zhi = Zhonghua xueyexue zazhi* **24**, 256-258 (2003).

202 Liao, J., Chen, H., Qi, M., Wang, J. & Wang, M. MLLT11-TRIL complex promotes the progression of endometrial cancer through PI3K/AKT/mTOR signaling pathway. *Cancer biology & therapy* **23**, 211-224, doi:10.1080/15384047.2022.2046450 (2022).

203 Lim, D. A. *et al.* Chromatin remodelling factor Mll1 is essential for neurogenesis from postnatal neural stem cells. *Nature* **458**, 529-533, doi:10.1038/nature07726 (2009).

204 Lin, C. H., Espreafico, E. M., Mooseker, M. S. & Forscher, P. Myosin drives retrograde F-actin flow in neuronal growth cones. *Neuron* **16**, 769-782, doi:10.1016/s0896-6273(00)80097-5 (1996).

205 Lin, H. J. *et al.* AF1q, a differentially expressed gene during neuronal differentiation, transforms HEK cells into neuron-like cells. *Brain research. Molecular brain research* **131**, 126-130, doi:10.1016/j.molbrainres.2004.07.022 (2004).

206 Lin, S. & Smith, G. M. Acetylation as a mechanism that regulates axonal regeneration. *Neural regeneration research* **10**, 1034-1036, doi:10.4103/1673-5374.160066 (2015).

207 Lintas, C. & Persico, A. M. Autistic phenotypes and genetic testing: state-of-the-art for the clinical geneticist. *Journal of medical genetics* **46**, 1-8, doi:10.1136/jmg.2008.060871 (2009).

208 Liu, T. *et al.* The retinoid anticancer signal: mechanisms of target gene regulation. *British journal of cancer* **93**, 310-318, doi:10.1038/sj.bjc.6602700 (2005).

209 Liu, Y., Foustoukos, G., Crochet, S. & Petersen, C. C. H. Axonal and Dendritic Morphology of Excitatory Neurons in Layer 2/3 Mouse Barrel Cortex Imaged Through Whole-Brain Two-Photon Tomography and Registered to a Digital Brain Atlas. *Frontiers in neuroanatomy* **15**, 791015-791015, doi:10.3389/fnana.2021.791015 (2021).

210 Liu, Y., Lee, J. W. & Ackerman, S. L. Mutations in the microtubule-associated protein 1A (Map1a) gene cause Purkinje cell degeneration. *The Journal of neuroscience : the official journal of the Society for Neuroscience* **35**, 4587-4598, doi:10.1523/JNEUROSCI.2757-14.2015 (2015).

211 López-Bendito, G. & Molnár, Z. Thalamocortical development: how are we going to get there? *Nature reviews. Neuroscience* **4**, 276-289, doi:10.1038/nrn1075 (2003).

212 Lu, J. & Pollard, T. D. Profilin binding to poly-L-proline and actin monomers along with ability to catalyze actin nucleotide exchange is required for viability of fission yeast. *Molecular biology of the cell* **12**, 1161-1175, doi:10.1091/mbc.12.4.1161 (2001).

213 Lyons-Warren, A. M., Herman, I., Hunt, P. J. & Arenkiel, B. R. A systematic-review of olfactory deficits in neurodevelopmental disorders: From mouse to human. *Neuroscience and biobehavioral reviews* **125**, 110-121, doi:10.1016/j.neubiorev.2021.02.024 (2021).

214 Magura, I. S. [Transmembrane ionic currents in the generation of action potential in giant neuron soma]. *Biofizika* **13**, 196-199 (1968).

215 Marchani, E. E. *et al.* Identification of rare variants from exome sequence in a large pedigree with autism. *Human heredity* **74**, 153-164, doi:10.1159/000346560 (2012).

216 Marcos, S. *et al.* Tubulin tyrosination is required for the proper organization and pathfinding of the growth cone. *PloS one* **4**, e5405-e5405, doi:10.1371/journal.pone.0005405 (2009).

217 Marín, O. & Rubenstein, J. L. R. Cell migration in the forebrain. *Annual review of neuroscience* **26**, 441-483, doi:10.1146/annurev.neuro.26.041002.131058 (2003).

218 McFarlane, H. G. *et al.* Autism-like behavioral phenotypes in BTBR T+tf/J mice. *Genes, brain, and behavior* **7**, 152-163, doi:10.1111/j.1601-183X.2007.00330.x (2008).

219 McKenna, W. L. *et al.* Tbr1 and Fezf2 regulate alternate corticofugal neuronal identities during neocortical development. *The Journal of neuroscience : the official journal of the Society for Neuroscience* **31**, 549-564, doi:10.1523/JNEUROSCI.4131-10.2011 (2011).

220 McMahon, K. A. *et al.* Mll has a critical role in fetal and adult hematopoietic stem cell self-renewal. *Cell stem cell* **1**, 338-345, doi:10.1016/j.stem.2007.07.002 (2007).

221 McQuaid, G. A., Lee, N. R. & Wallace, G. L. Camouflaging in autism spectrum disorder: Examining the roles of sex, gender identity, and diagnostic timing. *Autism : the international journal of research and practice* **26**, 552-559, doi:10.1177/13623613211042131 (2022).

222 Meier, S. M. *et al.* Obsessive-Compulsive Disorder and Autism Spectrum Disorders: Longitudinal and Offspring Risk. *PloS one* **10**, e0141703-e0141703, doi:10.1371/journal.pone.0141703 (2015).

223 Mensen, V. T. *et al.* Development of cortical thickness and surface area in autism spectrum disorder. *NeuroImage. Clinical* **13**, 215-222, doi:10.1016/j.nicl.2016.12.003 (2017).

224 Miyata, T., Kawaguchi, A., Okano, H. & Ogawa, M. Asymmetric inheritance of radial glial fibers by cortical neurons. *Neuron* **31**, 727-741, doi:10.1016/s0896-6273(01)00420-2 (2001).

225 Mockrin, S. C. & Korn, E. D. Acanthamoeba profilin interacts with G-actin to increase the rate of exchange of actin-bound adenosine 5'-triphosphate. *Biochemistry* **19**, 5359-5362, doi:10.1021/bi00564a033 (1980).

226 Moffat, J. J., Ka, M., Jung, E.-M. & Kim, W.-Y. Genes and brain malformations associated with abnormal neuron positioning. *Molecular brain* **8**, 72-72, doi:10.1186/s13041-015-0164-4 (2015).

227 Monroy, B. Y. *et al.* Competition between microtubule-associated proteins directs motor transport. *Nature communications* **9**, 1487-1487, doi:10.1038/s41467-018-03909-2 (2018).

228 Moon, H. M. & Wynshaw-Boris, A. Cytoskeleton in action: lissencephaly, a neuronal migration disorder. *Wiley interdisciplinary reviews. Developmental biology* **2**, 229-245, doi:10.1002/wdev.67 (2013).

229 Moore, S. 31-31 (Halifax, Nova Scotia, 2021).

230 Moore, S. A. & Iulianella, A. Development of the mammalian cortical hem and its derivatives: the choroid plexus, Cajal-Retzius cells and hippocampus. *Open biology* **11**, 210042-210042, doi:10.1098/rsob.210042 (2021).

231 Moreno-De-Luca, A. *et al.* Developmental brain dysfunction: revival and expansion of old concepts based on new genetic evidence. *The Lancet Neurology* **12**, 406-414, doi:10.1016/S1474-4422(13)70011-5 (2013).

232 Moy, S. S. *et al.* Sociability and preference for social novelty in five inbred strains: an approach to assess autistic-like behavior in mice. *Genes, brain, and behavior* **3**, 287-302, doi:10.1111/j.1601-1848.2004.00076.x (2004).

233 Mullen, R. J., Buck, C. R. & Smith, A. M. NeuN, a neuronal specific nuclear protein in vertebrates. *Development (Cambridge, England)* **116**, 201-211, doi:10.1242/dev.116.1.201 (1992).

234 Muller, J. *et al.* Sequence and comparative genomic analysis of actin-related proteins. *Molecular biology of the cell* **16**, 5736-5748, doi:10.1091/mbc.e05-06-0508 (2005).

235 Nabariya, D. K., Heinz, A., Derksen, S. & Krauß, S. Intracellular and intercellular transport of RNA organelles in CXG repeat disorders: The strength of weak ties. *Frontiers in molecular biosciences* **9**, 1000932-1000932, doi:10.3389/fmolb.2022.1000932 (2022).

236 Nadarajah, B., Brunstrom, J. E., Grutzendler, J., Wong, R. O. & Pearlman, A. L. Two modes of radial migration in early development of the cerebral cortex. *Nature neuroscience* **4**, 143-150, doi:10.1038/83967 (2001).

237 Nagy, J. *et al.* Altered neurite morphology and cholinergic function of induced pluripotent stem cell-derived neurons from a patient with Kleefstra syndrome and autism. *Translational psychiatry* **7**, e1179-e1179, doi:10.1038/tp.2017.144 (2017).

238 Nance, J. & Zallen, J. A. Elaborating polarity: PAR proteins and the cytoskeleton. *Development (Cambridge, England)* **138**, 799-809, doi:10.1242/dev.053538 (2011).

239 Nesler, K. R., Starke, E. L., Boin, N. G., Ritz, M. & Barbee, S. A. Presynaptic CamKII regulates activity-dependent axon terminal growth. *Molecular and cellular neurosciences* **76**, 33-41, doi:10.1016/j.mcn.2016.08.007 (2016).

240 Ngo, L. *et al.* TUBB5 and its disease-associated mutations influence the terminal differentiation and dendritic spine densities of cerebral cortical neurons. *Human molecular genetics* **23**, 5147-5158, doi:10.1093/hmg/ddu238 (2014).

241 Nieto, M. *et al.* Expression of Cux-1 and Cux-2 in the subventricular zone and upper layers II-IV of the cerebral cortex. *The Journal of comparative neurology* **479**, 168-180, doi:10.1002/cne.20322 (2004).

242 Nirschl, J. J., Ghiretti, A. E. & Holzbaur, E. L. F. The impact of cytoskeletal organization on the local regulation of neuronal transport. *Nature reviews. Neuroscience* **18**, 585-597, doi:10.1038/nrn.2017.100 (2017).

243 Nishimura, K. *et al.* Genetic analyses of the brain-derived neurotrophic factor (BDNF) gene in autism. *Biochemical and biophysical research communications* **356**, 200-206, doi:10.1016/j.bbrc.2007.02.135 (2007).

244 Nishiyama, J. Plasticity of dendritic spines: Molecular function and dysfunction in neurodevelopmental disorders. *Psychiatry and Clinical Neurosciences* **73**, 541-550, doi:10.1111/pcn.12899 (2019).

245 O'Leary, D. D. & Koester, S. E. Development of projection neuron types, axon pathways, and patterned connections of the mammalian cortex. *Neuron* **10**, 991-1006, doi:10.1016/0896-6273(93)90049-w (1993).

246 O'Neill, K. M. *et al.* Assessing effects on dendritic arborization using novel Sholl analyses. *Frontiers in cellular neuroscience* **9**, 285-285, doi:10.3389/fncel.2015.00285 (2015).

247 Ofek, G., Wiltz, D. C. & Athanasiou, K. A. Contribution of the cytoskeleton to the compressive properties and recovery behavior of single cells. *Biophysical journal* **97**, 1873-1882, doi:10.1016/j.bpj.2009.07.050 (2009).

248 Ogawa, M. *et al.* The reeler gene-associated antigen on Cajal-Retzius neurons is a crucial molecule for laminar organization of cortical neurons. *Neuron* **14**, 899-912, doi:10.1016/0896-6273(95)90329-1 (1995).

249 Ohki, T., Ohno, C., Oyama, K., Mikhailenko, S. V. & Ishiwata, S. i. Purification of cytoplasmic actin by affinity chromatography using the C-terminal half of gelsolin. *Biochemical and biophysical research communications* **383**, 146-150, doi:10.1016/j.bbrc.2009.03.144 (2009).

250 Ohta, H. *et al.* White matter alterations in autism spectrum disorder and attention-deficit/hyperactivity disorder in relation to sensory profile. *Molecular Autism* **11**, 77-77, doi:10.1186/s13229-020-00379-6 (2020).

251 Oma, Y. & Harata, M. Actin-related proteins localized in the nucleus: from discovery to novel roles in nuclear organization. *Nucleus (Austin, Tex.)* **2**, 38-46, doi:10.4161/nucl.2.1.14510 (2011).

252 Page, D. T., Kuti, O. J., Prestia, C. & Sur, M. Haploinsufficiency for Pten and Serotonin transporter cooperatively influences brain size and social behavior. *Proceedings of the National Academy of Sciences of the United States of America* **106**, 1989-1994, doi:10.1073/pnas.0804428106 (2009).

253 Pantaloni, D. & Carlier, M. F. How profilin promotes actin filament assembly in the presence of thymosin beta 4. *Cell* **75**, 1007-1014, doi:10.1016/0092-8674(93)90544-z (1993).

254 Parato, J. & Bartolini, F. The microtubule cytoskeleton at the synapse. *Neuroscience Letters* **753**, 135850-135850, doi:10.1016/j.neulet.2021.135850 (2021).

255 Parcelier, A. *et al.* AF1q/MLLT11 regulates the emergence of human prothymocytes through cooperative interaction with the Notch signaling pathway. *Blood* **118**, 1784-1796, doi:10.1182/blood-2011-01-333179 (2011).

256 Paredez, A. R. *et al.* An actin cytoskeleton with evolutionarily conserved functions in the absence of canonical actin-binding proteins. *Proceedings of the National Academy of Sciences of the United States of America* **108**, 6151-6156, doi:10.1073/pnas.1018593108 (2011).

257 Parikshak, N. N. *et al.* Genome-wide changes in lncRNA, splicing, and regional gene expression patterns in autism. *Nature* **540**, 423-427, doi:10.1038/nature20612 (2016).

258 Park, J. *et al.* AF1q inhibited T cell attachment to breast cancer cell by attenuating Intracellular Adhesion Molecule-1 expression. *Journal of Cancer Metastasis and Treatment* **2019**, doi:10.20517/2394-4722.2018.84 (2019).

259 Park, J. *et al.* AF1q is a novel TCF7 co-factor which activates CD44 and promotes breast cancer metastasis. *Oncotarget* **6**, 20697-20710, doi:10.18632/oncotarget.4136 (2015).

260 Pecci, A., Ma, X., Savoia, A. & Adelstein, R. S. MYH9: Structure, functions and role of non-muscle myosin IIA in human disease. *Gene* **664**, 152-167, doi:10.1016/j.gene.2018.04.048 (2018).

261 Pennington, K. *et al.* Prominent synaptic and metabolic abnormalities revealed by proteomic analysis of the dorsolateral prefrontal cortex in schizophrenia and bipolar disorder. *Molecular psychiatry* **13**, 1102-1117, doi:10.1038/sj.mp.4002098 (2008).

262 Piroli, M. E., Blanchette, J. O. & Jabbarzadeh, E. Polarity as a physiological modulator of cell function. *Frontiers in bioscience (Landmark edition)* **24**, 451-462, doi:10.2741/4728 (2019).

263 Pirone, D. M., Oberst, M. D., Stylianou, D. & Burbelo, P. D. The genomic structure of the human SPEC1 gene reveals complex splicing and close promoter proximity to the AF1q translocation gene. *Gene* **273**, 295-303, doi:10.1016/s0378-1119(01)00561-3 (2001).

264 Poirier, K. *et al.* Large spectrum of lissencephaly and pachygyria phenotypes resulting from de novo missense mutations in tubulin alpha 1A (TUBA1A). *Human mutation* **28**, 1055-1064, doi:10.1002/humu.20572 (2007).

265 Poirier, K. *et al.* Mutations in TUBG1, DYNC1H1, KIF5C and KIF2A cause malformations of cortical development and microcephaly. *Nature genetics* **45**, 639-647, doi:10.1038/ng.2613 (2013).

266 Poirier, K. *et al.* Mutations in the neuronal ß-tubulin subunit TUBB3 result in malformation of cortical development and neuronal migration defects. *Human molecular genetics* **19**, 4462-4473, doi:10.1093/hmg/ddq377 (2010).

267 Pollak, R. M. *et al.* Neuropsychiatric phenotypes and a distinct constellation of ASD features in 3q29 deletion syndrome: results from the 3q29 registry. *Molecular Autism* **10**, 30-30, doi:10.1186/s13229-019-0281-5 (2019).

268 Pollard, T. D. Actin and Actin-Binding Proteins. *Cold Spring Harbor perspectives in biology* **8**, doi:10.1101/cshperspect.a018226 (2016).

269 Purro, S. A. *et al.* Wnt regulates axon behavior through changes in microtubule growth directionality: a new role for adenomatous polyposis coli. *The Journal of neuroscience : the official journal of the Society for Neuroscience* **28**, 8644-8654, doi:10.1523/JNEUROSCI.2320-08.2008 (2008).

270 Quinlan, M. E., Heuser, J. E., Kerkhoff, E. & Mullins, R. D. Drosophila Spire is an actin nucleation factor. *Nature* **433**, 382-388, doi:10.1038/nature03241 (2005).

271 Radyushkin, K. *et al.* Neuroligin-3-deficient mice: model of a monogenic heritable form of autism with an olfactory deficit. *Genes, brain, and behavior* **8**, 416-425, doi:10.1111/j.1601-183X.2009.00487.x (2009).

272 Ramkumar, A., Jong, B. Y. & Ori-McKenney, K. M. ReMAPping the microtubule landscape: How phosphorylation dictates the activities of microtubule-associated proteins. *Developmental dynamics : an official publication of the American Association of Anatomists* **247**, 138-155, doi:10.1002/dvdy.24599 (2018).

273 Rangaraju, V., Lauterbach, M. & Schuman, E. M. Spatially Stable Mitochondrial Compartments Fuel Local Translation during Plasticity. *Cell* **176**, 73-84.e15, doi:10.1016/j.cell.2018.12.013 (2019).

274 Rauch, A. *et al.* Range of genetic mutations associated with severe non-syndromic sporadic intellectual disability: an exome sequencing study. *The Lancet* **380**, 1674-1682, doi:10.1016/S0140-6736(12)61480-9 (2012).

275 Reeves, R. & Beckerbauer, L. HMGI/Y proteins: flexible regulators of transcription and chromatin structure. *Biochimica et biophysica acta* **1519**, 13-29, doi:10.1016/s0167-4781(01)00215-9 (2001).

276 Rex, C. S. *et al.* Myosin IIb Regulates Actin Dynamics during Synaptic Plasticity and Memory Formation. *Neuron* **67**, 603-617, doi:10.1016/j.neuron.2010.07.016 (2010).

277 Rodan, L. H. *et al.* De Novo TUBB2A Variant Presenting With Anterior Temporal Pachygyria. *Journal of child neurology* **32**, 127-131, doi:10.1177/0883073816672998 (2017).

278 Rodríguez-Tornos, F. M. *et al.* Cux1 Enables Interhemispheric Connections of Layer II/III Neurons by Regulating Kv1-Dependent Firing. *Neuron* **89**, 494-506, doi:10.1016/j.neuron.2015.12.020 (2016).

279 Rogers, S. L. & Gelfand, V. I. Myosin cooperates with microtubule motors during organelle transport in melanophores. *Current biology : CB* **8**, 161-164, doi:10.1016/s0960-9822(98)70063-6 (1998).

280 Rogers, S. L. *et al.* Regulation of melanosome movement in the cell cycle by reversible association with myosin V. *The Journal of cell biology* **146**, 1265-1276, doi:10.1083/jcb.146.6.1265 (1999).

281 Ropars, V. *et al.* The myosin X motor is optimized for movement on actin bundles. *Nature Communications* **7**, 12456-12456, doi:10.1038/ncomms12456 (2016).

282 Rosahl, T. W. *et al.* Short-term synaptic plasticity is altered in mice lacking synapsin I. *Cell* **75**, 661-670, doi:10.1016/0092-8674(93)90487-b (1993).

283 Russell, G., Steer, C. & Golding, J. Social and demographic factors that influence the diagnosis of autistic spectrum disorders. *Social psychiatry and psychiatric epidemiology* **46**, 1283-1293, doi:10.1007/s00127-010-0294-z (2011).

284 Ryan, B. C., Young, N. B., Crawley, J. N., Bodfish, J. W. & Moy, S. S. Social deficits, stereotypy and early emergence of repetitive behavior in the C58/J inbred mouse strain. *Behavioural brain research* **208**, 178-188, doi:10.1016/j.bbr.2009.11.031 (2010).

285 Ryan, B. C., Young, N. B., Moy, S. S. & Crawley, J. N. Olfactory cues are sufficient to elicit social approach behaviors but not social transmission of food preference in C57BL/6J mice. *Behavioural brain research* **193**, 235-242, doi:10.1016/j.bbr.2008.06.002 (2008).

286 Rylaarsdam, L. & Guemez-Gamboa, A. Genetic Causes and Modifiers of Autism Spectrum Disorder. *Frontiers in cellular neuroscience* **13**, 385-385, doi:10.3389/fncel.2019.00385 (2019).

287 Sabo, S. L., Gomes, R. A. & McAllister, A. K. Formation of Presynaptic Terminals at Predefined Sites along Axons. *The Journal of Neuroscience* **26**, 10813-10825, doi:10.1523/JNEUROSCI.2052-06.2006 (2006).

288 Sadakata, T. *et al.* Autistic-like phenotypes in Cadps2-knockout mice and aberrant CADPS2 splicing in autistic patients. *The Journal of clinical investigation* **117**, 931-943, doi:10.1172/JCI29031 (2007).

289 Sahu, M. P., Nikkilä, O., Lågas, S., Kolehmainen, S. & Castrén, E. Culturing primary neurons from rat hippocampus and cortex. *Neuronal signaling* **3**, NS20180207-NS20180207, doi:10.1042/NS20180207 (2019).

290 Sainath, R. & Gallo, G. Cytoskeletal and signaling mechanisms of neurite formation. *Cell and Tissue Research* **359**, 267-278, doi:10.1007/s00441-014-1955-0 (2015).

291 Saito, T. In vivo electroporation in the embryonic mouse central nervous system. *Nature Protocols* **1**, 1552-1558, doi:10.1038/nprot.2006.276 (2006).

292 Sakakibara, A. *et al.* Dynamics of centrosome translocation and microtubule organization in neocortical neurons during distinct modes of polarization. *Cerebral cortex (New York, N.Y. : 1991)* **24**, 1301-1310, doi:10.1093/cercor/bhs411 (2014).

293 Sanders, Stephan J. *et al.* Multiple Recurrent De Novo CNVs, Including Duplications of the 7q11.23 Williams Syndrome Region, Are Strongly Associated with Autism. *Neuron* **70**, 863-885, doi:10.1016/j.neuron.2011.05.002 (2011).

294 Saxton, R. A. & Sabatini, D. M. mTOR Signaling in Growth, Metabolism, and Disease. *Cell* **168**, 960-976, doi:10.1016/j.cell.2017.02.004 (2017).

295 Sayyad, W. A., Amin, L., Fabris, P., Ercolini, E. & Torre, V. The role of myosin-II in force generation of DRG filopodia and lamellipodia. *Scientific reports* **5**, 7842-7842, doi:10.1038/srep07842 (2015).

296 Scala, F. *et al.* Layer 4 of mouse neocortex differs in cell types and circuit organization between sensory areas. *Nature communications* **10**, 4174-4174, doi:10.1038/s41467-019-12058-z (2019).

297 Scardigli, R., Bäumer, N., Gruss, P., Guillemot, F. & Le Roux, I. Direct and concentration-dependent regulation of the proneural gene Neurogenin2 by

Pax6. *Development (Cambridge, England)* **130**, 3269-3281, doi:10.1242/dev.00539 (2003).

298 Schaar, B. T. & McConnell, S. K. Cytoskeletal coordination during neuronal migration. *Proceedings of the National Academy of Sciences of the United States of America* **102**, 13652-13657, doi:10.1073/pnas.0506008102 (2005).

299 Schindelin, J. *et al.* Fiji: an open-source platform for biological-image analysis. *Nature methods* **9**, 676-682, doi:10.1038/nmeth.2019 (2012).

300 Schmidt, L. *et al.* Expanding the Phenotype of TUBB2A -Related Tubulinopathy: Three Cases of a Novel, Heterozygous TUBB2A Pathogenic Variant p.Gly98Arg. *Molecular Syndromology* **12**, 33-40, doi:10.1159/000512160 (2021).

301 Scholzen, T. & Gerdes, J. The Ki-67 protein: from the known and the unknown. *Journal of cellular physiology* **182**, 311-322, doi:10.1002/(SICI)1097-4652(200003)182:3<311::AID-JCP1>3.0.CO;2-9 (2000).

302 Schumann, C. M. & Amaral, D. G. Stereological Analysis of Amygdala Neuron Number in Autism. *The Journal of Neuroscience* **26**, 7674-7679, doi:10.1523/JNEUROSCI.1285-06.2006 (2006).

303 Semenova, I. *et al.* Regulation of microtubule-based transport by MAP4. *Molecular biology of the cell* **25**, 3119-3132, doi:10.1091/mbc.E14-01-0022 (2014).

304 Sept, D. & McCammon, J. A. Thermodynamics and kinetics of actin filament nucleation. *Biophysical journal* **81**, 667-674, doi:10.1016/S0006-3495(01)75731-1 (2001).

305 Shafrir, Y., ben-Avraham, D. & Forgacs, G. Trafficking and signaling through the cytoskeleton: a specific mechanism. *Journal of cell science* **113 (Pt 15)**, 2747-2757, doi:10.1242/jcs.113.15.2747 (2000).

306 Shen, L. *et al.* Cortical thickness abnormalities in autism spectrum disorder. *European child & adolescent psychiatry*, doi:10.1007/s00787-022-02133-0 (2022).

307 Silverman, J. L., Yang, M., Lord, C. & Crawley, J. N. Behavioural phenotyping assays for mouse models of autism. *Nature reviews. Neuroscience* **11**, 490-502, doi:10.1038/nrn2851 (2010).

308 Sivagnanasundaram, S., Crossett, B., Dedova, I., Cordwell, S. & Matsumoto, I. Abnormal pathways in the genu of the corpus callosum in schizophrenia pathogenesis: a proteome study. *Proteomics. Clinical applications* **1**, 1291-1305, doi:10.1002/prca.200700230 (2007).

309 Skotheim, R. I. *et al.* Novel genomic aberrations in testicular germ cell tumors by array-CGH, and associated gene expression changes. *Cellular oncology : the official journal of the International Society for Cellular Oncology* **28**, 315-326, doi:10.1155/2006/219786 (2006).

310 Smit-Rigter, L. *et al.* Mitochondrial Dynamics in Visual Cortex Are Limited In Vivo and Not Affected by Axonal Structural Plasticity. *Current biology : CB* **26**, 2609-2616, doi:10.1016/j.cub.2016.07.033 (2016).

311 So, C. W. *et al.* Analysis of MLL-derived transcripts in infant acute monocytic leukemia with a complex translocation (1;11;4)(q21;q23;p16). *Cancer genetics and cytogenetics* **117**, 24-27, doi:10.1016/s0165-4608(99)00136-3 (2000).

312 Song, Y. *et al.* Transglutaminase and polyamination of tubulin: posttranslational modification for stabilizing axonal microtubules. *Neuron* **78**, 109-123, doi:10.1016/j.neuron.2013.01.036 (2013).

313 Stanton-Turcotte, D. *et al.* Mllt11 Regulates Migration and Neurite Outgrowth of Cortical Projection Neurons during Development. *The Journal of Neuroscience* **42**, 3931-3948, doi:10.1523/JNEUROSCI.0124-22.2022 (2022).

314 Stoner, R. *et al.* Patches of disorganization in the neocortex of children with autism. *The New England journal of medicine* **370**, 1209-1219, doi:10.1056/NEJMoa1307491 (2014).

315 Stoykova, A., Fritsch, R., Walther, C. & Gruss, P. Forebrain patterning defects in Small eye mutant mice. *Development (Cambridge, England)* **122**, 3453-3465, doi:10.1242/dev.122.11.3453 (1996).

316 Stoykova, A., Götz, M., Gruss, P. & Price, J. Pax6-dependent regulation of adhesive patterning, R-cadherin expression and boundary formation in developing forebrain. *Development (Cambridge, England)* **124**, 3765-3777, doi:10.1242/dev.124.19.3765 (1997).

317 Strunk, C. J. *et al.* Elevated AF1q expression is a poor prognostic marker for adult acute myeloid leukemia patients with normal cytogenetics. *American journal of hematology* **84**, 308-309, doi:10.1002/ajh.21396 (2009).

318 Südhof, T. C. Neuroligins and neurexins link synaptic function to cognitive disease. *Nature* **455**, 903-911, doi:10.1038/nature07456 (2008).

319 Sudo, H. & Baas, P. W. Acetylation of microtubules influences their sensitivity to severing by katanin in neurons and fibroblasts. *The Journal of neuroscience : the official journal of the Society for Neuroscience* **30**, 7215-7226, doi:10.1523/JNEUROSCI.0048-10.2010 (2010).

320 Surguchev, A. P., Grigor'iants, R. A. & Urakov, V. N. [Natriuretic factor--a hormone produced by the atrium]. *Terapevticheskii arkhiv* **59**, 142-144 (1987).

321 Sylvén, C., Jansson, E., Cederholm, T., Hildebrand, I. L. & Beermann, B. Skeletal muscle depressed calcium and phosphofructokinase in chronic heart failure are upregulated by captopril--a double-blind, placebo-controlled study. *Journal of internal medicine* **229**, 171-174, doi:10.1111/j.1365-2796.1991.tb00326.x (1991).

322 Tabuchi, K. *et al.* A neuroligin-3 mutation implicated in autism increases inhibitory synaptic transmission in mice. *Science (New York, N.Y.)* **318**, 71-76, doi:10.1126/science.1146221 (2007).

323 Tammimies, K. *et al.* Association between Copy Number Variation and Response to Social Skills Training in Autism Spectrum Disorder. *Scientific Reports* **9**, 9810-9810, doi:10.1038/s41598-019-46396-1 (2019).

324 Taverna, E., Götz, M. & Huttner, W. B. The cell biology of neurogenesis: toward an understanding of the development and evolution of the neocortex. *Annual review of cell and developmental biology* **30**, 465-502, doi:10.1146/annurev-cellbio-101011-155801 (2014).

325 Thakurela, S. *et al.* Mapping gene regulatory circuitry of Pax6 during neurogenesis. *Cell discovery* **2**, 15045-15045, doi:10.1038/celldisc.2015.45 (2016).

326 Thomas, S. D., Jha, N. K., Ojha, S. & Sadek, B. mTOR Signaling Disruption and Its Association with the Development of Autism Spectrum Disorder. *Molecules (Basel, Switzerland)* **28**, doi:10.3390/molecules28041889 (2023).

327 Thomson, A. M. Neocortical layer 6, a review. *Frontiers in neuroanatomy* **4**, 13-13, doi:10.3389/fnana.2010.00013 (2010).

328 Tian, G. *et al.* Disease-associated mutations in TUBA1A result in a spectrum of defects in the tubulin folding and heterodimer assembly pathway. *Human molecular genetics* **19**, 3599-3613, doi:10.1093/hmg/ddq276 (2010).

329 Tiberio, P., Cavadini, E., Callari, M., Daidone, M. G. & Appierto, V. AF1q: a novel mediator of basal and 4-HPR-induced apoptosis in ovarian cancer cells. *PloS one* **7**, e39968-e39968, doi:10.1371/journal.pone.0039968 (2012).

330 Tiberio, P. *et al.* Involvement of AF1q/MLLT11 in the progression of ovarian cancer. *Oncotarget* **8**, 23246-23264, doi:10.18632/oncotarget.15574 (2017).

331 Tischfield, M. A. *et al.* Human TUBB3 mutations perturb microtubule dynamics, kinesin interactions, and axon guidance. *Cell* **140**, 74-87, doi:10.1016/j.cell.2009.12.011 (2010).

332 Toma, K., Kumamoto, T. & Hanashima, C. The timing of upper-layer neurogenesis is conferred by sequential derepression and negative feedback from deep-layer neurons. *The Journal of neuroscience : the official journal of the Society for Neuroscience* **34**, 13259-13276, doi:10.1523/JNEUROSCI.2334-14.2014 (2014).

333 Tsai, J.-W., Bremner, K. H. & Vallee, R. B. Dual subcellular roles for LIS1 and dynein in radial neuronal migration in live brain tissue. *Nature neuroscience* **10**, 970-979, doi:10.1038/nn1934 (2007).

334 Tse, C. O., Kim, S. & Park, J. Activation of Wnt signaling pathway by AF1q enriches stem-like population and enhance mammosphere formation of breast cells. *Biochemical and biophysical research communications* **484**, 884-889, doi:10.1016/j.bbrc.2017.02.018 (2017).

335 Tse, W. *et al.* Increased AF1q gene expression in high-risk myelodysplastic syndrome. *British journal of haematology* **128**, 218-220, doi:10.1111/j.1365-2141.2004.05306.x (2005).

336 Tse, W. *et al.* Elevated expression of the AF1q gene, an MLL fusion partner, is an independent adverse prognostic factor in pediatric acute myeloid leukemia. *Blood* **104**, 3058-3063, doi:10.1182/blood-2003-12-4347 (2004).

337 Tse, W., Zhu, W., Chen, H. S. & Cohen, A. A novel gene, AF1q, fused to MLL in t(1;11) (q21;q23), is specifically expressed in leukemic and immature hematopoietic cells. *Blood* **85**, 650-656, doi:10.1182/blood.V85.3.650.bloodjournal853650 (1995).

338 Tse, W., Zhu, W., Chen, H. S. & Cohen, A. A novel gene, AF1q, fused to MLL in t(1;11) (q21;q23), is specifically expressed in leukemic and immature hematopoietic cells. *Blood* **85**, 650-656 (1995).

339 Tueting, P. *et al.* The phenotypic characteristics of heterozygous reeler mouse. *Neuroreport* **10**, 1329-1334, doi:10.1097/00001756-199904260-00032 (1999).

340 Umeshima, H., Hirano T., Kengaku M. Microtubule-based nuclear movement occurs independently of centrosome positioning in migrating neurons. *Proceedings of the National Academy of Sciences of the United States of America* **104**, 16182-16187, doi:10.1073/pnas.0708047104 (2007)

341 van Bokhoven, H. Genetic and Epigenetic Networks in Intellectual Disabilities. *Annual Review of Genetics* **45**, 81-104, doi:10.1146/annurev-genet-110410-132512 (2011).

342 van Niekerk, E. A. *et al.* Methods for culturing adult CNS neurons reveal a CNS conditioning effect. *Cell reports methods* **2**, 100255-100255, doi:10.1016/j.crmeth.2022.100255 (2022).

343 Vessey, J. P. & Karra, D. More than just synaptic building blocks: scaffolding proteins of the post-synaptic density regulate dendritic patterning. *Journal of neurochemistry* **102**, 324-332, doi:10.1111/j.1471-4159.2007.04662.x (2007).

344 Voelker, J. & Arzube, M. [A new lung fluke from the coastal range of ecuador: Paragonimus ecuadoriensis n.sp. (paragonimidae, trematoda) (author's transl)]. *Tropenmedizin und Parasitologie* **30**, 249-263 (1979).

345 Walters, B. B. & Matus, A. I. Proteins of the synaptic junction. *Biochemical Society transactions* **3**, 109-112, doi:10.1042/bst0030109 (1975).

346 Wang, K. *et al.* Common genetic variants on 5p14.1 associate with autism spectrum disorders. *Nature* **459**, 528-533, doi:10.1038/nature07999 (2009).

347 Wang, T. *et al.* Large-scale targeted sequencing identifies risk genes for neurodevelopmental disorders. *Nature Communications* **11**, 4932-4932, doi:10.1038/s41467-020-18723-y (2020).

348 Watanabe, N. *et al.* Cryptic insertion and translocation or nondividing leukemic cells disclosed by FISH analysis in infant acute leukemia with discrepant molecular and cytogenetic findings. *Leukemia* **17**, 876-882, doi:10.1038/sj.leu.2402900 (2003).

349 Weber, K. L., Sokac, A. M., Berg, J. S., Cheney, R. E. & Bement, W. M. A microtubule-binding myosin required for nuclear anchoring and spindle assembly. *Nature* **431**, 325-329, doi:10.1038/nature02834 (2004).

350 Weiler, S. *et al.* Functional and structural features of L2/3 pyramidal cells continuously covary with pial depth in mouse visual cortex. *Cerebral cortex (New York, N.Y. : 1991)* **33**, 3715-3733, doi:10.1093/cercor/bhac303 (2023).

351 Weng, L.-q. *et al.* Aliskiren ameliorates pressure overload-induced heart hypertrophy and fibrosis in mice. *Acta pharmacologica Sinica* **35**, 1005-1014, doi:10.1038/aps.2014.45 (2014).

352 Werling, D. M. & Geschwind, D. H. Sex differences in autism spectrum disorders. *Current Opinion in Neurology* **26**, 146-153, doi:10.1097/WCO.0b013e32835ee548 (2013).

353 Whitman, M. C. *et al.* Two unique TUBB3 mutations cause both CFEOM3 and malformations of cortical development. *American journal of medical genetics. Part A* **170A**, 297-305, doi:10.1002/ajmg.a.37362 (2016).

354 Wrenn, C. C. Social transmission of food preference in mice. *Current protocols in neuroscience* **Chapter 8**, Unit 8.5G-Unit 8.5G, doi:10.1002/0471142301.ns0805gs28 (2004).

355 Wrenn, C. C., Harris, A. P., Saavedra, M. C. & Crawley, J. N. Social transmission of food preference in mice: methodology and application to galanin-overexpressing transgenic mice. *Behavioral neuroscience* **117**, 21-31 (2003).

356 Xi, F. *et al.* Calcium/calmodulin-dependent protein kinase II regulates mammalian axon growth by affecting F-actin length in growth cone. *Journal of cellular physiology* **234**, 23053-23065, doi:10.1002/jcp.28867 (2019).

357 Xu, Q. *et al.* Chromosomal microarray analysis in clinical evaluation of neurodevelopmental disorders-reporting a novel deletion of SETDB1 and illustration of counseling challenge. *Pediatric research* **80**, 371-381, doi:10.1038/pr.2016.101 (2016).

358 Yamada, K. M., Spooner, B. S. & Wessells, N. K. Axon growth: roles of microfilaments and microtubules. *Proceedings of the National Academy of Sciences of the United States of America* **66**, 1206-1212, doi:10.1073/pnas.66.4.1206 (1970).

359 Yamada, K. M., Spooner, B. S. & Wessells, N. K. Ultrastructure and function of growth cones and axons of cultured nerve cells. *The Journal of cell biology* **49**, 614-635, doi:10.1083/jcb.49.3.614 (1971).

360 Yamada, M., Clark, J. & Iulianella, A. MLLT11/AF1q is differentially expressed in maturing neurons during development. *Gene expression patterns : GEP* **15**, 80-87, doi:10.1016/j.gep.2014.05.001 (2014).

361 Yamada, M. *et al.* Cux2 activity defines a subpopulation of perinatal neurogenic progenitors in the hippocampus. *Hippocampus* **25**, 253-267, doi:10.1002/hipo.22370 (2015).

362 Yang, D. Y. J., Beam, D., Pelphrey, K. A., Abdullahi, S. & Jou, R. J. Cortical morphological markers in children with autism: a structural magnetic resonance imaging study of thickness, area, volume, and gyrification. *Molecular autism* **7**, 11-11, doi:10.1186/s13229-016-0076-x (2016).

363 Yang, L., Chen, L., Cai, C. & Li, H. Differential gene regulatory plasticity between upper and lower layer cortical excitatory neurons. *Molecular and cellular neurosciences* **90**, 22-32, doi:10.1016/j.mcn.2018.05.007 (2018).

364 Yang, M., Clarke, A. M. & Crawley, J. N. Postnatal lesion evidence against a primary role for the corpus callosum in mouse sociability. *The European journal of neuroscience* **29**, 1663-1677, doi:10.1111/j.1460-9568.2009.06714.x (2009).

365 Yang, M. & Crawley, J. N. Simple behavioral assessment of mouse olfaction. *Current protocols in neuroscience* **Chapter 8**, Unit 8.24-Unit 28.24, doi:10.1002/0471142301.ns0824s48 (2009).

366 Yang, M. *et al.* Social approach behaviors are similar on conventional versus reverse lighting cycles, and in replications across cohorts, in BTBR T+ tf/J, C57BL/6J, and vasopressin receptor 1B mutant mice. *Frontiers in behavioral neuroscience* **1**, 1-1, doi:10.3389/neuro.08.001.2007 (2007).

367 Yang, M., Zhodzishsky, V. & Crawley, J. N. Social deficits in BTBR T+tf/J mice are unchanged by cross-fostering with C57BL/6J mothers. *International journal of developmental neuroscience : the official journal of the International Society for Developmental Neuroscience* **25**, 515-521, doi:10.1016/j.ijdevneu.2007.09.008 (2007).

368 Yao, F. *et al.* Protein Biomarkers of Autism Spectrum Disorder Identified by Computational and Experimental Methods. *Frontiers in psychiatry* **12**, 554621-554621, doi:10.3389/fpsyt.2021.554621 (2021).

369 Yoshii, A., Zhao, J.-P., Pandian, S., van Zundert, B. & Constantine-Paton, M. A Myosin Va Mutant Mouse with Disruptions in Glutamate Synaptic Development and Mature Plasticity in Visual Cortex. *The Journal of Neuroscience* **33**, 8472-8482, doi:10.1523/JNEUROSCI.4585-12.2013 (2013).

370 Yoshimura, A. *et al.* Myosin-Va Facilitates the Accumulation of mRNA/Protein Complex in Dendritic Spines. *Current Biology* **16**, 2345-2351, doi:10.1016/j.cub.2006.10.024 (2006).

371 Yu, H. *et al.* Myo10 is required for neurogenic cell adhesion and migration. *In Vitro Cellular & Developmental Biology - Animal* **51**, 400-407, doi:10.1007/s11626-014-9845-z (2015).

372 Yu, H. *et al.* PtdIns (3,4,5) P3 Recruitment of Myo10 Is Essential for Axon Development. *PLoS ONE* **7**, e36988-e36988, doi:10.1371/journal.pone.0036988 (2012).

373 Yuan, A., Rao, M. V., Veeranna & Nixon, R. A. Neurofilaments at a glance. *Journal of cell science* **125**, 3257-3263, doi:10.1242/jcs.104729 (2012).

374 Yuba-Kubo, A., Kubo, A., Hata, M. & Tsukita, S. Gene knockout analysis of two gamma-tubulin isoforms in mice. *Developmental biology* **282**, 361-373, doi:10.1016/j.ydbio.2005.03.031 (2005).

375 Yuzwa, S. A. *et al.* Proneurogenic Ligands Defined by Modeling Developing Cortex Growth Factor Communication Networks. *Neuron* **91**, 988-1004, doi:10.1016/j.neuron.2016.07.037 (2016).

376 Zaboski, B. A. & Storch, E. A. Comorbid autism spectrum disorder and anxiety disorders: a brief review. *Future neurology* **13**, 31-37, doi:10.2217/fnl-2017-0030 (2018).

377 Zahr, S. K., Kaplan, D. R. & Miller, F. D. Translating neural stem cells to neurons in the mammalian brain. *Cell Death & Differentiation* **26**, 2495-2512, doi:10.1038/s41418-019-0411-9 (2019).

378 Zhang, H., Webb, D. J., Asmussen, H., Niu, S. & Horwitz, A. F. A GIT1/PIX/Rac/PAK Signaling Module Regulates Spine Morphogenesis and Synapse Formation through MLC. *The Journal of Neuroscience* **25**, 3379-3388, doi:10.1523/JNEUROSCI.3553-04.2005 (2005).

379 Zhang, S., Xiong, X. & Sun, Y. Functional characterization of SOX2 as an anticancer target. *Signal transduction and targeted therapy* **5**, 135-135, doi:10.1038/s41392-020-00242-3 (2020).

380 Zhao, Y. *et al.* Distinct molecular pathways for development of telencephalic interneuron subtypes revealed through analysis of Lhx6 mutants. *The Journal of comparative neurology* **510**, 79-99, doi:10.1002/cne.21772 (2008).

381 Zhou, F.-Q., Zhou, J., Dedhar, S., Wu, Y.-H. & Snider, W. D. NGF-induced axon growth is mediated by localized inactivation of GSK-3beta and functions of the microtubule plus end binding protein APC. *Neuron* **42**, 897-912, doi:10.1016/j.neuron.2004.05.011 (2004).

382 Zimmer, C., Tiveron, M.-C., Bodmer, R. & Cremer, H. Dynamics of Cux2 expression suggests that an early pool of SVZ precursors is fated to become upper cortical layer neurons. *Cerebral cortex (New York, N.Y. : 1991)* **14**, 1408-1420, doi:10.1093/cercor/bhh102 (2004).

APPENDIX A: Statistics

Figure	Analysis	n	P
2.2. B	Fold change of Mllt11 cDNA	4 ctrl, 3 cKO	0.0093
2.3. A	Body weight	8	>0.05
2.3. B	Brain weight	8	>0.05
2.3. C	Brain weight as % of body weight	8	>0.05
2.3. E	Distribution, total cells, cortical thickness E14.5	5	>0.05
2.3. F	Distribution, total cells, cortical thickness E16.5	7, 7, 5	<0.0001
2.3. G	Distribution, total cells, cortical thickness E18.5	5, 5, 4	0.0038, 0.0046, 0.0323, 0.0198, 0.0492, <0.0001
2.4. A	% Pax6 total cells E14.5	4	>0.05
2.4. B	% Pax6 total cells E16.5	4	>0.05
2.4. C	% Pax6 total cells E18.5	4	>0.05
2.4. D	% Sox2 total cells E14.5	3	0.0469
2.4. E	% Sox2 total cells E16.5	3	>0.05
2.4. F	% Sox2 total cells E18.5	4	>0.05
2.4. G	% Tbr2 total cells E14.5	4	>0.05
2.4. H	% Tbr2 total cells E16.5	4	>0.05
2.4. I	% Tbr2 total cells E18.5	4	0.0115, 0.0014, 0.0006,
2.5. A	% Ki67 total cells E14.5	4	>0.05
2.5. B	% Ki67 total cells E18.5	4	>0.05
2.5. C	Total EdU+ cells E14.5	4	>0.05
2.5. D	Total EdU+ cells E18.5	3	>0.05
2.5. E	Total CC3+ cells E14.5	3 ctrl, 5 cKO	>0.05
2.5. F	Total CC3+ cells E18.5	3 ctrl, 5 cKO	>0.05
2.6. A	% Satb2 total cells E14.5	4	>0.05
2.6. B	% Satb2 total cells E16.5	4	>0.05
2.6. C	% Satb2 total cells E18.5	4	0.0312, 0.0303, 0.0002, 0.0023, 0.0467

Figure	Analysis	n	P
2.6. D	% CDP total cells E14.5	5	>0.05
2.6. E	% CDP total cells E16.5	4	>0.05
2.6. F	% CDP total cells E18.5	5	0.0252, 0.0359, 0.0358, 0.0179,
2.6. G	Total tomato+ cells E14.5	5 ctrl, 6 cKO	>0.05
2.6. H	Total tomato+ cells E16.5	5	0.019
2.6. I	Total tomato+ cells E18.5	5	0.0344, <0.0001, <0.0001, 0.069, <0.0001, <0.0001
2.6. J	% Tbr1 total cells E14.5	4	>0.05
2.6. K	% Tbr1 total cells E16.5	4 ctrl, 5 cKO	>0.05
2.6. L	% Tbr1 total cells E18.5	4	0.0048
2.6. M	% Ctip2 total cells E14.5	4	0.0002, 0.0174
2.6. N	% Ctip2 total cells E16.5	4	0.0484, 0.0019, 0.0001
2.6. O	% Ctip2 total cells E18.5	4	>0.05
2.7. A	EdU+/Ctip2+ colabeled cells E14->E18.5	4	0.0278, 0.0104, 0.0173,
2.7. B	EdU+/Ctip2+ colabeled cells E16->E18.5	4	0.0146, 0.0261, 0.0349
2.7. C	EdU+/CDP+ colabeled cells E14->E18.5	4	0.0004, <0.0001, <0.0001, <0.0001
2.7. D	EdU+/CDP+ colabeled cells E16->E18.5	4	0.0077, 0.0001, 0.0008, <0.0001, <0.0001
2.7. E	% NeuN total cells E16.5	3	0.0023, 0.0345
2.7. F	% NeuN total cells E18.5	3	0.0315, 0.0002, <0.0001
2.8. A	Total EdU cells E14->E18.5	4	0.0027, 0.035, 0.0018, <0.0001, 0.0234, <0.0001, 0.0476
2.8. B	Total EdU cells E16-> E18.5	3	0.0063, 0.0011, 0.049, 0.0024,
2.8. F	Localization of GFP+ cells	3	0.0469, 0.0293
2.9. C	Nestin representative angle E14.5	4	>0.05
2.9. D	Nestin area E14.5	4	>0.05
2.9. E	Nestin dispersion E14.5	4	>0.05
2.9. H	Nestin representative angle E16.5	5	>0.05
2.9. I	Nestin area E16.5	5	>0.05
2.9. J	Nestin dispersion E16.5	5	>0.05
2.9. M	Nestin representative angle E18.5	3	>0.05

Figure	Analysis	n	P
2.9. N	Nestin area E18.5	3	>0.05
2.9. O	Nestin dispersion E18.5	3	>0.05
2.9. Q	P73+/Reelin+ cells E14.5	4	>0.05
2.9. S	P73+/Reelin+ cells E18.5	3	>0.05
3.2. B	Primary neurite length 24 HPP	3 individuals, 50 neurons/individual	0.0003
3.2. C	Total neurite length 24 HPP	3 individuals, 50 neurons/individual	<0.0001
3.2. D	Primary neurite length/total neurite length 24 HPP	3 individuals, 50 neurons/individual	<0.0001
3.2. F	Total neurites	3 individuals, 50 neurons/individual	<0.0001
3.2. G	Total neurite length 7 DPP	3 individuals, 50 neurons/individual	<0.0001
3.2. H	Sholl analysis 7 DPP	3 individuals, 50 neurons/individual	<0.0001
3.3. B	Total neurite length UL2/3	3 individuals, 30 neurons/individual	0.0101
3.3. C	Sholl analysis UL2/3	3 individuals, 30 neurons/individual	<0.0001
3.4. B	WM thickness E16.5	5	<0.0001
3.4. C	WM thickness E16.5 as % of cortical thickness	5	<0.0001
3.4. D	Cortical thickness - WM thickness E16.5	5	0.0332
3.4. F	WM thickness E18.5	4	<0.0001
3.4. G	WM thickness E18.5 as % of cortical thickness	4	>0.05
3.4. H	Cortical thickness - WM thickness E18.5	4	0.0332
3.5. C	PSD5/Synapsin I colocalization	2 individuals, 12-15 images/individual	0.04
3.5. D	PSD5/Synapsin I colocalization normalized to surface area	2 individuals, 12-15 images/individual	>0.05
3.5. E	cells/image	2 individuals, 12-15 images/individual	0.0036
3.5. F	PSD95/Synapsin I colocalization normalized to surface area/cell	2 individuals, 12-15 images/individual	>0.05
4.2. A	Male weight	Flox/+=15, Flox/+;Cre=20, cKO=17	0.0021, 0.0046, 0.0164, 0.0267
4.2. B	Female weight	Flox/+=13, Flox/+;Cre=17, cKO=14	0.0229, 0.0305

Figure	Analysis	n	P
4.3. A	Male olfactory habituation	Flox/+=11, Flox/+;Cre=11, cKO=11	>0.05
4.3. B	Female olfactory habituation	Flox/+=10, Flox/+;Cre=13, cKO=10	0.0299
4.3. C	Male olfactory dishabituation	Flox/+=11, Flox/+;Cre=11, cKO=11	>0.05
4.3. D	Female olfactory dishabituation	Flox/+=10, Flox/+;Cre=13, cKO=10	>0.05
4.4. A	Male water sniffing	Flox/+=11, Flox/+;Cre=11, cKO=11	0.0135
4.4. B	Female water sniffing	Flox/+=10, Flox/+;Cre=13, cKO=10	0.0313, 0.0064
4.4. C	Male water cumulative	Flox/+=11, Flox/+;Cre=11, cKO=11	0.0274
4.4. D	Female water cumulative	Flox/+=10, Flox/+;Cre=13, cKO=10	0.024
4.4. E	Male lemon sniffing	Flox/+=11, Flox/+;Cre=11, cKO=11	>0.05
4.4. F	Female lemon sniffing	Flox/+=10, Flox/+;Cre=13, cKO=10	>0.05
4.4. G	Male lemon cumulative	Flox/+=11, Flox/+;Cre=11, cKO=11	>0.05
4.4. H	Female lemon cumulative	Flox/+=10, Flox/+;Cre=13, cKO=10	>0.05
4.4. I	Male vanilla sniffing	Flox/+=11, Flox/+;Cre=11, cKO=11	0.0335
4.4. J	Female vanilla sniffing	Flox/+=10, Flox/+;Cre=13, cKO=10	>0.05
4.4. K	Male vanilla cumulative	Flox/+=11, Flox/+;Cre=11, cKO=11	>0.05
4.4. L	Female vanilla cumulative	Flox/+=10, Flox/+;Cre=13, cKO=10	>0.05
4.5. A	Male nonsocial odor 1	Flox/+=11, Flox/+;Cre=11, cKO=11	>0.05
4.5. B	Female nonsocial odor 1	Flox/+=10, Flox/+;Cre=13, cKO=10	>0.05
4.5. C	Male nonsocial odor 1 cumulative	Flox/+=11, Flox/+;Cre=11, cKO=11	>0.05
4.5. D	Female nonsocial odor 1 cumulative	Flox/+=10, Flox/+;Cre=13, cKO=10	>0.05
4.5. E	Male nonsocial odor 2	Flox/+=11, Flox/+;Cre=11, cKO=11	>0.05
4.5. F	Female nonsocial odor 2	Flox/+=10, Flox/+;Cre=13, cKO=10	>0.05

Figure	Analysis	n	P
4.5. G	Male nonsocial odor 2 cumulative	Flox/+=11, Flox/+;Cre=11, cKO=11	>0.05
4.5. H	Female nonsocial odor 2 cumulative	Flox/+=10, Flox/+;Cre=13, cKO=10	>0.05
4.6. A	Male social male odor	Flox/+=11, Flox/+;Cre=11, cKO=11	>0.05
4.6. B	Female social male odor	Flox/+=10, Flox/+;Cre=13, cKO=10	>0.05
4.6. C	Male social male odor cumulative	Flox/+=11, Flox/+;Cre=11, cKO=11	>0.05
4.6. D	Female social male odor cumulative	Flox/+=10, Flox/+;Cre=13, cKO=10	>0.05
4.6. E	Male social female odor	Flox/+=11, Flox/+;Cre=11, cKO=11	>0.05
4.6. F	Female social female odor	Flox/+=10, Flox/+;Cre=13, cKO=10	0.0073
4.6. G	Male social female odor cumulative	Flox/+=11, Flox/+;Cre=11, cKO=11	>0.05
4.6. H	Female social female odor cumulative	Flox/+=10, Flox/+;Cre=13, cKO=10	0.0261
4.7. A	Male social odor 1	Flox/+=11, Flox/+;Cre=11, cKO=11	>0.05
4.7. B	Female social odor 1	Flox/+=10, Flox/+;Cre=13, cKO=10	0.0009, 0.021, 0.0049
4.7. C	Male social odor 1 cumulative	Flox/+=11, Flox/+;Cre=11, cKO=11	>0.05
4.7. D	Female social odor 1 cumulative	Flox/+=10, Flox/+;Cre=13, cKO=10	0.0103
4.7. E	Male social odor 2	Flox/+=11, Flox/+;Cre=11, cKO=11	>0.05
4.7. F	Female social odor 2	Flox/+=10, Flox/+;Cre=13, cKO=10	>0.05
4.7. G	Male social odor 2 cumulative	Flox/+=11, Flox/+;Cre=11, cKO=11	>0.05
4.7. H	Female social odor 2 cumulative	Flox/+=10, Flox/+;Cre=13, cKO=10	>0.05
4.8. A	Male presentation order - scent nonspecific	Flox/+=11, Flox/+;Cre=11, cKO=11	>0.05
4.8. B	Female presentation order - scent nonspecific	Flox/+=10, Flox/+;Cre=13, cKO=10	0.0313, 0.0064, 0.0195. 0.0077, 0.0009, 0.0210, 0.0049
4.8. C	Male persentation order - scent nonspecific cumulative	Flox/+=11, Flox/+;Cre=11, cKO=11	>0.05
4.8. D	Female presentation order - scent nonspecific cumulative	Flox/+=10, Flox/+;Cre=13, cKO=10	0.0029, <0.0001, 0.0223

Figure	Analysis	n	P
4.8. E	Male presentation order - same vs. opposite sex	Flox/+=11, Flox/+;Cre=11, cKO=11	>0.05
4.8. F	Female presentation order - same vs. opposite sex	Flox/+=10, Flox/+;Cre=13, cKO=10	0.0313, 0.0064, 0.0195, 0.0077, 0.0073, 0.0084
4.8. G	Male presentation order - same vs. opposite sex cumulative	Flox/+=11, Flox/+;Cre=11, cKO=11	0.0024, 0.0136
4.8. H	Female presentation order - same vs. opposite sex cumulative	Flox/+=10, Flox/+;Cre=13, cKO=10	0.0029, <0.0001, 0.0223
4.8. I	Male scent-specific	Flox/+=11, Flox/+;Cre=11, cKO=11	>0.05
4.8. J	Female scent-specific	Flox/+=10, Flox/+;Cre=13, cKO=10	0.0313, 0.0064, 0.0084, 0.0073
4.8. K	Male scent-specific cumulative	Flox/+=11, Flox/+;Cre=11, cKO=11	>0.05
4.8. L	Female scent-specific cumulative	Flox/+=10, Flox/+;Cre=13, cKO=10	0.0410, 0.0011, 0.0143
4.9. A	Cumulative - nonsocial vs. social Flox/+ males	11	0.0008
4.9. B	Cumulative - nonsocial vs. social Flox/+;Cre males	11	0.0025
4.9. C	Cumulative - nonsocial vs. social cKO males	11	0.0018
4.9. D	Cumulative - nonsocial vs. social Flox/+ females	10	0.0057
4.9. E	Cumulative - nonsocial vs. social Flox/+;Cre females	13	<0.0001
4.9. F	Cumulative - nonsocial vs. social cKO females	10	0.0002
4.9. G	Nonsocial vs. social cumulative males	Flox/+=11, Flox/+;Cre=11, cKO=11	>0.05
4.9. H	Nonsocial vs. social cumulative females	Flox/+=10, Flox/+;Cre=13, cKO=10	0.035, 0.0004
4.10. A	Social approach - stranger 1 Flox/+ males	11	0.0103, 0.0004, <0.0001
4.10. B	Social approach - stranger 1 Flox/+;Cre males	11	<0.0001, <0.0001
4.10. C	Social approach - stranger 1 cKO males	11	0.001. <0.0001
4.10. D	Social approach - stranger 1 Flox/+ females	10	0.0001, 0.003, <0.0001
4.10. E	Social approach - stranger 1 Flox/+;Cre females	11	0.0002, <0.0001. 0.0001
4.10. F	Social approach - stranger 1 cKO females	10	0.0187, <0.0001, <0.0001

Figure	Analysis	n	P
4.10. G	Sociability index - empty vs. stranger 1 males	Flox/+=11, Flox/+;Cre=11, cKO=11	>0.05
4.10. H	Sociability index - empty vs. stranger 1 females	Flox/+=10, Flox/+;Cre=11, cKO=10	>0.05
4.11. A	Sniffing - stranger 1 males	Flox/+=11, Flox/+;Cre=11, cKO=11	>0.05
4.11. B	Sniffing - stranger 1 females	Flox/+=10, Flox/+;Cre=11, cKO=10	>0.05
4.11. C	Time investment ratio - stranger 1 males	Flox/+=11, Flox/+;Cre=11, cKO=11	>0.05
4.11. D	Time investment ratio - stranger 1 females	Flox/+=10, Flox/+;Cre=11, cKO=10	>0.05
4.12. A	Social approach - stranger 1 vs. stranger 2 Flox/+ males	11	0.02, 0.0004
4.12. B	Social approach - stranger 1 vs. stranger 2 Flox/+;Cre males	11	0.0076, 0.0001, <0.0001
4.12. C	Social approach - stranger 1 vs. stranger 2 cKO males	11	0.0415, 0.0005
4.12. D	Social approach - stranger 1 vs. stranger 2 Flox/+ females	10	0.0002, <0.0001
4.12. E	Social approach - stranger 1 vs. stranger 2 Flox/+;Cre females	11	0.0102, 0.0003
4.12. F	Social approach - stranger 1 vs. stranger 2 cKO females	10	0.0011, 0.0001
4.13. A	Sniffing - stranger 1 vs. stranger 2 Flox/+ males	11	>0.05
4.13. B	Sniffing - stranger 1 vs. stranger 2 Flox/+;Cre males	11	0.0231
4.13. C	Sniffing - stranger 1 vs. stranger 2 cKO males	11	0.0159
4.13. D	Sniffing - stranger 1 vs. stranger 2 Flox/+ females	10	>0.05
4.13. E	Sniffing - stranger 1 vs. stranger 2 Flox/+;Cre females	11	>0.05
4.13. F	Sniffing - stranger 1 vs. stranger 2 cKO females	10	>0.05
4.14. A	Time investment ratio - stranger 1 vs. stranger 2 Flox/+ males	11	>0.05
4.14. B	Time investment ratio - stranger 1 vs. stranger 2 Flox/+;Cre males	11	>0.05
4.14. C	Time investment ratio - stranger 1 vs. stranger 2 cKO males	10	>0.05
4.14. D	Time investment ratio - stranger 1 vs. stranger 2 Flox/+ females	10	>0.05

Figure	Analysis	n	P
4.14. E	Time investment ratio - stranger 1 vs. stranger 2 Flox/+;Cre females	11	>0.05
4.14. F	Time investment ratio - stranger 1 vs. stranger 2 cKO females	10	>0.05
4.14. G	Social novelty index - stranger 1 vs stranger 2 males	Flox/+=11, Flox/+;Cre=11, cKO=11	>0.05
4.14. H	Social novelty index - stranger 1 vs stranger 2 females	Flox/+=10, Flox/+;Cre=11, cKO=10	>0.05
4.15. A	Cued vs. non-cued food consumption Flox/+ males	1	>0.05
4.15. B	Cued vs. non-cued food consumption Flox/+;Cre males	12	>0.05
4.15. C	Cued vs. non-cued food consumption cKO males	12	>0.05
4.15. D	Cued vs. non-cued food consumption Flox/+ females	3	>0.05
4.15. E	Cued vs. non-cued food consumption Flox/+;Cre females	10	0.0482
4.15. F	Cued vs. non-cued food consumption cKO females	9	>0.05
4.15. G	Social transmission index males	Flox/+=1, Flox/+;Cre=12, cKO=11	>0.05
4.15. H	Social transmission index females	Flox/+=3, Flox/+;Cre=10, cKO=9	>0.05
4.16. A	% shredded nestlet males	Flox/+=12, Flox/+;Cre=12, cKO=11	>0.05
4.16. B	% shredded nestlet females	Flox/+=10, Flox/+;Cre=14, cKO=10	0.0215, 0.0497
4.16. C	Buried marbles males	Flox/+=12, Flox/+;Cre=12, cKO=11	>0.05
4.16. D	Buried marbles females	Flox/+=10, Flox/+;Cre=14, cKO=10	>0.05
4.18. A	Sleeping males	Flox/+=11, Flox/+;Cre=11, cKO=11	>0.05
4.18. B	Sleeping females	Flox/+=10, Flox/+;Cre=13, cKO=10	>0.05
4.18. C	Digging males	Flox/+=11, Flox/+;Cre=11, cKO=11	>0.05
4.18. D	Digging females	Flox/+=10, Flox/+;Cre=13, cKO=10	>0.05
4.18. E	Jumps males	Flox/+=11, Flox/+;Cre=11, cKO=11	>0.05
4.18. F	Jumps females	Flox/+=10, Flox/+;Cre=13, cKO=10	>0.05

Figure	Analysis	n	P
4.18. G	Climbs males	Flox/+=11, Flox/+;Cre=11, cKO=11	>0.05
4.18. H	Climbs females	Flox/+=10, Flox/+;Cre=13, cKO=10	>0.05
4.18. I	Rearing males	Flox/+=11, Flox/+;Cre=11, cKO=11	>0.05
4.18. J	Rearing females	Flox/+=10, Flox/+;Cre=13, cKO=10	>0.05
4.18. K	Grooming males	Flox/+=11, Flox/+;Cre=11, cKO=11	>0.05
4.18. L	Grooming females	Flox/+=10, Flox/+;Cre=13, cKO=10	>0.05
4.19. A	Grooming - habituation males	Flox/+=10, Flox/+;Cre=11, cKO=11	>0.05
4.19. B	Grooming - habituation females	Flox/+=10, Flox/+;Cre=11, cKO=10	>0.05
4.19. C	Grooming - stranger 1 males	Flox/+=11, Flox/+;Cre=11, cKO=11	>0.05
4.19. D	Grooming - stranger 1 females	Flox/+=10, Flox/+;Cre=11, cKO=10	>0.05
4.19. E	Grooming - stranger 2 males	Flox/+=11, Flox/+;Cre=11, cKO=11	>0.05
4.19. F	Grooming - stranger 2 females	Flox/+=10, Flox/+;Cre=11, cKO=10	>0.05
4.20. A	Grooming Flox/+ males	10	0.0189
4.20. B	Grooming Flox/+;Cre males	11	0.0269
4.20. C	Grooming cKO males	11	0.0471
4.20. D	Grooming Flox/+ females	10	0.0026, 0.0005
4.20. E	Grooming Flox/+;Cre females	11	0.0158
4.20. F	Grooming cKO females	10	0.0391
4.20. G	Grooming - cumulative males	Flox/+=10, Flox/+;Cre=11, cKO=11	>0.05
4.20. H	Grooming - cumulative females	Flox/+=10, Flox/+;Cre=11, cKO=10	>0.05
4.21. A	Entries - habituation males	Flox/+=10, Flox/+;Cre=11, cKO=11	>0.05
4.21. B	Entries - habituation females	Flox/+=10, Flox/+;Cre=11, cKO=10	>0.05
4.21. C	Entries - empty vs. stranger 1 Flox/+ males	10	>0.05
4.21. D	Entries - empty vs. stranger 1 Flox/+;Cre males	11	>0.05
4.21. E	Entries - empty vs. stranger 1 cKO males	11	>0.05

Figure	Analysis	n	P
4.21. F	Entries - empty vs. stranger 1 Flox/+ females	10	>0.05
4.21. G	Entries - empty vs. stranger 1 Flox/+;Cre females	11	>0.05
4.21. H	Entries - empty vs. stranger 1 cKO females	10	>0.05
4.21. I	Total entries - stranger 1 males	Flox/+=10, Flox/+;Cre=11, cKO=11	>0.05
4.21. J	Total entries - stranger 1 females	Flox/+=10, Flox/+;Cre=11, cKO=10	>0.05
4.22. A	Entries - stranger 1 vs. stranger 2 Flox/+ males	10	>0.05
4.22. B	Entries - stranger 1 vs. stranger 2 Flox/+;Cre males	11	>0.05
4.22. C	Entries - stranger 1 vs. stranger 2 cKO males	11	>0.05
4.22. D	Entries - stranger 1 vs. stranger 2 Flox/+ females	10	>0.05
4.22. E	Entries - stranger 1 vs. stranger 2 Flox/+;Cre females	11	>0.05
4.22. F	Entries - stranger 1 vs. stranger 2 cKO females	10	>0.05
4.22. G	Total entries - stranger 1 + stranger 2 males	Flox/+=10, Flox/+;Cre=11, cKO=11	>0.05
4.22. H	Total entries - stranger 1 + stranger 2 females	Flox/+=10, Flox/+;Cre=11, cKO=10	>0.05
4.23. A	Total entries - cumulative males	Flox/+=10, Flox/+;Cre=11, cKO=11	>0.05
4.23. B	Total entires - cumulative females	Flox/+=10, Flox/+;Cre=11, cKO=10	>0.05
4.23. C	Total entries - habituation vs. stranger 1 vs. stranger 2 Flox/+ males	10	<0.0001, 0.0007
4.23. D	Total entries - habituation vs. stranger 1 vs. stranger 2 Flox/+;Cre males	11	0.0011, 0.0004
4.23. E	Total entries - habituation vs. stranger 1 vs. stranger 2 cKO males	11	<0.0001, <0.0001
4.23. F	Total entries - habituation vs. stranger 1 vs. stranger 2 Flox/+ females	10	0.0049, 0.0024
4.23. G	Total entries - habituation vs. stranger 1 vs. stranger 2 Flox/+;Cre females	11	<0.0001, 0.0002

Figure	Analysis	n	P
4.23. H	Total entries - habituation vs. stranger 1 vs. stranger 2 cKO females	10	0.0066, 0.0048